

FINITE-ELEMENT AND LATTICE BOLTZMANN BASED NUMERICAL  
MODELING OF ENVIRONMENTAL MASS TRANSFER PROCESSES

By

Yusong Li

Dissertation

Submitted to the Faculty of the  
Graduate School of Vanderbilt University  
in partial fulfillment of the requirements

for the degree of

DOCTOR OF PHILOSOPHY

in

Environmental Engineering

August, 2005

Nashville, Tennessee

Approved:

Eugene J. LeBoeuf

Prodyot K. Basu

David S. Kosson

M. Douglas LeVan

Douglas H. Fisher

Louis Hampton Turner, IV

Copyright © 2005 by Yusong Li  
All Rights Reserved

To my grandparents, Renqing Li and Zhaoyi Li,  
my parents, Tianhui Li and Tinghua Zhou,  
my brother Ruosong Li,  
and  
my beloved husband Yong Zhang,  
who made all of this possible,  
for their love, endless encouragement and patience

## ACKNOWLEDGEMENTS

Reflecting back on this enjoyable and painful five year Ph.D study, I would like to express my gratitude to all those people who helped, supported and accompanied me.

First of all, I would like to thank my advisor, Eugene J. LeBoeuf, for supporting me, and for providing motivation and guidance throughout my dissertation research. As my teacher and mentor, he guided me into the wonderful world of scientific research. I am greatly indebted to him for his availability, inspiration, criticism, humor and optimism. His technical and editorial advice is essential to the completion of this dissertation.

I would like to express my appreciation to my co-advisor Professor P.K. Basu. I feel very fortunate to sit in his class on the first day of my study and work closely with him since then. His guidance on numerical modeling is critical for completing this dissertation. His support and suggestions on my future plans are invaluable.

My thanks also go to Drs. David S. Kosson, M. Douglas LeVan, Douglas H. Fisher, and Louis Hampton Turner, IV for serving on my dissertation committee, for contributing their time and offering valuable comments on my research work. Especially I would like to thank Dr. Turner who spent many hours helping me on Web-based modeling part.

I have had big pleasure to work with a number of members in our research group, Terra Baranowski, Kati Young Bell, Rossane Delapp, Ravi Palakodeti, Leslie Shor, Yuanjian Sun, Wei Wang, Wen Yu and Lu Zhang. I appreciate their time to listen to my research presentations, their kindness to provide criticism and suggestions, and the

opportunity that informs me much broader environmental engineering topics other than my research focuses. Particularly, the friendship with Rossane Delapp is much appreciated. I will always cherish her suggestions related to both my graduate studies and life.

Special thanks are due to my officemates, Zhiyong Guo, Marci Recher, Natasha Smith, and Kristen E. Shepherd. I am very grateful to a warm and harmonious environment they provide to me. We share numerous good discussions on our study, research and life. Their encouragements on my research and their helps on my life will be in my memory forever.

No one has been more important to me in the pursuit of my degree than my family. I would like to thank my grandparents, who brought me up until I was twelve-year old and cultured early seeds of my education. I would also like to express my deep gratitude to my parents, for their high expectations and profound influences on my outlook in life. I also appreciate my brother, who always sets high standard for me and serves as my model in both life and study.

Last, but most importantly, I am greatly indebted to my devoted husband Yong Zhang. I appreciate his patience on listening to me endlessly talk about my research. I appreciate that he accompanied me numerous nights work late in the school. I appreciate his strong confidence in my ability to accomplish my research goals. His encouragements and supports have been the true origins of completing this work. His love forms the root of my happiness.

This dissertation is supported in part through a grant by the National Science Foundation, and the Vanderbilt Department of Civil and Environmental Engineering.

# TABLE OF CONTENTS

	PAGE
<b>DEDICATION.....</b>	<b>iii</b>
<b>ACKNOWLEDGEMENTS .....</b>	<b>iv</b>
<b>LIST OF TABLES .....</b>	<b>x</b>
<b>LIST OF FIGURES .....</b>	<b>xii</b>
<b>CHAPTER</b>	
<b>I. INTRODUCTION.....</b>	<b>1</b>
1.1 Perspective .....	1
1.2 Research Significance .....	6
1.3 Research Hypothesis .....	7
1.4 Research Objectives .....	7
1.5 Organization of the Dissertation .....	8
<b>II. LITERATURE REVIEW .....</b>	<b>11</b>
2.1 Introduction.....	11
2.2 Mass Transfer at the Macroscale .....	11
2.2.1 Completely Mixed Reactors .....	13
2.2.2 Plug Flow with Dispersion Reactors.....	14
2.2.3 First Order Mass Transfer Models.....	17
2.2.4 Diffusion Models .....	24
2.2.5 Summary of Macroscale Mass Transfer Models .....	32
2.3 Microscale Mass Transfer Processes .....	33
2.3.1 Intrisorbent Diffusion.....	33
2.3.2 Diffusion in Synthetic Macromolecules .....	37
2.3.3 Sorption Isotherm Models.....	40
2.4 Modeling Fluid Flow in Porous Media.....	48
2.4.1 Models of Porous Media.....	48
2.4.2 Modeling Fluid Flow through Porous Media.....	53
2.5 Lattice Boltzmann Methods.....	56

2.5.1	Introduction to Lattice Boltzmann Methods .....	56
2.5.2	Advantages of Lattice Boltzmann Methods.....	59
2.5.3	Lattice Boltzmann Modeling Flows in Porous Media .....	60
2.5.4	Improvements of Boundary Conditions.....	61
2.5.5	Lattice Boltzmann Methods on Irregular Grids .....	62
2.5.6	LBM Simulations of Solute Transport in Fluid Flow .....	64
2.6	Summary .....	69
<b>III.</b>	<b>DEVELOPMENT OF A WEB-BASED MASS TRANSFER PROCESSES LABORATORY.....</b>	<b>71</b>
3.1	Introduction .....	71
3.2	Learning Theory and the Importance of the Laboratory in Engineering Education.....	71
3.3	Web-Based Education.....	74
3.3.1	Web-Based Education Overview .....	74
3.3.2	Categories of Web-Based Education Tools .....	75
3.4	Mass Transfer Processes Research and Education .....	79
3.5	Mass Transfer Process Laboratory.....	83
3.5.1	Overview.....	83
3.5.2	Conceptual Model.....	84
3.5.3	Mathematical Models.....	86
3.5.4	Numerical Methods.....	94
3.5.5	The Mass Transfer Process Laboratory Website .....	96
3.5.6	Example Applications .....	112
3.6	Mass Transfer Process Laboratory System Architecture.....	117
3.6.1	Architecture Overview.....	117
3.6.2	Architecture Specifications.....	120
3.7	SUMMARY .....	129
<b>IV.</b>	<b>STOCHASTIC MODELING OF THE PERMEABILITY OF RANDOMLY GENERATED POROUS MEDIA .....</b>	<b>131</b>
4.1	Introduction.....	131
4.2	Numerical Methods.....	134
4.2.1	Porous Media Generation .....	134
4.2.2	LBM Simulation .....	136
4.2.3	FORM .....	138
4.2.4	Proposed Algorithm.....	141
4.3	Illustrative Examples .....	143
4.3.1	Example Model Domains .....	143

4.3.2	Evaluations of the LBM Model .....	144
4.4	Numerical Results .....	145
4.4.1	Permeability Statistics .....	145
4.4.2	Applicability of Permeability Distributions .....	148
4.4.3	Comparison with Monte Carlo Simulations .....	150
4.5	Summary .....	153
<b>V.</b>	<b>A LEAST SQUARES FINITE ELEMENT SCHEME FOR LATTICE BOLTZMANN METHOD ON UNSTRUCTURED MESHES .....</b>	<b>156</b>
5.1	Introduction .....	156
5.2	Numerical Formulations .....	160
5.2.1	Numerical Derivation .....	160
5.2.2	Boundary Conditions .....	164
5.2.3	Implementation Issues .....	164
5.3	Analysis of LSFE-LBM .....	167
5.3.1	Accuracy Analysis .....	167
5.3.2	Stability Analysis .....	168
5.4	Numerical Results .....	175
5.4.1	Poiseuille Flow .....	175
5.4.2	Couette Flow .....	177
5.4.3	Flow past a Circular Cylinder .....	178
5.4.4	Flow in Porous Media .....	181
5.5	Summary .....	184
<b>VI.</b>	<b>USE OF LSFE-LBM TO STUDY MASS TRANSFER PROCESSES .....</b>	<b>187</b>
6.1	Introduction .....	187
6.2	LSEF-LBM for Solute Transport .....	189
6.3	Validation of LSFE-LBM .....	190
6.3.1	Diffusion between Two Parallel Walls .....	190
6.3.2	Diffusion with Reactive Boundary .....	193
6.4	Use of LSFE-LBM to Simulate Mass Transfer in a Single Particle System .....	195
6.4.1	Problem Description .....	195
6.4.2	Liquid Phase Boundary Condition .....	197
6.4.3	Intraparticle Diffusion .....	200
6.4.4	Analysis of the Single Particle System .....	203
6.4.5	Numerical Simulations .....	206



6.5	Use of LSFE-LBM to Simulate Mass Transfer in Porous Media.....	213
6.5.1	Introduction.....	213
6.5.2	System Setting .....	216
6.5.3	Influence of Pore Structural Configurations.....	217
6.5.4	Influences of Soil Organic Matter.....	223
6.6	Summary .....	232
<b>VII.</b>	<b>CONCLUSIONS AND FUTURE RESEARCH NEEDS .....</b>	<b>234</b>
7.1	Overview.....	234
7.2	Summary .....	235
7.2.1	Development of a Web-Based Mass Transfer Process Laboratory (MTVLab).....	236
7.2.2	Stochastic Modeling of the Permeability of Randomly Generated Porous Media.....	237
7.2.3	Development of a Least Squares Finite Element Lattice Boltzmann Method (LSFE-LBM).....	238
7.2.4	Use of a Least Squares Finite Element Lattice Boltzmann Method to Study Fluid Flow and Mass Transfer Processes.....	240
7.3	Recommendations for Future Research.....	242
7.3.1	Future directions on expanding MTVLab.....	242
7.3.2	Future directions on advancing LBM FORM.....	243
7.3.3	Future directions on advancing LSFE-LBM.....	244
7.3.4	Future directions on investigating mass transfer processes using LSFE-LBM .....	245
	<b>REFERENCES.....</b>	<b>247</b>

## LIST OF TABLES

<b>TABLE</b>	<b>PAGE</b>
3-1 Mass Transfer Processes Included in the Model.....	86
3-2 Boundary Conditions for CMFR and CMBR. ....	87
3-3 Parameters for MTVLab Example Applications. ....	114
4-1 Particle Size Distribution Parameters Employed in This Work.....	144
4-2 Statistical Properties of Derived Permeability CDFs.....	146
5-1 A Comparison of Accuracy and Stability Characteristics of FD-LBM, CGDBE, and LSFE-LBM for the Pure Advection Equation on a Uniform Mesh. ....	169
5-2 Comparison of Geometric and Dynamic Parameters of Flow past a Circular Cylinder with Previous Studies.....	180
6-1 Parameters of the Single Particle System.....	206
6-2 Parameters of Numerical Tests for Region PNE.....	207
6-3 Parameters of Numerical Tests for Region LEA.....	208
6-4 Parameters of Numerical Tests for Region IND.....	210
6-5 Parameters of Numerical Tests for Defining the Intraparticle Diffusion Region.....	211
6-6 An Analysis of BTCs of Numerical Tests for Defining the Intraparticle Diffusion Region. ....	212
6-7 Porous Media Domains Used for Studying the Influence of Soil Structure Configurations on Solute Transport.....	218
6-8 Distributions of Remaining Phenanthrene in Simulated Porous Media Domains at a Time of 30 Pore Volumes.....	220
6-9 Porous Media Domains with Varied Humic Acids and Kerogen Contents Used for Studying the Influence of SOMs on Solute Transport.....	224
6-10 Freundlich Isotherm Model Parameters for Phenanthrene Sorption on Humic Acids and Kerogen at 25 °C (LeBoeuf and Weber 2000).....	226

6-11	Nonequilibrium Reaction Rates of Phenanthrene Sorption on Humic Acid and Kerogen. ....	226
6-12	Intraparticle Diffusion Coefficients for Phenanthrene Diffusion into Humic Acids and Kerogen (LeBoeuf and Weber 2000) .....	226

## LIST OF FIGURES

FIGURE	PAGE
2-1 Macroscopic and Microscopic of Mass Transfer Processes. ....	12
2-2 Completely Mixed Reactors for Coupling Macroscale and Microscale Mass Transport.....	14
2-3 Control Volume for One-Dimensional Transport through Porous Media .....	15
2-4 Influence of Sorption Kinetics on the Breakthrough Curve. ....	16
2-5 Conceptualization of the Multiprocess Nonequilibrium Models.....	20
2-6 Hopfenberg-Frisch Chart of Anomalous Transport Phenomena .....	37
2-7 Schematic Characterization of Absorption and Adsorption Processes .....	40
2-8 Langmuir Model. ....	42
2-9 BET Model.....	43
2-10 Freundlich Sorption Isotherm. ....	45
2-11 Sorption Processes on the Discrete Heterogeneous Sorbent.....	45
2-12 A Spatially-Periodic Porous Media Model .....	49
2-13 Bethe Network Model.....	50
2-14 A Cross Section of a Typical Porous Media, (a) Realistic, and (b) a Network Model. ....	51
2-15 Depiction of Two- and Three-Dimensional Network Models .....	51
2-16 A Two-Dimensional Particle Packing Model of Randomly Distributed Disks .....	52
2-17 A Nine-Velocity (D2Q9) Lattice Model.....	57
3-1 General Information Flow within MTVLab. ....	84
3-2 MTVLab Conceptual Model.....	85
3-3 Uptake by a Sphere from a CMBR. ....	95

3-4	Concentration Distributions at Various Times in a Sphere with Initial Concentration $C_i$ and Surface Concentration $C_0$ .	96
3-5	An Example Welcome Page.	97
3-6	An Example Page of Project Description.	98
3-7	An Example Page of System Data Input.	98
3-8	An Example Page of Particle Definition.	99
3-9	An Example Page of Diffusion Processes Definition.	100
3-10	An Example Page of Defining Particle Properties.	101
3-11	An Example of User-Specified Output Page.	102
3-12	An Example Confirmation Page.	103
3-13	An Example Model Status Page.	104
3-14	An Example of General Results Page.	105
3-15	Example Concentration Output Menu.	106
3-16	An Example Concentration Profile Output Presented by a Radar Graph.	107
3-17	An Example Mass Uptake Output Presented by a Pie Graph.	108
3-18	An Example Mass Flux Output Presented by a Line Graph.	109
3-19	MTVLab Help and Tutorial Modules.	110
3-20	Particle Sorption and Desorption Processes in a CMFR.	116
3-21	Particle Sorption and Desorption Processes in a CMBR.	116
3-22	A Comparison of Particle Concentration Profiles During Sorption and Desorption Processes for a CMFR and a CMBR.	117
3-23	Mass Transfer Processes Virtual Laboratory System Architecture.	119
3-24	MTVLab FlowChart.	121
3-25	Example CORBA Architecture.	127
4-1	Example Randomly-Generated Porous Media at Porosity 0.45.	136
4-2	Flow Chart for the LBM FORM Algorithm.	142

4-3	Influence of Particle Mean Diameter on Porous Media Permeability CDF for Domains with Geometric Mean Particle Diameter $D = 50 \mu\text{m}$ and Differing COV. ....	146
4-4	Influence of Particle Sorting on Porous Media Permeability CDF for Domains with Geometric Mean Particle Diameter $D = 50 \mu\text{m}$ and Differing COV. ....	147
4-5	Comparison of FORM-Derived Permeability CDF with Most Commonly Used Normal Distribution CDF, Gamma Distribution CDF, and Lognormal Distribution CDF on the Simulation Domains with Differing Geometric Mean Particle Diameter and COV. ....	149
4-6	A Comparison of Monte Carlo Simulation Results and FORM Results for the Simulation Domain with Particle Mean Diameter $D = 25 \mu\text{m}$ and $\text{COV} = 0.01$ . ....	152
5-1	Schematic Plot of Neighboring Point Distribution around the Point $(i,j)$ in a Uniform Triangular Mesh for LSFE-LBM. ....	170
5-2	Stability Boundaries as Function of Mean Velocity $u$ and Collision Frequencies $\omega$ for Selected $dt/dl$ when $\tau = 1.0$ . ....	173
5-3	Stability Boundaries as Function of Mean Velocity $u$ and Collision Frequencies $\omega$ for Selected $\tau$ when $dt/dl = 1.0$ . ....	174
5-4	Comparison of LSFE-LBM Solution (points) and Analytical Solution (line) for Normalized Velocity Profile for Poiseuille Flow. . ....	176
5-5	Comparison of LSFE-LBM Solution and Analytical Solution for Couette flow. ....	178
5-6	Unstructured Mesh for Flow past a Circular Cylinder. ....	179
5-7	An Example of Unstructured Mesh for Flow in the Porous Media. ....	182
5-8	A Comparison of the Performance of Traditional LBM and LSFE-LBM on Simulating Flow in the Porous Media. ....	184
6-1	Figure 6-1. Diffusion between Two Parallel Walls. ....	191
6-2	Comparison of LSFE-LBM Solution (points) and Analytical Solution (line) for Diffusion between Two Parallel Walls. ....	192
6-3	Diffusion between Two Parallel Walls with a Reactive Boundary Condition. ..	193
6-4	An Illustration of an Upper Wall Boundary Condition at the Micro-Scale. ....	194

6-5	Comparison of LSFE-LBM Solution (points) and Analytical Solution (line) for Diffusion Between Two Parallel Walls with a Reactive Boundary Condition under Different Damkohler Numbers. ....	195
6-6	An Illustration of Fluid Flow and Solute Transport Through and Around a Circular Particle. ....	196
6-7	An Illustration of Boundary Conditions at the Solid-Liquid Interface. ....	198
6-8	An Illustration of the LBM Boundary Condition at the Solid-Liquid Interface.....	199
6-9	An Illustration of a Finite Difference Discretization of a Circular Particle with a Cylindrical Coordinate System. ....	200
6-10	An Illustration of Relationships among Mass Transfer Processes in a Single Particle System. ....	203
6-11	Graphic Representation of Mass Transfer Regimes of a Single Particle System.....	205
6-12	Break Through Curves in Region PNE.....	205
6-13	Break Through Curves in Region LEA. ....	208
6-14	Break Through Curves in Region IND. ....	210
6-15	An Illustration of Fluid Flow and Solute Transport through a Porous Medium. ....	216
6-16	BTCs of Phenanthrene Removal from Contaminated Porous Media with Varied Particle Sorting Levels.....	219
6-17	A Relationship between Permeability and the Amount of Mass remaining in a Porous media.....	221
6-18	Breakthrough Curves of Phenanthrene Removal from Contaminated Porous Media with Varied SOM Contents.....	228
6-19	Tailing Concentrations of Phenanthrene Removal from Contaminated Porous Media with Varied Humic Acids and Kerogen contents.....	228
6-20	Changes of Phenanthrene Concentrations in SOMs with Different Humic Acids and Kerogen Contents when Removal of Phenanthrene from Contaminated Porous Media. ....	231

# CHAPTER I

## INTRODUCTION

### 1.1 Perspective

Chemical contamination of subsurface environments are increasing in concern in the United States due to the growing percentage of the population dependent on groundwater as their sole water supply (Freeze and Cherry 1979). Successful remediation of chemically contaminated groundwater, soil, and sediments is thus an important undertaking for environmental engineers and scientists. To provide for effective and efficient groundwater contamination prevention and remediation systems, however, engineers and scientists must first possess a clear understanding of the complex processes controlling the mass distribution, transportation, reaction, and transformation of contaminants in the subsurface system. In order to model contaminant movement at the field scale correctly, an accurate depiction of the rate-limited mass transfer processes controlling the distribution of contaminants at the particle scale and the pore scale is critical.

Recent research, however, has shown that mass transfer processes at the particle scale are subjected to highly nonlinear processes. For example, Weber and coworkers (Weber and Huang 1996; Huang, Young et al. 1997; LeBoeuf and Weber 1997; Weber, LeBoeuf et al. 2001) have demonstrated that natural organic matter (NOM) derived from soils and sediments may be represented as a dual mode sorbent containing both rubbery and glassy components, and that diffusion of contaminants into and out of the glassy



domain contributes to slower sorption-desorption rates. The Distributed Reactivity Model (DRM), originally applied to equilibrium systems and later extended to heterogeneous natural solids under non-equilibrium conditions, provides a framework to characterize the influence of variably reactive domains of soil and sediment particles on sorption processes (Weber , McGinley et al. 1992; Young and Weber 1995; Weber and Huang 1996; Huang, Young et al. 1997; LeBoeuf and Weber 1997; Huang and Weber 1998). Further, additional studies (LeBoeuf and Weber 1997; LeBoeuf and Weber 2000; LeBoeuf and Weber 2000; Schaumann and Antelmann 2000; Young and LeBoeuf 2000; DeLapp and LeBoeuf 2004; DeLapp, LeBoeuf et al. 2004; Schaumann and LeBoeuf 2004), support analogies between NOM and synthetic organic macromolecules, and thus, well-developed theories for diffusion in organic polymers could be applied to NOM-controlled intrasorbent diffusion (Weber, LeBoeuf et al. 2001).

These complex depictions of mass transfer processes at the particle scale necessitate the employment of more evolved conceptual models, and use of often highly nonlinear numerical methods, which thus provide a great educational challenge. While traditional approaches to instruction have, and continue to be, effective in teaching mass transfer processes, recent studies suggest that exclusive use of this approach is not sufficient (Gillett 2001; Hyde and Karney 2001; Koehn 2001). Depending too heavily on traditional forms of instruction, including formal lectures and homework, may limit students' exposure to one or two stages of the four progressive, yet interrelated, stages of the Kolb Learning Cycle (Kolb 1984) ((i) concrete experience; (ii) active experimentation; (iii) reflective observation; and (iv) abstract conceptualization), and thus may limit their learning retention. Engineering students prefer active processing

(Anderson 1991); use of more active stages, i.e., concrete experiences, can greatly enhance their learning experiences. Web-based virtual laboratory environments, where students can gain a personalized experience and make intelligent decisions, has been widely recognized as a powerful substitute to traditional education strategies (Brusilovsky, Eklund et al. 1998; Goeller 1998; Kerrey and Isakson 2000; Kirschner and Paas 2001; Iskander 2002), including instruction of mass transfer processes (Katz, Weathers et al. 1997; Katz, Weathers et al. 1998; Reardon 2001). Current Web-based teaching activities relating to mass transfer processes education, however, are often provided at the most basic levels of instruction. Further, combining high-level computation requirements for modeling mass transfer processes with Web-based user-friendly features greatly increases the technical challenges of employing such systems across the Internet. It is in this light that we provided a proof-of-principle framework from which to develop more sophisticated Web-based models that can employ computationally efficient, high-level computer programs (e.g., FORTRAN, C++). Here, we developed a mass transfer processes virtual laboratory (MTVLab) for individuals involved in coursework, research, and professional practice to improve the general understanding of controlling mass transfer processes in environmental systems.

In parallel to our effort to enhance mass transfer process education by incorporating state-of-the-art mass transfer models at the particle scale with Web-based education, this research seeks to better evaluate mass transfer processes at the pore scale. Traditional models employing *ideal* contaminant transport processes represented by local equilibrium assumptions and linear sorption processes often fail to adequately model observed processes, suggesting other, *non-ideal* factors are influencing observed

behaviors. These non-ideal factors include physical and chemical heterogeneity of soils and sediments (Haggerty and Borelick 1995; Haggerty and Gorelick 1998), nonequilibrium, rate-limiting, slow sorption/desorption behaviors (Pignatello and Xing 1996; Luthy, Aiken et al. 1997; Weber, LeBoeuf et al. 2001), and variable advection patterns associated with complex soil particle geometries (Brusseau, Jessup et al. 1989; Brusseau, Jessup et al. 1991). In the past thirty years, mass transfer models have evolved in their ability to incorporate the primary non-ideal factors, from first-order reaction models (Lapidus and Amundson 1952; Coats and Smith 1964; Van Genuchten and Wierenga 1976; Travis and Etnier 1981; Brusseau, Jessup et al. 1989; Connaughton, Stedinger et al. 1993; Pedit and Miller 1994; Chen and Wagenet 1995; Haggerty and Borelick 1995; Culver, Hallisey et al. 1997; Haggerty and Gorelick 1998) to diffusion models (Miller and Weber 1984; Miller and Weber 1988; Ball and Roberts 1991; Pedit and Miller 1994; Cunningham, Werth et al. 1997; Haggerty and Gorelick 1998; Werth and Hansen 2002), from single site model (Lapidus and Amundson 1952) to multi-site model (Brusseau, Jessup et al. 1989; Pedit and Miller 1994; Haggerty and Borelick 1995; Pedit and Miller 1995), and from deterministic approaches to stochastic approaches (Cunningham, Werth et al. 1997; Haggerty and Gorelick 1998; Werth and Hansen 2002). Although these models provide enhanced abilities to capture the heterogeneity of soils, it remains difficult to explicitly quantify pore tortuosity, particle geometry, and pore size distribution within as employed in these models. Additionally, variability in flow rates and solute concentrations may also affect mass transfer characteristics, further suggesting the need to extend current mass transfer models to account for porous media geometry (Pignatello and Xing 1996), the first step of which is to develop a numerical model for

fluid flow capable of reproducing the physics of fluid flow in porous media to provide for improved simulations of controlling mass transfer processes.

Different approaches have been applied to model flow through porous media, for example, effective-medium approximation (EMA) (Choy 1999), renormalization (King 1989), percolation theory (Reyes and Jensen 1985; Sahimi 1994), volume-averaging method (Whitaker 1999), (Quintard and Whitaker 1994; Quintard and Whitaker 2000), network models (Koplik and Lasseter 1984; Aviles and LeVan 1991; Russell and LeVan 1997; Blunt 2001), Laplacian methods (Durlfisky 1991; Efendiev and Durlfisky 2002), and multi-grid homogenization methods (Knappek 1998; Moulton, Dendy et al. 1998). Each of these methods, however, are based upon some level of averaging, and thus none of them can fully represent the details of what may occur within individual pores (Sahimi 1995; Succi 2001). In the late 1980s', lattice Boltzmann models (LBM) were successfully introduced into fluid flow simulations (Rothman 1988; Cancelliere, Chang et al. 1990; Chen, Diemer et al. 1991). The particle-like nature of LBM enables the representation of complex pore structures with fundamental mechanical events (e.g., bounce back), while permitting recovery of macroscopic flow behavior within very small pore spaces (Succi 2001). LBM has been viewed as the most promising method for simulating complex problems of flow in natural porous media (Chen and Doolen 1998; Wolf-Gladrow 2000).

Traditional LBM, however, is restricted to construction on a uniform grid, which can significantly reduce further applications of LBM in flow through porous media where the complex geometry of micropores cannot be well fit to a uniform lattice. By coupling LBM with traditional numerical methods such as Finite Difference, Finite Volume, and Finite Element methods, the applicability of LBM can be extended to irregular

unstructured grids (Cao, Chen et al. 1997; Mei and Shyy 1998; Peng, Xi et al. 1998; Peng, Xi et al. 1999; Lee and Lin 2001; Sofonea and Sekerka 2003). It is in this light that we developed a new finite element lattice Boltzmann method, which utilizes a least squares finite element method (LSFE) in space and a Crank-Nicolson method in time. This method is able to solve fluid flow and mass transfer problems in domains that contain complex or irregular geometric boundaries by using finite element methods' geometric flexibility and numerical stability, while employing efficient and accurate least squares optimization. LSFE-LBM is a powerful tool to assist the numerical modeling efforts of elucidating the relative contributions of transport- and sorption/desorption-related nonequilibrium factors on mass transfer processes in subsurface systems.

## **1.2 RESEARCH SIGNIFICANCE**

To achieve successful remediation of contaminated groundwater, it is critical for engineers and scientists to possess a clear understanding of the complex mass transfer processes that may occur in the subsurface environment. The presence of physical and chemical heterogeneity of subsurface systems, as well as the inherent complexity associated with microscale rate-limiting mass transfer processes, provide for significant challenges to accurate prediction of the fate and transport of chemical constituents within the subsurface. Development of improved modeling techniques, based on extensions of a lattice Boltzmann method adapted to the specific research needs identified within this dissertation, will facilitate a more accurate prediction of the fate and transport of contaminants in subsurface environments. Provision of these models through a Web-based environment will provide students, faculty, and professionals a convenient and

efficient tool to improve the understanding of controlling mass transfer processes in environmental systems. The novel Web-based modeling system architecture developed by this work will provide a proof-of-principle framework from which to develop more sophisticated Web-based models that can employ computationally efficient, high-level computer programs.

### **1.3 Research Hypothesis**

This research addresses the following hypotheses:

- I. A Web-based virtual laboratory, incorporating recent advances in mass transfer processes research, as a complement to the existing practices, will serve as a powerful tool to enhance current mass transfer processes education.
- II. Advanced pore-scale numerical models, capable of capturing the physics of fluid flow and solute transport in complex pore geometries, will facilitate a better understanding of complex mass transfer processes.

### **1.4 Research Objectives**

In this work we seek to improve the general understanding of controlling mass transfer processes in environmental systems by developing advanced numerical methods and a virtual mass transfer laboratory (MTPVLab). Based on the aforementioned hypotheses, the following two general objectives with several sub-objectives are proposed:

- I. Development of a user-friendly, graphical user interface, Web-based modeling system for students and researchers to study state-of-the-art mass transfer processes. This objective is delineated into three tasks:
  - I-1. Development of finite element-based numerical modules for identified state-of-the-art mass transfer mechanisms.
  - I-2. Development of user-friendly graphical user interfaces (GUIs) for input, output, and help modules.
  - I-3. Development of a proof-of-principle software architecture from which to develop more sophisticated Web-based models that can employ computationally efficient, high-level computer programs (e.g., FORTRAN, C++).
  
- II. Development of advanced numerical models to better investigate mass transfer processes in porous media
  - II-1. Use of a proper pore-scale method, e.g. LBM, to study characteristics of fluid flow in randomly generated porous media.
  - II-2. Development of a novel least squares finite element lattice Boltzmann method (LSFE-LBM) to more efficiently model fluid flow in porous media.
  - II-3. Use of LSFE-LBM to study fluid flow and mass transfer processes in randomly generated porous media.

## **1.5 Organization of the Dissertation**

This dissertation is organized into seven chapters. Chapter I includes an introduction to the research topic, its significance to environmental engineering, and the

stated hypotheses and objectives. Chapter II provides necessary background information and insights into the current state-of-the-art concepts and models that are being used to study mass transfer processes. Chapter III details the development of a Web-based mass transfer processes virtual laboratory. Chapter IV presents an innovative stochastic method to study permeability of randomly generated porous media by coupling a first order reliability method (FORM) with LBM. Chapter V describes the numerical derivations, validations, stability and accuracy analysis, and successful applications of LSFE-LBM to simulate flow fields in randomly generated porous media. Chapter VI extends LSFE-LBM to study solute transport in porous media. Finally, Chapter VII summarizes the main conclusions from the dissertation and addresses future areas of research.

A bibliography of the manuscripts associated with this dissertation is listed below:

### **Chapter III: Development of a Web-based Mass Transfer Processes Laboratory**

- Li, Y., LeBoeuf, E. J., Basu, P. K., and Turner, L.H. *Development of a Web-Based Mass Transfer Processes Laboratory: System Development and Implementation*. Computer Applications in Engineering Education, 11: 25-39, 2003.
- Li, Y., LeBoeuf, E. J., Basu, P. K., and Turner, L.H. *A Web-based interactive virtual laboratory system for environmental mass transfer processes*. International Journal of Engineering Education (in review).

### **Chapter IV: Stochastic Modeling of the Permeability of Randomly Generated Porous Media**

- Li, Y., LeBoeuf, E. J., Basu, P. K., and Mahadaven, S. *Stochastic Modeling of the Permeability of Randomly-Generated Heterogeneous Porous Media*. Advances in Water Resources, 28 (8): 835-844, 2005.

### **Chapter V: A Least Squares Finite Element Scheme for Lattice Boltzmann Method on Unstructured Meshes**

- Li, Y., E.J. LeBoeuf, and P.K. Basu, *Least squares finite element lattice Boltzmann method*. Physical Review E, 69 (6), Art. No., 06570(R). 2004.
- Li, Y., E.J. LeBoeuf, and P.K. Basu, *A Least Squares Finite Element Scheme for Lattice Boltzmann Method on Unstructured Meshes*. Physical Review E (in review).



## **Chapter VI: Use of LSFE-LBM to Study Mass Transfer Processes**

- *Li, Y., LeBoeuf, E.J. and Basu, P.K. Use of a Least Squares Finite Element Lattice Boltzmann Method to Study Fluid Flow and Mass Transfer Processes. Proceedings of the 2005 International Conference on Computational Science, May, 2005*
- *Li, Y., LeBoeuf, E. J. and Basu, P. K. Pore-scale modeling of the effects of transport - related and sorption/desorption processes on solute transport in heterogeneous porous media. Water Resources Research (in preparation).*

## **CHAPTER II**

### **LITERATURE REVIEW**

#### **2.1 Introduction**

This chapter consists of six sections providing an extensive review of the background and theories related to this research. Subsequent to this introduction, an overview of current macroscale solute fate and transport models is presented in Section 2.2, followed by a discussion of important microscale rate-limiting mass transfer processes, including diffusion and sorption processes, in Section 2.3. Modeling fluid flow through porous media is explored in Section 2.4, while Section 2.5 discusses the lattice Boltzmann method (LBM), a promising method for simulating complex problems of fluid flow in natural porous media. Section 2.6 summarizes current state-of-the-art research efforts, and highlights the specific research objectives of this study.

#### **2.2 Mass Transfer at the Macroscale**

Mass transfer is an essential part of many environmental processes within natural or engineered systems, such as water and wastewater treatment, air emissions control, and groundwater and soil remediation systems. In this research, our focus is on the subsurface environment and the mass transfer processes that may be responsible for controlling removal of organic chemicals from soils and sediments.

Two different scales are often involved in mass transfer processes: macroscale and microscale (Figure 2-1). Macroscale mass transfer processes include phenomena affecting the movement of constituents in the bulk of a system and across its boundaries

(Weber and DiGiano 1996), such as advection and dispersion. Microscale mass transfer processes include short-range diffusion and sorption processes that occur primarily at interfaces between phases (Weber and DiGiano 1996).

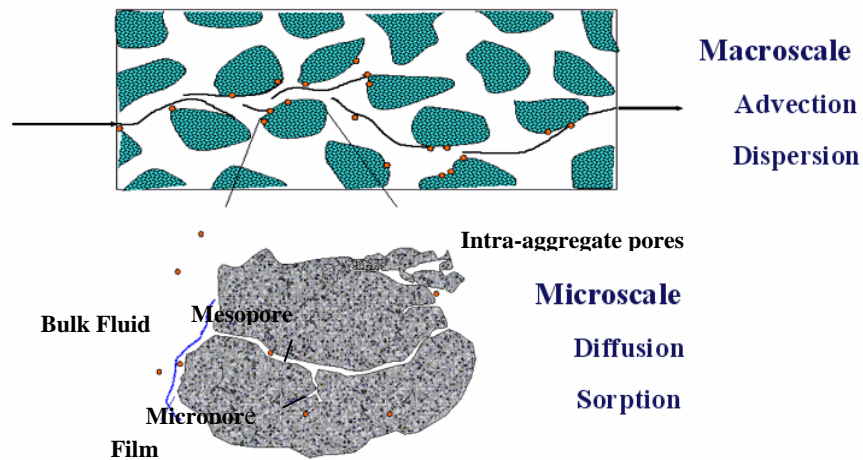


**Figure 2-1. Macroscopic and Microscopic of Mass Transfer Processes.**

Processes involved in mass transfer in the subsurface can be classified as (Brusseau and Rao 1989; Brusseau and Rao 1990; Weber, McGinley et al. 1991; Brusseau 1998): (i) advective-dispersive transport from bulk solution to the boundary layer of a soil or sediment particle; (ii) film diffusion across the adsorbed water to the surface of a particle; and (iii) diffusion within the particle itself (i.e., intrasorbent diffusion). Since these processes act in series, the slowest process will represent the rate-limiting step. Subsurface systems are also complicated by the presence of variable fluid flow patterns, causing transitions between laminar and turbulent flow. The critical value of the Reynolds number, at which fluid flow changes from laminar to turbulent, has been found by various investigators to range between 1 and 12 for subsurface systems (Scheidegger 1974). Although fluid flow in groundwater is generally laminar in nature,

the flow pattern and the residence times of fluid elements within the system may also influence the time available for mass transfer.

Two types of ideal reactors, i.e., completely mixed reactors and plug flow reactors, are often employed to simplify flow patterns and reduce or effectively eliminate some mass transfer processes. The applications of completely mixed reactors to model environmental systems include completely mixed flow reactors (CMFRs) and completely mixed batch reactors (CMBRs), which will be discussed in Section 2.2.1. Plug flow reactors, discussed in Section 2.2.2, are often employed in conjunction with advection-dispersion-reaction (ADR) equations, i.e., plug flow with dispersion reactor (PFDR), to model observed behaviors of natural porous media systems.

### 2.2.1 Completely Mixed Reactors

A CMFR or CMBR reactor provides for a system representing a suspension of sorbent particles in a bulk solution. As illustrated in Figure 2-2, a CMBR has no inflow or outflow, while a CMFR involves a continuous inflow and outflow. The well-mixed nature of CMFR and CMBR provide for uniform solute distribution in the bulk solution (i.e., no thermal or concentration gradient), although not necessarily constant concentration in a CMBR. Solute transport into or out of the suspended solid particles (i.e. adsorption and desorption processes), can be modeled through application of microscopic mass transfer models, which is discussed in detail in Section 2.3. If the mixing intensity is high, film diffusion will not be significant compared to intrasorbent diffusion in a well-mixed system (Weber and Miller 1988), and thus, the rate of change of mass in the solution phase will equal to rate of change of mass in the solid phase:

$$\text{CMBR: } V \frac{\partial C}{\partial t} = -D_s V \frac{\partial q}{\partial t}, \quad (2-1)$$

$$\text{CMFR: } V \frac{\partial C}{\partial t} = QC_{in} - QC - D_s V \frac{\partial q}{\partial t}, \quad (2-2)$$

where:

- $V$  = solution volume [ $L^3$ ];
- $C$  = solute concentration [ $M/L^3$ ];
- $D_s$  = concentration of solid particle (sorbent) in the solution [ $M/L^3$ ];
- $Q$  = flow rate in a CMFR [ $L^3/T$ ]; and
- $C_{in}$  = solute concentration in the inflow of a CMFR [ $M/L^3$ ].

System mass uptake in CMFRs and CMBRs can be derived through a mass balance on the solute where solutes lost from solution are balanced with solute gain by the sorbent particles(Weber and DiGiano 1996).

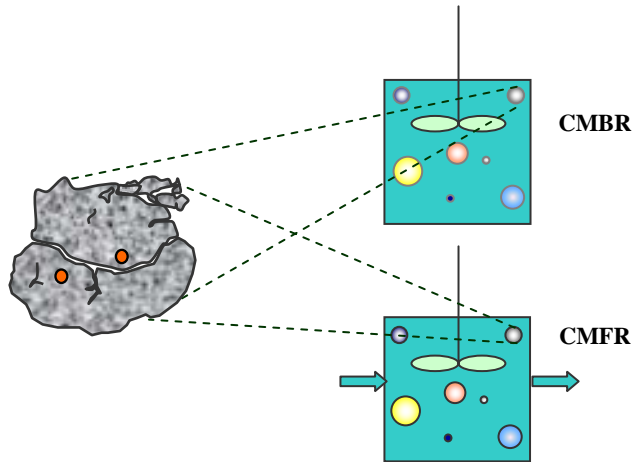


**Figure 2-2. Completely Mixed Reactors for Coupling Macroscale and Microscale Mass Transport.**

### 2.2.2 Plug Flow with Dispersion Reactors

Plug flow with dispersion reactor (PFDR) incorporates a dispersion term to account for the deviation from ideal plug flow behavior. In PFDR, macroscale advection

and dispersion are responsible for movement of solute through the bed, while inter-phase and intra-particle transport control sorption and diffusion rates. A one-dimensional advection-dispersion-reaction (ADR) model can be established based on a mass balance analysis on a control volume shown in Figure 2-3.

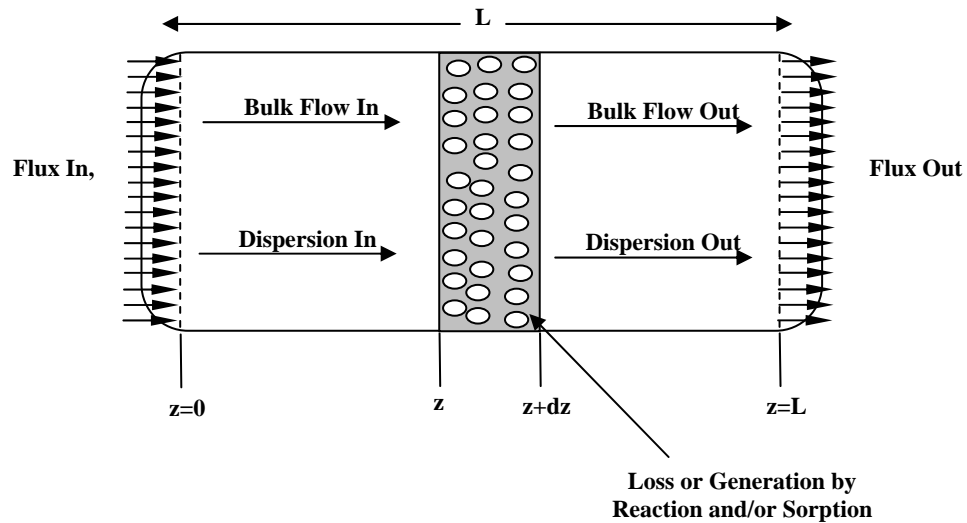


**Figure 2-3. Control Volume for One-Dimensional Transport through Porous Media (after Weber et al., 1991).**

The ADR model can be expressed as:

$$\frac{\partial C}{\partial t} = -v_z \frac{\partial C}{\partial z} + D_h \frac{\partial^2 C}{\partial z^2} - \frac{\rho_s(1-\varepsilon)}{\varepsilon} \frac{\partial q}{\partial t} \quad (2-3)$$

where:

- $C$  = solute concentration in the solution phase [ $M/L^3$ ];
- $v_z$  = the component of liquid-phase pore velocity in the  $z$  direction [ $L/T$ ];
- $\rho_s$  = the density of solid phase [ $M/L^3$ ];
- $\varepsilon$  = the porosity of the bed [-]; and
- $D_h$  = the hydrodynamic dispersion coefficient [ $L/T^2$ ].

Microscale linear or nonlinear sorption processes can be coupled with the ADR model through its sorption term,  $\frac{\partial q}{\partial t}$ . Initially, due to the slow movement of groundwater, it is assumed that microscale diffusion and sorption processes are much faster than macroscale advection and dispersion process, and thus, local sorption equilibrium should prevail, i.e., local equilibrium assumption (LEA). Numerous studies (Karickhoff and Brown 1978; Freeman and Cheung 1981; Di Toro and Horzempa 1982; Ball 1989; Harmon 1992; Carroll, Harkness et al. 1994; Farrell and Reinhard 1994; Farrell and Reinhard 1994; Weber and Huang 1996; Werth and Reinhard 1997; Werth and Reinhard 1997; Werth and Hansen 2002), however, cast doubt on the applications of LEA through the observation of long term sorption/desorption processes following an initial fast uptake. The resulting influence on macroscopic mass transfer phenomena are asymmetrical breakthrough curves, with earlier breakthrough and tailing, as shown in the Figure 2-4.

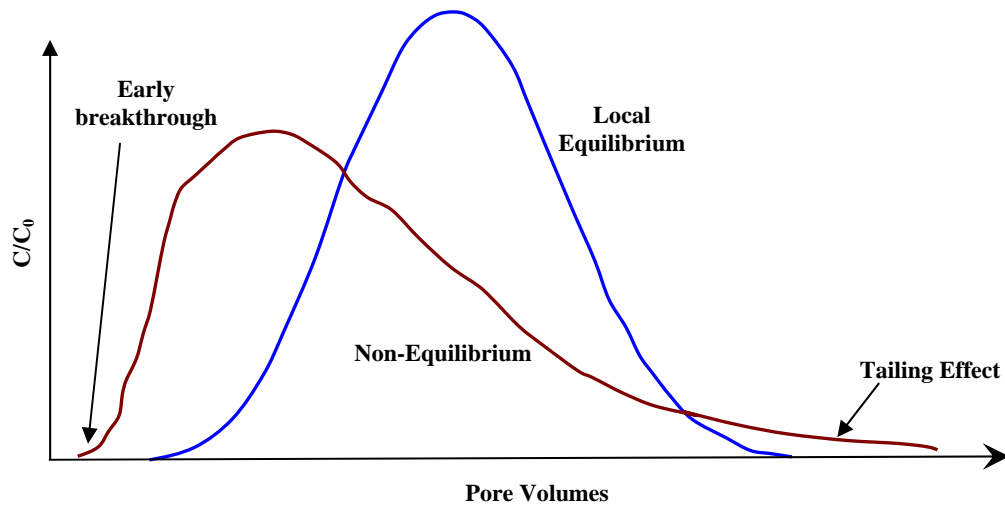


**Figure 2-4. Influence of Sorption Kinetics on the Breakthrough Curve.**

This two stage sorption-desorption phenomena can be attributed to many factors (Brusseau, Jessup et al. 1989; Brusseau 1994), including transport related factors (e.g., different advection pattern) and sorption related factors (e.g., chemical nonequilibrium reactions, and intrasorbent diffusion). Attempts to capture sorption kinetics can be classified into two types of mass transfer models, i.e., first order reaction based (Section 2.2.3) and diffusion model based (Section 2.2.4), both of which strive to include transport-related factors in the model.

### 2.2.3 First Order Mass Transfer Models

First order mass transfer models utilize a first order reaction to describe observed non-equilibrium mass transfer processes. An important advantage of this type of model is its simplicity, such that it does not require specific geometric information of the porous media.

#### 2.2.3.1 One-Site Models

Very early efforts to capture sorption kinetics treat the sorption rate as a function of the concentration difference between the solid and solution phases, which is a combination of effects from sorption and desorption (Lapidus and Amundson 1952; Brusseau and Rao 1990):

$$\frac{\partial q}{\partial t} = k_d \frac{\theta}{\rho} C - k_d' q, \quad (2-4)$$

where:

$C$	=	solute concentration in the solution [M/L <sup>3</sup> ];
$q$	=	solute concentration in the solid phase [M/M];
$k_d$	=	sorption rate coefficient [L <sup>3</sup> /M];
$k_d'$	=	desorption rate coefficient [L <sup>3</sup> /M];
$\rho$	=	soil bulk density [M/L <sup>3</sup> ]; and



$\theta$  = volumetric water content [-].

This over-simplified model failed to predict experimental data (Brusseu and Rao 1989; Brusseu and Rao 1990), and was thus replaced by two site models, which can be classified as chemical based two-site models and physical based two-site models which attribute non-equilibrium phenomena to sorption related and transport-related processes, respectively.

### 2.2.3.2 Two-Site First Order Models

Chemical based two site models attribute non-equilibrium to sorption-related factors, and envision the sorbent as two types of sites, where first order reaction controls at Type 1 sites, and assumes local equilibrium at Type 2 sites (Selim, Davidson et al. 1976; Cameron and Klute 1977; Travis and Etnier 1981):

$$\text{Type 1 site: } \frac{\partial q_1}{\partial t} = k[(1 - \phi)K_p C - q_1], \quad (2-5)$$

$$\text{Type 2 site: } \frac{\partial q_2}{\partial t} = \phi K_p \frac{\partial C}{\partial t}, \quad (2-6)$$

where:

- $q_1$  = solute concentration in the Type 1 sites [M/M];
- $q_2$  = solute concentration in the Type 2 sites [M/M];
- $k$  = the mass transfer coefficient for type 1 site [1/T];
- $K_p$  = the partitioning coefficient [ $L^3/M$ ]; and
- $\phi$  = the fraction of Type 2 sites [-];

Physical-based two-site models attribute non-equilibrium to transport-related factors, and envision the liquid phase in the porous medium as two regions (Coats and Smith 1964; Van Genuchten and Wierenga 1976): a mobile region and an immobile region. A first order reaction connects the solute transfer between two regions, while sorption processes in both regions are assumed as instantaneous sorption equilibrium:

$$\theta_m \frac{\partial C_m}{\partial t} + \theta_{im} \frac{\partial C_{im}}{\partial t} + f\rho \frac{\partial S_m}{\partial t} + (1-f)\rho \frac{\partial S_{im}}{\partial t} = \theta_m D \frac{\partial^2 C_m}{\partial z^2} - v_m \theta_m \frac{\partial C_m}{\partial z} \quad (2-7)$$

$$\frac{\partial S}{\partial t} = KnC^{n-1} \frac{\partial C}{\partial t} \quad (2-8)$$

$$\theta_{im} \frac{\partial C_{im}}{\partial t} + (1-f)\rho \frac{\partial S_{im}}{\partial t} = \alpha(C_m - C_{im}) \quad (2-9)$$

where:

$m$	=	refers to mobile regions;
$im$	=	refers to immobile regions;
$\theta_m$	=	the fractions of soil filled with mobile regions [-];
$\theta_{im}$	=	the fractions of soil filled with immobile regions [-];
$v_m$	=	average pore water velocity in the mobile solution[L/T];
$\alpha$	=	first order reaction coefficient [1/T];
$n$	=	Freundlich sorption coefficient [-].
$S$	=	the sorbed concentration [M/M]; and
$f$	=	the fraction of sorption sites in dynamic region [-].

Although two-site models typically achieve good results in representing experimental data, Brusseau et al. (Brusseau, Jessup et al. 1989) point out that their major constraint lies in the fact that they attribute the observed nonequilibrium to a single process, which in fact may be affected by multiple chemical and physical factors.

### 2.2.3.3 Multi-Site Models

The multiprocess nonequilibrium (MPNE) model proposed by Brusseau et al. (1989) is specifically formulated for nonequilibrium caused by a combination of transport and sorption related processes.

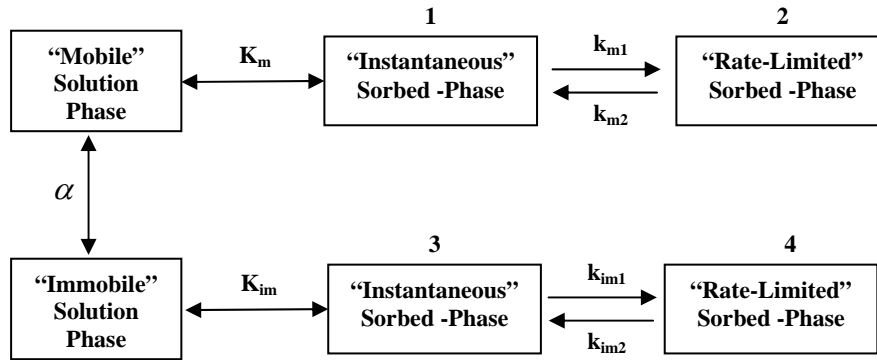


**Figure 2-5. Conceptualization of the Multiprocess Nonequilibrium Models (after Brusseau et al., 1989).**

It is clear from Figure 2-5 that MPNE actually is a coupling of chemical- and physical-based two-site models described in Section 2.2.3.2. Inherited from a physical-based two-site model primarily for liquid phases consisting of mobile and immobile regions, MPNE also employs a chemical based two-site model in that sorption sites are separated into instantaneous and rate-limited portions. In this model, only Domain 1 possesses instantaneous mass transfer with the mobile solution, the other three domains are all rate-limited by either diffusive mass transfer between mobile and immobile region or slow sorption processes.

Realizing the diversity of transport and sorption processes at the grain scale, some studies (Pedit and Miller 1994; Haggerty and Borelick 1995) have extended multi-site model. Instead of two mobile and immobile regions, Haggerty's model (Haggerty and Borelick 1995) postulate a mobile region combining with N distinct immobile regions. Those N distinct immobile regions can reflect various microscale mass transfer processes, e.g. diffusion, adsorption, and dissolution, although they are also expressed in the form of first order reactions. This model may be stated as:

$$\frac{\partial c_m}{\partial t} + \sum_{j=1}^N \beta_j \frac{\partial (c_{im})_j}{\partial t} = \nabla \cdot \left( \frac{D}{R_m} \nabla c_m \right) - \frac{v}{R_m} \nabla c_m - \frac{q}{\theta_m R_m} (\hat{c} - c_m) \quad (2-10)$$

$$\frac{\partial (c_{im})_j}{\partial t} = \alpha_j [c_m - (c_{im})_j], \quad j = 1, 2, \dots, N \quad (2-11)$$

where:

- $c_m$  = solute concentration in the mobile phase [M/L<sup>3</sup>];
- $D$  = the hydrodynamic dispersion coefficient [L/T<sup>2</sup>];
- $R_m$  = the retardation factor of the mobile zone [-];
- $v$  = the pore water velocity [L/T];
- $q$  = a source or sink of water [1/T];
- $\theta_m$  = the porosity of mobile zone [-];
- $\alpha_j$  = the apparent first –order mass transfer coefficient for the  $j$ th immobile zone [-];
- $\beta_j$  = the capacity ratio of the  $j$ th immobile zone [-];
- $N$  = the number of immobile zones [-]; and
- $(c_{im})_j$  = the concentration in the  $j$ th immobile zone [-].

This multi-site model can accurately predict rates of mass transfer in a bulk sample of a Borden sand containing a mixture of different grain sizes and diffusion rates (Haggerty and Borelick 1995). The multi-site formulation of first order reaction models allows for consideration of a comparatively broad range of sorption site heterogeneity. However, because too many parameters are included in the models, experimentally measuring all the parameters involved is not realistic.

#### 2.2.3.4 Stochastic First Order Reaction Models

It has been argued that some soil properties, such as intraparticle porosity and pore size distributions, can vary for individual solid particles (Weber , McGinley et al. 1992), and thus the discrete interpretation employed by two-site and multi-site models may not be sufficient to characterize the heterogeneity of soil. An alternative approach is

to use a continuous distribution function to characterize the multiple sites with different first order reaction rates.

Connaughton et al. (Connaughton, Stedinger et al. 1993) envisioned soils as a continuum of particles ordered by a desorption rate constant. The probability that a randomly selected solute is located on a soil particle with first order desorption rate  $k$  is simulated by a gamma probability density function  $f(k)$ .

$$f(k) = \frac{\beta^\alpha k^{\alpha-1} \exp(-\beta k)}{\int_0^\infty x^{\alpha-1} \exp(-x) dx} \quad (2-12)$$

where:

$\beta$  = a scale parameter [-]; and  
 $\alpha$  = a shape parameter [-].

$\beta$  serves to determine both the mean and standard deviation of the  $k$ , and  $\alpha$  indicates whether many soil particles have very small first order desorption rate the hydrodynamic dispersion coefficient. The smaller  $\alpha$  is, the slower the desorption process. This model was employed to simulate desorption of naphthalene from contaminated soils and found that the gamma distribution model fit experimental data better than a two-site model.

Similarly, in Chen and Wagenet 's model (Chen and Wagenet 1995), sorption sites are grouped based on a gamma probability density function for both the equilibrium linear partitioning portion and the first order sorption portion. The model was applied to fixed bed reactors, leading to improved interpretation of the slow tailing effects in nonequilibrium breakthrough curves.

Pedit and Miller (Pedit and Miller 1994) treat the sorbent phase solute concentration, partitioning coefficient, and first-order mass transfer coefficient as random variables. In a batch reactor, the bulk fluid phase solute concentration is given by:

$$\frac{dC_b(t)}{dt} = \frac{M_s}{V} \int_0^\infty \int_0^\infty f_m(K_d, k_{fo}) k_{fo} [S_e(t) - S(t)] \times dK_d dk_{fo} - \lambda_b C_b(t) \quad (2-13)$$

where:

$k_{fo}$	=	first order reaction coefficient [1/T];
$K_d$	=	partitioning coefficient [ $L^3/M$ ];
$f_m(K_d, k_{fo})$	=	mass fraction probability density function [-];
$S_e(t)$	=	the sorbent-phase solute concentration for a particle or collection of sorption sites at equilibrium with the bulk fluid phase solute concentration [M/M];
$S(t)$	=	the sorbent phase solute concentration for a particle of collection of sorption sites with locally defined sorption parameter values $K_d$ and $k_{fo}$ [M/M].

Comparing to several other modeling approaches, e.g. multi-site first order model and diffusion model, it is found that this model, with a log-normal distribution, provides the best fit of all two parameter models tested, and performed nearly as well as the best three parameter models.

A finite difference formulation with both the gamma distribution and lognormal distribution of the first order rate coefficient was developed by Culver et al. (Culver, Hallisey et al. 1997) for both completely mixed batch reactors and fixed-bed reactors. For desorption of TCE from long-term contaminated soils, this model also provided significantly improved simulations of aqueous concentrations as compared to the two-site models.

## 2.2.4 Diffusion Models

No matter how sophisticated first-order reaction model may be, a first-order reaction is often a poor representation of the microscale sorption and diffusion processes. For example, Miller and Weber (Miller and Weber 1986) observed that a first-order mass transfer model under-predicted early uptake in batch sorption studies. Thus many studies (Miller and Weber 1984; Miller and Weber 1988; Ball and Roberts 1991; Pedit and Miller 1994; Cunningham, Werth et al. 1997; Haggerty and Gorelick 1998; Werth and Hansen 2002) engaged in coupling more mechanistic based explainable diffusion models with macroscopic ADR equations. During the past thirty years, diffusion based models developed from single mechanism models, to dual resistance models, two mechanism models, multiple particle class models, and stochastic diffusion models.

### 2.2.4.1 Single Mechanism Diffusion Models

One site diffusion models envision all microscopic mass transfer occur within the same environment, and often utilize Fickian diffusion based models to describe the microscale transfer processes in the solid phase:

$$\frac{\partial q_r}{\partial t} = \frac{D}{r^{(v-1)}} \frac{\partial}{\partial r} \left[ r^{(v-1)} \frac{\partial q_r}{\partial r} \right], \quad (2-14)$$

where:

- $q_r$  = the solid phase concentration at microscale [M/M];
- $D$  = diffusion coefficient [L/T<sup>2</sup>]; and
- $v$  = the dimensionality of the microscale particles [-].

$v=1$  refers to a layered particle;  $v=2$  represents a cylindrical particle; and  $v=3$  denotes a spherical particle. Based on the detailed concentration derived from this microscale solution, an average concentration for the particle can be generated as:

$$q_{avg} = \frac{v}{a^v} \int_0^a q_r dr, \quad (2-15)$$

where  $a$  is the distance from the center to the edge of the solid particle. This averaged value can then be substituted into the sorption term,  $\frac{\partial q}{\partial t}$ , of the ADR equation to compute the microscale behavior within the macroscale.

#### 2.2.4.2 Dual Resistance Diffusion Models

The above mentioned diffusion models assume that film resistance is negligible. Under some circumstances, for example in non-well mixed system with very slow flow rate, film resistance may be at the same order of magnitude as intraparticle diffusion. In such cases, dual resistance models (Miller and Weber 1984; Crittenden, Hutzler et al. 1986) may be applied. In dual resistance models, the sorption term in the ADR equation is replaced by a film mass transfer term as:

$$\frac{\partial C}{\partial t} = -v_z \frac{\partial C}{\partial z} + D_h \frac{\partial^2 C}{\partial z^2} - \frac{(1-\varepsilon)}{\varepsilon} \frac{3}{R} k_f (C - C_\delta), \quad (2-16)$$

where:

- $C_\delta$  = the concentration at the outside of film [M/L<sup>3</sup>];
- $k_f$  = the mass transfer coefficient in the film [1/T]; and
- $R$  = the radius of spherical particle [L].

At the surface of particle, liquid film phase concentration and solid phase concentration follow the boundary relationship:

$$\frac{k_f}{\rho_s} (C - C_\delta) = D_s \frac{\partial q}{\partial r}, \quad \text{at } r = R \quad (2-17)$$

where,  $D_s$  is the surface diffusion coefficient. Moreover, solute transport inside the solid particle may be expressed by Fickian diffusion:



$$\frac{\partial q}{\partial t} = \frac{1}{r^2} \frac{\partial}{\partial r} \left( r^2 D \frac{\partial q}{\partial r} \right) \quad (2-18)$$

#### 2.2.4.3 Two Mechanism Diffusion Models

Although the single mechanism and dual resistance diffusion models incorporate Fickian diffusion as a mechanism explaining the microscopic mass transfer processes, they neglect the inherent sorbent heterogeneity caused by microscale variations in physical and chemical properties. Ball and Roberts (Ball and Roberts 1991) attribute the driving force for microscale mass transfer as pore diffusion and surface diffusion. For a batch reactor, combining with Fick's first law, a mass balance over the spherical porous sorbent can lead to their model:

$$\varepsilon_i \frac{\partial C}{\partial t} + \rho_a \frac{\partial q}{\partial t} = \varepsilon_i \frac{D_p}{r^2} \frac{\partial}{\partial r} \left[ r^2 \frac{\partial C}{\partial r} \right] + \rho_a \frac{D_s}{r^2} \frac{\partial}{\partial r} \left[ r^2 \frac{\partial C}{\partial r} \right], \quad (2-19)$$

where:

- $\varepsilon_i$  = the internal porosity of particle [-];
- $\rho_a$  = apparent density of the solid particle [M/L<sup>3</sup>]; and
- $D_s$  = the effective surface diffusion coefficient [L/T<sup>2</sup>].

Ball and Roberts's (Ball and Roberts 1991) model achieved excellent agreement with their experiment data of long term sorption of halogenated organic chemicals by aquifer material, and was able to find a strong correlation between grain radius and rates of uptake.

#### 2.2.4.4 Multiple Particle Class Models

The aforementioned models only consider one type of particle, with uniform chemical and physical properties. Sorbent heterogeneity, however, suggests that, single particle class models will not be sufficient to characterize mass transfer processes in the heterogeneous systems such as soils and sediments. Pedit and Miller (Pedit and Miller

1995) developed a model including multiple-particle classes with different physical and sorptive properties. The model combines an instantaneous equilibrium faction with a rate-limited pore diffusion process. At the same time, it accounts for first-order degradation reactions in both the bulk fluid phase and inside the particles. For a CMBR, the solute concentration at the macroscale bulk fluid-phase is given by:

$$\left(1 + \frac{M_s}{V} \sum_{i=1}^{n_p} f_m^i f_e^i \frac{dq_e^i(t)}{dC_b(t)}\right) \frac{dC_b(t)}{dt} = -\frac{M_s}{V} \sum_{i=1}^{n_p} f_m^i \left( \frac{3k_b^i}{a^i \rho_a^i} [C_b(t) - C_p^i(r = a^i, t)] + f_e^i \lambda_e^i q_e^i(t) \right) - \lambda_b C_b(t), \quad (2-20)$$

and the particle scale concentration given by rate-limited intraparticle pore diffusion processes is expressed as:

$$\left( \theta_p^i + \rho_a^i \frac{\partial q_r^i(r, t)}{\partial C_p^i(r, t)} \right) \frac{\partial C_p^i(r, t)}{\partial t} = \frac{\theta_p^i D_p^i}{r^2} \frac{\partial}{\partial r} \left( r^2 \frac{\partial C_p^i(r, t)}{\partial r} \right) - \theta_p^i \lambda_p^i C_p^i(r, t) - \rho_a^i \lambda_r^i q_r^i(r, t) \quad (2-21)$$

where:

$M_s$	=	mass of solids [M];
$V$	=	volume of bulk fluid [L <sup>3</sup> ];
$i$	=	the particle class index [-];
$n_p$	=	number of particle classes [-];
$f_e^i$	=	is the fraction of equilibrium-type sorption sites of particle class $i$ [-];
$q_e^i(t)$	=	the solid –phase solution concentration of particle class $i$ at equilibrium with the bulk fluid-phase solute concentration [M/M];
$i$	=	the particle class index [-];
$k_b^i$	=	the boundary layer mass transfer coefficient of particle class $i$ [1/T];
$C_b(t)$	=	the bulk fluid-phase solute concentration [M/L <sup>3</sup> ];
$a_i$	=	the particle radius of particle class $i$ [L];
$\rho_a^i$	=	the apparent particle density of particle class $i$ [M/L <sup>3</sup> ];
$C_p^i(r, t)$	=	the intraparticle fluid phase solute concentration of particle class $i$ [M/L <sup>3</sup> ];

- $\lambda_e^i$  = the equilibrium type solid phase first-order reaction rate coefficient for particle class  $i$  [1/T];
- $\lambda_b$  = the bulk fluid-phase first-order reaction rate coefficient [1/T];
- $\lambda_p^i$  = the intraparticle fluid-phase first-order reaction rate [1/T];
- $\lambda_r^i$  = the intraparticle solid-phase first order reaction rate coefficient [1/T];
- $\theta_p^i$  = the intraparticle porosity of particle class  $i$  [-]; and
- $q_r^i(r,t)$  = intraparticle solid-phase solute concentration of particle class  $i$  [M/M].

Pedit and Miller's (Pedit and Miller 1994; Pedit and Miller 1995) results indicated that multiple-particle class models provide a more accurate representation of long-term sorption rate data than traditional single-particle class approaches.

#### 2.2.4.5 Stochastic Diffusion Models

In parallel to the stochastic approaches for first order reaction models, stochastic methods have also been applied to diffusion models, commonly through a continuous probability distribution function for the diffusion coefficients. Cunningham et al. (Cunningham, Werth et al. 1997) consider soil aggregates as spherical particles with water filled mesopores and micropores. Microscale mass transfer was decomposed to a fast portion and a slow portion. A fast local equilibrium is assumed to exist between the solute dissolved in the mesoporous water and the solute adsorbed on the mesopore walls. The slow, rate-limiting process was attributed to pore diffusion process within the micropores. A gamma probability density function was utilized to describe the distribution of rate-limiting diffusion coefficient. They demonstrated that an analytical solution can be derived for average solute concentrations in the particle, and thus using a gamma distribution of diffusion coefficient is no more demanding than using a single value for the diffusion coefficient.

Haggerty (Haggerty and Gorelick 1998) proposed a novel distributed diffusion model based on one dimensional diffusion along individual pathways within particle grains. Each pathway, identified by the apparent diffusion coefficient  $D_a$  and the length  $l$ , follows a lognormal distribution of  $D_a/l^2$ . It is reasonable to include several pathways in a single aggregate, and thus, even a single aggregate may have a distribution of diffusion rate coefficients. Haggerty's model was applied to simulate Farrell and Reinhard (Farrell and Reinhard 1994)'s experimental results, and found this lognormal distribution model provide a better fit. Comparing with Cunningham's (Cunningham, Werth et al. 1997) model, Haggerty's model can better capture variations of diffusion rates in a single particle; however, it did not explicitly differentiate between the fast and slow diffusion processes as modeled by Cunningham et al. (Cunningham, Werth et al. 1997).

More recently, Werth and Hansen (Werth and Hansen 2002) proposed a spherical diffusion model based on a gamma distribution of diffusion rate constants for sorption and desorption, respectively. The uniqueness of this model is to capture the combinations of the exposure concentration and exposure time by probability functions. The model was successfully applied to simulate the effects of concentration history on desorption kinetics profiles for trichloroethene (TCE), and thus represents a more mechanistically explainable approach to capture the effects of heterogeneity on slow desorption.

It is worthy noting here that stochastic approaches, both for first order reaction models and diffusion models, acclaimed outstanding ability to fit the experimental data, and more important in explaining the tailing effects for soil column breakthrough curves. Further, a continuous distribution function only needs two parameters, i.e. a mean and a standard deviation, so that it does not need more parameters than the two site models. It

thus appears that stochastic approaches may produce an ability to model well a wide range of situation. However, employing the probability density function for some critical modeling parameters (e.g. diffusion coefficient) is arbitrary and it generally void of physical or mechanistic explanation (Pignatello and Xing 1996).

#### *2.2.4.6 Particle Geometry and Size*

The increased accuracy achieved by diffusion models are based on a certain geometric description of the porous medium. For mathematical simplicity, most models mentioned above assume a spherical shape and uniform aggregate size. Natural porous media, however, involve complex particle shapes and various aggregate size distributions. It has been shown that (Rasmuson 1985; Rasmuson 1985) particle shapes will influence the uptake rate especially for the long-term sorption processes, such that spherical aggregates are the slowest and the slabular particles show the fastest uptake rate. Meanwhile, Ball and Roberts (Ball and Roberts 1991) noted that aggregate size will also influence mass uptake rates, such that the rate of approach to equilibrium was greater for smaller size aggregates. Thus, models with uniform shape and size will not be sufficient to simulate the diversity of particles found in natural porous media.

As an attempt to apply simplified models to some more realistic situations, Rao et al. (Rao and Jessup 1982; Brusseau and Rao 1990) tried to approximate mass transfer processes in nonspherical particles by equivalent spheres such that the sphere volume is equal to the volume of the nonspherical aggregates. Van Genuchten (Van Genuchten 1985) presented a method to transform soil aggregates with different shapes into a uniformly sized spherical aggregate with similar diffusion characteristics to the original

aggregate. The transformation is achieved by employing a geometry dependent shape factor, defined as:

$$\gamma_s = \frac{D_a \theta L}{a^2 q R_{im}}, \quad (2-22)$$

where:

$D_a$	=	the effective diffusion coefficient of the soil matrix [L/T <sup>2</sup> ];
$\theta$	=	porosity [-];
$a$	=	spherical aggregate radius [L];
$q$	=	the macroscopic fluid flow specific discharge [L <sup>3</sup> /T];
$R_{im}$	=	is the immobile phase retardation factor [-]; and
$L$	=	soil column depth [L].

This method extends the physical diffusion models to different particle shapes, including spheres, cylinders and slabs; however, it is limited to uniformly sized aggregates.

Aggregate size distributions, as well as aggregate shape variations, are critical for particle characterization applying diffusion models to heterogeneous particles. By computing an equivalent radius from the volume-weighted radii of different aggregate-size class, Rao et al. (Rao and Jessup 1982) presented a method to reduce a range of spherical aggregate sizes to a single equivalent aggregate class. Combining the shape transformation method of van Genchten (Van Genuchten 1985) with Rao's (Rao and Jessup 1982) size equivalent methods, natural porous media aggregates with complex shapes and different sizes can thus be simplified to an equivalent spherical aggregate of an equivalent uniform size.

### 2.2.5 Summary of Macroscale Mass Transfer Models

Non-ideal solute transport processes in the subsurface system can be attributed to three types of factors: (1) heterogeneous soil physical and chemical properties (Haggerty and Borelick 1995; Haggerty and Gorelick 1998), such as the types of soil particles, their hydraulic conductivity, porosity and pore distributions; (2) nonequilibrium rate limiting slow sorption desorption behaviors (Pignatello and Xing 1996; Luthy, Aiken et al. 1997; Weber, LeBoeuf et al. 2001), such as pore diffusion, intraorganic matter diffusion; and (3) different advection patterns due to complex soil particle geometries (Brusseau, Jessup et al. 1989; Brusseau, Jessup et al. 1991). Successful mass transfer models, which are able to capture all those influential factors, need to possess the ability to: (1) accurately interpret the rate-limiting mass transfer processes at the particle scale; (2) accurately model the complex flow advection behavior in the natural porous media.

Most models discussed in this section, however, for mathematic simplification, are built upon a completely mixed batch reactor, or a plug flow with dispersion reactor. Thus, most are incapable of addressing the influence of fluid flow patterns on solute transport processes. Recent studies, however, indicate that particle configurations and geometries will significantly affect mass transfer processes in the subsurface environment (Knutson, Werth et al. 2001). It is thus of great importance to extend the above mentioned mass transfer models to account for porous media geometry (Pignatello and Xing 1996). The first step is to develop a numerical model for fluid flow capable of reproducing enough of the physics of real fluids in real porous media. Sections 2.4 and 2.5 address the current state of the art research efforts in modeling fluid flow in porous media.

On the other hand, macroscale mass transfer models have evolved in an effort to better capture the rate-limiting mass transfer processes at the particle scale. The evolution of first order reaction models, from one site, to two site, multi-site, and eventually continuous probability distributions, vividly displays efforts to better simulate the influence of soil heterogeneity on rate-limiting mass transfer processes. The diffusion modeling approach, evolving from a single Fickian diffusion mechanism, to multiple diffusion mechanisms, and stochastic models, itself, is a step beyond the first order reaction approach in terms of improving our mechanistic understanding of non-linear sorption processes. However, without an accurate depiction of the rate-limiting mass transfer processes controlling the distribution of contaminants within soils and sediments at the particle scale, one cannot expect to model contaminant movement correctly, and thus it is important to examine microscale mass transfer research efforts as a means to better link aforementioned macroscale models to more mechanistic-based microscale systems. Section 2.3 addresses the current state-of-the-art research efforts on microscale mass transfer processes.

## **2.3 Microscale Mass Transfer Processes**

### **2.3.1 Intrapore Diffusion**

Intrapore diffusion processes include surface diffusion, pore diffusion, Knudsen diffusion, and intraorganic matter diffusion. Since these processes act in parallel, the faster mechanism will control the overall mass transfer rate.



#### *2.3.1.1 Surface Diffusion*

Surface diffusion accounts for the diffusion process where solute migrates along the wall surfaces of the internal pores. It can be considered important when concentrations of the sorbate are several orders of magnitude greater than that in the solution (de Boer 1968), which happens when sorbents possess continuous surfaces comprised by organic materials (Weber, LeBoeuf et al. 2001), e.g., activated carbon. In natural systems, surface diffusion is significant when soils and sediments present very high organic contents.

#### *2.3.1.2 Pore Diffusion*

Reinhard and coworkers (Farrell and Reinhard 1994) postulated that diffusion in hydrophobic micropores (Werth and Reinhard 1997), or the mineral pore surfaces with a natural organic matter coat (Gu, Schmitt et al. 1994; Kaiser and Guggenberger 2000), may be the rate-limiting mass transfer step. Werth and Reinhard (Werth and Reinhard 1999) found that counter-diffusion in slow desorbing sites can be sterically hindered, and thus, they concluded that slow diffusion takes place inside micropores. More recently, the correlation of rate with micropore size was demonstrated by Castilla et al. (Castilla, Werth et al. 2000), where slow desorption can be controlled by diffusion from successively smaller width micropores. Although the pore diffusion mechanism was explored by a number of researchers (Ball and Roberts 1991; Ball and Roberts 1991; Werth and Reinhard 1997; Werth and Reinhard 1997), simulation results using this model often underestimated observed short-term desorption rates, and overestimated the observed long-term desorption rate (LeBoeuf 1998). An explanation for this lack of model agreement with experiment data is that, instead of the solute retardation through

local sorption equilibrium on pore walls, the slow desorption results from diffusion into and out of organic matter with and along pore walls, which implicate that intraorganic matter diffusion (Section 2.3.1.4) is the real controlling process.

#### *2.3.1.3 Knudsen Diffusion*

When the dimensions of the micropores are on the same order as the dimension of the solute molecule, Knudsen diffusion may occur. Knudsen diffusion is attributed to constraints of the confining medium, or non-Fickian and anomalous diffusion attributed to intraorganic matter diffusion. The confinement in Knudsen diffusion can have a number of impacts on the transport of molecules within them (Drake and Klafter 1990; Chatong and Massoth 1993; Werth and Reinhard 1997), including increasing effective viscosity within a micropore and significant reduction in molecular transport through micropores. Although it is possible for Knudsen diffusion to occur in mineral matrices (Farrell and Reinhard 1994), studies suggest that intraorganic matter diffusion often controls the mass transfer of hydrophobic organic compounds when natural organic matter (NOM) is present (Xing and Pignatello 1997; Huang and Weber 1998).

#### *2.3.1.4 Intraorganic Matter Diffusion*

Intraorganic matter diffusion theory suggests that NOM accounts the primary diffusive resistance in soils and sediments (Weber, LeBoeuf et al. 2001). Weber and co-workers envisioned soil particle as a three-domain substance: mineral domain, rubbery organic matter domain, and a glassy organic matter domain (Weber and Huang 1996). While the rubbery region may manifest fast linear sorption behavior, the glassy region is proposed to exhibit nonlinear sorption behavior, slower sorption rates, and possible sorption-desorption hysteresis (Weber and Huang 1996; Huang, Young et al. 1997;

LeBoeuf and Weber 1997). The Distributed Reactivity Model (DRM), which originally applied to equilibrium systems and later extended to heterogeneous natural solids under non-equilibrium conditions, provided a framework to characterize the influences of different energetic reactivity domains of soil particles on intraorganic matter processes.(Weber , McGinley et al. 1992; Young and Weber 1995; Weber and Huang 1996).

Intraorganic matter diffusion has been proposed as a rate-limiting mechanism for hydrophobic organic matter sorption by a number of researchers (Weber, LeBoeuf et al. 2001) with various evidences, including (1) the increase of desorption rate with the swelling of soil organic matter matrix (Freeman and Cheung 1981);(2) lower mass transfer coefficient related to higher organic matter contents in the sorbents (Carroll et al., 1994);(3) the decrease of Freundlich isotherm  $n$  values with increased time (Weber and Huang, 1996); (4) the reduce of intraorganic diffusion rates by the increasing sorptive interaction within the organic matrix (Ball and Roberts, 1991a); and (5) the agreements of diffusion coefficients between the bi-rate desorption in the NOM and in rubbery and glassy macromolecules (Carroll et al.). Given these observed phenomena associated with intraorganic matter diffusion, it is nature to make analogies between NOM and synthetic organic macromolecules. Recently, LeBoeuf and co-workers demonstrated that NOM possesses many macromolecular characteristics, including glass transition temperatures (temperatures marking the transitions from glassy, hard, relatively rigid states to rubbery, soft, relatively flexible states) (LeBoeuf and Weber 1997; LeBoeuf and Weber 2000; Schaumann and Antelmann 2000; Young and LeBoeuf 2000; DeLapp, LeBoeuf et al. expected 2003; DeLapp and LeBoeuf expected January 2004). Given the apparent

relevance of NOM and synthetic organic macromolecules behavior, many observations can be drawn from well-developed theories about diffusion in synthetic organic macromolecules to NOM-controlled intrasorbent diffusion (Weber, LeBoeuf et al. 2001).

### 2.3.2 Diffusion in Synthetic Macromolecules

Categorized based on their relative rate of solute diffusion and relaxation or reconfiguration of a macromolecular structure, four different types of diffusion phenomena occur in organic macromolecules: Case I (Fickian), Case II, Super Case II, and anomalous or nonFickian diffusion (Hopfenberg and Frisch 1969), as illustrated in the Figure 2-6.

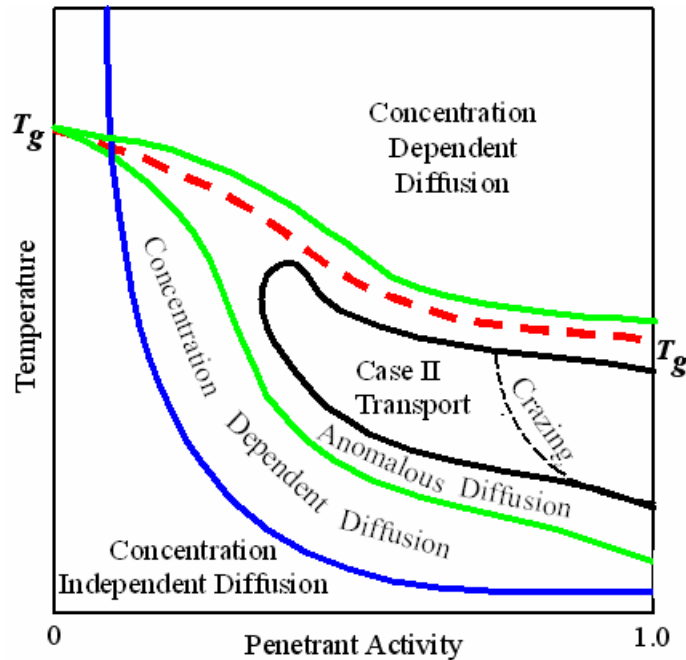


**Figure 2-6. Hopfenberg-Frisch Chart of Anomalous Transport Phenomena (after Vieth, 1991 from Hopfenberg and Frisch, 1969).**

### 2.3.2.1 Fickian Diffusion

Case I, or Fickian diffusion, occurring only at very low solute concentrations or low temperatures, refers to rates of diffusion that are orders of magnitude slower than the relaxation rates of the macromolecule. The rate of Fickian diffusion is explained by the direct relationship between the velocity with which a solute moves and its thermodynamic driving forces (chemical potential):

$$F = -D \frac{\partial C}{\partial x}, \quad (2-22)$$

where:

$$\begin{aligned} F &= \text{the rate of transfer per unit area of section [M/L}^2\text{T]}; \\ C &= \text{the concentration of solutes [M/L}^3\text{]}; \\ D &= \text{diffusion coefficient [L/T}^2\text{]}; \end{aligned}$$

When Fickian diffusion controls, the mass uptake is proportional to  $t^{1/2}$  (Crank 1975).

### 2.3.2.2 Case II Diffusion

If the rate of diffusion is extremely fast relative to the macromolecule relaxation rate, Case II diffusion will be observed. Solutes in the organic macromolecules are affected by both mechanical stress and chemical potentials (Harmon, Lee et al. 1987). At high solute concentrations, swelling is required to relieve mechanical stress and to accommodate solute molecules. When swelling controls kinetics, there is a linear relationship between the mass uptake and time (Harmon, Lee et al. 1987). Case II diffusion causes the development of a sharp front of solute moving at a constant velocity from regions of high swelling (high mobility, rubber-like state) to regions of low swelling (low mobility, glass-like state). Case II diffusion only occurs below the glass transition temperature, and above certain concentrations of solutes.

### *2.3.2.3 Super Case II Diffusion*

Super Case II represents an extreme example of Case II diffusion, observed at higher concentrations than Case II diffusion while also below the glass transition temperature (Hopfenberg and Frisch 1969). Super Case II diffusion can result in the crazing or cracking of the macromolecule surface. In the natural system, it may occur when soil particles are immersed in the pure organic solvent, where the solute concentration is big enough to cause local fracture of the soil particles.

### *2.3.2.4 Anomalous Transport*

Diffusion processes ranging from ideal Fickian diffusion to Case II (relaxation or swelling controlled) sorption may also be observed for a given solute/macromolecule system if a sufficient range of temperature and solute activity is traversed experimentally (Hopfenberg and Frisch 1969). Anomalous or nonFickian diffusion occurs when relaxation rates and diffusion rates are comparable, and can be considered intermediate to Case I and Case II behavior. Due to initially low solute concentrations, anomalous diffusion often begins with a rapid relaxation independent phase, followed by a temporary desorption, and subsequent long term relaxation in the swelling macromolecules matrix (Berens and Hopfenberg 1978). Assuming the diffusion coefficient and the solute velocity is constant, Berens and Hopfenberg (Berens and Hopfenberg 1978) considered anomalous transport as the linear superposition of phenomenologically independent contributions from Fickian diffusion and macromolecular relaxations. Dual sorption theory, assuming that glassy macromolecules contain micro-holes, postulated that two concurrent modes of sorption exists in the macromolecules, has also been employed to explain anomalous transport phenomena.

Based on this concept, besides the normal dissolution in the bulk macromolecules, an abnormal non-linear Langmuir-type sorption, which accounts for the long term slow process, exists within fixed micro-hole sites (Vieth and Howell 1976) within the sorbents.

### 2.3.3 Sorption Isotherm Models

Sorption isotherm models describe the equilibrium distribution of contaminants between and among the constituent phases and interfaces of systems under constant temperature. Based on the degree of interaction between sorbate and sorbent, sorption processes can be broadly classified as absorption and adsorption. Absorption is a process in which solute migrates from one phase and dissolves into another phase, while adsorption is a phenomena restricted to the accumulation of dissolved substances at interfaces between the solution and adsorbent (Weber and DiGiano 1996), as illustrated in Figure 2-7. Sorption process often causes retardation of diffusive transport under transient conditions, and thus, it is essential for the quantification of solute transport.

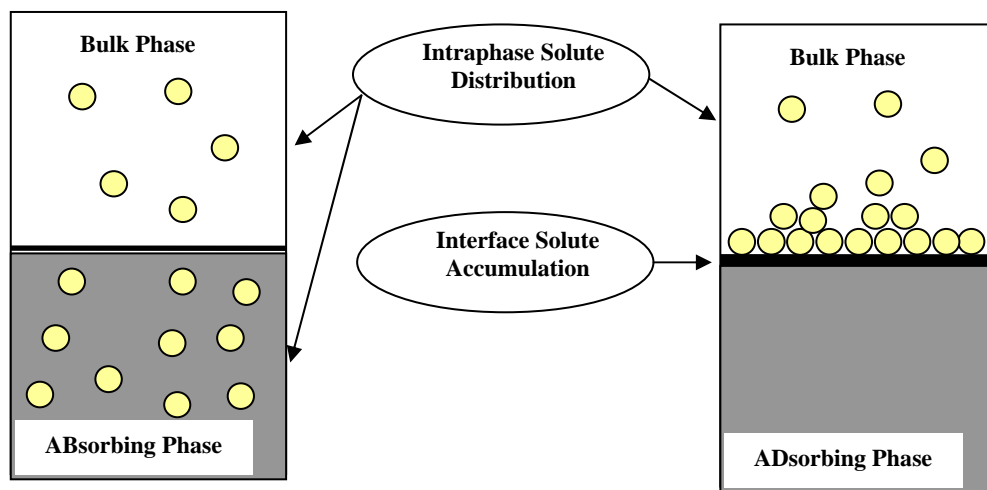


**Figure 2-7. Schematic Characterization of Absorption and Adsorption Processes (after Weber and Digiano, 1996).**

### 2.3.3.1 Linear Model

The linear isotherm model, the simplest relationship between the solid phase and liquid phase concentrations, expresses the accumulation of solute within the sorbent as a function that is directly proportional to the solution phase concentration:

$$q_e = K_d C_e, \quad (2-24)$$

where:

$q_e$	=	equilibrium sorbed concentration [M/M];
$K_d$	=	distribution coefficient [ $L^3/M$ ]; and
$C_e$	=	equilibrium aqueous concentration [ $M/L^3$ ].

The linear sorption isotherm model has been correlated to the absorption of hydrophobic compounds into an organic matter. When soil particles possess very high organic carbon content, partitioning process will appear to allow solute dissolve into organic matter. Partitioning coefficient is often directly related to the mass fraction of organic carbon in soil, or related to an octanol-water partition coefficient (Weber and Digiano, 1996).

Linear isotherm can also be applied to describe adsorption processes, however, in this case, implicating that the energies of sorption are uniform with increasing concentration and the loading of sorbent is low (Weber, McGinley et al. 1991). For adsorption process, it is only valid within Henry's region, where solute accumulation on the surface is very low. Due to its mathematical simplicity, linear sorption isotherm is still very widely used, albeit often incorrectly.

### 2.3.3.2 Langmuir Model

The Langmuir sorption isotherm includes two primary assumptions: (1) the sorption energy for each molecule is the same and independent of surface coverage; and



(2) sorption occurs only on localized sites and involves no interactions between sorbed molecules (Weber and Digiano, 1996). Thus, the Langmuir model leads to a monomolecular layer of solute on the surface, as illustrated in the Figure 2-8.

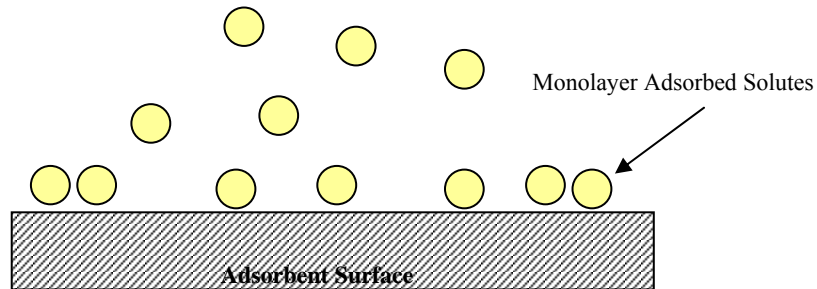


**Figure 2-8. Langmuir Model.**

The Langmuir model can be derived through the balance between the rates of condensation and evaporation of gas molecules at a solid surface, and is expressed as:

$$q_e = \frac{Q_0 b C_e}{1 + b C_e}, \quad (2-25)$$

where :

- $q_e$  = equilibrium sorbed concentration [M/M];
- $Q_0$  = Langmuir capacity coefficient [M/M];
- $b$  = Langmuir intensity coefficient [L<sup>3</sup>/M]; and
- $C_e$  = equilibrium aqueous concentration [M/L<sup>3</sup>]

It is worthy to note that the Langmuir intensity coefficient,  $b$ , is related to the net enthalpy of adsorption,  $dH_a$ :

$$b = \beta_{a,h} \exp\left(\frac{-dH_a}{RT}\right), \quad (2-26)$$

where  $\beta_{a,h}$  has a characteristic value for a particular adsorption reaction. Given the value of  $b$  from equilibrium tests at different temperatures, the thermodynamic character of the adsorption, i.e. net enthalpy, can be determined by the linearized relationship:

$$\ln b = \ln \beta_{a,h} - \frac{-dH_a}{R} \frac{1}{T} . \quad (2-27)$$

Due to its homogeneous site energies assumption, the Langmuir model itself often can not provide good modeling results for many natural systems. However, it can be used in conjunction with other isotherm models to describe sorption of heterogeneous systems. For example, it has been successfully combined with linear portioning isotherm by the dual mode model to describe the sorption in the heterogeneous media (Vieth et al., 1976).

#### 2.3.3.3 Brunauer-Emmett-Teller (BET) Model

Including the adsorption of multiple layers of molecules, the BET model can be considered as an extension of the Langmuir model, as illustrated in the Figure 2-9. Moreover, the BET model differentiates the energy between the first layer and the subsequent layers. It assumes that the energy associated with the first layer is comparable to the heat of adsorption, while the energy associated with the subsequent layers is the heat of condensation (Benefield, Judkins et al. 1982; Adamson 1990).

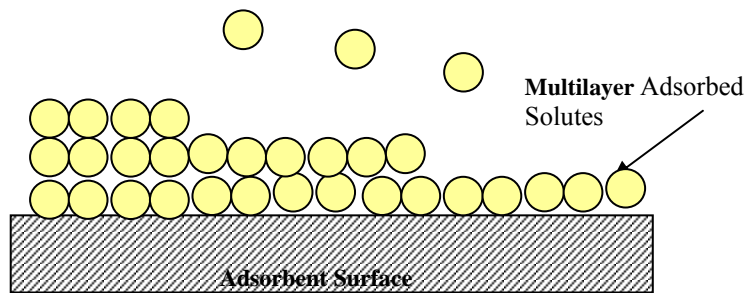


**Figure 2-9. BET Model.**

The BET model may be expressed as:

$$q_e = \frac{\beta C_e Q_0}{(C_s - C_e)[1 + (\beta - 1)(C_e / C_s)]}, \quad (2-28)$$

where  $C_s$  is the saturation concentration of the solute.  $\beta$  is like  $b$  in the Langmuir model that it indicates the relationship with the energy of adsorption:

$$\beta = \exp\left(\frac{-dH_a}{RT}\right), \quad (2-29)$$

where  $dH_a$  is the net enthalpy of adsorption of the first layer of adsorbate.

#### 2.3.3.4 Freundlich Model

The Freundlich model describes the sorption equilibrium by an exponential relationship:

$$q_e = K_F C_e^n, \quad (2-30)$$

where:

$$\begin{aligned} K_F &= \text{Freundlich capacity coefficient [M/M][L}^3\text{/M]}^n; \text{ and} \\ n &= \text{Freundlich sorption intensity exponent [-].} \end{aligned}$$

Although originally presented as an empirical model, the Freundlich model can be derived by the summation of a series of Langmuir models with different and constant adsorption energies (Weber and DiGiano 1996). Thus, the Freundlich model in fact accounts for the heterogeneous energy sites through the value of  $n$ . As illustrated in Figure 2-10,  $n=1$  indicates linear sorption.  $n>1$  represents an unfavorable sorption process because sorption decreases sharply with lower concentration.  $n<1$  represents a favorable sorption process, because sorption uptake capacities of the solid phase increase sharply from low solution concentration to high concentration. It is also worth noting that the decrease of  $n$  indicate an increasingly heterogeneous adsorption sites.

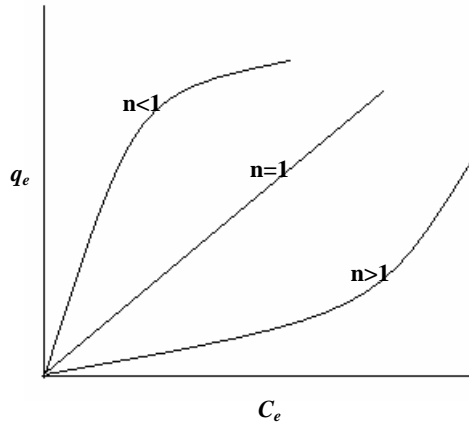


**Figure 2-10. Freundlich Sorption Isotherm.**

*2.3.3.5 Composite Isotherm Models*

Although the Freundlich model can capture the heterogeneity of environmental sorption processes, it assumes a continuous site energy distribution. Many environmental sorbents, as illustrated in Figure 2-11, however, may present discrete or discontinuous characteristics.

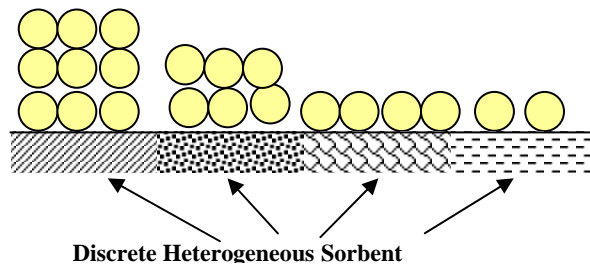


**Figure 2-11. Sorption Processes on the Discrete Heterogeneous Sorbent (after Weber and Digiano, 1996).**

In these circumstances, a composite isotherm, consisting of a summation of the contributing sorption processes, can be applied. The Dual mode model (Vieth and Howell 1976) is an example of a composite isotherm model, where linear dissolution occurs in

the bulk organic matter, while Langmuir sorption associated with adsorption of solute to fixed sites within the matrix. DRM developed by Weber and coworkers (Weber , McGinley et al. 1992; Young and Weber 1995; Weber and Huang 1996; Huang, Young et al. 1997; LeBoeuf and Weber 1997; Huang and Weber 1998) is also an attempt to capture the combination of linear and nonlinear sorption, as noted below:

$$q_{eT} = x_l K_{DT} C_e + \sum_{i=1}^m x_{nl} K_{Fi} C_e^{n_i} \quad (2-31)$$

where:

- $q_{eT}$  = the sorbed phase concentration per unit mass of sorbent [M/M];
- $x_{nl}$  = the mass fraction of sorbent with nonlinear sorption [-];
- $K_{Fi}$  = the Freundlich sorption coefficient for component  $i$  [M/M][L<sup>3</sup>/M]<sup>n</sup>;
- $n$  = Freundlich sorption exponent for component  $i$  [-].

The DRM model envisioned the soil particle into three domains, namely, mineral domain, glassy domain and rubbery domain. The Freundlich sorption model is employed to describe the non-linear adsorption in the glassy domain. Meanwhile, a linear term is utilized to model the adsorption at the surface of mineral domain, and the partitioning process in the rubbery domain.

It is interesting to compare the dual mode model and the DRM model here, where two major differences can be identified. First and most importantly, the dual mode model treats the glassy domain as a constant energy site by using a single Langmuir sorption model; however, DRM treats the nonlinear adsorption as a set of multiple reactions involving different sites energy by employing a Freundlich sorption model, which is actually the summation of multiple Langumir models (Weber et al., 1992). The second difference lies in the different explanations on the linear terms in two models. The portioning term in the dual mode model account only for the partitioning processes in the

rubbery phase. DRM, however, attributes the linear term to both adsorption on the mineral site and partitioning into rubbery organic matter.

### 2.3.3.6 Polanyi-Manes Model

It is reasonable, in some circumstances, to postulate that the adsorption domain of soils and sediments may be comprised of micro-porous non-polar surfaces (Xia and Ball 1999). In such cases, a pore-filling model based on the Polanyi potential theory may be applicable. In Polanyi potential theory, an adsorption potential, depending on proximity to the surface and the nature of the sorbate is assumed:

$$\varepsilon_{sw} = RT \ln(S_w / C_e), \quad (2-32)$$

where:

$\varepsilon_{sw}$	=	effective adsorption potential [cal/mol];
$S_w$	=	solubility of the solute at temperature T [M/L <sup>3</sup> ];
$C_e$	=	the equilibrium concentration of the solute [M/L <sup>3</sup> ]; and
$R$	=	the ideal gas constant 8.314 J/mol K.

Adsorption will take place whenever the strength of the field, independent of temperature, is great enough to compress the solute to a partial pressure greater than its vapor pressure (Vermeulen, LeVan et al. 1987). The Polanyi – Manes model accounts partitioning processes for common organic matter, and pore filling effects for fixed-pore carbonaceous adsorbents, which can be stated as (Xia and Ball 2000; Xia and Pignatello 2001):

$$q_e = K_d C_e + Q_0' \rho \times 10 \left[ a \left( \frac{\varepsilon_{sw}}{V_m} \right)^{b'} \right] \quad (2-33)$$

where:

$\rho$	=	solute molecular density [M/L <sup>3</sup> ];
$Q_0'$	=	the adsorption volume capacity at saturation [L <sup>3</sup> /M];
$K_d$	=	the partitioning coefficient [L <sup>3</sup> /M]; and
$a, b$	=	fitting parameters [-].

The Polanyi – Manes models often works well with nonpolar sorbent with well-defined pore structures, such as soot, charcoals, and kerogens (Xia and Ball 2000).

## **2.4 Modeling Fluid Flow in Porous Media**

While it is obvious that the variability of flow rate and solute concentration at the pore scale will affect mass transfer characteristics, proper pore-scale modeling efforts will further assist the exploration of micro-scale soil/sediment structure configurations on mass transfer. This section addresses the current state-of-the-art research studies in modeling fluid flow in the porous media.

### 2.4.1 Models of Porous Media

Accurate numerical simulation of fluid flow in porous media requires the description of porous media morphology, which remains a formidable problem. A realistic model for porous media should include both geometry properties, such as shape and volume, and topological properties, such as pore interconnectivity. In many cases, however, the type of model that can be employed is dependent on the modeling method, and more importantly, computational limitations. Thus, it is important to construct models that are able to closely mimic the heterogeneity of actual porous media, and at the same time are sufficiently efficient to allow simulation of flow and transport phenomena with reasonable computational effort.

#### *2.4.1.1 One-Dimensional Model*

A one-dimensional model envisions the pore space as a collection of cylindrical tubes in parallel or in series (Scheidegger 1974). The radii of tubes are uniform or

determined by the pore size distribution. This type of model cannot account for the interconnectivity of the pores, so that the predictions are typically grossly in error (Scheidegger 1974).

#### 2.4.1.2 Spatially-Periodic Models

Spatially periodic models are represented by a periodic structure with unit cells of circular cylinder arrays. Figure 2-12 is an example of a spatially-periodic porous medium.

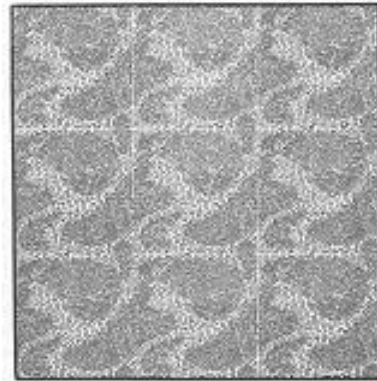


**Figure 2-12. A Spatially-Periodic Porous Media Model (after Sahimi, 1995).**

Sangani and Acrivos (Sangani and Acrivos 1983) first used spatially-periodic models to calculate the permeability of the system. Meanwhile, the spatially-periodic model was also employed to study hydrodynamic dispersion (Carbonell and Whitaker 1983; Eidsath, Carbonell et al. 1983), and found good agreement between the model predictions and experimental values. However, it is worth noting that this agreement is built upon the fact that experimental systems used in those studies were based on a simplified periodic, man-made porous media, instead of natural porous media. Spatially-periodic models actually only represent an approximation of natural porous media, and thus do not contain enough real heterogeneity.



### 2.4.1.3 Network Models

Network models can be classified into two broad categories, branching network models and closed loop network models (Sahimi 1995). The Bethe lattice (Flory 1941) is an example of a branching network model, illustrated in Figure 2-13.

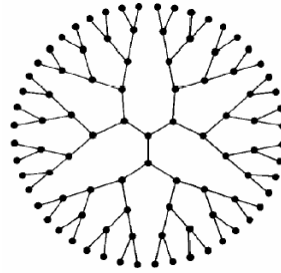


**Figure 2-13. Bethe Network Model (after Sahimi et al., 1990).**

The advantage of a branching network model is that it is often possible to derive analytical solutions (Sahimi 1995) to describe the fluid flow. Due to the lack of closed loops of pore connectivity, however, the model fails to describe the topology of real porous media.

Closed loop network models of porous media, which were first introduced by Fatt (Fatt 1956; Fatt 1956; Fatt 1956) in 1956, are intuitively appealing and have been very widely used. In a closed network model, pore bodies representing large void spaces are connected by pore throats representing narrow openings. Figure 2-14 illustrates a mapping from a two-dimensional real porous media to a network model:

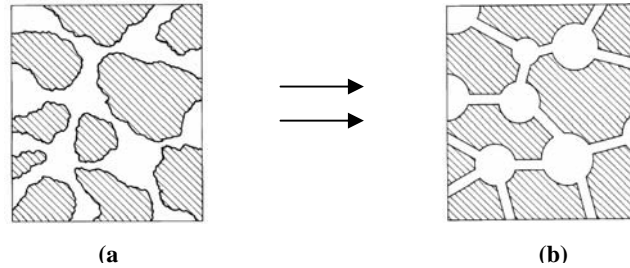


**Figure 2-14. A Cross Section of a Typical Porous Media, (a) Realistic, and (b) a Network Model (after Koplík and Lasseter, 1984).**

For simplicity, pore bodies are often represented by spheres whose radii follow the corresponding pore size distribution of the porous media under consideration. Similarly, throats are simplified as cylindrical shapes, and often are uniformly arranged as regular lattice (Lowry and Miller 1995; Held and Celia 2001). Figure 12-5 is an example of two-dimensional and three-dimensional closed network models on a regular lattice.

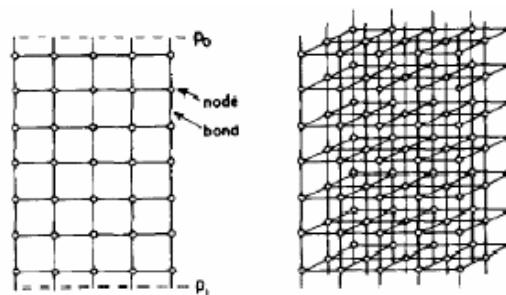


**Figure 2-15. Depiction of Two- and Three-Dimensional Network Models (after Aviles and LeVan, 1991).**

A significant difficulty of using a closed network model is how to derive a network model from a given porous media, namely, the reconstruction of porous media (Adler, Thovert et al. 2002), which includes characterization of the structure of the porous media,

forms of the pore size distributions, and pore interconnectivity. Recently, statistical reconstruction algorithms were employed to construct two-dimensional (Vogel and Roth 1998; Liang, Philippi et al. 1999; Tsakiroglou and Payatakes 2000; Vogel and Roth 2001) and three-dimensional (Bakke and Oren 1997) network models from given digital representations of the porous media.

#### *2.4.1.4 Particle Packing Models*

Particle packing models are different from the models mentioned above in that instead of simplifying the pore spaces, they idealize the solid particles. Particle models envision porous media as particles of certain geometries distributed in the continuum. Because packing of disks in two-dimension or spheres in three-dimension can represent a wide range of random media, such as suspensions, porous media, composite materials, and atomic structures, computer simulations of particle packing models have drawn increased attention (Torquato 2002). Figure 2-16 is an example of a two-dimensional particle packing model.



**Figure 2-16. A Two-Dimensional Particle Packing Model of Randomly Distributed Disks (after Sahimi, 1995).**

For a three-dimensional sphere, regular packing schemes include cubic, rhombohedral, orthorhombic, and tetragonal-sphenoidal (Harr 1977). Packing of particles representing a

natural porous media, however, is influenced by several factors, including the shape of particles, the distribution of particle sizes, and packing schemes, and is often implemented by the use of a random packing technique.

Through random packing, particle locations are randomly generated subject to constraints, such as no particle overlap and structure stability. Two major types of particle packing algorithms currently exist: sequential addition and collective rearrangement. Sequential addition packing models sequentially fill an initially empty domain with randomly placed particles (Bennett 1972; Jullien and Meakin 1987) while maintaining a stable structure. Sequential addition packing algorithms perform well for relatively large, homogeneous spheres. However, they tend to yield relatively loose packing structures, and provide no explicit mechanism to control the produced porosity (Yang, Miller et al. 1996). Collective rearrangement methods often include two steps: (i) definition of an initial distribution of particles; and (ii) iterative rearrangement of the particles to attain a structurally stable state (Yang, Miller et al. 1996). Initial particle size distributions are often based on lognormal distributions (Bear 1972; Scheidegger 1974), while spherical distributions of the particles follow a uniform distribution. Iterative rearrangement methods include Monte Carlo simulation and molecular dynamics techniques, which are often very computationally intensive (Yang, Miller et al. 1996).

#### 2.4.2 Modeling Fluid Flow through Porous Media

Modeling fluid flow through porous media in groundwater involves multiscale phenomena: microscale (molecular level), mesoscale (single pore level), macroscale (multiple pores) and megascale (field size level). A central challenge is to understand

how macroscale flow characteristics depend on microscale geometry of the pore space and the physical characteristics of the fluid and solid (Sahimi 1995). A starting point of the problem is typically Darcy's law (Scheidegger 1974):

$$q = -K \cdot \nabla p, \quad (2-34)$$

where:

$$\begin{aligned} q &= \text{specific flow rate [L/T];} \\ K &= \text{permeability constant [L}^3\text{T/M]; and} \\ \nabla p &= \text{pressure gradient [-].} \end{aligned}$$

Darcy's law assumes a linear relationship between the pressure gradient and the specific flow rate. The permeability constant,  $K$ , represents averaged effects of complex porous structures. A great challenge in modeling flow in porous media is to accurately predict permeability by developing a model at the mesoscopic level that is capable of reproducing enough of the physics of real fluids in real porous media.

Many elegant approaches, which borrow most of the powerful tools of modern statistical mechanics, such as effective-medium approximation (EMA), renormalization, percolation theory, and volume-averaging methods, have been applied in order to more accurately estimate the equivalent permeability of random porous media (Renard and Marsily 1997). If the property fluctuations are small, EMA can provide reliable estimates of effective permeability (Sahimi 1995). In EMA, porous media is visualized as a heterogeneous medium constructed by side by side placement of homogeneous blocks; a single, known permeability block is embedded in the homogeneous matrix of unknown permeability to generate an expression for the equivalent permeability (Choy 1999). For systems with larger variations in permeability, King (King 1989) first applied renormalization methods to calculate equivalent permeability, which represents a porous

medium through analogy of with an electric network. Percolation theory (Reyes and Jensen 1985; Sahimi 1994), which addresses complex systems comprised of objects that may or may not be connected by analyzing the percolation transition point, has also been applied to estimate equivalent permeability of materials within two phases, one of which is non-permeable (Kirkpatrick 1973). Whitaker and his group used a volume-averaging method (Whitaker 1999) to solve the Navier-stokes equation in porous media, and eventually was able to estimate the permeability of the porous media while considering its geometry (Quintard and Whitaker 1994; Quintard and Whitaker 2000), although the closure problem remains very complex (Sahimi, 1995).

Many advanced numerical simulation methods have also been developed to solve fluid flow in porous media when property parameters are available (Wen and Gomez-Hernandez 1996). Network models (Koplik and Lasseter 1984; Aviles and LeVan 1991; Russell and LeVan 1997; Blunt 2001) consist of pores of variable radius connected to neighboring pores by variable sizes of throats. Here, fluid flow is solved for a single pore first, from which a solution of nodal pressures for every interior node of a network can be derived, finally resulting in an equivalent permeability. Laplacian methods (Efendiev and Durlofsky 2002), named for their dependence on the solution of the Laplace equation, often simulates a block isolated from the rest of the aquifer by assuming certain boundary conditions; for example, periodic boundary conditions (Durlofsky 1991), and thus an equivalent permeability can be estimated based on the resulting pressure gradient and specific flow rate. Laplacian methods are comparatively more accurate, although very computational intensive (Wen and Gomez-Hernandez 1996). Combining multigrid modeling techniques and homogenization methods, multigrid homogenization methods

(Knappek 1998; Moulton, Dendy et al. 1998) have been developed to calculate coarse grid permeability. Although it is claimed that multigrid homogenization methods reach a compromise between computational cost and the accuracy for estimating equivalent, it appears these methods are not stable in some special cases (Knappek 1998).

While each of the aforementioned methods have been successful to some context, each is based upon a certain level of averaging, and thus none can fully represent the complete details of flow within micropores (Succi 2001). In the late 1980s', lattice Boltzmann models (LBM) were successfully introduced into fluid flow simulations (Rothman 1988; Cancelliere, Chang et al. 1990; Chen, Diemer et al. 1991). Because of its ease of modeling complex pore geometries (Bernsdorf, Durst et al. 1999), LBM has been viewed as the most promising method for simulating complex problems of flow in natural porous media. A brief review of LBM is given in the subsequent section.

## **2.5 Lattice Boltzmann Methods**

### **2.5.1 Introduction to Lattice Boltzmann Methods**

Lattice Boltzmann methods originated from lattice gas automata (LGA) (Frisch, Hasslacher et al. 1986), which is based on concepts from the kinetic theory of gases. Instead of homogeneous and continuous materials, LGA views fluids as arrays of discrete particles living on a discrete lattice, evolving with some interactive rules, i.e., propagation and collision rules. First, each particle advances one node to a neighboring lattice site. If two or more particles arrive at the same site, collision between the particles will occur, and the velocity of each particle is then subject to change due to the effects of

the collision. Collision rules are selected such that mass and momentum conservation are satisfied at each node on the lattice. Despite its microscopic basis, LGA is capable of modeling macroscopic flow phenomena, with the simplest possible lattice (triangular) capable of accurately modeling two-dimensional fluid flow (Rothman 1997). The most widely used method used today, however, is the two-dimensional, nine-velocity model (D2Q9) (Wolf-Gladrow 2000), as illustrated in Figure 2-17.

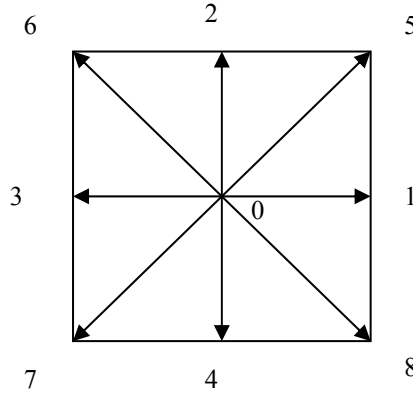


**Figure 2-17. A Nine-Velocity (D2Q9) Lattice Model.**

In the D2Q9 model, the velocity vectors,  $\bar{c}_i$  are defined in the following manner:

$$\bar{c}_i = \begin{cases} (0,0) & (i=0) \\ c_s \left( \cos \left[ (i-1) \frac{\pi}{2} \right], \sin \left[ (i-1) \frac{\pi}{2} \right] \right) & (5 \leq i \leq 8) \\ c_s \sqrt{2} \left( \cos \left[ (i-5) \frac{\pi}{2} + \frac{\pi}{4} \right], \sin \left[ (i-5) \frac{\pi}{2} + \frac{\pi}{4} \right] \right) & (1 \leq i \leq 4) \end{cases} \quad (2-35)$$

where  $c_s$  is the computational speed of sound, representing the maximum speed that may be achieved on the lattice.



LBM inherits most of the features of LGA, except that instead of tracking the movement of single particles, a collective population representing a cloud of microscopic particles is studied, thus overcoming many of the disadvantages of LGA, such as statistical noise and complex collision rules (Succi 2001). The following two steps can express LBM:

$$\text{Propagation: } f_i(\bar{x} + \bar{c}_i, t + 1) = f_i(\bar{x}, t) \quad (2-36)$$

$$\text{Collision: } f_i(\bar{x} + \bar{c}_i, t + 1) - f_i(\bar{x}, t) = \Omega_i \quad (2-37)$$

where,  $f_i$  represents the probability of finding a particle in the position  $\bar{x}$  at time  $t$  that is moving with velocity  $\bar{c}_i$ .  $\Omega_i$  denotes a collision operator representing the rate of change of  $f_i$  resulting from a collision. Utilizing a linearized, single time relaxation model (Bhatnagar, Bross et al. 1954) derived from kinetic theory, the collision operator may be defined as:

$$\Omega_i = -\frac{1}{\tau}(f_i - f_i^{eq}) \quad (2-38)$$

where  $\tau$  is the relaxation time which controls the rate of approach toward equilibrium, which is related to the viscosity of the fluid.  $f_i^{eq}$  is an equilibrium distribution analogous to the Maxwellian distribution, which is given by:

$$f_i^{eq} = \rho \omega_i \left( 1 + \frac{\bar{u} \cdot \bar{c}_i}{c_s^2} + \frac{(\bar{u} \cdot \bar{c}_i)^2 - c_s^2 \bar{u}^2}{2c_s^4} \right) \quad (2-39)$$

where  $\omega_i$  is the weighting parameter for each velocity direction. The density per node,  $\rho$ , the macroscopic velocity,  $\bar{u}$ , the fluid pressure  $P$ , and the kinematic viscosity  $\nu$  are defined by

$$\rho = \sum_i f_i; \quad \rho \bar{u} = \sum_i f_i c_i \quad ; \quad P = \rho c_s^2 \quad ; \quad \nu = c_s^2 \left( \tau - \frac{1}{2} \right) \quad (2-40)$$

It has been shown (Chen, Chen et al. 1992) that use of the Chapman-Enskog procedure allows the lattice Boltzmann discretization equation to recover the Navier-Stokes equations with a truncation error proportional to the square of the Mach number ( $Ma = u/c_s$ , where  $u$  is the characteristic flow velocity and  $c_s$  the speed of sound).

### 2.5.2 Advantages of Lattice Boltzmann Methods

A remarkable characteristic of LBM is its simplicity, such that the state of the fluid needs to be identified only at the lattice nodes, and the Navier-Stokes equation can be replicated by microscopic particle collision and propagation. Computations, based only on propagation and collision, is thus less complex relative to traditional computational fluid dynamics (CFD) methods. Moreover, local collision characteristics provide the opportunity for parallelism of the computer programming code, potentially enhancing computational efficiency.

Another striking advantage of LBM is that it can address complex boundary conditions. The bounce back boundary condition, where particles will bounce back when moving towards solid walls, is very easy to implement. Bernsdorf et al. (Bernsdorf, Durst et al. 1999) compared the performance of LBM with finite volume methods for the prediction of incompressible fluid flows. Their results suggest that finite volume methods appear to be more efficient for simple geometries. For complex geometries, finite volume methods' computational requirements increased greatly, while computational requirements for LBM first decreased with increasing complexity of the obstacle structure and became almost independent from it for highly complex structures (Bernsdorf, Durst et al. 1999).

### 2.5.3 Lattice Boltzmann Modeling Flows in Porous Media

The particle like nature of LBM allows one to address complex pore structures with fundamental mechanical events (e.g., bounce back), while permitting recovery of macroscopic flow behavior in very small pore spaces (Succi 2001). This attractive feature makes LBM an excellent numerical tool for simulating flows in complicated geometries, such as flow through porous media.

Rothmann first applied LBM for simulating flow through porous media in 2-D, and verified Darcy's law in complex geometries (Rothman 1988). Succi et al. (Succi, Foti et al. 1989) provided a reasonable estimate of porous media permeability as a function of porosity by applying the LBM in 3-D. Cancelliere et al. (Cancelliere, Chang et al. 1990) subsequently refined Succi's results with a better representation of the microgeometry through random positioning of penetrable spheres of equal radii. Later, Heijs and Lowe (Heijs and Lowe 1995) used the LBM to validate the Carman-Kozeny equation utilizing a computed tomography clay soil image, observing that the Carman-Kozeny equation provided a less successful estimation of permeability relative to LBM. Recent studies have applied and extended LBM to simulation of flow through porous media in various areas, such as multiphase flow (Shan and Doolen 1996; Knutson, Werth et al. 2001), non-Newtonian flow (Boek, Chin et al. 2003), and multiscale flow simulation (Kang, Zhang et al. 2002). At the same time, the method itself has undergone additional enhancements (Chen and Doolen 1998), especially in terms of deriving more accurate boundary conditions and extension to inclusion of irregular grids.

#### 2.5.4 Improvements of Boundary Conditions

Despite the success of LBM in many situations, the complex micro-geometry of many porous media systems suggests a need to provide for improved boundary conditions. In earlier work, boundary conditions in LBM were directly adopted from the LGA method (Chen and Doolen 1998). For example, the bounce back boundary condition, in which particles moving in the direction of a wall will exit the wall in the opposite direction from which they came, is commonly employed at walls to obtain a no-slip velocity condition (Rothman 1988; Ziegler 1993). Although the bounce back boundary condition can be easily implemented, it possesses several shortcomings (Gallivan, Noble et al. 1997), including low accuracy (first-order accuracy) and an inability to apply to moving walls. Several new boundary conditions were thus proposed. Skordos (Skorodos 1993) proposed to include velocity gradients in the equilibrium distribution function at the wall nodes. By calculating the particle distributions contributed by nodes just inside the wall, Nobel et al. (Noble, Chen et al. 1995) was able to maintain a proper hydrodynamic boundary condition while executing a regular LBM procedure. Maier et al. (Maier, Bernard et al. 1996) modified the bounce back condition to nullify net momentum tangent to the wall and to preserve momentum normal to the wall. By introducing a counter slip velocity into the equilibrium distribution function, Inamuro et al. (Inamuro, Yoshino et al. 1995) eliminated slip velocity at the wall. A second-order extrapolation scheme was proposed by Chen et al. (Chen, Martinez et al. 1996) to obtain unknown particle distribution functions. The above-mentioned boundary conditions yield good results for flat walls, however, curved boundaries are often approximated by a series of stairs that leads to a reduction of numerical accuracy.

Recently, an accurate curved boundary treatment method, which can preserve the geometry and still keep second order accuracy for the velocity field, was proposed by Filippova and Hanel (Filippova and Hanel 1998) and improved and further extended to three-dimension by Mei et al. (Mei, Luo et al. 1999). The appearance and further development of curved boundary conditions will likely provide substantial contributions towards improved simulation of practical fluid flow situations in porous media.

### 2.5.5 Lattice Boltzmann Methods on Irregular Grids

As noted previously, LBM originated from LGA where particles propagate from one site to the other on a regular lattice, limiting LBM to uniform grids. This limitation seriously reduces the rate of further applications of LBM to flow through porous media where the complex geometry of micropores cannot be well-fit to a uniform lattice (Succi, Amati et al. 1995). Motivated by the consideration of extending the applicability of LBM to irregular grids, He et al. (He, Luo et al. 1996) proposed an interpolation-supplemented LBM, which can be implemented on an irregular rectangle, and later, has been extended to a general curvilinear coordinate system (He and Doolen 1997). However, in this approach collisions still take place on the grid points, and the topology of the grid is still not arbitrary (Peng, Xi et al. 1998).

Recently, it has been shown that, while the coupling between discretization of velocity spaces and physical space is an essential part of LGA dynamics, it is not crucial for LBM (Cao, Chen et al. 1997). In this light, LBM can be viewed as a special finite difference scheme of the Boltzmann equation:

$$\frac{\partial f_i}{\partial t} + \bar{c}_i \cdot \bar{\nabla} f_i = \Omega_i \quad (i = 1, 2, \dots, N) \quad (2-41)$$

where  $N$  is the number of different velocities in the model. Thus, any discretization of the Boltzmann equation, such as Finite Differences (FD), Finite Volumes (FV) and Finite Elements (FE) method may suffice to recover Navier-Stokes equations (Cao, Chen et al. 1997). Linking LBM with these well-established numerical techniques will enable LBM to address much broader geometries (Succi 2001).

Succi's work group (Amati, Succi et al. 1997) was the first to propose a finite volume formulation of the LBM, where a piece-wise linear interpolation scheme was used to estimate the volume-averaged particle distribution in a non-uniform coarse lattice. Another volumetric formulation of LBM was developed by Chen (Chen 1998), which can be applied to arbitrary meshes while achieving exact conservation laws and equilibrium balance conditions. Peng et al. (Peng, Xi et al. 1998; Peng, Xi et al. 1999; Xi, Peng et al. 1999) also proposed another version of Finite Volume LBM (FVLBM) for both triangular and rectangular elements. Their scheme is claimed to be very flexible for internal and external boundaries, however, there is a reduction in computational efficiency compared with classical LBM (Peng, Xi et al. 1999).

Based on Runge-Kutta time marching schemes and various spatial discretization schemes, Chen and coworkers (Sofonea and Sekerka 2003) combined FD and LBM in several ways. A central difference scheme was proposed by Cao et al. (Cao, Chen et al. 1997) in Cartesian coordinates, and was later extended to curvilinear coordinates with non-uniform grids (Mei and Shyy 1998). The proposed Finite Difference LBM (FDLBM) scheme has been successfully applied in several fluid simulations (Chen and Doolen 1998), including single-phase flow through three-dimensional digitized rock fractures under varied simulated confining pressures (Kim and Lindquist 2003).

While the number of studies combining LBM and FD/FV continues to expand, few studies have addressed the generation of finite element LBM (FELBM). As an early effort to combine FE methods with LBM, Lee and Lin (Lee and Lin 2001) presented a characteristic Galerkin discrete Boltzmann equation (CGDBE), which implements a Taylor-Galerkin procedure for the discrete Boltzmann equation. With appropriate boundary conditions, their method results in accurate solutions with little numerical diffusion. This method, however, is limited by its conditional stability associated with the explicit expression of the convection term. FE methods, famous for their superior numerical stability and geometry flexibility over FD and FV methods, suggest FELBM may be an appealing alternative to FVLBM and FDLBM. Further research on combining FE method with LBM is necessary and will likely yield promising results.

#### 2.5.6 LBM Simulations of Solute Transport in Fluid Flow

LBM simulation of solute transport involves the recovery of the Navier-Stokes equation, the continuity equation, and advection-diffusion-reaction equations. Emphasizing the different areas of foci, current research efforts can be classified into three categories, including (i) solute transport in fluid flow without reaction; (ii) solute transport in fluid flow with reaction in the bulk fluid; and (iii) solute transport in fluid flow with reaction at the solid liquid interfaces.

##### *2.5.6.1 Solute Transport without Reaction*

Research achievements in LBM simulation of miscible fluids flow provided the foundation for modeling inert solute transport in fluid flow. The color model is the earliest approach to simulate miscible flow mixture, which was first developed by Holme

and Rothman (Holme and Rothman 1992). In this model, red and blue particle distribution functions were introduced to represent two components. The evolution of the particles is the same as if they were not colored, but the color of the particles is redistributed after collision while keeping color conserved. Based upon the idea of Holme and Rothman, Flekkøy (Flekkøy 1993) introduced another color model, which also distinguishes the particles as either red or blue. Two relaxations, however, take place for the sum of the distribution functions or the mass density of the two components, and for the difference of the distribution functions or the relative amount of two components. It is shown that proper choice of eigenvalues of the collision operator can reduce the Holme and Rothman model to the Flekkøy model.

Assuming that solutes are in sufficiently low concentration such that they do not influence the flow, instead of collaborated red and blue particles, other research efforts introduced a separate particle distribution function to model solute particles. Employing a lattice model with four velocities and one rest particle, Alvarez-Ramirez (Alvarez-Ramirez, Nieves-Mendoza et al. 1996) developed a LBM to simulate diffusion and calculate the effective diffusivity in a quiescent heterogeneous media. Nobel (Noble 1997) formulated a LBM for two dimensional advection-diffusion equations, where a four velocity model is employed to model solute particles with known velocity fields. Knutson (Knutson, Werth et al. 2001) successfully applied Nobel's method to simulate solute transport from distributed non-aqueous phase liquids blobs in a two-dimensional porous medium. In a similar manner, Inamuro et al. (Inamuro, Yoshino et al. 2002) proposed another LBM for an isothermal binary miscible fluid mixture. Analyzing the method by asymptotic theory demonstrated that the solute concentration can be derived



with relative errors of the same order as the lattice spacing. The method was later applied to simulate flow and heat/mass transfer problems in a three-dimensional porous structure (Yoshino and Inamuro 2003).

More recent efforts incorporate innovative techniques and theories to simulate solute transport in fluid flow. Merks et al. (Merks, Hoekstra et al. 2002) demonstrated the utilization of a moment propagation method for modeling advection-diffusion in LBM. In this method, after each streaming and collision step, a scalar quantity is released in the lattice, part of which stays on the lattice while the remaining fraction is distributed over the neighboring nodes according to the probability that a carrier fluid particle moves after collision. Luo and Girimaji (Luo and Girimaji 2003) applied kinetic theory to derive a two-fluid LBM for binary mixture, in which mutual collisions and self-collisions are treated independently, such that both miscible and immiscible fluids can be simulated by sampling the sign of the mutual-collision term. This model provides a thermodynamically consistent lattice Boltzmann theory for simulating multi-component fluids.

While most research efforts assume isotropic dispersion processes, Zhang and coworkers (Zhang, Bengough et al. 2002) presented a LBM for two-dimensional advection and anisotropic dispersion processes, where an anisotropic dispersion coefficient is derived through utilizing a directionally dependent relaxation time. The method was later extended to solve three-dimensional solute transport problem in variably saturated porous media (Zhang, Bengough et al. 2003).

#### *2.5.6.2 Solute Transport with Reaction in the Bulk Fluid*

Shortly after the appearance of LBM hydrodynamic models, Kingdon and Schofield (Kingdon and Schofield 1992) formulated the first lattice Boltzmann model for

chemical reaction in a flow system. In this model, solute is assumed to be sufficiently dilute such that advection is primarily due to bulk fluid flow. The diffusion of solute is controlled by the relaxation of the distribution function to the corresponding equilibrium status. The chemical reaction was incorporated by adding a source term in the lattice Boltzmann equation. In a similar manner, Dawson et al. (Dawson, Chen et al. 1993) proposed a LBM for reaction-diffusion advected by velocities governed by the Navier-Stokes equation. The collision term in this model was defined by a summation of a reactive term and a non-reactive term, where a BGK collision term is employed for the non-reactive term, and the reactive collision term is associated with the reaction processes under consideration. Dawson's model has been applied to simulate so called Turing instability (Chen, Dawson et al. 1995) phenomenon described by Sel'kov model. Qian and Orszag (Qian and Orszag 1995) developed another LBM to simulate diffusion driven system with an irreversible reaction  $A+B \rightarrow C$ , where the general reaction-diffusion equation is derived under the assumption of local diffusive equilibrium. Compared with asymptotic analysis results and a cellular automaton model, Qian's model is easier to apply when no analytic or asymptotic results exist, and is faster, simpler, and more accurate than a cellular automaton model. Utilizing LBM with 13 velocities on a two-dimensional square lattice, Weimar and Boon (Weimar and Boon 1996) reported another LBM model for studying nonlinear reaction. As opposed to the common approach that uses the same velocity set for the reactants as for the fluid, this model adopted a smaller set of velocities, i.e., five velocities, for the reactive species. This model was successfully applied to study the effect of turbulent mixing on pattern formation in the Brusselator model.

### *2.5.6.3 Solute Transport with Reaction at the Solid-Liquid Interface*

As opposed to reaction in the bulk fluid, particular interests of some researchers focused on studying the coupled solute transport and chemical reactions at the solid liquid interfaces. Wells et al. (Wells, Janecky et al. 1991) first studied chemical reactions including dissolution and precipitation at mineral surfaces. Allowing wall nodes to serve as sources or sinks for mass of a dissolved component, this lattice gas automata model simulates mass transfer rates as a function of the disequilibrium between fluid and mineral, represented by a mass transfer probability function. Dissolution processes are simulated by turning a wall node into a fluid node following a period of unsaturated conditions, while precipitation processes are reversed for a super-saturated condition. In 2000, He et al. (He, Li et al. 2000) extended Wells model to a LBM BGK formula, utilizing D2Q9 lattice models for both fluid flow and solute transport while assuming the mass transport of the solute has no effect on the fluid flow. Coupling the surface reaction with the diffusion between the wall and bulk fluid, the reaction kinetics were explicitly incorporated through boundary conditions. Here, boundary conditions are properly treated based upon the observation that, at a stationary wall, the non-equilibrium portion of the distribution function is proportional to the dot product of its microscopic velocity and the concentration gradient. Following application to convection-diffusion processes in channels with simple geometry, He's model (He, Li et al. 2000) was extended to simulate the evolution of pore geometry due to dissolution by HCL in arbitrary geometries and with locally unsteady state reactions (Kang, Zhang et al. 2002). More recently, Kang et al. (Kang, Zhang et al. 2003) further applied the model to explore the

effects of several dimensionless parameters (i.e., Peclet and Peclet-Damkohler numbers) on the coupled dissolution and precipitation processes in a simplified porous medium.

Meanwhile, it is worthy to mention another LBM model addressing reaction on solid wall surfaces, developed by Zhang and Ren (Zhang and Ren 2003). This model simulates one-dimensional vertical leaching processes. A five-direction LBM model, including two horizontal directions, two vertical directions, and a static direction is vertically bounded by two reactive walls, where the reactions at the walls are assumed to take place at two different rates. The solutes in solution and on the wall are in instant equilibrium on the fast wall; while a first-order kinetic reaction rate was applied to the mass transfer between the solutes in solution on the slow wall. The leaching of atrazine through soil columns was simulated based upon the experimentally-derived parameters, and the results of this LBM model agree well with the measured breakthrough curves and a non-equilibrium two site convection-dispersion model.

## **2.6 Summary**

The background and theories presented in this chapter provide insight into current state-of-the-art research efforts to identify mass transfer processes mechanisms and modeling strategies. Mechanisms identifying rate-limiting mass transfer processes contributing to observed contaminant slow sorption and subsequent hysteretic desorption have been extensively studied in the past thirty years. Meanwhile, modeling strategies have evolved to better capture sorption and transport related nonequilibrium. However, few of these studies address the contribution of pore scale configurations and advection patterns on the identified rate-limiting mass transfer processes. The primary reason for

the lack of research in this area derives from the intrinsic complexity of using traditional CFD methods to model groundwater flow and its integration with the myriad mass transfer processes occurring in the heterogeneous porous media of subsurface systems. Employment of new modeling methods for groundwater flow and mass transfer, i.e., LBM, and adapting it to this specific research need, for example, combining LBM with traditional numerical methods, may provide a promising technique to better predict fluid flow in subsurface environments. On the other hand, LBM-based approaches have been extended to numerous mass transfer processes, including both pure diffusion processes and diffusion-advection processes. Capture of the influences of rate-limiting mass transfer processes at the particle scale, however, presents several challenges in identifying proper solid-liquid boundary conditions, and proper relationships between macroscale non-linear sorption parameters and microscale parameters.

## **CHAPTER III**

### **DEVELOPMENT OF A WEB-BASED MASS TRANSFER PROCESSES LABORATORY**

#### **3.1 Introduction**

This chapter begins with a brief literature review of engineering education learning theories, followed with a discussion of Web-based education. Section 3.4 presents strategies for incorporating mass transfer processes research into Web-based education in terms of Kolb's Learning Cycle. Section 3.5 provides a detailed description of a Web-based mass transfer processes virtual laboratory (MTVLab), including its conceptual model, mathematical models, input/output interfaces, and the Help and tutorial module. Section 3.6 depicts the technical details of the system architecture of MTVLab. This Chapter concludes with a summary and identification of needs for future work.

#### **3.2 Learning theory and the importance of the laboratory in engineering education**

Behaviorism, cognitivism, and constructivism represent three fundamental theories of learning processes (Good and Brophy 1990). Behaviorism theory concentrates on observable behavior, and stresses that learning occurs when a correct response is demonstrated following a specific environmental stimulus. The behavioral instructional approach is especially effective in facilitating the learning of introductory-level topics. Describing knowledge acquisition as a mental activity rather than a straight stimulus-response, cognitivism theory views the student as an active participant in the learning

process, and recognizes that meaningful and well-organized information is easier to learn and remember. Cognitive education strategies work well in teaching environments associated with strong cognitive emphases, such as analytic reasoning and algorithmic problem solving. Constructivism theory suggests that learning is an active process of constructing a personal interpretation of the world, where learning should take place in realistic settings. Constructivist strategies are especially well-suited for advanced or expertise-level knowledge acquisition, such as advanced chemical mass transfer processes, where the student is required to make intelligent decisions within the learning environment.

Constructivism views the learning process as a progression of activities consisting of four separate stages: (i) having an experience; (ii) reviewing the experience; (iii) drawing conclusions from the experience, and (iv) taking an action to confirm the conclusion or generation of a new experience (Gillett 2001). The aims of constructivist strategies are often synonymous with the aims of engineering education, which demands not only the development of the abilities to accept, evaluate, or use information, but also development of skills in identifying, defining, and problem solving (Kolari and Savander-Ranne 2000). Following constructivist theory, engineering education can activate and encourage learners to work and learn in new and complex engineering surroundings, both independently and in teams.

Laboratory experiences, which imitate the uncertainty and complexity of authentic life practices, are essential elements in constructivism education (Wang, Laffey et al. 2001), and thus engineering education. Several studies (Su and Huang 1999; Kolari and Savander-Ranne 2000) suggest that laboratory experiences can achieve positive

influences on learning skills, understanding concepts, cognitive abilities, and attitudes. For example, Su and Huang (Su and Huang 1999) illustrated that the quality of the laboratory environment, and the frequency of the laboratory experience, can account for 10% to 24% of students' attitudes toward science, and 5% to 27% of students' academic achievements in science subjects. Besides improving students' understanding of theories and principles, laboratory teaching can promote engineering awareness (England and Field 1989; Abu-Khalaf 1998), improve their ability to diagnose and correct unacceptable process performance (Myers 1994), and perform economic evaluations (Langrish and Davies 1995).

Several types of laboratory experiences are active in engineering education today. Demonstration experiments, as a first-level laboratory experience, provide students the opportunity to observe particular phenomena in a classroom setting as a means to link theory with practice. A second-level laboratory experience can be derived from the analysis of data collected during an in-class demonstration. Third-level laboratory experiences include experiments carried out by the students under close supervision, while fourth-level experiences may include open-ended labwork. Strongly-guided labwork is beneficial in developing students' experimental skills, while open-ended labwork, where students have autonomy in making experimental protocol decisions, not only enhance experimental skills, but also assist students in developing independent scientific thinking.

In recent years, a great deal of effort has focused on the integration of new technologies such as multimedia video, audio, and animation, and computers, with associated software, into the laboratory experience. These new technologies are used for



data collection (Ko, Chen et al. 2000), model building and interactive demonstration (Shin and Yoon 2000; Shin, Yoon et al. 2002), analysis and graphical representation of data (Iskander 2002), and for combinations of these technologies (Sere, Leach et al. 1998). A comprehensive survey on the current practice in laboratory education by Sere et al. (Sere, Leach et al. 1998) suggests that use of new technologies for model building during labwork stimulates students to think more about the conceptual background of a specific lab situation than most other contexts of labwork. Recent advances in the use of the Internet in educational settings suggest that laboratories conducted through use of the World Wide Web (hereinafter referred to as 'the Web') may provide increased opportunities for laboratory experiences (Chu 1999).

### **3.3 Web-Based Education**

#### **3.3.1 Web-Based Education Overview**

Web-based education possesses many advantages for engineering educators over other instructional approaches, including use of individual software packages (Brusilovsky, Eklund et al. 1998; Goeller 1998; Kerrey and Isakson 2000; Kirschner and Paas 2001; Iskander 2002). First, Web-based instruction presents information in a non-linear style, allowing students to explore new information via browsing and cross-referencing activities. In such a constructivist, Web-based environment, students are provided more freedom to develop their own metacognitive strategies based on individual backgrounds and experiences (Good and Brophy 1990). Second, Web-based teaching supports active learning processes emphasized by constructivist theory. In a Web-based

modeling system, *vis-à-vis* reading, students possess the ability to interactively adjust the parameters of a system, which can then be evaluated and displayed in real time. Instead of passively accepting information, students take an active role in the learning process, and knowledge acquisition can be achieved in a more interesting and meaningful way. A third feature of Web-based education is enhanced understanding through improved visualization. Visual learning is the preferred mode for engineering students (Wankat and Oreovicz 1993), and Web-based tools that can provide clear, colorful, and interesting images can lead to improved degrees of understanding. A fourth advantage of Web-based education is its convenience. Access to the Internet enables education to occur at anyplace, at anytime (Kerrey and Isakson 2000). Through Web-based systems, students are provided the opportunity to study at a location they want, and at a time they like. Creating a learning environment that can accommodate individual schedules can thus improve the rate of learning, especially for well-prepared, senior or graduate level students (Whelan 1997; Brusilovsky, Eklund et al. 1998).

### 3.3.2 Categories of Web-Based Education Tools

Several categories of Web-based educational tools have been developed, including Web-based instruction systems, intelligent tutoring systems, virtual laboratories, and Web-based modeling systems.

#### 3.3.2.1 *Web-Based Instruction System*

Web-based instruction systems represent a developing branch of computer-aided instruction (CAI). This type of instruction emphasizes the use of the Web for transfer of educational information, and it may be considered as a replacement or a supplement to

traditional delivery methods of lectures and textbooks. Example information that may be distributed through this venue includes course instructional material, example problems, figures, questions, and exams. HyperText Markup Language (HTML) and JavaScript often provide the foundation of such systems (Crown 1999; Crown 2001), and, on occasion, database technology is employed (Chu 1999). An online homework system developed by Nakavachara (Nakavachara 2001), which makes use of ColdFusion (Macromedia, San Francisco, California) for database connection, and MATLAB (The MathWorks, Inc., Natick, Massachusetts) as a computational engine, provides a good example of Web-based instruction.

#### *3.3.2.2 Intelligent Tutoring System*

Intelligent tutoring systems (ITS) use artificial intelligence techniques to formulate models of an expert's knowledge and that of a student's knowledge, and then intervenes with tutorial advice when differences between the two models become evident (Roschelle, Kaput et al. 1998). ITS can alter instruction content and rate based on real-time tracking and evaluation of students' needs and knowledge levels, which often need to be fulfilled by employing advanced artificial intelligence techniques. Most Web-based ITS utilize short questionnaires or quizzes implemented with HTML forms and common gateway interface (CGI) programs to determine a student's knowledge level (Roschelle, Kaput et al. 1998; Shin, Yoon et al. 2002). One such system is designed to assign students knowledge-level appropriate chemical engineering laboratory sessions based on the record of student performances in prior laboratories and exams (Shin, Yoon et al. 2002). Recently, multimedia, in the form of video and audio, were incorporated into a Web based ITS as a means to improve the rate of learning (Stern and Woolf 2000).

### *3.3.2.3 Virtual Laboratory*

Virtual laboratories emphasize the creation of an interactive, multi-dimensional visualization of a laboratory environment, with some possessing the ability to remotely control actual instruments (Roschelle, Kaput et al. 1998; Book, Koeppen et al. 2002). While numerous examples of virtual laboratories exist (Mosterman, Dorlandt et al. 1994), most virtual laboratory systems use general sever/client models as a basis for their system architecture, with specific elements of the architecture customized to meet demands of the particular application. Virtual Reality Modeling Language (VRML) is also widely employed (Dong and Zhu 2002; Shin 2002) in most systems due to the extensive use of advanced graphics and multimedia technology, including three-dimensional animation, sound, and artificial sensory devices. Ko's (Ko, Chen et al. 2000) system may represent a typical example, where a double client-server structure is implemented by using JavaScript and HTML for the graphic interface on the client side, Laboratory Virtual Instrument Engineering Workbench (LabVIEW, National Instruments, Baltimore, Maryland) for local instrument control, inetCAM (Inetcam, Inc., San Diego, California) as a video server, and Common Gateway Interface (CGI) for communication between the client and Web server. Other technologies and components, including Java Input-Output Application Programming Interfaces (API), Java Applet, Java Database Connectivity (JDBC), Java Servlet, and Microsoft Access database (Microsoft Corporation, Redmond, Washington), are also used in virtual laboratories (Book, Koeppen et al. 2002).

### *3.3.2.4 Web-Based Modeling System*

Web-based modeling systems can be useful tools to assist teaching of high-level, complex engineering principles in a stimulating manner (Kerrey and Isakson 2000). Like

ITS and virtual laboratories, these systems typically use interactive interfaces to guide students through the learning process, but as important, they also possess great computational capacity. With this added computational element, these systems often possess the potential of expanding from the role of an educational tool to that of a research tool. Example applications of Web-based modeling systems include simulating livestock grazing effects on pastures (Mohtar, Zhai et al. 2000), teaching modules for internal combustion engines to edify fundamental thermodynamic and heat transfer concepts (Kirkpatrick, Lee et al. 1997), simulation engines for custom project management education (Marin 2000) and fluid mechanics and aerodynamics (Higuchi 2001), and a gas turbine simulator that provides an interactive graphical environment for rapid and efficient analysis of user-defined gas turbine systems (Reed and Afjeh 1998).

Combining high-level computation capacity with Web-based user-friendly features, however, greatly increases the technical challenges of employing such systems across the Internet. Some of these challenges arise from a need to interface several aspects of the overall Web-based model, including high-level computer languages that drive the numerical models, databases to collect input and output data, graphics and possibly spreadsheet packages to generate model outputs, and interfaces to communicate with users' browsers. Other challenges arise from recognizing that not all Web browsers support the same computer languages, and the need for computational efficiency, since many of the models involve complex calculations. In an effort to overcome these challenges, most of the aforementioned example systems (Kirkpatrick, Lee et al. 1997; Reed and Afjeh 1998; Higuchi 2001) employ Java Applet as the dominant technology to

construct interactive graphical programs that are easily distributed across the Internet, and are then run on the user's machine using Java (Reed and Afjeh 1998).

While generally robust in its ability to overcome many of these challenges, Java Applet may be restrictive when examining its long-term applicability to Web-based models that are likely to grow considerably more complex, and address an ever-growing variety of problems. For example, many simulation codes already exist in languages such as C/C++ or FORTRAN (FORmula TRANslation). Use of Java Applet requires considerable work to translate the existing numerical code to Java. A second restriction is related to speed of download and computational efficiency. Java Applet often has large initial download overhead, making the appearance of the first page very slow. Moreover, as an interpreted system, Java is typically an order of magnitude less computationally efficient relative to C (Eckel 2000). A third concern is availability. If not present on their computer, first-time users may be required to download Java. Although free, the download process might be restricted by the computer ability of users, and may be prohibited in computer laboratories and public Internet bars.

To improve the quality of Web-based education, enhancements to the variety of architectures available for Web-based modeling are required. These enhancements must be able to address each of the aforementioned challenges, and yet remain flexible to address potential system modifications in the future.

### **3.4 Mass Transfer Processes Research and Education**

The approaches used for teaching and conducting research into mass transfer processes often take differing paths; teaching usually involves formal lectures,

homework, modeling (usually analytical), and sometimes, but often not, actual wet laboratories. Fundamental research of mass transfer processes usually incorporates state-of-the-art experimental apparatus coupled with state-of-the-art analytical or numerical modeling. While students may be well-grounded in the fundamental theories of mass transfer processes after completion of coursework, they may not be as well prepared to transition to practicing engineering and conducting state-of-the-art research for several reasons, including: (i) inability to apply known concepts to new problems; (ii) inability or reluctance to construct numerical models; and (iii) unfamiliarity with wet-laboratory procedures. While the latter problem can be easily overcome through relatively short train-up periods addressing laboratory procedures specific to a project, the former problems usually must be overcome through additional coursework and experience with understanding the sensitivity of mass transfer models to changes in model parameters through use of developed models. Further, while traditional approaches to instruction have, and continue to be, effective in teaching mass transfer processes, recent studies suggest that exclusive use of this approach is not enough (Gillett 2001; Hyde and Karney 2001; Koehn 2001). An examination of learning processes may thus assist in identifying additional instructional techniques that can optimize the overall educational experience. In particular, Kolb (1984) provides an especially appealing description of the learning process that may be most applicable to science and engineering education.

Kolb (Kolb 1984) portrays successful learning as a cyclical process between various stages of learning. This cyclical process, defined as “The Kolb Learning Cycle,” involves four progressive, yet interrelated, stages: (1) concrete experience (CE); (2) active experimentation (AE); (3) reflective observation (RO); and (4) abstract

conceptualization (AC). In the CE stage, learners rely on senses to take in information. The information is then transformed into internal knowledge by carefully thinking, watching, and making decisions during the RO stage. Through logical analysis and systematic planning, learners are able to move to AC, where they think and learn concepts. During the AE stage, learning involves experimenting, and many other hands-on activities. Finally, learners return from active experimentation to concrete experience to complete the learning cycle; albeit with a very different level of understanding, accompanied by higher level learning and thinking skills (Egan 1997), such as critical thinking and problem solving skills.

Depending too heavily on traditional forms of instruction, including formal lectures (RO) and homework (AE), may limit students' exposure to one or two stages of the learning cycle, and thus confine their learning retention. Engineering students prefer active processing (Anderson 1991), and thus will learn better if more active stages, i.e., concrete experiences, also are involved. For example, studies of engineering students by Stice (Stice 1987) and Wankat and Oreovicz (Wankat and Oreovicz 1993) suggest that learning retention of up to 90 percent is achieved when all four stages of the Kolb Learning Cycle are employed, while only 20 percent of the material is retained if only abstract conceptualization is used.

Although originally conceptualized in terms of wet laboratories, the CE stage of the Kolb Learning Cycle also can be achieved by using new instructional techniques that employ advanced information technology such as computer-assisted teaching, multimedia-based instruction, and Web-based learning (Goeller 1998; Kerrey and Isakson 2000; Iskander 2002). In each of these activities, students can actively explore



concepts, models and designs, and eventually enhance their problem solving skills. Review of numerous prior studies (Abbas and Al-Bastaki 2002) suggest that a 32% reduction in average instruction time may be realized through use of computer-based technology.

Recent trends in mass transfer education also involve use of advanced technologies. For example, Katz and co-workers (Katz, Weathers et al. 1997; Katz, Weathers et al. 1998) constructed a multimedia-based laboratory module for a contaminant fate and transport course, which includes interactive tutorials, instructional video, annotated spreadsheets, and simulations of field-scale transport. Reardon (Reardon 2001) presents an example use of the Internet in mass transfer education through establishment of a course Web site, including on-line distribution of instructional material, example problems, figures, questions, and exams.

In this study, we attempt to further the use of Web-based tools in mass transfer processes education and research through development of a user-friendly problem solving environment, where users are able to define, model, and compare and contrast certain mass transfer processes, all in the confines of one program. MTVLab is an appealing Web-based system to assist in the instruction of mass transfer processes in a number of ways: (1) it completes the Kolb Learning Cycle for mass transfer education by creating an active learning environments to explore, visualize, compare and contrast mass transfer processes; (2) it minimizes computational effort, and thus allows students to focus on developing problem solving strategies; and (3) it provides an opportunity for users to more easily explore highly nonlinear processes where no analytical solutions exist, thus

saving time in developing numerical models, and instead focusing efforts on improved understanding of mass transfer processes.

The remaining portion of this chapter provides descriptions of each of the elements comprising MTVLab (Section 3.5) and the technical architecture of the system (Section 3.6).

### **3.5 Mass Transfer Process Laboratory**

#### 3.5.1 Overview

MTVLab is comprised of interactive user-friendly input interfaces, customizable output interfaces, illustrative Help and Tutorial sections, a relational database, and a finite element in space and finite difference in time numerical engine (Figure 3-1).

Upon access to the welcome page of MTVLab, each user can gain access to the Help and Tutorial modules to obtain detailed descriptions of each component of the program, as well as example applications described within the Case Studies section. First-time users are invited to participate in the registration process. Following registration, users can enter input interface pages, where they can define a modeling project, including reactor type, initial conditions, specific mass transfer process, and particle characteristics. Upon completion of the input component of the laboratory, users may run the numerical model representing their chosen reactor and particle characteristics by selecting the Execute button. Model simulation status and estimated time for completion are displayed continuously. Model output results, including concentration, mass uptake, and mass flux

data, are presented in tabular and graphical forms to users through use of Excel (Microsoft Corporation, Redmond, Washington) spreadsheets.

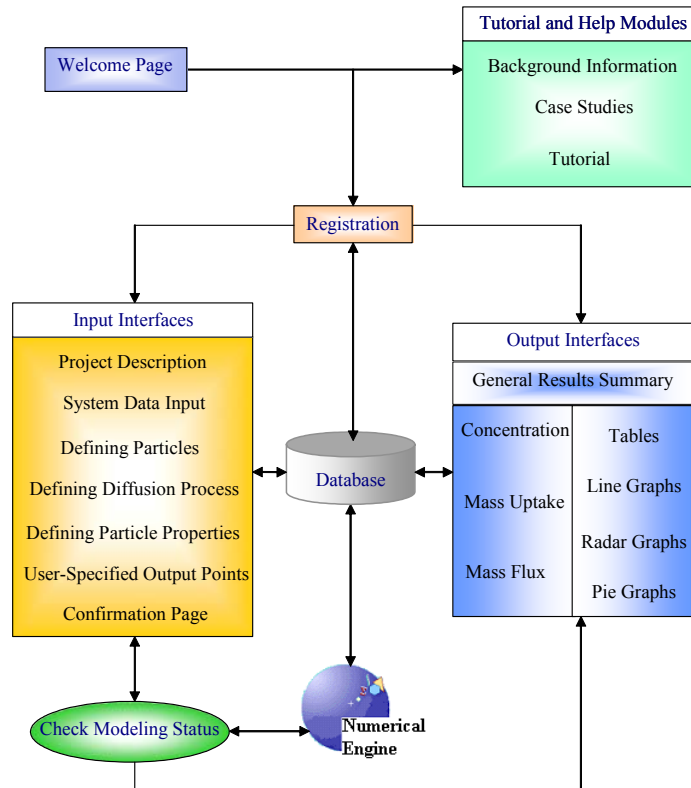


**Figure 3-1. General Information Flow within MTVLab.**

### 3.5.2 Conceptual Model

MTVLab provides a virtual environment for users to model solute mass transfer into or out of spherical particles in two types of ideal reactors: a completely mixed flow reactor (CMFR) and a completely mixed batch reactor (CMBR). Figure 3-2 illustrates a conceptual model of MTVLab, where sorbate diffusion processes occur in spherical particles in a CMBR and a CMFR.

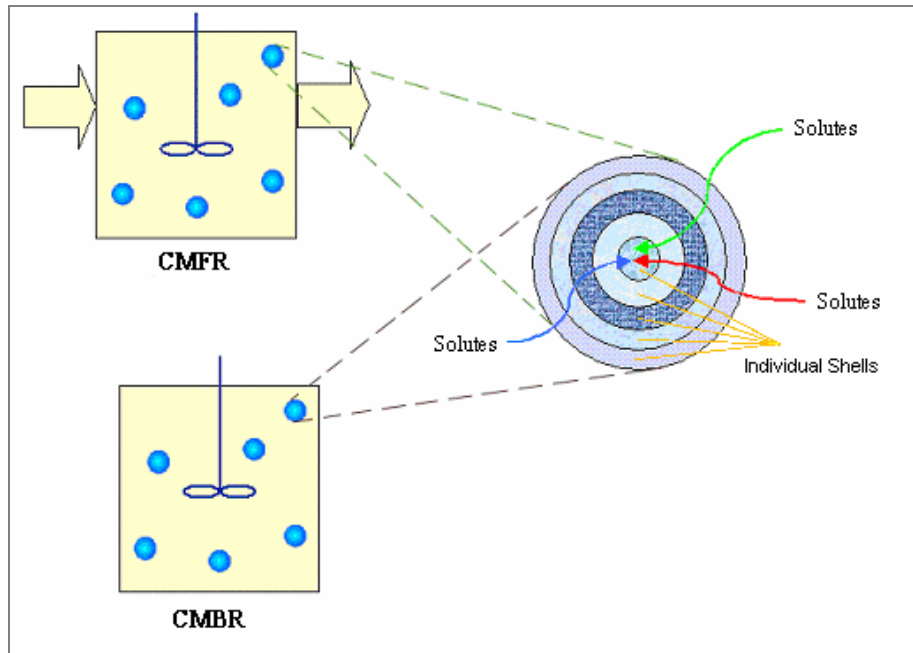


**Figure 3-2. MTVLab Conceptual Model.**

Currently, up to five different types of particles may be defined with each particle possessing specific properties including size, initial conditions (solid-phase and liquid-phase concentrations), physical and chemical properties, and sorption/diffusion processes. Up to five separate reactive domains are also allowed within each particle, where users can define different physical and chemical properties of each domain.

Twelve types of complex mass transfer processes are available for modeling as listed in Table 3-1. Fickian and non-Fickian diffusion models are employed to represent nonequilibrium sorption processes, and linear and/or nonlinear sorption isotherms are utilized to account for equilibrium sorption. Further, based on recognized analogies between NOM and synthetic organic macromolecules, several well-developed synthetic organic macromolecule diffusion models, e.g. Case II diffusion and relaxation models, are employed to describe mass transfer processes in NOM.

**Table 3-1. Mass Transfer Processes Included in the Model.**

Fickian diffusion (no sorption)	Fickian diffusion + Linear sorption + Langmuir sorption
Fickian diffusion + Linear sorption	Fickian diffusion + Linear sorption + Langmuir sorption 1 + Langmuir sorption 2
Fickian diffusion + Langmuir sorption	Fickian diffusion + Linear sorption + Freundlich sorption
Fickian diffusion + Freundlich sorption	Fickian diffusion + Linear sorption + Polanyi sorption
Fickian diffusion + Polanyi sorption	
Case II Diffusion	Relaxation Model

### 3.5.3 Mathematical Models

Mathematical models used to describe mass transfer processes in the subsurface environment enforce the law of conservation of mass allowing for diffusion, advection, interphase mass exchange, chemical reaction, and the presence of sources and sinks. In the special case involving aforementioned mass-transfer rate-limited processes, and for very small flow velocities, advection can be ignored. A general mathematical model for mass transfer in a spherical particle can thus be reduced to (Crank 1975):

$$D_e \left( \frac{\partial^2 C}{\partial r^2} + \frac{2}{r} \frac{\partial C}{\partial r} \right) = \varepsilon_d \frac{\partial C}{\partial t} + (1 - \varepsilon_d) \rho_s S \quad (3-1)$$

where:

$r$	=	the spherical coordinate [L];
$C$	=	concentration of solute in the particle [M/L <sup>3</sup> ];
$D_e$	=	the effective diffusion coefficient [L <sup>2</sup> /T];
$\varepsilon_d$	=	porosity of the diffusion domain [-];
$\rho_s$	=	solid phase density [M/L <sup>3</sup> ];
$S$	=	sorbed solute in the solid phase [M/MT].

Initial conditions, including initial concentration of solution in the reactor, and initial solid phase concentration in the particle, are defined by user input. Different

reaction domains within each particle may also possess different initial concentrations, effectively allowing for sorption, desorption, or combinations of sorption and desorption processes.

Boundary conditions are determined based on selection of one of two types of ideal reactors, CMFR and CMBR. For both reactors, it is assumed that there is no mass transfer flux in the center of the particle. For CMFR, the liquid-phase concentration at the surface of the particle is set equal to a constant concentration of solute in the solution. For CMBR, the rate at which a sorbate leaves solution is set equal to the rate it enters the surface of the spherical particles, where the liquid-phase sorbate concentration at the surface of particles is assumed equal to the solution concentration. The boundary conditions for both CMFR and CMBR are summarized in Table 3-2.

**Table 3-2. Boundary Conditions for CMFR and CMBR. Where  $R$  is the radius of a particle;  $C$  is the liquid phase concentration of a particle;  $D_e$  is the effective diffusion coefficient of a particle;  $S_p$  is the surface area of a particle;  $C_a$  is the constant solution concentration in CMFR;  $V$  is the volume of the solution;  $N$  is the number of particle included in the reaction.**

CMFR	CMBR
$D_e \left. \frac{\partial C}{\partial r} \right _{r=0} = 0$ $C = C_a, \quad \text{at } r = R$	$D_e \left. \frac{\partial C}{\partial r} \right _{r=0} = 0$ $\frac{V}{N} \frac{\partial C}{\partial t} + S_p D_e \left. \frac{\partial C}{\partial r} \right _{r=R} = 0$

Brief descriptions of the mathematical models for each mass transfer processes listed in Table 3-1 are provided in the following sections.

### 3.5.3.1 Fickian Diffusion (No sorption)

If diffusing species possess low chemical activities (e.g., low partial pressures or low concentrations), Fick's First Law can be applied to explain the mass transfer process.

Following equation could be used to describe this process:

$$D_a \left( \frac{\partial^2 C}{\partial r^2} + \frac{2}{r} \frac{\partial C}{\partial r} \right) = \frac{\partial C}{\partial t} \quad (3-2)$$

where:

$$\begin{aligned} D_a &= \text{apparent diffusivity coefficient [L}^2\text{/T]}; \\ R &= \text{the space coordinate in the particle [L]; and} \\ t &= \text{time [T]}. \end{aligned}$$

### 3.5.3.2 Fickian Diffusion + Linear Sorption

The simplest case of sorption isotherm behavior is observed under conditions of linear distribution between sorbent and solute (sorbate) characterized by a linear isotherm. Employing Fickian diffusion to represent the nonequilibrium sorption process, and linear sorption accounting for equilibrium, following particle scale mass transfer model can be derived:

$$\frac{D_l / \tau}{1 + \left( \frac{(1 - \varepsilon_d) \rho_s}{\varepsilon_d} \right) K_d} \left( \frac{\partial^2 C}{\partial r^2} + \frac{2}{r} \frac{\partial C}{\partial r} \right) = \frac{\partial C}{\partial t} \quad (3-3)$$

where:

$$\begin{aligned} K_d &= \text{distribution coefficient [L}^3\text{/M]}; \\ D_l &= \text{free liquid diffusivity [L}^2\text{/t] of the solute}; \\ \tau &= \text{tortuosity factor [-]} \end{aligned}$$

### 3.5.3.3 Fickian Diffusion + Freundlich Sorption

Sorption processes are often nonlinear functions of the aqueous phase concentration of the solute. In natural soils and sediments, a Freundlich isotherm model often describes nonlinear sorption processes very well (e.g., Huang and Weber, 1996;

Young and Weber, 1995.). Combining Fickian diffusion and Freundlich sorption processes yields the following model:

$$\frac{\varepsilon_d D_l}{\tau} \left( \frac{\partial^2 C}{\partial r^2} + \frac{2}{r} \frac{\partial C}{\partial r} \right) = \left( \varepsilon_d + (1 - \varepsilon_d) \rho_s n K_f C^{n-1} \right) \frac{\partial C}{\partial t} \quad (3-4)$$

where:

$$\begin{aligned} K_f &= \text{Freundlich capacity coefficient [M/M][L}^3/\text{M]}^n; \text{ and} \\ n &= \text{Freundlich sorption intensity exponent [-].} \end{aligned}$$

#### 3.5.3.4 Fickian Diffusion +Langmuir Sorption

Based on a homogeneous surface site energy assumption, a Langmuir sorption model may be employed. Combining Langmuir sorption with Fickian diffusion yields the following model:

$$\frac{\varepsilon_d D_l}{\tau} \left( \frac{\partial^2 C}{\partial r^2} + \frac{2}{r} \frac{\partial C}{\partial r} \right) = \left( \varepsilon_d + (1 - \varepsilon_d) \rho_s \frac{Q_0 b}{(1 + bC)^2} \right) \frac{\partial C}{\partial t} \quad (3-5)$$

where:

$$\begin{aligned} Q_0 &= \text{Langmuir capacity coefficient [M/M]; and} \\ b &= \text{Langmuir intensity coefficient [L}^3/\text{M].} \end{aligned}$$

#### 3.5.3.5 Fickian Diffusion +Polanyi Sorption

Polanyi sorption theory could apply to any particulate matter with well-defined pore structure and with surfaces that are sufficiently nonpolar to allow natural organic chemicals to strongly out-compete water for the adsorption space (Xia and Ball 2000). Combining the following equations, we may obtain a model to describe Fickian diffusion coupled with Polanyi sorption:

$$\frac{\varepsilon_d D_l}{\tau} \left( \frac{\partial^2 C}{\partial r^2} + \frac{2}{r} \frac{\partial C}{\partial r} \right) = \varepsilon_d \frac{\partial C}{\partial t} + (1 - \varepsilon_d) \rho_s \frac{\partial q}{\partial t} \quad (3-6)$$

$$q = Q_0 10^{a'(RT \ln(S_w/C)/V)^{b'}} \cdot \rho \quad (3-7)$$



where:

$R$	=	ideal gas constant (cal/mol-K);
$T$	=	temperature (K)
$Q_o$	=	adsorption volume capacity at saturation [ $L^3/M$ ];
$S_w$	=	aqueous solubility [ $M/L^3$ ];
$V$	=	the bulk molar volume of the adsorbate at the temperature of adsorption [ $L^3/mol$ ];
$a', b'$	=	fitting parameters; and
$\rho$	=	solute density [ $M/L^3$ ].

### 3.5.3.6 Fickian Diffusion + Linear Sorption + Langmuir Sorption (Dual-Mode Model)

Although not widely used by itself in the environmental literature due to its assumption of homogeneous surface site energies (Weber, McGinley et al. 1992), the Langmuir model can be used in conjunction with other isotherm models to describe sorption of more heterogeneous systems. In a heterogeneous medium, non-linear sorption isotherms can be decomposed into a linear component that accounts for normal dissolution and a non-linear Langmuir-type component that accounts for immobilization of penetrant molecules at fixed sites within the medium (LeBoeuf and Weber 1997). Combining the Fickian diffusion and dual sorption theory, we obtain:

$$\frac{\varepsilon_d D_l}{\tau} \left( \frac{\partial^2 C}{\partial r^2} + \frac{2}{r} \frac{\partial C}{\partial r} \right) = \varepsilon_d \frac{\partial C}{\partial t} + (1 - \varepsilon_d) \rho_s \frac{\partial q}{\partial t}$$

$$q = K_d \cdot C + \frac{Q_o b C}{1 + b C} \quad (3-8)$$

### 3.5.3.7 Fickian Diffusion + Linear Sorption + Langmuir Sorption 1, 2

The Distributed Reactivity Model developed by Weber and coworkers (Weber, McGinley et al. 1992; Young and Weber 1995; Weber and Huang 1996; Huang, Young et al. 1997; LeBoeuf and Weber 1997; Huang and Weber 1998) is based on the hypothesis that energetic differences among or within individual soil and sediment particles result in different combinations of linear and nonlinear contributions to overall

sorption. The two different Langmuir sorption models here represent two different energetic sites. The model, including a linear phase partitioning component and two Langmuir-type isotherm components, thus represent select cases of the Distributed Reactivity Model. Combining with the nonequilibrium Fickian diffusion process, we obtain:

$$\frac{\varepsilon_d D_l}{\tau} \left( \frac{\partial^2 C}{\partial r^2} + \frac{2}{r} \frac{\partial C}{\partial r} \right) = \varepsilon_d \frac{\partial C}{\partial t} + (1 - \varepsilon_d) \rho_s \frac{\partial q}{\partial t}$$

$$q = K_d \cdot C + \frac{Q_0 b C}{1 + b C} + \frac{Q_0 b C}{1 + b C} \quad (3-9)$$

### 3.5.3.8 Fickian Diffusion + Linear Sorption + Freundlich Sorption

Freundlich sorption may be approximated as a summation of several distinct Langmuir-type (i.e., capacity-limited and relatively constant energy) nonlinear adsorption at different sites in a heterogeneous matrix (LeBoeuf 1998). Based on DRM theory, the nonlinear component of adsorption includes a set of multiple reactions involving different sites of different energy. A model combining linear sorption and Freundlich sorption is thus often applied to account for multiple sorption domains of different reactivity at the soil-sediment particle scale. Again, combining with Fickian diffusion process yields the following model:

$$\frac{\varepsilon_d D_l}{\tau} \left( \frac{\partial^2 C}{\partial r^2} + \frac{2}{r} \frac{\partial C}{\partial r} \right) = \varepsilon_d \frac{\partial C}{\partial t} + (1 - \varepsilon_d) \rho_s \frac{\partial q}{\partial t}$$

$$q = K_d \cdot C + K_f \cdot C^n \quad (3-10)$$

### 3.5.3.9 Fickian Diffusion + Linear Sorption + Polanyi Sorption

The sorption of non-polar and low-polar organic chemicals on natural sorbents can be interpreted as an additive combination of partitioning and adsorption (Xia and Ball 2000). A model which can incorporate linear partitioning with Polanyi sorption is a two-

domain model proposed to separately account for contributions from partition by ordinary organic matter and adsorption, or, more accurately, pore-filling, by fixed-pore carbonaceous adsorbents (Xia and Pignatello 2001).

$$\frac{\varepsilon_d D_l}{\tau} \left( \frac{\partial^2 C}{\partial r^2} + \frac{2}{r} \frac{\partial C}{\partial r} \right) = \varepsilon_d \frac{\partial C}{\partial t} + (1 - \varepsilon_d) \rho_s \frac{\partial q}{\partial t}$$

$$q = K_d \cdot C + Q_0 10^{a'(RT \ln(S_w/C)/V)^b} \cdot \rho \quad (3-11)$$

### 3.5.3.10 Case II Diffusion

The transport of organic molecules in glassy polymers often does not obey Fickian behavior. When the relaxation rate of individual macromolecular chains are much slower than the diffusion rate of the solute, Case II diffusion may be observed. It only occurs below a polymer glass transition temperature, and above certain concentrations of solute. Case II diffusion is characterized by linear kinetics and a sharp diffusion front, and it occurs in polymer penetrant systems in which the penetrant substantially swells the polymer (Thomas and Windle 1980; Thomas and Windle 1982). Harmon proposed an equation for the total flux in terms of the sum of two fluxes; one Fickian diffusion and the other Case II transport (Harmon 1992):

$$J = -D \frac{\partial C}{\partial x} + vC \quad (3-12)$$

Mass balance in spherical particle provides the following equation:

$$\frac{\partial C}{\partial t} = D \frac{\partial^2 C}{\partial r^2} + \frac{2D}{r} \frac{\partial C}{\partial r} - v \frac{\partial C}{\partial r} \quad (3-13)$$

where:

- $v$  = constant velocity of Case II diffusion front [L/T];
- $C$  = concentration of solute in the particle [M/L<sup>3</sup>]; and
- $D$  = apparent diffusivity coefficient [L<sup>2</sup>/T].

### 3.5.3.11 Relaxation Model

Both concentration-gradient-controlled diffusion and relaxation-controlled swelling contribute to the rate and the extent of penetrant sorption in glassy polymers. Diffusion processes ranging from ideal Fickian diffusion to Case II (relaxation or swelling controlled) sorption may be expected for a given penetrant/polymer system if a sufficient range of temperature and penetrant activity is traversed experimentally (Hopfenberg and Frisch 1969). The sorption process is considered here as the linear superposition of phenomenological independent contributions from Fickian diffusion and polymeric relaxations:

$$M_t = M_{t,F} + M_{t,R} \quad (3-14)$$

where:

$$\begin{aligned} M_t &= \text{total mass uptake by the soil particle [M];} \\ M_{t,F} &= \text{mass uptake due to Fickian diffusion and adsorption [M];} \\ M_{t,R} &= \text{mass uptake due to relaxation process [M].} \end{aligned}$$

The relaxation process is assumed to be first order in the concentration difference (Berens 1978), which can be expressed as:

$$\frac{dM_{t,R}}{dt} = k_r (M_{\infty,R} - M_{t,R}) \quad (3-15)$$

where:

$$\begin{aligned} M_{\infty,R} &= \text{ultimate mass uptake due to relaxation [M]; and} \\ k_r &= \text{relaxation rate constant [1/T].} \end{aligned}$$

Thus, total mass uptake due to Fickian diffusion, adsorption and relaxation processes can be expressed as:

$$\frac{M_t}{M_\infty} = \frac{M_{t,F}}{M_\infty} + (1 - f_d)[1 - \exp(-k_r t)] \quad (3-16)$$

where:

$$\begin{aligned} M_\infty &= \text{total ultimate mass uptake [M];} \\ f_d &= \text{mass uptake percentage due to diffusion and adsorption [-].} \end{aligned}$$

### 3.5.4 Numerical Methods

In a CMBR or CMFR, if the mixing intensity is high, transport of solute to the surface of the solid phase does not limit the sorption rate, and thus, the rate of change of mass in the solution phase can be set equal to the rate of solute mass change in the particle. Thus, the modeling task reduces to solving microscale mass transfer problems. Through establishment of a mass balance between the particles at every instant of time based on conservation of total system mass consisting of mass of solute in the solution and mass of solute within all of the particles, solution concentration can be derived for multiple particle cases.

The mathematical model is solved through use of a discrete numerical scheme using *hp*-finite element in space and finite difference in time. Use of the *hp*-version of finite element method ensures that the non-smoothness of the response can be accounted for easily without the need to resort to upwind-mixed finite element technique to avoid spurious perturbations (Basu, Hsiao et al. 1993). Spatial discretization is accomplished using spherical shell elements, while temporal modeling is based on discretization using backward difference. The unknown function  $C(r,t)$  for an element is approximated by:

$$C(r,t) = \sum_{j=1}^{p+1} C_j(t) N_j(\zeta) \quad (3-17)$$

Here  $C_j$  are spatial constants but vary with time,  $N_j$  are shape functions which are integrals of Legendre polynomial in terms of the standard element coordinate  $-1 \leq \zeta \leq 1$ .

Using the weighted residual method and applying discretization, the following matrix equation is obtained for the system at the  $k^{\text{th}}$  time step.

$$\left[ \left( \frac{[M]}{\Delta t^k} + \theta[K] \right) \right] \{C\}^k = \left[ \left( \frac{[M]}{\Delta t^k} \right) - (1-\theta)[K] \right] \{C\}^{k-1} \quad (3-18)$$

where:

- $[M]$  = matrix containing integrals of product of shape functions;
- $[K]$  = matrix containing integrals of product of derivatives of shape functions;
- $\Delta t^k$  =  $k^{\text{th}}$  time step;
- $\theta$  = temporal approximation parameter with value depending on the scheme use;
- $\{C\}^k$  = approximation concentration at the  $k^{\text{th}}$  time step.

Non-linearity of physical parameters was accounted for through an iterative scheme. Implementations were accomplished in FORTRAN 90, where each of the aforementioned mass transfer processes cases was successfully modeled. For the simplest cases (i.e., Fickian diffusion without sorption, Fickian diffusion with linear sorption), analytical solutions are available for both CMFR and CMBR (Crank 1975). Figures 3-3 and Figure 3-4 illustrate the similarity of results of the numerical solutions relative to the analytical solutions.

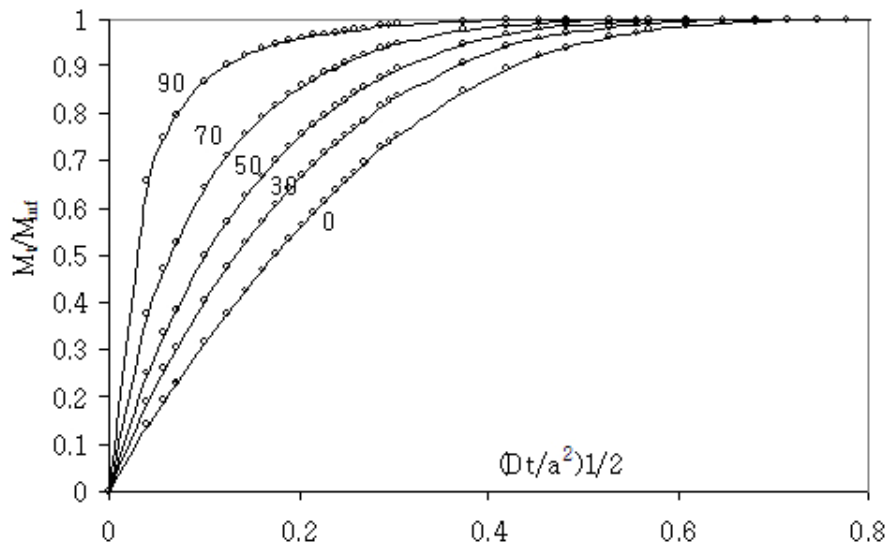


**Figure 3-3. Uptake by a Sphere from a CMBR. Numbers on curves represent the percentage of solute taken up by the particle at equilibrium. Solid lines represent analytical solutions, and points represent numerical solutions.**

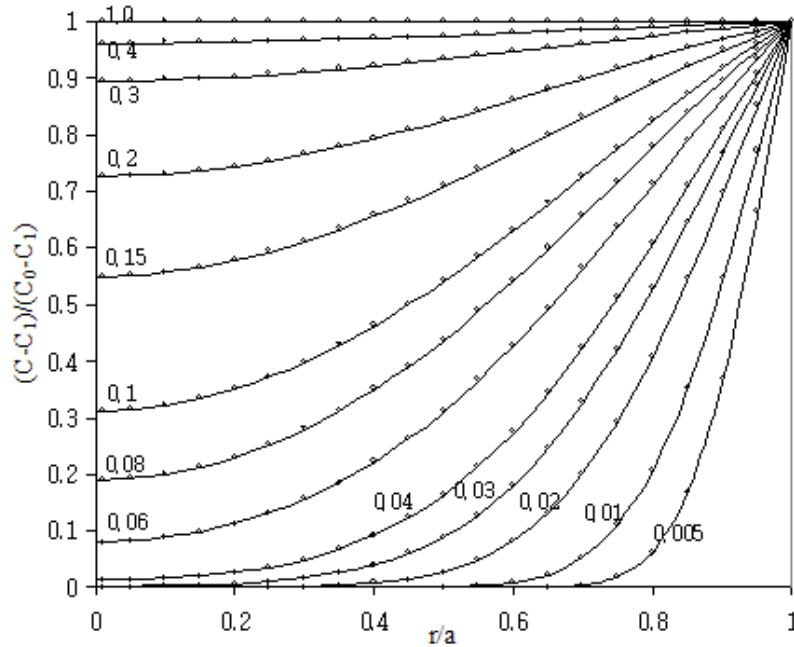


**Figure 3-4. Concentration Distributions at Various Times in a Sphere with Initial Concentration  $C_1$  and Surface Concentration  $C_0$ . Numbers on curves represent values of  $Dt/a^2$ . Lines represent analytical solutions, and points represent numerical solutions.**

### 3.5.5 The Mass Transfer Process Laboratory Website

#### 3.5.5.1 Welcome and Registration

As shown in Figure 3-5, the Welcome page represents the gateway to MTVLab, through which users can access Help and Tutorial modules, the registration system, and Input and Output interfaces. Users can access the Help and Tutorial modules from the Welcome page by clicking on the large ‘Welcome’ picture. First-time users will be led to the registration system, where they are required to complete information fields, including username, password, and contact information. This information is used by MTVLab to uniquely identify each user within the system. Registered users may directly enter the MTVLab from the Welcome page.

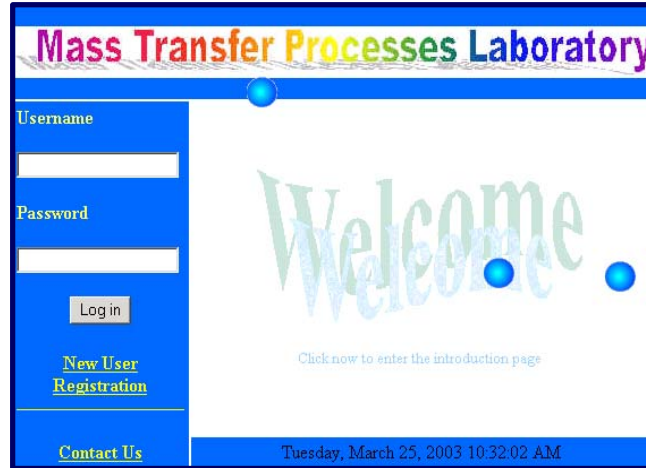


**Figure 3-5. An Example Welcome Page.**

### *3.5.5.2 Input Interface*

A set of interactive input interface Web pages are logically presented to lead users through the simulation process. Input information includes project description, definition of the reactor configuration, determination of the number of particles in the system, selection of mass transfer processes, identification of the model parameters involved in the specific processes, locations and times of user-specified data collection points, and simulation period.

***Project Description.*** The Project Description page presents different formats for first-time users and previously registered users. First-time users are prompted to open a new project by inputting the project name and description. A Project Description page containing information of the latest project entered is presented to previously registered users. Users can then choose to edit the existing project or open a new project. Users may also choose to view the results if the existing project simulation run is complete. An example Project Description page is provided in Figure 3-6.



Welcome *lisa*, please follow the wizard to do modeling.

## Mass Transfer Processes Laboratory

**Project Selection** Help

<p><input type="radio"/> Edit Project <b>lisa</b></p> <hr/> <p><input checked="" type="radio"/> Open a new project</p> <p><small>(input new project name and description in the right column)</small></p> <hr/> <p><input type="radio"/> Results for project <b>lisa</b></p>	<p>Project Name:</p> <p><input type="text" value="lisa"/></p> <p>Project Description:</p> <div style="border: 1px solid gray; padding: 5px; min-height: 40px;"> <p>This is a test page for tutorial!</p> </div>
--	---

**Figure 3-6. An Example Page of Project Description.**

*System Data Input.* In this page, users define overall system information, including reactor type, the volume of solution within the reactor, initial solution concentration, the number of different types of particles, and simulation duration. An example system data input page is provided in Figure 3-7.

## Mass Transfer Processes Laboratory

**System data Input** Help

Solution volume ( <i>liter</i> ):	<input type="text"/>
Initial solution concentration ( <i>mg/l</i> ):	<input type="text"/>
The number of particles:	<input type="text" value="1"/>
Time duration: <input type="text" value="seconds"/>	<input type="text"/>

---

Transient state, completely mixed flow reactor  
 Transient state, completely mixed batch reactor  
 Steady state

**Figure 3-7. An Example Page of System Data Input.**

**Particle Definition.** An equivalent number of particles to that defined in the System Data Input page is displayed on this screen. Selection of a particular particle leads users to subsequent pages to define the mass transfer process and particle properties. Colors of the displayed particles change from bright blue to pale blue upon completion of data entry for that particle. An example page of particle definition is provided by Figure 3-8.

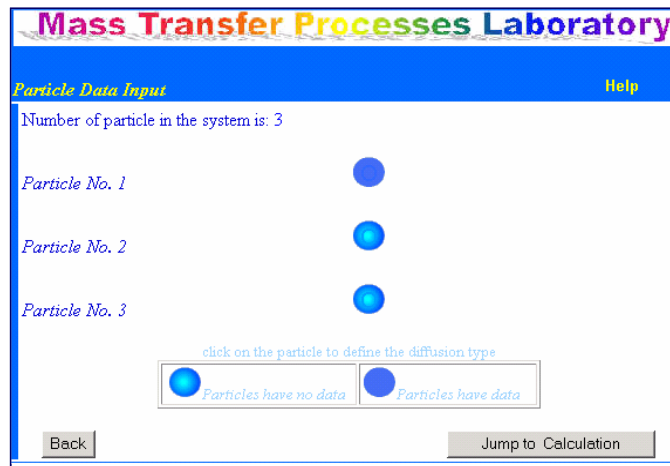


**Figure 3-8. An Example Page of Particle Definition.**

**Diffusion Processes Definition.** Corresponding to the particle selected in the previous page, users provide the particle radius, the number of shells (i.e., reaction domains), and the diffusion type. Users can choose one mass transfer process among the provided twelve mass transfer processes including linear and nonlinear sorption, and Fickian and nonFickian diffusion processes. An example page of diffusion processes definition is provided by Figure 3-9.

**Mass Transfer Processes Laboratory**

Please input the data for particle No. 1 Help

Radius of particle No. 1( *mm* ):

Number of shells in particle No. 1:

---

Select the diffusion type for particle No.1:

<i>Fickican Diffusion</i>	<i>Non-Fickican Diffusion</i>
<input type="radio"/> <i>No Sorption</i>	
<input type="radio"/> <i>Linear Sorption</i>	
<input type="radio"/> <i>Freundlich Sorption</i>	
<input type="radio"/> <i>Langmuir Sorption</i>	
<input type="radio"/> <i>Polanyi Sorption</i>	<input type="radio"/> <i>CaseII diffusion</i>
<input type="radio"/> <i>Linear Sorption + Langmuir Sorption</i>	<input type="radio"/> <i>Relaxation model</i>
<input type="radio"/> <i>Linear Sorption + Langmuir Sorption 1 + Langmuir Sorption 2</i>	<input type="radio"/> <i>Dual Domain model</i>
<input type="radio"/> <i>Linear Sorption + Freudlich Sorption</i>	
<input type="radio"/> <i>Linear Sorption + Polanyi Sorption</i>	

**Figure 3-9. An Example Page of Diffusion Processes Definition.**

*Defining Particle Properties.* This page provides data entry fields for particles' physical and chemical properties. This page is custom-formatted based on information provided in the previous page. For example, based on the number of defined shells for a particular particle, a corresponding picture is displayed to help users visualize its physical structure. Based on the diffusion type, corresponding model parameters are also shown in the input tables. For each particle, users first locate the position of each shell, then they input basic

properties for each shell, including initial solid phase concentration, porosity, tortuosity, and density. Finally, the required model parameters, e.g., diffusion coefficient, for the corresponding mass transfer process is provided by the user for each shell. Figure 3-10 provides an example page of defining particle properties.

**Mass Transfer Processes Laboratory**

**Particle No. 1 Shell Data** Help

**Shell Location**

Diagram showing a particle with two shells: Shell No. 1 (inner) and Shell No. 2 (outer). Three points are marked: Point 1 at the center, Point 2 at the boundary of Shell No. 1, and Point 3 at the boundary of Shell No. 2.

Point	Location (mm, from center of particle)
1	0.0
2	<input type="text"/>
3	1.0

**Diffusion/Sorption Properties** (No Sorption)

Shell No.	Apparent Diffusion Coefficient (mm <sup>2</sup> /s)	Initial Concentration (mg/l)
1	<input type="text"/>	<input type="text"/>
2	<input type="text"/>	<input type="text"/>

**Figure 3-10. An Example Page of Defining Particle Properties.**

**User-Specified Output.** Upon completion of all required input, users are afforded the opportunity to define spatial and temporal data collection points for each particle type for which they are interested in obtaining data. Upon project execution, model-specified and user-specified points are available as model output. An example of the user-specific output page is present in Figure 3-11.

**Mass Transfer Processes Laboratory**

*Particle No.1 output points* Help

Please specify the points you wish to be included in the output :

Point	$r(mm)$
1	0.0
2	0.0
3	0.0
4	0.0
5	0.0
6	0.0
7	0.0
8	0.0
9	0.0
10	0.0
16	0.0
17	0.0
18	0.0
19	0.0
20	0.0

$R=1.0mm$

**Figure 3-11. An Example of User-Specified Output Page.**

**Confirmation Page.** Following completion of all input information, a confirmation page is displayed to allow users the opportunity to review all entered data. If satisfied with their design, users may select the Submit button to start the numerical simulation process. Users may choose to reconstruct the input pages should they desire to make a change. A sample confirmation page is provided in Figure 3-12.

# Mass Transfer Processes Laboratory

Following data are stored in the database

[Help](#)

**Project Information:**

User Name: lisa  
 Project Name: lisa  
 Project Description: test linear sorption

**General Data:**

Solution Volume (liter): 1.0  
 Initial Solution Concentration (mg/l): 1.5  
 The number of Particles: 1  
 Problem Type: Transient state, completely mixed flow reactor  
 Time duration(seconds): 7776000.0

**Particle Data:**

**Particle**

**No.1**

Diffusion Type: Fickian Diffusion + Freundlich Sorption  
 The Number of Shells: 1  
 Radius (mm): 1.0

Shell Data for Particle #1:

Shell No.	Inner Radius (mm)	Outer Radius (mm)	Solid phase initial concentration (mg/kg)	Diffusion Coefficient (mm <sup>2</sup> /s)	Porosity	Tortuosity	Density (g/cm <sup>3</sup> )	K <sub>f</sub>	n
1	0.0	1.0	0.0	6.0E-7	0.5	1.2	1.35	2.0	0.8

Following spatial locations of particle No. 1 will be included in the output (r[mm]=):



**Figure 3-12. An Example Confirmation Page.**

**Model Status.** Once executed, the approximate time for model completion is displayed on the screen. Users may select the model status button to update the modeling status. During this time, users may choose either to wait for the results on-line, or close the Web browser and return at a later time to retrieve results. Upon completion of a simulation run, users are able to access the output interface by selecting the Show Results button. Figure 3-13 provides an example model status page.



**Figure 3-13. An Example Model Status Page.**

### *3.5.5.3 Output Interface*

The MTVLab output module possesses three objectives: (1) provide sufficient information without overwhelming users with excessive data; (2) present information in a customizable manner; and (3) provide a meaningful visualization of model output data. To achieve these objectives, MTVLab embeds Excel spreadsheets into the Web page, and groups the results in terms of graphs and data tables. Data tables provide detailed results from the numerical modeling process, and can be copied, pasted, or exported directly from the on-line Excel table to local Excel files by clicking on a single button. Graphical outputs provide informative displays of output data as line, radar, or pie graphs. The MTVLab output system is very flexible in that data information can be displayed for a particular particle, shell, and location in the particle (when applicable), and for more than one hundred time points by interactively changing data collection locations and times. Further, the output interface is presented in such a way so as to present an overall summary of modeling results that is integrated with detailed results for each particle.

**General Results Summary.** Access to the output portion of MTVLab generates a report summarizing results of the simulation. Information displayed includes (1) summarized project description, including project name, reactor type, the number of particles, and simulation duration; (2) solution and liquid phase concentrations in the middle of shells for each particle; and (3) particle mass uptake represented by color-coded bars corresponding to referenced concentrations displayed along a time axis from the beginning of the simulation to its completion. Selecting the corresponding hot button leads users to detailed Concentration, Mass Uptake and Mass Flux results pages. Figure 3-14 provides an example of General Results Page.

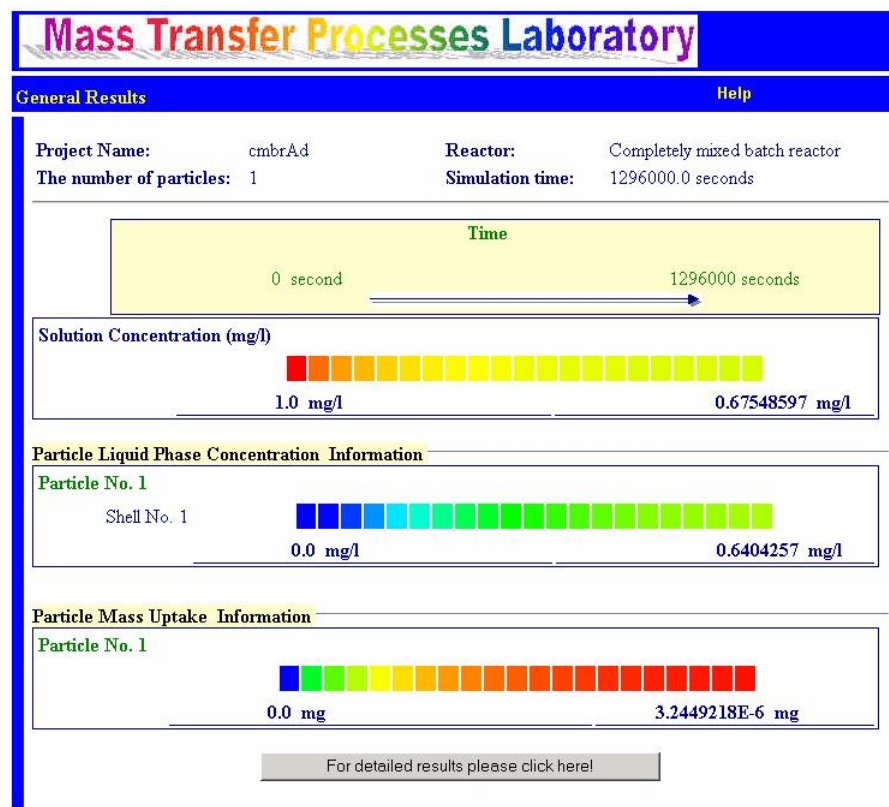


**Figure 3-14. An Example of General Results Page.**



**Concentration Results Output.** Detailed concentration results, including liquid phase concentration and solid phase concentration, are provided for each particle type as spatial concentration profile graphs, concentration versus time graphs, and comprehensive concentration data tables. Figure 3-15 presents the concentration output menu.

**Mass Transfer Processes Laboratory** Help

Concentration Mass Uptake Mass Flux

**GRAPHS**

Concentration Profile Overview Particle No. 1 Type: Liquid phase concentration

Concentration Profile Radar Graph Particle No. 1

Concentration Profile Line Graph Time: 6000.0 seconds Type: Liquid phase concentration

Concentration vs. Time Overview (Line Graph) Particle No. 1 Time phase: 0 seconds to 6000.0 seconds Type: Liquid phase concentration

Concentration vs. Time (Line Graph) Particle No. 1 Location: 0 mm (from center) Time Phase: 0 seconds to 6000.0 seconds Type: Liquid phase concentration

**DATA TABLES**

Concentration Overview Table Particle No. 1 Time Phase: 5980.0 seconds to 6000.0 seconds

Detailed Concentration Data

Submit

**Figure 3-15. Example Concentration Output Menu.**

In the menu, the Concentration Profile Overview section presents a concentration vs. radial line graph that provides visual display of the spatial change of solute concentration at five specific time points. Users can then select to display a concentration profile line graph or radial graph at more than one hundred additional time points. Users may also display a concentration vs. time line graph for user-defined spatial locations in each particle type at more than one hundred time points. In addition, concentration output data for fifty equally-spaced locations and all user-defined locations at more than two hundred time points are summarized in a tabulated Excel spreadsheet. Concentration data for standard output locations including particle center, particle surface, the center of all the shells, and user-defined locations are also presented in a separate concentration overview table. Figure 3-16 provides an example concentration profile output presented by a radar graph.

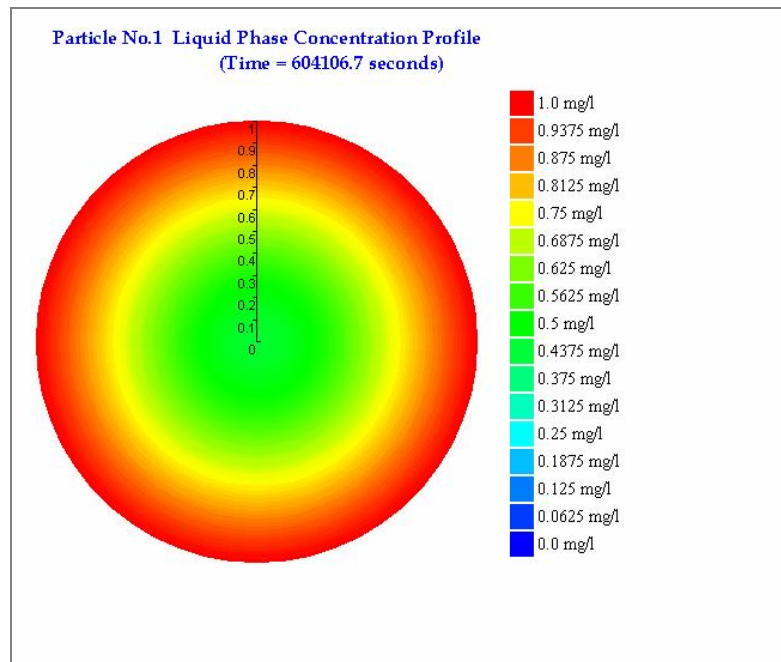


**Figure 3-16. An Example Concentration Profile Output Presented by a Radar Graph.**

**Mass Uptake Results Output.** Detailed mass uptake results, including liquid phase mass uptake, solid phase mass uptake, and total mass uptake, are presented as mass uptake versus time graphs, relative mass uptake percentage pie graphs, and comprehensive mass uptake data tables at both the particle-level and shell-level for each type of particle in the system. Mass uptake for particles or for shells in a designated particle is displayed as mass uptake vs. time line graphs. Pie graphs illustrate the relative mass uptake percentages among the particles in the system or among the shells in a designated particle at more than one hundred time points. A particle mass uptake table summarizes tabular information for each particle, while a shell-level mass uptake table summarizes mass uptake results for a designated particle. Figure 3-17 provides an example of mass uptake percentage output in the format of pie graph.

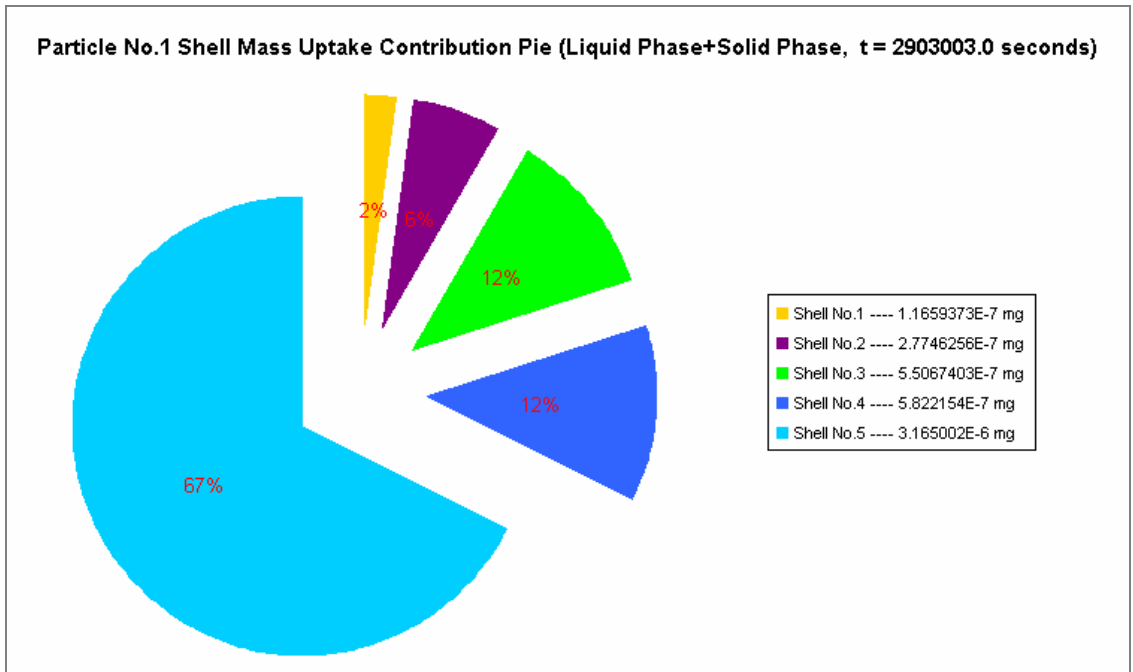


**Figure 3-17. An Example Mass Uptake Output Presented by a Pie Graph.**

**Mass Flux Results Output.** A mass flux profile for a designated particle is presented by a mass flux vs. radial line graph, and a mass flux vs. time line graph is presented at user-defined locations in the particle for more than one hundred time points. Similar to that provided for Concentration output, a mass flux table and a detailed mass flux data table are used to summarize the mass flux data at more than two hundred time points for more than fifty standard and user-defined locations in the particle. Figure 3-18 is an example mass flux output presented by a line graph.

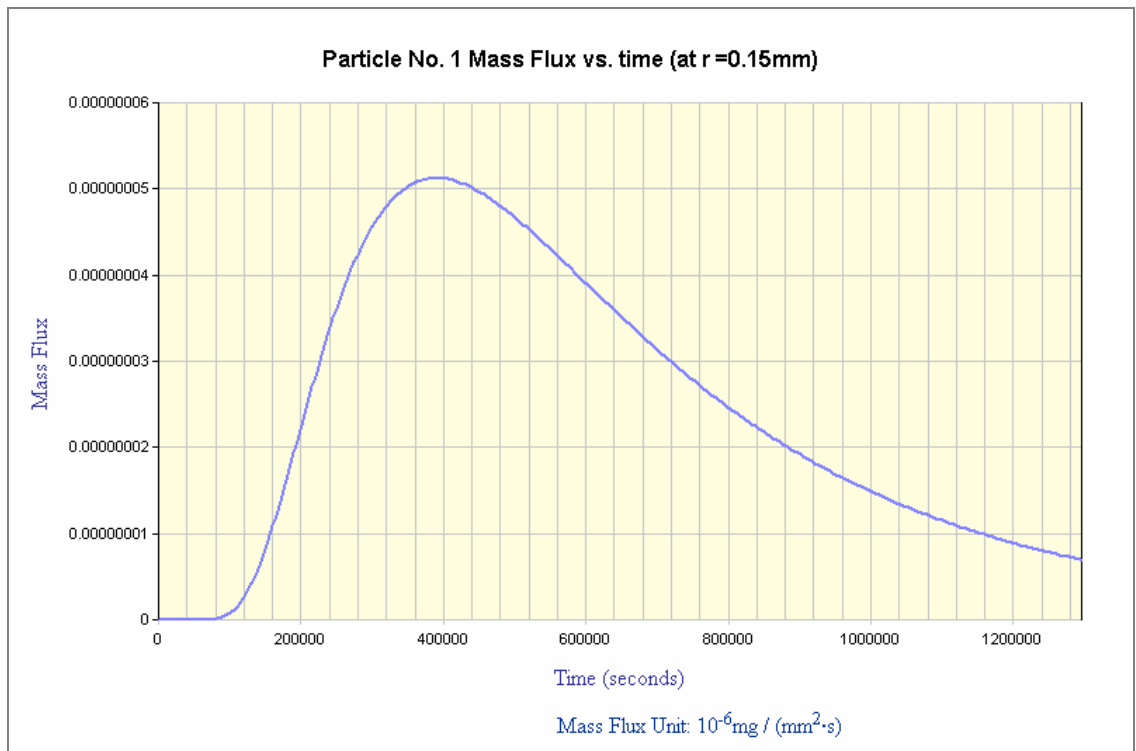


**Figure 3-18. An Example Mass Flux Output Presented by a Line Graph.**

#### 3.5.5.4 Tutorial and Help Modules

Successful use of MTVLab requires users to possess the ability to not only understand the basic principles behind mass transfer processes, but also the aptitude to

navigate the MTVLab Web site. MTVLab Tutorial and Help modules are designed to highlight basic mass transfer-related principles and theories, orient users with the purpose and structure of the laboratory, and to provide step-by-step instructions for full laboratory utilization. Figure 3-19 illustrates the help and tutorial page of MTVLab.

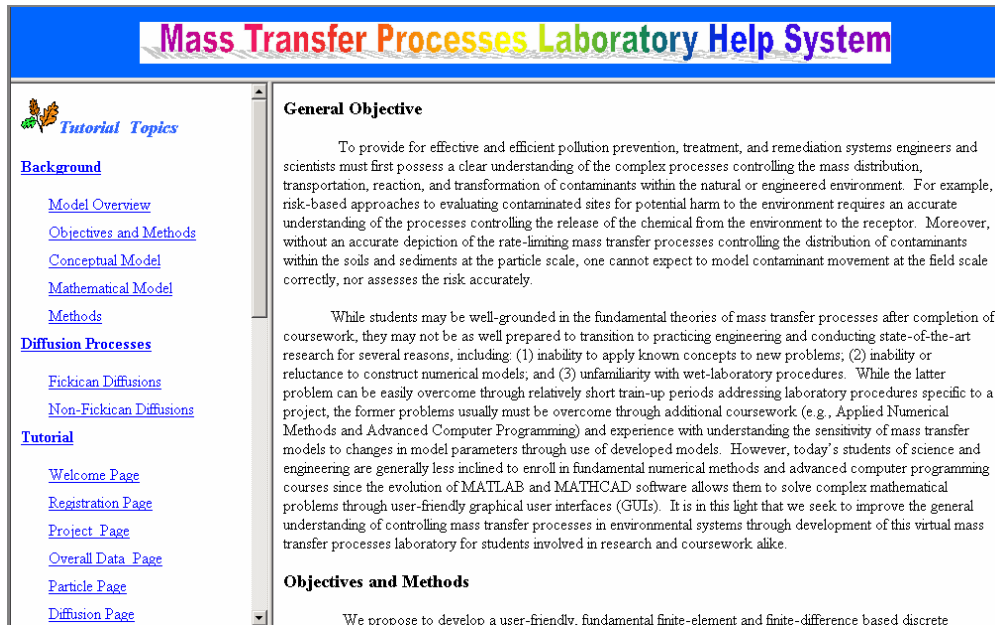


**Figure 3-19. MTVLab Help and Tutorial Modules.**

**Help Module.** The Help module provides descriptions of the MTVLab framework, including purpose and motivation for development of the laboratory, conceptual model employed, and mathematical and numerical models used. In addition, MTVLab Help provides an overview of basic theories, governing equations, and application areas of each of the twelve mass transfer processes used in MTVLab (Table 3-1).

**Tutorial.** The Tutorial module includes operating instructions, explanations of input parameters, and illustrations of relevant mass transfer theories. Should users have a question on a particular entry they may click on the Help button located at the upper right

corner of each Web page. The user is then directed to a tutorial page, which presents an image of the Web page of the initial query. The user is then instructed to click on the location where the difficulty was encountered (e.g., number of shells in a particle), wherein the tutorial provides detailed explanations of corresponding operations. Another function of the Tutorial module is the provision of links from the current screen to related background information. For example, when inputting parameters for a certain diffusion type, it is very common for users to be unfamiliar with the definition of particular model parameters. Selecting respective tutorial topics lead users to corresponding background information, where a specific diffusion process is explained in detail, and the parameters' meanings are discussed.

***Case Studies.*** Many meaningful, solved problems are included in the Case Studies module of MTVLAB in an effort to provide an in-depth illustration of diffusion and sorption behavior under numerous initial conditions, boundary conditions, particle characteristics, and diffusion and sorption methods. Case Study 1 examines how the numerical solutions developed in the finite-element and finite-difference-based numerical model used in this laboratory compare to available analytical solutions. Case Study 2 evaluates the differences in rates of mass uptake or release realized by particles subjected to two different reactor conditions: CMFR and CMBR. Case Study 3 explores the effect of particle size under three different scenarios. Case Study 4 examines the influence of varying sorption isotherm parameters on diffusion-limited mass transfer. Case Study 5 examines several examples of how differing shell properties can influence the diffusion process.

### 3.5.6 Example Applications

#### 3.5.6.1 Background

As previously discussed, the overarching goal of MTVLab is to provide a user-friendly, Web-based environment for students and research professionals to more fully understand and evaluate a number of mass-transfer processes. Currently, MTVLab is undergoing further development to incorporate additional particle shapes (i.e., cylinders and slabs) and non-well-mixed systems, including the use of a lattice Boltzmann method to determine velocity profiles within user-defined reactor domains (e.g., users can define the pore structure or particle size distribution of particles within a fixed-bed reactor). Further, MTVLab is undergoing further validation and development in environmental engineering courses at Vanderbilt University. The following discussion provides an example of how MTVLab may be employed in a graduate-level course (in this case, ENVE 270, Environmental Thermodynamics, Kinetics and Mass Transfer at Vanderbilt University).

ENVE 270 addresses fundamental environmental processes while providing necessary tools to solve a broad range of environmental problems including equilibrium phenomena, process dynamics, and mass transfer processes. MTVLab is introduced in the course as part of an in-class tutorial following traditional instruction in sorption and diffusion processes. Situated in a computer laboratory, students become familiar with the program through an instructor-led tour of the Help and Tutorial modules of MTVLab. Following the initial tour, students are led through a hands-on demonstration of the use of the program to solve a relatively simple mass transfer problem. After demonstrating their ability to understand and use the program, the students are provided opportunities to

solve additional problems and case studies using MTVLab. Part of the learning value of this effort stems from the use of previously solved homework problems as part of their new assignment, where students can compare their previous analytical solutions with the numerical solutions from MTVLab. Further, students are able to solve much more complex problems previously unsolvable using analytical techniques, thus promoting their critical thinking and problem solving skills. Following is an example application of the use of MTVLab in solving an advanced mass transfer processes problem.

### 3.5.6.2 Example Application

Clean spherical particles (radius,  $r = 1$  mm; diffusion coefficient,  $D = 6.0 \times 10^{-7}$  mm<sup>2</sup>/s; porosity,  $\varepsilon = 50\%$ ; tortuosity,  $\tau = 1.2$ ; density,  $\rho = 1.35$  g/cm<sup>3</sup>; partitioning coefficient,  $K_d = 1.0$  cm<sup>3</sup>/g) of mass 1.0 kg are dropped into a pond of water ( $V = 1,760,839$  mm<sup>3</sup>) contaminated with an organic chemical (e.g., trichloroethylene (TCE)) at a concentration of 1 mg/l. Assuming that the pond is well-mixed allows one to assume that each of the particles may be assigned an equivalent volume of 10 mm<sup>3</sup> {equivalent volume for each particle = [No. of Particles]/[Total Reactor Volume] = [((1.0 kg)(1000 g/kg)(1 particle/(4/3π(0.1 cm)<sup>3</sup>))/((1.35 g/cm<sup>3</sup>))]/[ 1,760,839 mm<sup>3</sup>] = (176,839 Particles)/(1,760,839 mm<sup>3</sup>) = 1 Particle/10 mm<sup>3</sup>}. Scenarios: (i) Assuming that TCE will diffuse into the spherical particles, and the diffusion process will be Fickian with linear sorption, what is the equilibrium concentration of TCE in the particle if the pond is modeled as a CMBR *vis'-a-vis'* a CMFR (with contaminated water flowing into the pond)? (ii) What is the TCE concentration in the particle if, following attainment of equilibrium described in scenario (i), clean water replaces the contaminated water in each of the reactors?



*Step 1: Problem Identification*

Users examine the given information to identify that two separate MTVLab simulations are required to answer the first question associated with scenario (i) concerning sorption processes: one for the CMFR, and one for the CMBR. Following attainment of equilibrium within the two reactors, two additional simulations are required to model the desorption processes based on an initial particle concentration derived from the sorption equilibrium concentration obtained in scenario (i).

*Step 2: Model Definition and Simulation*

Here, users define the model to simulate by specifying initial and boundary conditions, and corresponding parameter values. Using the input wizard interfaces of MTVLab, users select the appropriate reactor configuration, sorption type, and diffusion type based on information derived from the problem statement and Step 1. Upon completion of data input, users select the “calculation” button to perform the numerical simulation. Table 3-3 summarizes model parameters for each of the four simulations required in this application.

**Table 3-3. Parameters for MTVLab Example Applications.**

Example Name	Reactor Type	Initial Solution Concentration (mg/l)	Particle Solid Phase Initial concentration (mg/kg)
Project 1	CMFR	1.0	0.00
Project 2	CMBR	1.0	0.00
Project 3	CMFR	0.0	1.00
Project 4	CMBR	0.0	0.67

*Step 3. Examination of Results.*

Upon completion of the simulation, users have the opportunity to explore and analyze the results based on the given output formats; e.g., data tables and graphs, or they may choose to download the data within Excel spreadsheets to analyze and display the data in their own preferred format. Figures 3-20 and 3-21 summarize the MTVLab Concentration Profile Overview line graphs for simulations 1 and 3 (CMBR), and simulations 2 and 4 (CMFR), respectively. By defining user-specified time points, users may also view the changes of concentration profiles during the sorption/desorption process in colorful radar graphs, as illustrated in Figure 3-22.

*Step 4. Problem Generalization.*

MTVLab provides a convenient environment for users to compare different conditions in a particular scenario or contrast different scenarios; thus allowing users to make connections, generalize results, and develop critical thinking skills. In the aforementioned application, users are able to examine the differences in concentration profile and mass uptake achieved by a CMBR relative to a CMFR. Users may also use MTVLab to model the same scenarios, but with different sorption or diffusion types, or different particle types and sizes, so that they can derive a better understanding of the effects of differing particle properties on overall mass transfer processes. Innumerable other scenarios may also be created by using MTVLab, providing an opportunity for comparing and contrasting results, while improving users' critical thinking ability, and at the same time significantly reducing the time required to setup and solve similar problems using analytical solutions (when available), or numerical models when analytical solutions are not obtainable.

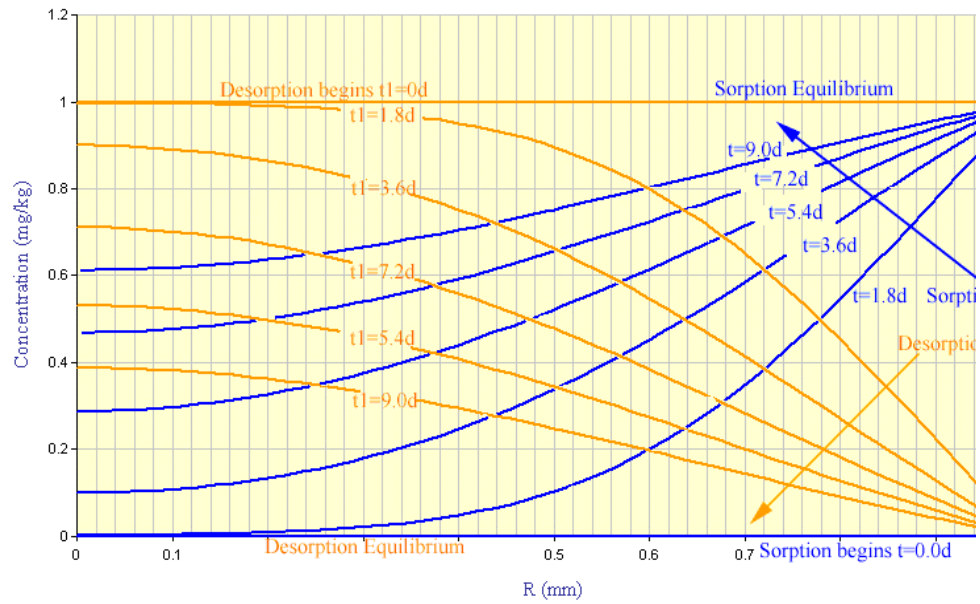


**Figure 3-20. Particle Sorption and Desorption Processes in a CMFR.**

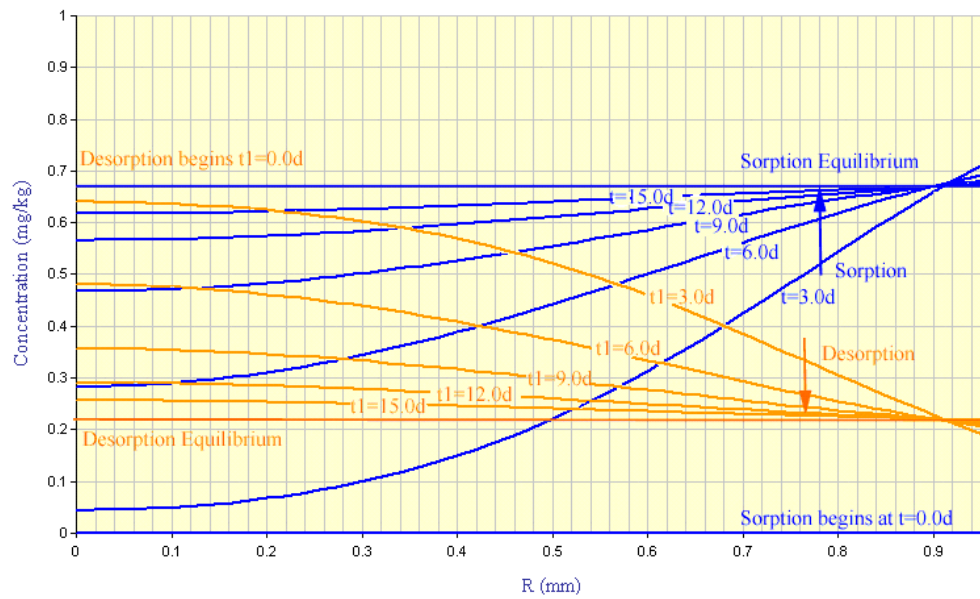


**Figure 3-21. Particle Sorption and Desorption Processes in a CMBR.**

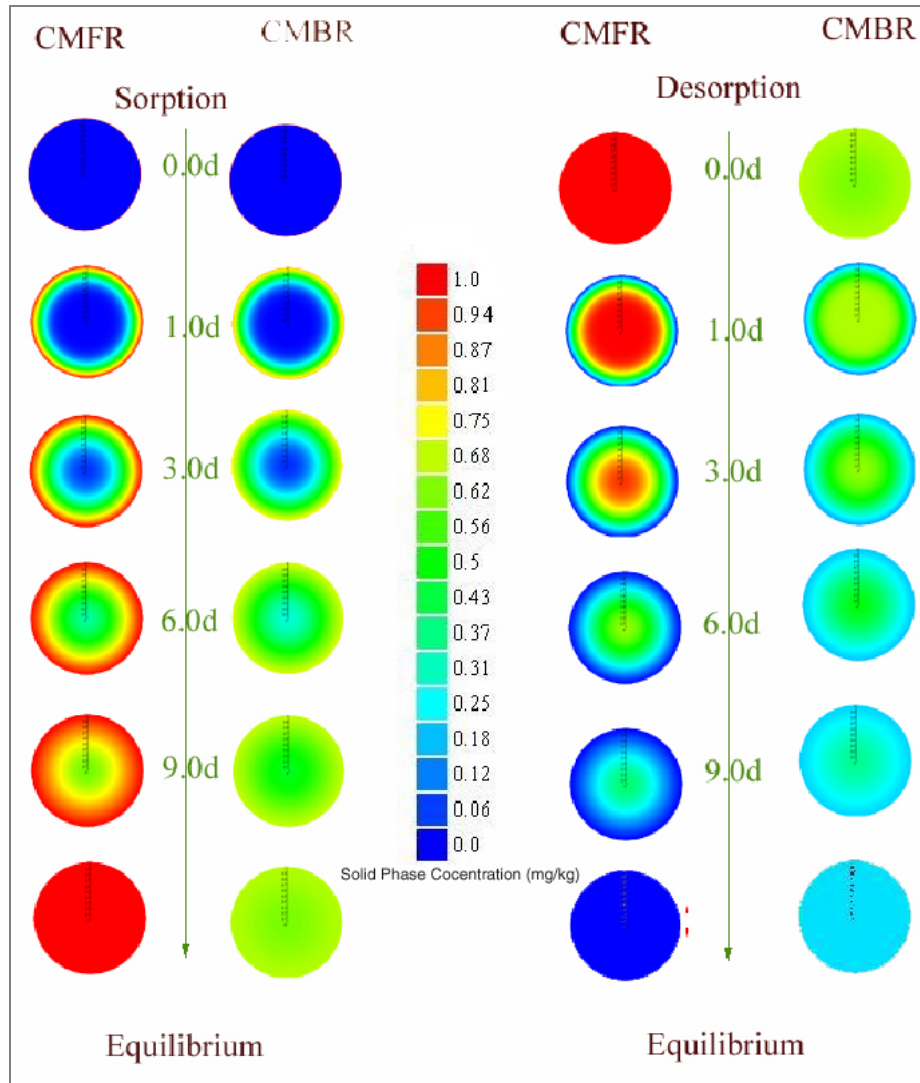


**Figure 3-22. A Comparison of Particle Concentration Profiles During Sorption and Desorption Processes for a CMFR and a CMBR.**

### 3.6 Mass Transfer Process Laboratory System Architecture

#### 3.6.1 Architecture Overview

The Model-View-Controller (MVC) design model serves as the basis for the system architecture of MTVLab. The objective of MVC is to separate the input and output interfaces and the modeling portion of the program into three different

components: the “Model”, the “View”, and the “Controller”. In the MTVLab application, the “Model” includes several server-resident applications, including the numerical model and a database. Common Object Request Broker Architecture (CORBA) serves as a communication protocol. The “View” displays and retrieves information from the user, including interfaces that graphically display model data to the user. The “Controller”, through use of the Java Server Pages (JSP) and Java Beans, interprets mouse and keyboard inputs from the user to make appropriate changes to the “Model” and “View”. The advantage of the MVC paradigm is that it effectively limits and defines the interaction between interface components and underlying problem-domain classes. Relative to the aforementioned web-based model systems, the MTVLab system architecture is especially appealing for a number of reasons: (i) it supports various programming languages and also supports the mixing of these languages allowing the use of the most appropriate one for a given task; (ii) it allows for the execution of the numerical engine and the web server on different computers by employing CORBA technology; (iii) it accepts different database management systems by using Open Database Connectivity (ODBC); and (iv) it provides downloadable, well-organized, highly-visual, and easily edited output through use of a popular spreadsheet program (Excel, Microsoft Office Web Components, Version 9.0.0.2710). Figure 3-23 provides a general illustration of the MVC architecture employed in this laboratory.

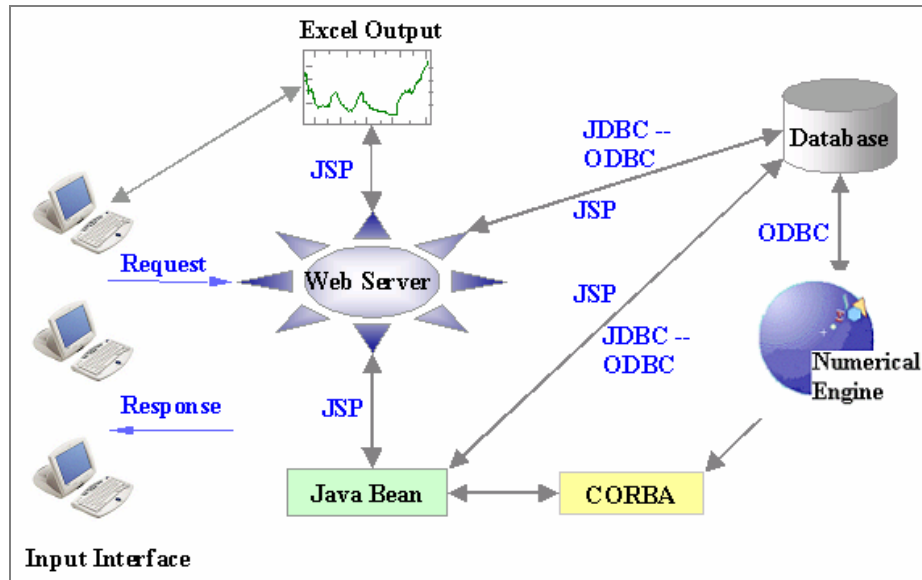


**Figure 3-23. Mass Transfer Processes Virtual Laboratory System Architecture.**

Briefly, the MVC architecture of MTVLab was developed as follows: the finite-element- and finite-difference-based numerical engine used in MTVLab was developed in C++ and FORTRAN for use on the server, while interactive input/output interfaces were constructed with Hypertext Markup Language (HTML), JavaScript and JSP. In MPTL, users input data via Internet Explorer (Microsoft Corporation, Redmond, Washington). The web server accepts the data using JSP, which creates Java Beans to hold and manage the information. JSP and the Java Beans handle the transmission and storage of the information in the database, thereby building a simulation request. When the simulation request is complete and valid, users use Internet Explorer to initiate the execution of the simulation request. CORBA functions as a bridge to pass the simulation request from the JSP and Java Beans to the numerical engine to begin the simulation process. The numerical engine obtains the input data and parameters from the simulation request and the database via ODBC. During the simulation, the numerical engine

provides program output to the database, again using ODBC. Simulation results, in the form of tables and graphs, are then generated from data retrieved from the database using JSP and Java Beans and displayed through Excel. This information is summarized in a detailed flowchart provided in Figure 3-24.

### 3.6.2 Architecture Specifications

A number of software development tools were utilized in the development of this program. This section describes these components in detail, including descriptions of why a particular tool was selected, how it was used, and, in the case of particular software packages, how the software was interfaced with other software.

#### 3.6.2.1 *Web Server*

A web server acts as a gateway for users' browsers (e.g., Internet Explorer) to access the laboratory model. A number of web sever software programs are available, including Microsoft Internet Information Server (Microsoft Corporation, Redmond, Washington), Apache web server (The Apache Software Foundation, Wilmington, Delaware), and IBM WebSphere (IBM Corporation, Armonk, New York). Because MTVLab employs a JSP environment with Windows 2000 (Microsoft Corporation, Redmond, Washington) system software, the web server must be capable of delivering JSP. In this case, Tomcat (The Apache Software Foundation, Wilmington, Delaware, Version 3.2.3) was employed as the web server software since, unlike other servers, Tomcat delivers on both JSP and Servlets (<http://java.sun.com/products/jsp/tomcat/>), and is a very good server for developing and testing JavaSever Pages (Bergsten 2001).

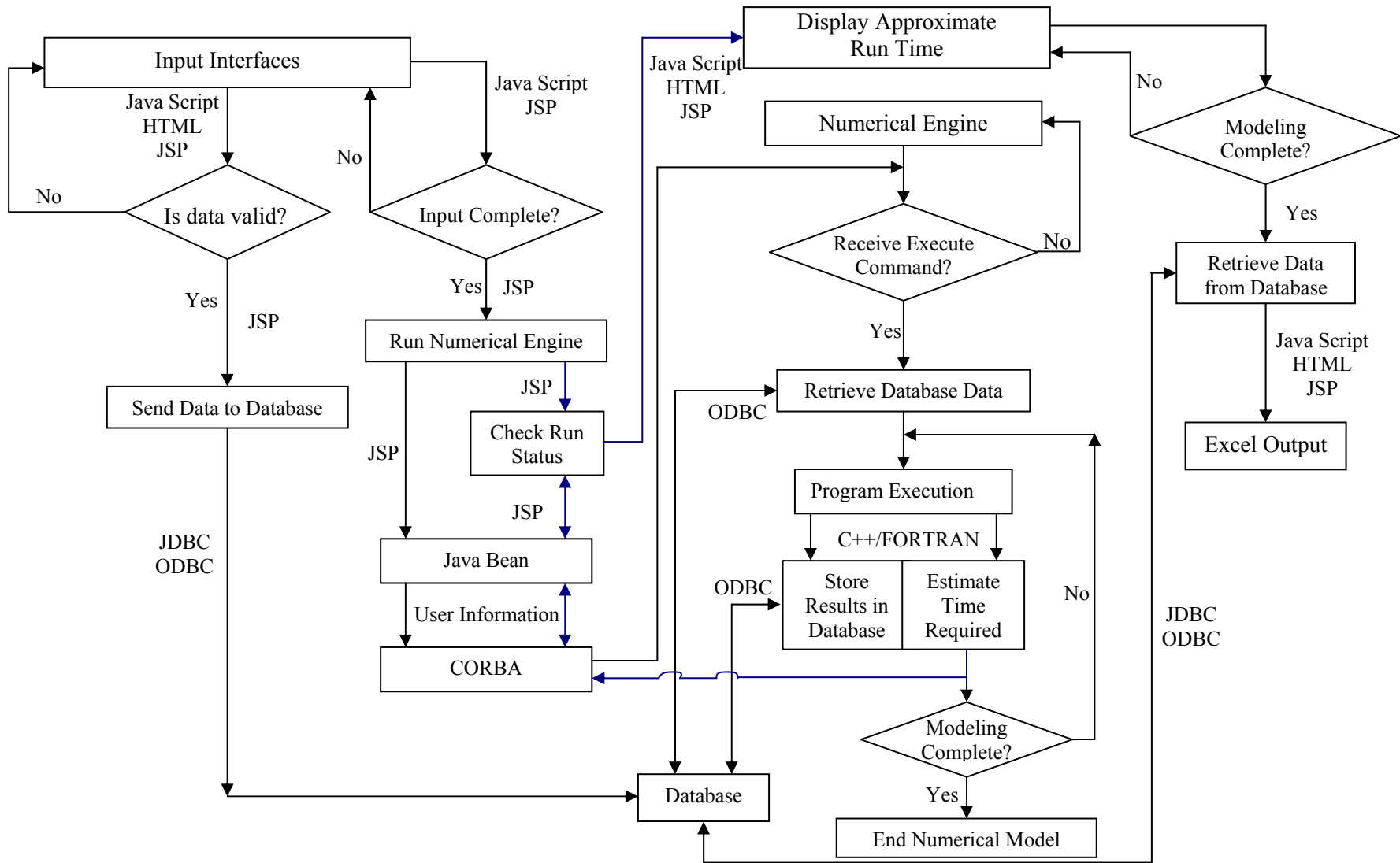


Figure 3-24. MTVLab FlowChart.



### *3.6.2.2 JavaServer Pages (JSP)*

Server-based scripting languages such as Perl, Active Sever Pages (ASP), PHP (recursive acronym for "Hypertext Preprocessor"), ColdFusion, and JSP, provide a means to develop dynamic, robust, and easily maintained input and output interfaces. Each scripting language possesses unique features; each with its own particular advantages/disadvantages (Bloomberg, Kawski et al. 1997). JSP was selected for use in MTVLab because it combines the most important features of available alternatives, plus it possesses several unique characteristics. Like other scripting languages, JSP can be embedded with HTML, and allows the development of customized tag libraries. JSP is different in that it provides access to Java APIs, allowing for easy integration of JSP with existing Java files. JSP is also generally more efficient than other scripting languages (Bergsten 2001). For example, JSP pages are compiled and loaded only once, while ASP, Perl, and PHP require reinterpretation for each new client request. In MTVLab, JSP provides dynamic input/output interfaces, and transfers data between input/output interfaces and Java Beans, and between input/output interfaces and the database.

### *3.6.2.3 Java Beans*

Java Beans are reusable Java components that can be recognized and manipulated within visual application builder environments. Value beans and utility beans are two primary types of Java Beans (Bergsten 2001) in a JSP-based application. Value beans carry information, while utility beans perform actions such as retrieving data from a database. In MTVLab, value beans are used to encapsulate information, such as user ID, reactor type, and particle properties. Utility beans are employed to transmit and retrieve

data to/from the database, transmit an execution message to the numerical model, and query the status of the numerical simulation.

#### *3.6.2.4 Database*

Web-based modeling systems are typically supported by relational databases capable of storing structured data required by the program (Jansons and Cook 2002). A relational database places all information in tables, links tables through shared attributes, and controls redundancy to maintain logical relationships. Several database programs exist, including Structured Query Language (SQL) Server (Microsoft Corporation, Redmond, Washington), MySQL (MySQL AB Company, West Edmonds, WA), Access (Microsoft Corporation, Redmond, Washington), and Oracle (Oracle Corporation, Redwood Shores California). While each database program provides relatively similar relational database functions and capabilities, SQL Server 2000 (Microsoft Corporation, Redmond, Washington), was selected for use in MTVLab based primarily on its availability.

Database characteristics of interest include data storage limits, simplicity of programming for customizable solutions, ease of integration into web-based applications, and query performance. For example, initial evaluations of the overall performance of MTVLab indicated that an unreasonable length of time was required for presentation of modeling results. Improvements in the logical design through optimized queries, and installation of powerful database indexes for frequently used queries, provided significantly increased performance.

### 3.6.2.5 Numerical Engine

Because of its robust compiler designed for high-performance technical computing, the availability of useful subroutines from numerous library sources, and its popularity among many engineering applications, FORTRAN compilers are still commonly employed in solving complex problems requiring extensive computations (e.g., Netlib (<http://www.netlib.org/>)). Previous uses of FORTRAN-based numerical codes in web-based modeling systems, however, appear to be limited, since the FORTRAN language lacks sufficient support for directly connecting to databases (Jansons and Cook 2002) and is not well suited to handling input and output through web servers. These problems are easily overcome, however, by creating a MTVLab C++ shell, or wrapper, for the FORTRAN program core. C++ possesses the ability to easily communicate with the database for data input/output.

Mixed FORTRAN/C++ language development is relatively simple to employ when the same versions of Visual C++ and Visual FORTRAN are used. In MTVLab, Compaq Visual FORTRAN Professional Edition 6.6.0 (Compaq Computer Corporation, Tallahassee, Florida ) and Microsoft Visual C++ 6.0 (Microsoft Corporation, Redmond, Washington) were employed to create the numerical model. Editing, debugging, linking, and compiling both software packages are accomplished transparently within Microsoft Visual Studio (Microsoft Corporation, Redmond, Washington). Special consideration, however, must be given for calling, naming, and argument passing conventions between FORTRAN and C++. In addition, if different versions of FORTRAN and C++ are used, FORTRAN code must be compiled separately, and the compiled file is required to be added to the C++ program.

### *3.6.2.6 Database – Numerical Application Connection: ODBC*

To provide an interface between applications and an underlying database, Application Programming Interfaces (APIs) are required. Microsoft SQL Server 2000 supports several classes of APIs for C++ programs: Object Linking and Embedding (OLE DB), ODBC, Embedded SQL for C, and DB-Library for C. Embedded SQL for C and DB-Library are two relatively old APIs, and no future versions of SQL Server will include the files required to perform programming on applications that use these APIs. ODBC is a platform- and database-neutral standard designed to access relational SQL data. A striking advantage of ODBC is its flexibility which makes it possible for users to replace one database program with another without extensive coding (Jansons and Cook 2002). For example, use of ODBC makes it very easy to replace SQL Server 2000 with any other database management system (DBMS) such as Microsoft Access or Oracle. OLE DB, which has evolved from ODBC, can access both relational and non-relational information. OLE DB is creating a better known presence (Ling, Yen et al. 2000); however, ODBC is still considered the more established interface. As such, ODBC is recommended for employment in web-based modeling systems, as utilized in this system.

ODBC includes an ODBC Administrator and a list of database drivers including SQL Server driver. In MTVLab, the C++/FORTRAN application calls ODBC functions to communicate with the ODBC SQL Server driver, and submit SQL statements. The SQL Server driver then translates the application's SQL statements into commands that the SQL Server understands, passes SQL statements to the data source, and returns results to the application.

### *3.6.2.7 Database – JSP Connection: JDBC*

JDBC provides connectivity between a Java program and a database. JSP, which uses Java as its underlying language, requires use of JDBC to communicate with a database. Similar to ODBC, JDBC relies on drivers, rewritten for each specific DBMS, to convert the JDBC functions to the corresponding DBMS. JDBC can be used directly in JSP pages, but this often leads to excessively large programming code. A better approach is to develop a set of custom action elements based on JDBC. In MTVLAB, custom actions developed by Bergsten (Bergsten 2001) are used to achieve JSP and database connectivity.

### *3.6.2.8 Common Object Request Broker Architecture (CORBA)*

CORBA is a platform-independent, language-independent architecture that allows applications to communicate with one another no matter where they are located. CORBA technology is employed in MTVLab to enable communication between JSP and the numerical engine. Figure 3-25 illustrates the flow of information using CORBA technology in MTVLab.

In MTVLab, users issue requests to the numerical engine via web pages employing Java Beans. Object Request Broker (ORB), the core layer of CORBA, serves as a client-server bridge, routing requests from the client (i.e. applications that send messages requesting services) to the server (i.e. applications that actually implement the requesting messages), passing model parameter information, and returning the results. To allow both client and server access to ORB, an interface must be established through an Interface Definition Language (IDL). To make the IDL interface understandable to the server-based numerical engine, it is compiled to C++ by OMNI ORB 4.0.0 (AT&T

Laboratories, Cambridge, Massachusetts), resulting in files called IDL skeletons. On the client side, Java IDL is used to compile the IDL interface to Java language used in Java Bean, and the resulting files are called IDL stubs. Skeletons and stubs serve as proxies for servers and clients, respectively.

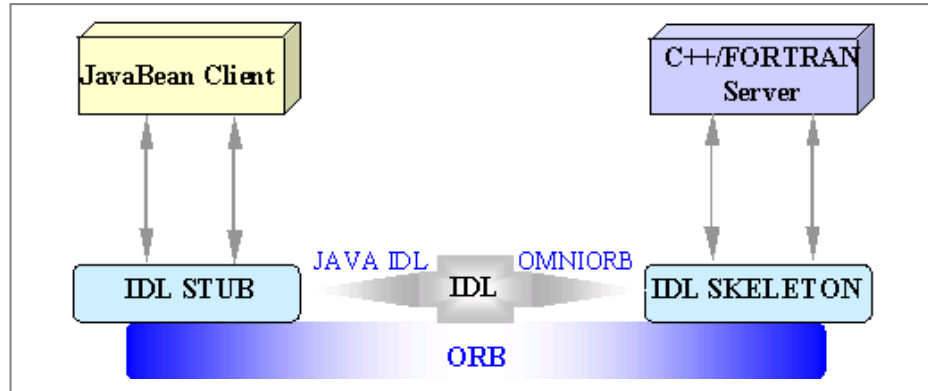


**Figure 3-25 Example CORBA Architecture.**

During operation, Java Bean client initiates a client request by calling stubs. ORB receives the call, finds the server, passes the parameters and operation, and calls the server through a skeleton. After the server completes the program execution, ORB returns the results back to the client through stubs. In MTVLab, a Naming Service, which associates clients with locations and information, is employed to locate the client and the server by their usernames. By using Naming service, the Java Bean client and the numerical engine server do not necessarily need to be installed on the same computer.

#### *3.6.2.9 Specifications for Input Interfaces*

HTML is used for building the static frame of each interface page, while JavaScripts and JSP are embedded into HTML for dynamic contents. Running at the client site, JavaScript helps create truly interactive web pages through programming, and

it is also used to validate user input before submission to the web server. Running on the server, JSP is used to develop dynamic web pages and build the bridge between web pages and the database in real time.

There are two distinguishing features of the MTVLab input system. First is the logical organization. The input interfaces are logically organized like a wizard, leading users in a step by step manner to build models. A wizard style interface is intuitive and very easy to use, which effectively avoids overwhelming users with too much information on each page (Chu 1999). The second feature is interactivity. As stated before, with JDBC technology, the input interface can communicate with a relational database in real time. For example, data input into the interface will be transmitted to a database immediately. In addition, whenever users log into their accounts, the data of their latest projects can be displayed. This automatic data retrieval mechanism is convenient in that users do not need to remember, copy, or store the models they have previously submitted. They can work whenever they want, wherever they have access to the Internet.

#### *3.6.2.10 Specifications for Output Interfaces*

The basic structure of the output interface is the same as the input interface, where HTML comprises the main static structure of the output interface, while JSP and JavaScripts provide dynamic contents. The most striking characteristic of MTVLab output is the use of Excel. There are two important reasons that Excel is used to present MTVLab output results. First, Excel is a powerful, yet easy to understand spreadsheet program for organizing, editing, and plotting data. The second reason is that Excel is the most widely used spreadsheet tool in the world (Bott and Leonhard 1999), ensuring that a

large number of users already possess familiarity with its use. As part of Microsoft Office Web Components, Excel combines seamlessly with other content in the web page. In order to dynamically generate customized Excel tables, lines, or graphs based on user requests, JDBC is used to retrieve the necessary data from the database and JSP code is used to generate the Extensible Markup Language (XML) strings which define the Excel data.

### **3.7 Summary**

Mass transfer processes form the foundation of many environmental processes including water treatment, wastewater treatment, and surface and groundwater contaminant transport modeling, and thus represent a core component of environmental engineering and science. Recent research achievements in mass transfer mechanisms at the particle scale employed evolved conceptual models, and used highly nonlinear numerical methods, which thus provide a great educational challenge. In this study, we propose to develop a Web-based modeling tool to improve mass transfer processes education, especially for better conveying state-of-the-art understanding of mass transfer mechanisms at the particle scale.

Learning theories and the use of laboratories in engineering education were utilized as a background to argue for the further development of web-based education tools. Limitations in the use of current web-based models were highlighted in terms of the need to develop more robust system architectures to address the complexity of sophisticated mass transfer numerical models. Applicability of Web-based education to mass transfer processes was addressed in the context of The Kolb Learning Cycle.



Presentation of the web-based modeling system, MTVLab, provided a proof-of-principle framework from which to develop more sophisticated Web-based models that can employ computationally efficient, high-level computer programs (e.g., FORTRAN, C++). MTVLab will help improve mass transfer processes education in several aspects, including (i) provision of an interactive problem-solving environment; (ii) improved visualization of abstract concepts; and (iii) decreased users' time devoted to mathematical or numerical modeling.

While MTVLab is able to help enhance mass transfer processes education, it cannot be used as a sole replacement to other instructional means; rather, it is intended as a complement to existing practices. MTVLab is best utilized as a means to follow-up course lectures and homework on mass transfer processes principles. Only after addressing the basic theories in class will MTVLab be able to reinforce the topics covered, and assist users' understanding through visualization of the various processes. Another consideration in the use of Web-based educational tools like MTVLab is that users' navigation within hypermedia systems can cause confusion and disorientation due to their nonlinear structure (i.e., users can jump from one location to another without any logical sequence of information presented between the two links). Web-based instructional tools may thus require a high degree of maturity on the part of the student (e.g., MTVLab is recommended for senior undergraduate or graduate-level students). Moreover, Web-based instruction provides opportunities for self-paced study. This, however, may decrease the contact time between students and teachers. Communication mechanisms between students and instructors such as on-line questionnaires and instant help should thus be included whenever possible.

## CHAPTER IV

### STOCHASTIC MODELING OF THE PERMEABILITY OF RANDOMLY GENERATED POROUS MEDIA

#### 4.1 Introduction

It is well-recognized that fluid flow in subsurface porous media is strongly influenced by spatial variability and heterogeneity (Scheidegger 1974). Proper modeling of groundwater flow within this environment thus involves capture of multiscale phenomena, including microscale- (molecular), mesoscale- (single pore), macroscale- (multiple pores), and megascale- (field) level systems. A central challenge arising from this situation is to understand how macroscale characteristics of fluid flow depend on microscale geometry of pore spaces and physical characteristics of the fluid and solid (Sahimi 1995).

Specific permeability is an important macroscale parameter representing averaged microscale characteristics of fluids and porous media. At the macroscale, specific permeability for single-phase flow can be described within the context of Darcy's law for low Reynolds numbers:

$$q = -\frac{k}{\mu}(\nabla p + \rho g \nabla z) \quad (4-1)$$

where:

$k$	=	the specific permeability [ $L^2$ ];
$q$	=	the specific flow rate [ $L/T$ ];
$\mu$	=	the viscosity of the fluid [ $M/LT$ ];
$\nabla p$	=	the pressure gradient [ $M/L^2T^2$ ];
$\rho$	=	the fluid density [ $M/L^3$ ];
$g$	=	the gravitational acceleration [ $L/T^2$ ]; and

$z$  = the vertical coordinate [L].

Furthermore, many empirical methods, such as the Hazen method and Kozeny theory (Scheidegger 1974), have related specific permeability with microscale properties of porous media, including particle size, sorting level, and porosity. For example, the Kozeny equation may be expressed as:

$$k = \frac{\phi^3}{cS^2} \quad (4-2)$$

where:

$\phi$  = porosity [-];  
 $c$  = the Kozeny coefficient [-]; and  
 $S$  = the specific surface area [1/L], defined by the ratio of particle surface area exposed to fluid per unit volume.

The heterogeneous nature of soils derived in part from the randomness of particle size distributions, porosities, and pore structures, however, suggests that soil and sediment permeability is also subject to randomness and uncertainty. This uncertainty is well-recognized, and numerous studies have employed stochastic methods to model groundwater flow in subsurface porous media by assuming a permeability probability density function, including the use of normal (Sitar, Cawlfeld et al. 1987), lognormal (Hamed, Bedient et al. 1996; Skaggs and Barry 1997; Lu and Zhang 2003), and gamma (Cooke, Mostaghimi et al. 1995; Johnston 1998) distributions. Although it is widely understood that the selection of a particular probability density function will markedly influence simulation results (Woodbury and Sudicky 1991; Cooke, Mostaghimi et al. 1995), few studies (Woodbury and Sudicky 1991; Turcke and Kueper 1996; Kennedy and Woodbury 2002) describe the manner in which to construct a permeability probability density function. These studies primarily focus on experimental determination

of probability density functions for permeability at the field scale. Developing numerically-derived distributions will be more economically efficient, although such efforts face several technical challenges, namely: (i) restriction on the computational resources available to employ numerous Monte-Carlo-type statistical simulations and (ii) difficulty in accurately capturing influences of microscale uncertainties with macroscale permeability uncertainty.

Recently, several analytical reliability approximation methods, e.g., first-order reliability method (FORM) and second-order reliability method (SORM), have been used in the environmental field to model groundwater flow and contaminant transport (Sitar, Cawfield et al. 1987; Hamed, Bedient et al. 1996; Skaggs and Barry 1996), and surface water quality (Portielje, Hvitved-Jacobsen et al. 2000; Maier, Lence et al. 2001). Possessing greater efficiency than traditional Monte-Carlo-type simulations, these methods can greatly decrease computational demands. In addition, lattice Boltzmann methods (LBM) have been applied to estimate the permeability of porous media (Rothman 1988; Zhang, Zhang et al. 2000; Pan, Hilpert et al. 2001; Manwart, Aaltosalmi et al. 2002; Keehm, Mukerji et al. 2004). Due to its ability to address fluid flow in complex micropore geometries, researchers have used LBM to help to relate microscale uncertainties with macroscale permeability uncertainty. In this paper, we present a mathematical framework to construct a probability density function for permeability that (i) employs LBM to estimate permeability based on fluid flow in complex micropore geometries, and (ii) utilizes FORM to derive the stochastic characteristics of porous media permeability. In this way, probability density functions for permeability can be constructed with reasonable computational efforts based on more easily obtained media

properties, e.g., porosity and particle size distribution. Although permeability CDFs constructed by LBM FORM in this study focus on the pore scale, this effort has the potential to provide valuable information for correctly constructing permeability CDFs at the field scale (Eggleston and Rojstaczer 2001).

Descriptions of numerical methods employed in this work follow this introduction. This discussion includes a brief introduction to porous media generation methods, the theoretical basis for use of LBM to model fluid flow, and the statistical basis for FORM, concluding with a general description of the proposed algorithm. The subsequent section exemplifies implementation of LBM FORM in several example domains of interest, including discussion of statistical properties of the generated permeability density function, and the accuracy and efficiency of the new method. Following a brief summary, the manuscript concludes by highlighting directions for further enhancements of the proposed method.

## **4.2 Numerical Methods**

### **4.2.1 Porous Media Generation**

Accurate numerical simulation of fluid flow in porous media requires detailed descriptions of porous media morphology, which should include geometric properties such as particle or pore shape and volume, and topological properties such as pore interconnectivity. In many cases, however, the type of model that can be employed is dependent on the modeling method, and more importantly, limited computational resources. It is thus important to construct models that are able to closely mimic the

heterogeneity of actual porous media, and at the same time are sufficiently efficient to allow simulation of flow and transport phenomena with reasonable computational effort. In this study, porous media are envisioned as a statistical distribution of non-overlapping circular disks representing soil particles distributed in a rectangular two-dimensional uniform continuum representing the pore space through which a fluid flows.

As first proposed by Gardner , particle size distributions in soil are often assumed to be lognormal in nature (Lerman 1979). Buchan noted that approximately one-half of the U.S. Department of Agriculture (USDA) textural classification triangle could be adequately modeled by a lognormal distribution. Since a standard lognormal distribution implies zero and infinity for the smallest and largest particle sizes, respectively, modified lognormal distributions were developed to constrain the upper and lower extremes of the particle size. Recently, Fredlund et al. proposed a new model based on a unimodal mathematical function, which is believed to provide improved representations of particle size distributions relative to lognormal distributions. This model's ease of use, however, is limited by its employment of five fitting parameters; our study thus employs a modified lognormal distribution to describe particle size distribution, assuming that all particle sizes reside in a 95% confidence interval to eliminate extremely large or small particles.

Modifying the algorithm proposed by Yang et al.(Yang, Miller et al. 1996) for a three dimensional sphere packing, a two-step collective rearrangement technique is developed to generate random porous media. First, particles with size distributions following a modified lognormal distribution are generated until the required porosity is satisfied. The particles are then assigned to a two dimensional domain by assuming a

uniform distribution of particle locations. Based on this initial, possibly overlapped configuration (i.e., one particle may overlap another particle), an iterative arrangement process is applied to achieve an overlap-free condition. During each iteration, the largest particle is selected for relocation if there is any overlap with another particle; if overlap occurs, its spatial location is adjusted until the overlap is removed, and then registered in the final non-overlap location. The procedure continues with the next largest particle, etc. until all particles are registered in their final non-overlap location. Periodic boundary conditions are maintained at all boundaries throughout the iteration process. Figure 4-1 provides an illustration of several of the generated random porous media employed in this study.

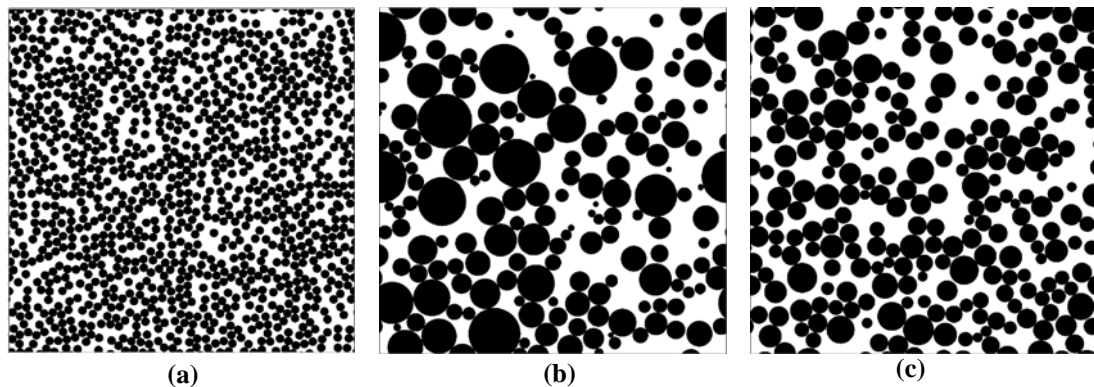


**Figure 4-1. Example Randomly-Generated Porous Media at Porosity 0.45. (a) geometric mean diameter is 25  $\mu\text{m}$  and coefficient of variation (COV) 0.01; (b) geometric mean diameter is 50  $\mu\text{m}$  and COV 0.6; (c) geometric mean diameter is 50  $\mu\text{m}$  and COV 0.3.**

#### 4.2.2 LBM Simulation

LBM (Rothman 1988; Chen and Doolen 1998; Wolf-Gladrow 2000) is a mesoscopic approach for simulating computational fluid dynamics by solving a discretized Boltzmann equation. An attractive feature of LBM is the ease of addressing

complex boundary conditions by implementing very simple schemes. Numerous works have successfully applied LBM in modeling fluid flow in porous media and quantification of porous media permeability (Rothman 1988; Cancelliere, Chang et al. 1990; Heijs and Lowe 1995; Pan, Hilpert et al. 2001).

LBM models fluids as particle distributions residing on a discrete lattice, propagating to their adjacent lattice nodes, and colliding with other particles to redistribute momentum. In this study, a two-dimensional, nine-velocity lattice model (D2Q9) (Wolf-Gladrow 2000) is employed.. The evolution process can be expressed by the equation:

$$f_i(\bar{x} + \bar{c}_i, t + 1) = f_i(\bar{x}, t) + \frac{1}{\tau} [f_i^{eq}(\bar{x}, t) - f_i(\bar{x}, t)] \quad (4-3)$$

where,  $f_i$  represents the particle distribution in position  $\bar{x}$  at time  $t$ , moving with velocity  $\bar{c}_i$ ,  $\tau$  is the relaxation time which controls the rate of approach towards equilibrium, and  $f_i^{eq}$  is an equilibrium distribution parameter. It has been shown (Chen, Chen et al. 1992) that the Navier-Stokes equation can be recovered from this discretized Boltzmann equation for incompressible flow, with a truncation error proportional to the square of the Mach number ( $M_a = u / c_s$ , where  $u$  is the characteristic flow velocity, and  $c_s$  is the speed of sound (usually set to  $1/\sqrt{3}$  for the D2Q9 model)). The density per node,  $\rho$ , the macroscopic velocity,  $\bar{u}$ , the fluid pressure  $P$ , and the kinematic viscosity  $\nu$  are defined by

$$\rho = \sum_i f_i; \quad \rho \bar{u} = \sum_i f_i c_i \quad ; \quad P = \rho c_s^2 \quad ; \quad \nu = c_s^2 \left( \tau - \frac{1}{2} \right) \quad (4-4)$$



A non-slip boundary condition is imposed at the solid and liquid interfaces by implementing a bounce-back rule that reverses the momentum of particles approaching the solid wall. Periodic boundary conditions are maintained at the inlet and outlet of the domain. A pressure gradient is imposed by maintaining a density difference between the inlet and the outlet of the simulation domain; thus at very small Reynolds numbers, the permeability of simulated porous domains can be estimated by Darcy's law based on the imposed pressure gradient and specific flow rate derived from LBM simulation.

#### 4.2.3 FORM

FORM originated from reliability analysis in structural engineering, and is an attractive alternative to computationally intensive Monte Carlo methods (Sitar, Cawlfeld et al. 1987). In this paper, we implement FORM to construct permeability cumulative distribution functions (CDFs) for randomly generated porous media. A description of the FORM procedure is presented below.

In reliability analysis, a function  $M(x_1, x_2, \dots, x_n)$  is often formulated to describe the performance of a system. The system performance is considered in terms of two states, 'failure' or 'safe', depending on whether the performance function is less than or greater than zero, respectively. A limit state surface may then be defined as the boundary between the failure and safe regions, i.e.,  $M(x_1, x_2, \dots, x_n) = 0$ . In this study, the performance function evaluates whether the calculated permeability of a simulation domain is smaller than some selected target value  $g_i$ :

$$M(x_1, x_2, \dots, x_n) = G(x_1, x_2, \dots, x_n) - g_i \quad (4-5)$$

The limit state surface may thus be defined at  $G = g_i$ . The probability of failure, i.e.,  $G$  is less than  $g_i$ , can be defined:

$$F_G(g) = p(G \leq g_i) = \int \dots \int_{G \leq g} f_X(x_1, x_2, \dots, x_n) dx_1 dx_2 \dots dx_n \quad (4-6)$$

where  $f_X(x_1, x_2, \dots, x_n)$  is the joint probability density function for random variables  $x_1, x_2, \dots, x_n$ . Equation 4-6 is difficult to evaluate for many reasons, including (i) difficulty of evaluating multidimensional integration, (ii) lack of statistical information for the joint probability density function,  $f$ ; and (iii) the complexity in evaluating the performance function. The objective of FORM is to derive an estimation of  $F_G$  based on a first-order Taylor series expansion of the performance function.

If random variables,  $x_i$ s, are correlated non-normal functions, they should be transformed to the space of uncorrelated reduced normal functions (Haldar and Mahadevan 2000). On the transformed limit state surface, the point closest to the origin is defined as the ‘design point’, representing the most likely failure point. This minimum distance from the origin in the transformed space can be computed as

$$\beta = -\bar{\alpha}^T \cdot \bar{x}^* \quad (4-7)$$

where,  $\alpha$  is a unit vector normal to the limit state surface and directed toward  $G < g_i$ , and  $x^*$  is the design point . The first-order approximation of the failure probability can be obtained as:

$$p(G \leq g_i) = \Phi(-\beta) \quad (4-8)$$

where  $\Phi()$  is the standard normal cumulative probability operator (Haldar and Mahadevan 2000). This approximation is accurate if the limit state surface is nearly flat in the neighborhood of the design point.

The design point is determined by solving an optimization problem that minimizes the distance from the origin in the reduced normal space to the limit state surface. A Newton-Raphson-type recursive algorithm, proposed by Rackwitz and Fiessler (Rackwitz and Fiessler 1978), as described in equation 4-8, is implemented here:

$$\bar{x}'_{k+1} = \frac{1}{|\nabla G(\bar{x}'_k)|^2} [\nabla G(\bar{x}'_k)^t \bar{x}'_k - G(\bar{x}'_k)] \nabla G(\bar{x}'_k) \quad (4-9)$$

where,  $k$  denotes the iteration number, and  $\nabla G(\bar{x}'_k)$  represents the gradient vector of the performance function at  $\bar{x}'_k$ . The Rackwitz-Fiessler method linearizes the performance function at each iteration point, and uses the derivatives to find the next iteration point. The entire CDF can be constructed by repeating this FORM procedure to estimate the probability of the calculated permeability is smaller than a series of  $g_i$  values in equation 4-8.

In many applications, FORM requires only a small number of iterations for convergence. When the performance function is in implicit or numerical form, however, extra effort, for example, a finite difference scheme (equation 4-10), may be required to derive the gradient of the performance function.

$$\frac{\partial G(\bar{x})}{\partial x_i} = \frac{G(x_i + \Delta x_i) - G(x_i - \Delta x_i)}{2\Delta x_i} \quad (4-10)$$

Here, the step,  $\Delta x_i$ , is chosen as a small fraction of the standard deviation of random variables. Thus, the number of function evaluations required by each iteration of FORM will be  $2n+1$ , where  $n$  is the number of random variables.

#### 4.2.4. Proposed Algorithm

Since porosity data are widely available for many soil types and it can be accurately and routinely determined in laboratories, porosity statistics are generally easier to obtain than statistics for porous media permeability. An underlying assumption of this work is that the porosity of the simulated domain is a random variable. Figure 4-2 presents a summary flowchart describing the proposed algorithm, as detailed below. First, an initial value for porosity is generated based on the probability distribution of the random variable porosity; it is then combined with a given particle size distribution to generate a random porous medium. LBM is then implemented to estimate the permeability of the generated domain. Based on the particular porosity and the particle size distribution, the resulting micropore configuration is subject to uncertainty. With sufficiently large numbers of samples, however, the average permeability of randomly-generated porous media will approach a constant value dependent only on the porosity and the particle size distribution (Koponen, Kataja et al. 1997). The simulation is considered converged if the relative error of the average permeability corresponding to the value derived from the previous number of samples is consistently less than 1% for five consecutive iterations. In this study, we found at least 25 samples were required to achieve a stable average permeability. Upon determination of an average permeability, the Rackwitz-Fiessler formula is employed to calculate the probability that the average permeability of the randomly-generated porous media is smaller than a  $g_i$ . As illustrated in Figure 4-2, a particle size distribution is employed, but it is utilized to generate porous medium configurations as part of the performance function. Porosity is thus the only random variable for FORM input. In this situation, the Rackwitz-Fiessler iteration scheme

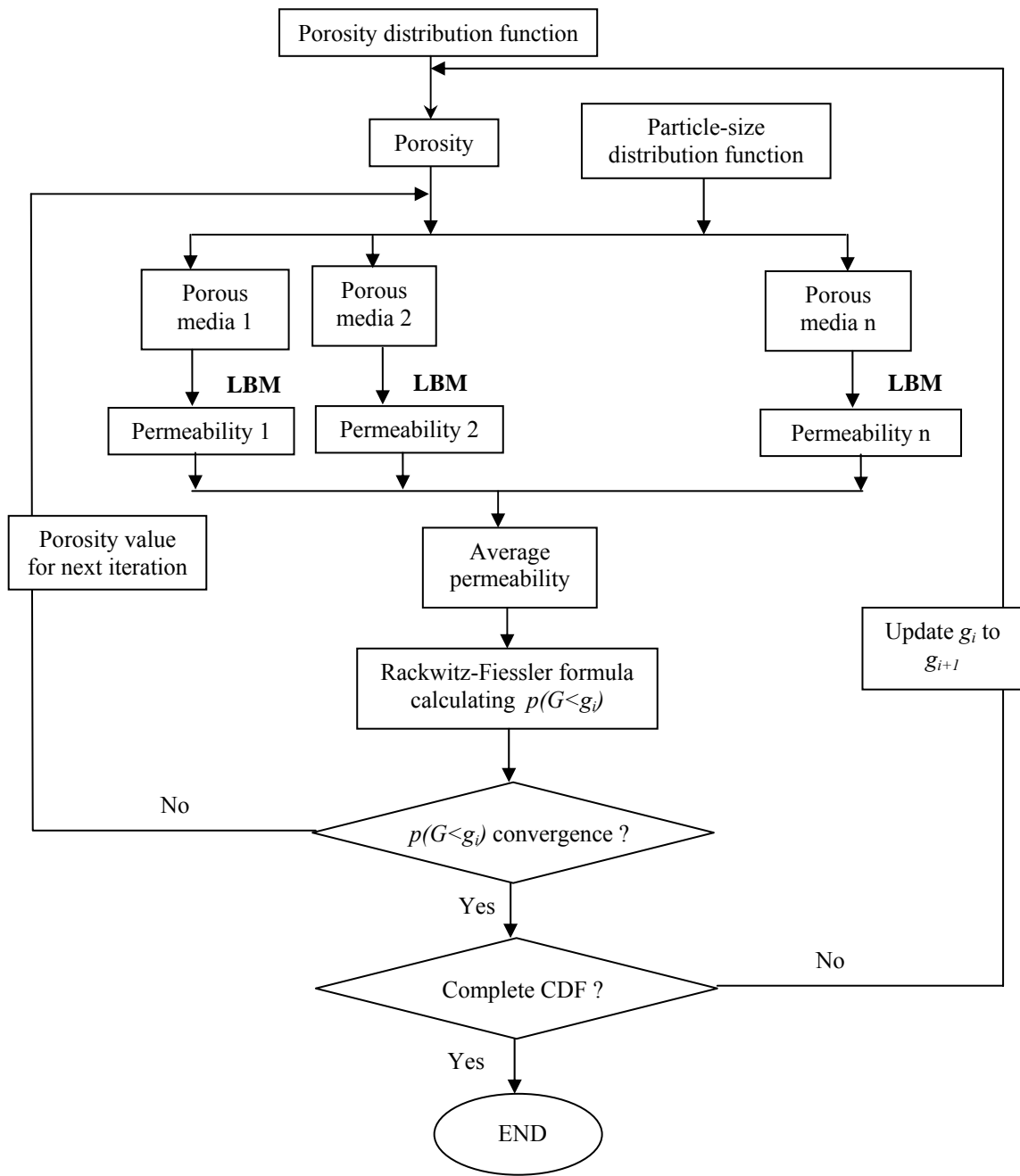


**Figure 4-2. Flow Chart for the LBM FORM Algorithm.**

(Rackwitz and Fiessler 1978) becomes a one dimensional Newton formula as expressed in equation 11:

$$x'_{k+1} = \frac{1}{\frac{\partial G(x'_k)}{\partial x}} \left[ \frac{\partial G(x'_k)}{\partial x} x'_k - G(x'_k) \right] \quad (11)$$

Points on the CDF curve corresponding to  $g_i$  are generated when the Rackwitz-Fiessler iteration scheme achieves convergence. Repeating this procedure for a series of  $g_i$  values enables the construction of the entire CDF.

### 4.3 Illustrative Examples

#### 4.3.1 Example Model Domains

Simulations included use of randomly-generated porous media with domain size 1 mm × 1 mm, and geometric mean particle diameters of 25 μm, 50 μm, and 100 μm, depicting particle sizes representative of very coarse silt to very fine sand. The particle size distribution employs a modified lognormal distribution, using a 95% confidence interval for particle size to eliminate extreme values. The influence of particle sorting characteristics on permeability was also examined by varying the coefficient of variance (COV) of the particle diameters, i.e., COV of 0.01, 0.31 and 0.66, which correspond to very well-sorted, moderately sorted, and poorly sorted sediments. Summaries of the particle size distributions for simulated domains are listed in Table 4-1, while illustrations of the domains are presented in Figure 4-1.

**Table 4-1. Particle Size Distribution Parameters Employed in This Work.**

<b>Geometric Mean Diameter (<math>\mu\text{m}</math>)</b>	<b>COV</b>	<b>Rmax/Rmin</b>	<b>Sorting</b>	<b>Lattice Size</b>
25	0.01	1.04	Very well sorted	800 x 800
50	0.01	1.04	Very well sorted	400 x 400
	0.31	3.24	Moderately sorted	400 x 400
	0.66	10.51	Poorly sorted	540 x 540
100	0.01	1.04	Very well sorted	300 x 300

#### 4.3.2. Evaluations of the LBM Model

A series of numerical simulations were conducted to evaluate LBM accuracy, its ability to estimate permeability, and numerical resolution requirements for the aforementioned example domains. Poiseuille flow was first simulated to test the accuracy of the LBM model. Numerical experiments with different channel widths were performed while holding the relaxation time,  $\tau$ , and Reynolds number,  $R_e$ , constant. Relative errors for the whole channel are calculated as

$$\varepsilon = \frac{1}{N} \sqrt{\sum_{i=1}^N (u_i^{(n)} - u_i^{(a)})^2}, \quad (4-12)$$

where  $N$  is the number of lattice nodes along the channel width, and  $u_i^{(n)}$  and  $u_i^{(a)}$  are the numerical and analytical solutions, respectively. The relative error and the channel width present a linear relationship with a slope of  $-2.1$  on a log graph, which indicates a second order convergence of this LBM model in the spatial discretization, as described elsewhere (Maier, Kroll et al. 1998; Wolf-Gladrow 2000; Pan, Hilpert et al. 2001). The influence of  $\tau$  on the accuracy of the LBM model was verified by numerical experiments employing different  $\tau$  values from 0.6 to 1.2 with a step size of 0.2, which provide a local minimum of the relative error at  $\tau = 0.8$ .

To investigate the ability of LBM to accurately estimate permeability, LBM was employed with the randomly generated porous media under varying pressure gradient conditions. A linear relationship between pressure gradient and specific rate is identified with a low Reynolds number, i.e.,  $R_e < 0.01$ , which is consistent with applicable regions for Darcy's law (Bear 1972; Rothman 1988). In this study,  $R_e$  is restricted to values less than 0.01, and permeability is estimated as the ratio of flow rate and pressure gradient. Effects of spatial discretization on permeability estimation for randomly generated porous media were investigated by varying the density of numerical grids on simulation domains. Results indicate that estimated permeability converges to a stable value with increasing spatial resolution, as stated elsewhere (Maier, Kroll et al. 1998; Pan, Hilpert et al. 2001). For COV of 0.01 and 0.31, the number of grids per mean particle diameter,  $m$ , should be greater than 20 to achieve convergence on  $k_s$ , while  $m$  should be greater than 27 to achieve convergence for COV of 0.66. Specific lattice sizes employed in LBM simulations are listed in Table 4-1.

## **4.4 Numerical Results**

### **4.4.1 Permeability Statistics**

For the purpose of simplicity, a normal distribution with mean of 0.5 and COV of 0.12 is assumed for the random variable porosity. Under this condition, the probability of a negative porosity is as small as  $1.5e-5$ . A summary of statistical properties of the derived CDFs for the sample domains is presented in Table 4-2. The influence of particle



size distributions on permeability CDFs are further illustrated in Figure 4-3 and Figure 4-4.

**Table 4-2. Statistical Properties of Derived Permeability CDFs.**

Geometric Mean Diameter ( $\mu\text{m}$ )	Diameter COV	Permeability Mean (Darcy)	Permeability COV	Chi-Square Test Significance Level		
				Normal	Lognormal	Gamma
25	0.01	1.54	1.36	0.04	0.001	0.11
50	0.01	6.22	1.30	0.007	1E-05	0.015
	0.31	8.71	1.10	0.002	2E-06	0.002
	0.66	12.11	1.00	0.02	1E-04	0.16
100	0.01	17.36	1.54	0.048	0.0004	0.01

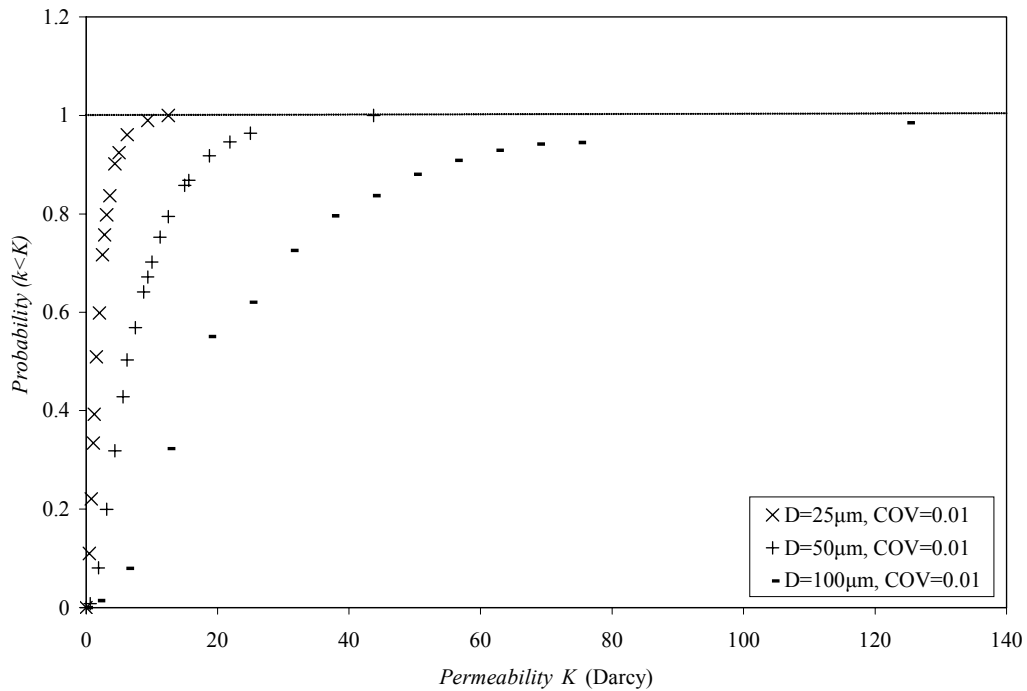


**Figure 4-3. Influence of Particle Mean Diameter on Porous Media Permeability CDF for Domains with Geometric Mean Particle Diameter  $D = 50 \mu\text{m}$  and Differing COV.**

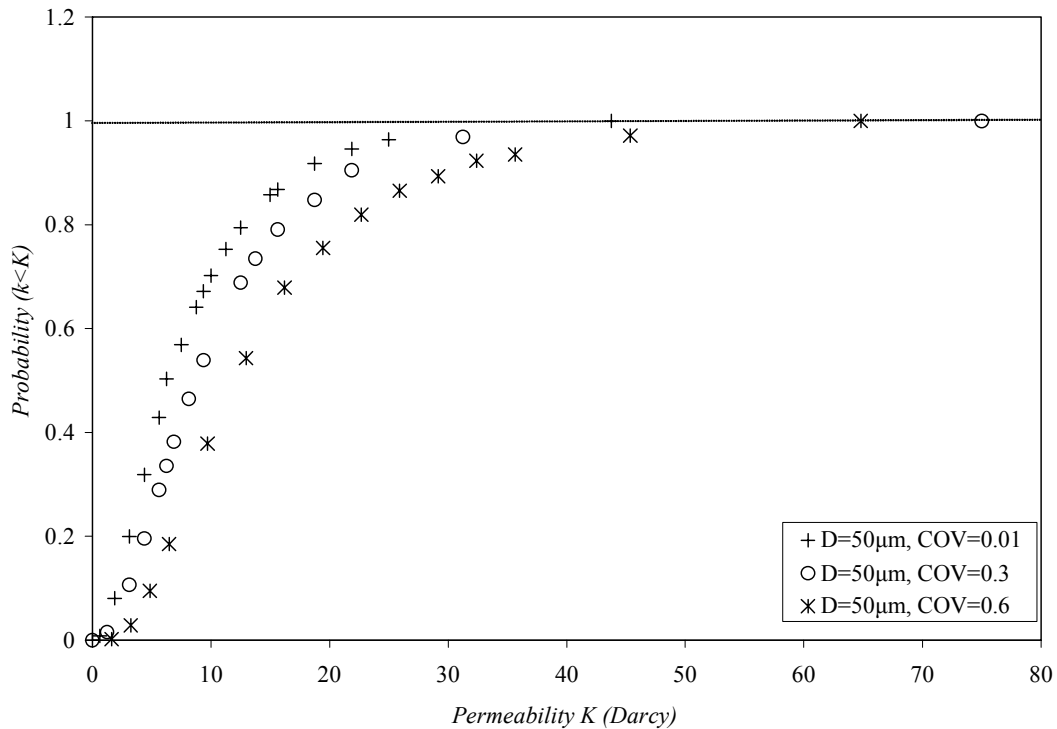


**Figure 4-4. Influence of Particle Sorting on Porous Media Permeability CDF for Domains with Geometric Mean Particle Diameter  $D = 50 \mu\text{m}$  and Differing COV.**

First, it is observed that domains with larger particle mean diameters or higher particle diameter COVs possess larger mean permeability values and higher probabilities of achieving larger permeability values. This phenomenon can be explained in terms of specific surface area, or the ratio of particle surface area in contact with fluid per unit volume. Specific surface areas are larger for the domains, which are well sorted or possess smaller particle mean diameters. Higher specific surface areas suggest greater surface area in contact with fluid, causing increased frictional resistance to fluid flow, thus leading to a reduction in permeability.

Second, it is shown in Table 4-2 that permeability COVs of all domains generally lie in the range of 1.0 to 1.5, which is about 10 times larger than the porosity COV of

0.12. This suggests that permeability is subjected to greater uncertainty than porosity. In addition, permeability COVs of domains with mean diameter 50  $\mu\text{m}$  range from 1.0 to 1.3, although the particle diameter COVs change 66 times from 0.01 to 0.66. This indicates that, although the particle diameter COV will influence the permeability mean value, it will not directly affect the uncertainty of permeability. We believe it is the uncertainty of micropore structure configurations derived from porosity and particle size distributions that actually lead to the larger uncertainties in permeability.

#### 4.4.2 Applicability of Permeability Distributions

Chi-square tests were applied to the derived permeability CDFs based upon normal, lognormal, and gamma distributions. The chi-square test significance levels are listed in Table 2, where a smaller significance level suggests that the model result is less significantly different from the given probability function, representing a better model fit. In this work, a lognormal distribution appears to provide the lowest significance level for all five modeling domains. Further exploration of the ability of normal, lognormal, and gamma distributions to describe permeability is provided in Figure 4-5, which illustrates corresponding CDFs utilizing LBM FORM derived mean and COV.

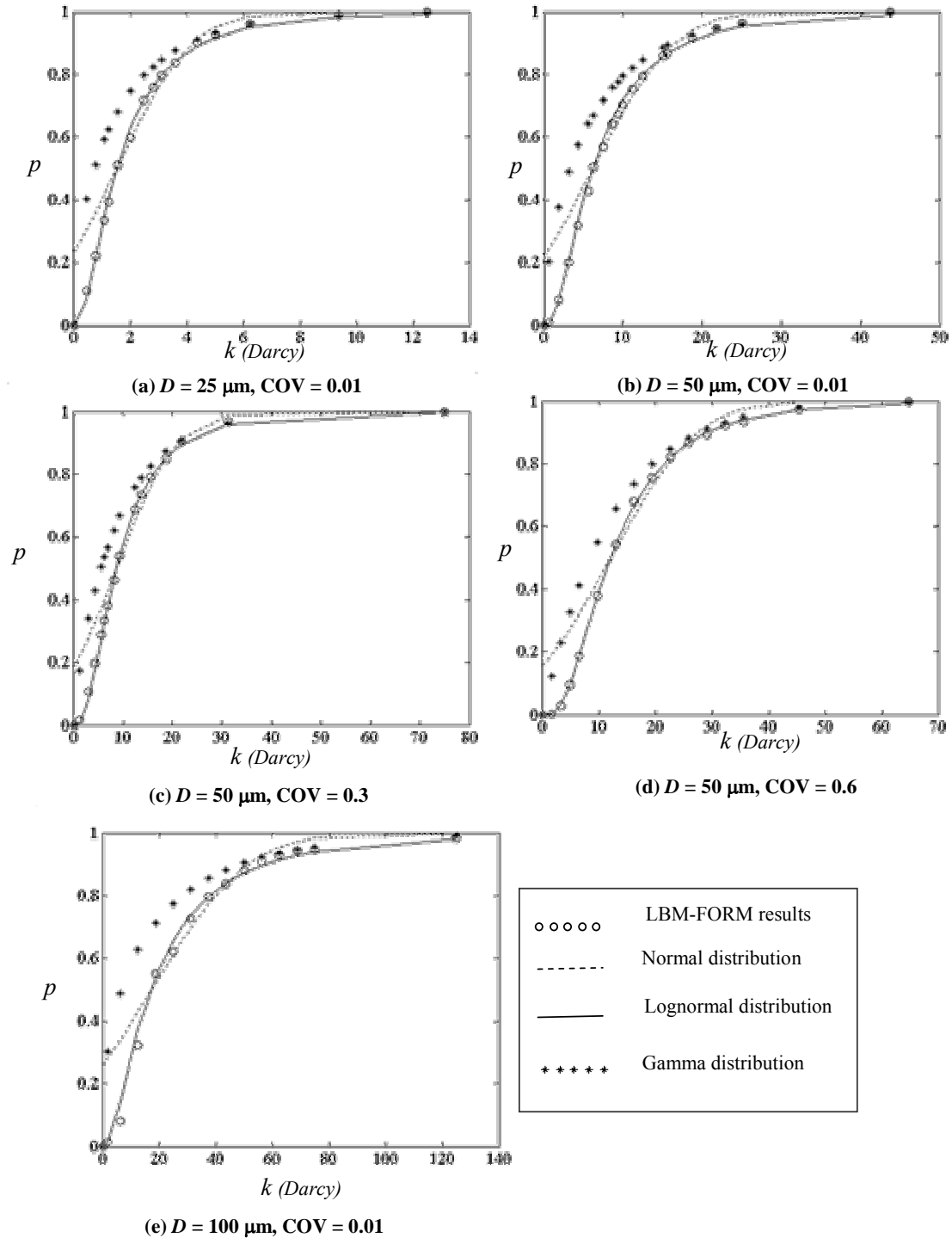


**Figure 4-5. Comparison of FORM-Derived Permeability CDF with Most Commonly Used Normal Distribution CDF, Gamma Distribution CDF, and Lognormal Distribution CDF on the Simulation Domains with Differing Geometric Mean Particle Diameter and COV.**

It is clear that normal distributions fail to represent the LBM FORM results at low probability, which can be attributed to normal distributions' allowance for the negative permeability values at extremely low probability. Although the Gamma distribution is limited to only positive values of permeability, it appears to overestimate the probability for the lower permeability. The failure of the Gamma distribution is likely associated with the constant nature of COV, i.e., the Gamma distribution  $COV = 1/\sqrt{2}$ , regardless of the mean value, which is incapable of fully describing the high uncertainty of porous media permeability. In this study, the lognormal distribution performs very well in describing the FORM-derived permeability CDF both at low and high probability regions, which are actually implied from two important characteristics of the lognormal distribution (i) exclusion of negative values and (ii) high right skewness. The applicability of the lognormal distribution to permeability in this study also agrees well with Woodbury and Sudicky (Woodbury and Sudicky 1991), who evaluated more than 1000 samples for the Borden aquifer, suggesting that the lognormal distribution can be employed to describe the permeability distribution.

#### 4.4.3 Comparison with Monte Carlo Simulations

Monte Carlo simulation is a useful tool capable of addressing stochastic problems when only a basic working knowledge of probability and statistics is available. Given sufficient simulations, the Monte Carlo method can provide accurate simulation results in a simple but computationally demanding manner (Haldar and Mahadevan 2000). Evaluation of the necessary number of simulations required to guarantee the accuracy is thus critical in the proper employment of the Monte Carlo method. As opposed to

common approaches that establish the number of model runs based upon experience or simplified tests, this study determined the required number of simulations by relating it to the relative error and probability based on equation (Haldar and Mahadevan 2000),

$$\varepsilon\% = \sqrt{\frac{(1-p)}{N \times p}} \times 200\% \quad (4-13)$$

where,  $\varepsilon$  is the error,  $p$  is probability and  $N$  is the number of simulations required. This equation was derived by considering the number of failures in  $N$  trials as a binomial distribution, then approximating the binomial distribution with a normal distribution, and estimating the 95% confidence interval of the estimated probability of failure .

For the purpose of validation, Monte Carlo simulations were implemented on the domain with a particle mean diameter of 25  $\mu\text{m}$  and  $\text{COV} = 0.01$ . Equation 4-13 indicates that, for  $p = 0.1$ , at least 14,400 Monte Carlo runs are required to achieve an error less than 5%. As discussed in Section 4.2.4, the uncertainty of micropore structures for a given porosity and particle size distribution necessitates at least 25 simulations of different configurations to achieve a stable average permeability. 360,000 LBM simulations will thus be required to construct a CDF for  $p > 0.1$ . In this study, the computing time required for LBM modeling of permeability depended on permeability values, varying from 0.5 to 10 hours on a Dell Precision 650 Workstation; with longer convergence times associated with higher permeability domains or denser numerical discretization resolutions. It is thus not feasible to perform all 360,000 LBM simulations due to computational limitations. Our approach to overcome this problem included (i) performing a smaller number of simulations based on available computing resources and (ii) quantitatively defining the relative error of Monte Carlo results based on equation 12, which serves as a basis to evaluate the relative accuracy of LBM FORM results.

1,600 Monte Carlo runs were computed, corresponding to 40,000 LBM simulations. Constructed CDFs are plotted in Figure 4-6 and compared well with FORM results. When the probability exceeds 0.4, the largest relative error between the two methods is approximately 3.4%. The largest relative error for the entire CDF is 8.5%, occurring at the point  $p = 0.12$ , the smallest probability point simulated. Based on Equation 12, 1600 Monte Carlo runs will provide an error of less than 6% for probabilities larger than 0.4, and an error of 13.5% for  $p = 0.12$ . LBM FORM results are thus within the relative error range of the Monte Carlo method, suggesting the relatively high accuracy of this method.

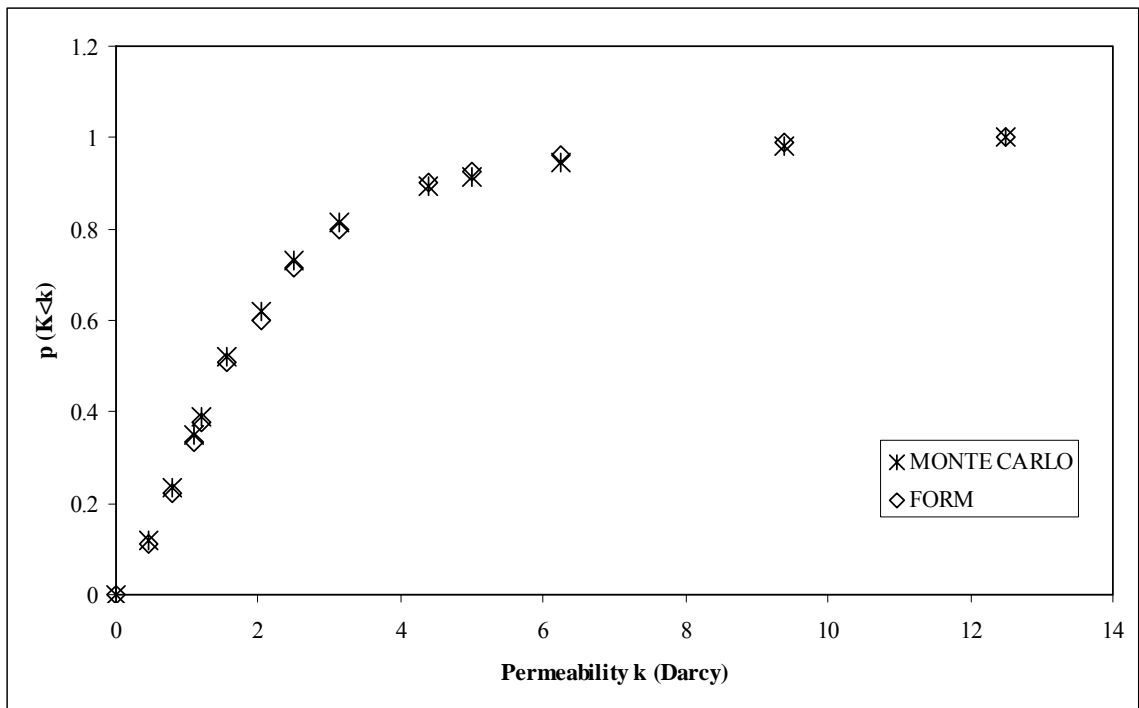


**Figure 4-6. A Comparison of Monte Carlo Simulation Results and FORM Results for the Simulation Domain with Particle Mean Diameter  $D = 25 \mu\text{m}$  and COV = 0.01.**

The FORM method employed in this work can achieve convergence within two to six iterations. Each iteration involves 3 function evaluations to calculate average permeability and gradient values. Although 15 points were used to construct the CDF employed in this work, 10 points are usually sufficient to generate a CDF (Haldar and Mahadevan 2000). Assuming an average of 4 FORM iterations to achieve convergence, 3 function evaluations for calculating average permeability and its gradient values, and 10 points on a CDF, approximately 120 averaged permeability values must be computed to construct a CDF through FORM. This is approximately 1/13 times the 1,600 Monte Carlo simulations used in this study, and approximately 1/120 times the required 14,400 Monte Carlo simulations needed to construct a CDF possessing an error less than 5% when  $p > 0.1$ , indicating the relatively high efficiency of LBM FORM relative to Monte Carlo simulations.

#### **4.5 Summary**

Permeability, as a function of particle size distribution, porosity, and packing, is often the greatest source of uncertainty in simulating fate and transport of contaminants in the subsurface environment. Although permeability has previously been assumed as a random variable in groundwater modeling, the restriction on computational resources and the difficulty in relating microscale and macroscale uncertainties have resulted in reduced efforts to construct probability density functions for permeability. In this study, we proposed a new approach, LBM FORM, based on more easily derived porosity statistics and particle size distribution, to construct permeability CDFs through the combination of LBM and FORM.



LBM FORM was implemented to construct permeability CDFs of five randomly generated porous media; each possessing different particle size distributions. Results show that the domains with larger mean particle diameter or higher particle diameter COV tend to possess a higher probability of achieving larger permeability. Permeability values are subjected to higher uncertainty than the porosity and particle diameters because of the uncertainty of the micropore structure configurations. Lognormal distributions modeled well the permeability CDF constructed for a variety of domains examined in this study. Accuracy of the proposed method was confirmed by comparison with Monte Carlo simulations for one example simulation domain. The largest relative error is approximately 3.4% when the probability exceeds 0.4, and is 8.5% when probability is less than 0.4, both of which are within the relative error associated with the Monte Carlo method. Further, this work demonstrated that the Monte Carlo method is severely limited by computational requirements, making it extremely difficult to accurately construct an entire permeability CDF curve by Monte Carlo; LBM FORM, however, was found to be approximately 13 to 120 times more efficient than traditional Monte Carlo simulations.

The primary contribution of this effort derives from the development of a new approach to calculate permeability CDFs by combining LBM and FORM. Although it provides higher accuracy and efficiency than Monte-Carlo simulations, it is worthy to note several directions for enhancements of the method. First, the LBM method implemented in this study is in the BGK form (Bhatnagar, Bross et al. 1954) with a linear collision operator. The accuracy of permeability based on BGK LBM is dependent on the fluid viscosity and thus on the relaxation time. We chose an optimized value of the

relaxation time  $\tau$  ( $\tau = 0.8$ ) to eliminate this dependency. In the future, we suggest the use of more sophisticated LBM schemes to simulate fluid flow in porous media. For example, a two relaxation time (TRT) LBM (d'Humieres, Ginzburg et al. 2002; Lallemand, d'Humieres et al. 2003) will be able to annihilate the permeability dependence on the viscosity with a specific choice of the free eigenvalues. Further, the convergence rate is accelerated when using higher viscosity values for a TRT LBM. A second potential enhancement of the method is associated with the reliability method employed. While FORM performed well in example domains in this study, more advanced methods, such as SORM or other modified forms of FORM, might be required for situations that are more complicated. Finally, the simulation results in this work are based on randomly generated, two-dimensional simplified porous media. Future modeling efforts will benefit from use of more sophisticated porous media packing modules to more closely reflect actual field situations. Applications of the proposed framework with more sophisticated LBM and reliability methods for three-dimensional porous media should greatly assist future researchers in advancing fundamental understanding of the primary factors influencing permeability within porous media.

## CHAPTER V

### A LEAST SQUARES FINITE ELEMENT SCHEME FOR LATTICE BOLTZMANN METHOD ON UNSTRUCTURED MESHES

#### 5.1 Introduction

In the last decade, LBM has been developed as an effective tool to simulate complex fluid flow problems (Benzi, Succi et al. 1992; Chen and Doolen 1998). Historically, LBM originated from lattice gas automata (LGA), which views fluids as arrays of particles residing on a discrete lattice, evolving with specific interactive propagation and collision rules. Improvements to LBM relative to LGA include extending single particle occupation variables to particle distribution functions (McNamara and Zanetti 1988), developing of a linearly stable collision operator (Higuera, Succi et al. 1989; Higuera and Jim'enez 1989), and utilizing a single time relaxation approximation (Chen, Chen et al. 1991), which provides LBM an improved capability to eliminate statistical noise and enhanced computational efficiency. LBM, similar to LGA, however, is restricted to uniform lattice structures, which severely limits its potential application to many practical problems, e.g., flow in porous media, where representations of complex pore geometry require a very fine uniform lattice, thus necessitating additional computing resources (Succi, Amati et al. 1995). More recently, it was determined that, although the coupling between discretization of velocity spaces and physical spaces is an essential part of LGA dynamics, it is not critical for LBM (Sterling and Chen 1996). It is in this light that many efforts were forwarded to improve LBM such that it is able to more flexibly apply to non-uniform grids. Those improvements can be classified as: (i) interpolation

techniques; (ii) grid refinement techniques; and (iii) numerical lattice Boltzmann methods.

Interpolation techniques, first proposed by He, Luo, and Dembo (He, Luo et al. 1996), extend LBM to non-uniform rectangular meshes by interpolating the density distribution at the grid sites from the square lattices. An extension of this technique is a Taylor-series expansion and least-squares-based LBM proposed by Shu, Niu, and Chew (Shu, Niu et al. 2002). Instead of direct interpolation, a Taylor series expansion is implemented to estimate the density function at the grid sites, and a least-squares scheme is implemented to minimize errors. Although this approach removes the rectangular shape restriction and possesses a meshless feature, collisions still take place on the grid points. More recently, a local time step technique (Imamura, Suzuki et al. 2005) was applied to this interpolation supplemented LBM, which greatly reduces CPU time required to obtain steady-state solutions.

Grid refinement techniques refine the lattice locally where more precision is required or the geometry is more complex, passing the data between fine and coarse lattices via a particular algorithm. Filippova and Hänel (Filippova and Hanel 1998) coupled LBM with a local second order hierarchical grid refinement and boundary fitting scheme. The new approach not only possesses an improved ability to treat curved boundaries, but also provides higher computational accuracy, especially in thin boundary layers where solutions possess highly anisotropic features. Utilizing a multigrid architecture, Lin and Lai (Lin and Lai 2000) proposed a composite block-structured LBM, which allows one-way interaction at the post-streaming stage without rescaling the discrete distribution function. Pointing out that Lin's algorithm is inaccurate, and that

Filippova's approach presents singularity for  $\tau = 1$ , Dupuis and Chopard (Dupuis and Chopard 2003) proposed an alternative grid refinement algorithm, which can accelerate the flow settlement process a thousand times faster than a single grid resolution. Grid refinement techniques present a promising direction for the development of LBM; however, its limited application to regular rectangular grid structures restricts the flexibility of these methods.

Numerical lattice Boltzmann methods combine LBM with traditional numerical methods such as finite difference (FD), finite volume (FV), and finite element (FE) methods to increase computational efficiency and accuracy, while adapting LBM to irregular mesh. Based on Runge-Kutta time discretization and various spatial discretization schemes, Chen and coworkers (Cao, Chen et al. 1997; Chen 1998) combined FD and LBM in number of ways. The central difference scheme was first proposed by Cao et al. (Cao, Chen et al. 1997) in Cartesian coordinates, and was later extended to curvilinear coordinates with non-uniform grids (Mei and Shyy 1998). Nannelli and Succi (Nannelli and Succi 1992) proposed the first finite volume formulation of LBM. Later, Amati, Succi, and Benzi (Amati, Succi et al. 1997) presented a finite volume formulation of the LBM, where a piece-wise linear interpolation scheme was used to estimate the volume-averaged particle distribution in a non-uniform coarse lattice. Another volumetric formulation of LBM was developed by Chen (Chen 1998), which can be applied to arbitrary mesh while achieving exact adherence to conservation laws and equilibrium conditions (Chen 1998). Peng and co-workers (Peng, Xi et al. 1998; Peng, Xi et al. 1999; Xi, Peng et al. 1999) proposed additional versions of the finite volume LBM (FV-LBM) using both triangular and rectangular elements, which appears

to be flexible for both internal and external boundaries. More recently, this method was further developed from both theoretical and practical aspects by S. Ubertini and coworkers (Ubertini, Bella et al. 2003; Ubertini and Succi 2005), who demonstrated that the method does not present significant numerical viscosity effects (at the second order) in the mesh size. As an early effort to combine FE methods with LBM, Lee and Lin (Lee and Lin 2001; 2003) presented a characteristic Galerkin discrete Boltzmann equation (CGDBE), which implements a Taylor-Galerkin procedure.

Traditionally, FE methods (Strang and Fix 1973) have allowed simulation of more complex, and hence, realistic geometries relative to FD and FV methods. In standard Computational Fluid Dynamics (CFD), FV methods, however, are more widespread. A significant reason lies in the nature of the convection operators of fluid flow, which are first order, and thus non-self-adjoint. For equations with non-self-adjoint operators, the classical Galerkin method is often corrupted by spurious oscillations or wiggles (Jiang 1998). Least-squares finite element (LSFE) method, on the other hand, was recently shown to be a robust and efficient way to solve non-self-adjoint equations. It always leads to symmetric, positive definite, linear systems of equations without using techniques such as upwinding, staggered grids and operator splitting techniques (Ding 1999). Compared with Taylor-Galerkin-based FE methods, LSFE method possesses improved stability. Furthermore, for more complex systems, Taylor-Galerkin-based FE methods may promote oscillations at discontinuities (Jiang 1998) or at solid-liquid interfaces with boundary layers or high velocity gradients. Those oscillations may be suppressed by adding dissipation terms like those in 'upwind' and 'artificial viscosity' schemes, which, however, are dependent on the specific parameters of the problem. For non-self-adjoint

systems, such as the lattice Boltzmann equation, it is thus reasonable to apply LSFE, which represents a promising approach to extend LBM to more practical and complex domains while simultaneously benefiting from finite element methods' superior stability and flexibility. It is in this light that we implement a new FE-LBM, which utilizes LSFE in space and a Crank-Nicolson scheme in time.

This chapter details the derivation and example applications of LSFE-LBM. Subsequent to this introduction, a numerical formulation section, including a numerical derivation of the LSFE-LBM and a discussion of important implementation issues, is presented, followed by a thorough theoretical analysis of the accuracy and stability of the method. The implementation of LSFE-LBM is exemplified through two-dimensional incompressible Poiseuille flow, Couette flow, flow past a circular cylinder, and flow in porous media. The chapter concludes by summarizing the advantages of the LSFE-LBM, and a discussion of its future potential.

## 5.2 Numerical Formulations

### 5.2.1 Numerical Derivation

The starting point of LSFE-LBM is the discrete lattice Boltzmann equation

$$\frac{\partial f_i}{\partial t} + \bar{c}_i \cdot \bar{\nabla} f_i = \Omega_i \quad (i = 1, 2, \dots, N) \quad (5-1)$$

where  $f_i$  represents the particle velocity distribution function,  $\bar{c}_i$  is the velocity along the  $i$ -th direction,  $N$  is the number of different velocities in the model, and  $\Omega_i$  denotes the

collision operator which is commonly approximated by the Bhatnagar-Gross-Krook model (Bhatnagar, Gross et al. 1954)

$$\Omega_i = -\frac{1}{\tau}(f_i - f_i^{eq}) \quad (5-2)$$

where  $\tau$  is the relaxation time,  $f_i^{eq}$  is the local equilibrium given by

$$f_i^{eq} = \rho \omega_i \left( 1 + \frac{\bar{u} \cdot \bar{c}_i}{c_s^2} + \frac{(\bar{u} \cdot \bar{c}_i)^2 - c_s^2 \bar{u}^2}{2c_s^4} \right) \quad (5-3)$$

in which  $\omega_i$  is the weighting parameter for each velocity direction. The nodal density  $\rho$  and the macroscopic velocity  $\bar{u}$  is defined by

$$\rho = \sum_i f_i \quad \rho \bar{u} = \sum_i f_i c_i \quad (5-4)$$

Nine possible directional velocities are used in this study, where  $\omega_i$  in equation (5-3) equals 4/9 for  $i = 0$ , 1/9 for  $i = 1,2,3,4$ , and 1/36 for  $i = 5,6,7,8$ . The nine velocities are defined as

$$\bar{c}_i = \begin{cases} (0,0) & (i = 0) \\ c_s \left( \cos \left[ (i-1) \frac{\pi}{2} \right], \sin \left[ (i-1) \frac{\pi}{2} \right] \right) & (1 \leq i \leq 4) \\ c_s \sqrt{2} \left( \cos \left[ (i-5) \frac{\pi}{2} + \frac{\pi}{4} \right], \sin \left[ (i-5) \frac{\pi}{2} + \frac{\pi}{4} \right] \right) & (5 \leq i \leq 8) \end{cases} \quad (5-5)$$

Construction of LSFE-LBM first considers application of the  $\theta$ -method to treat time-space approximations. Setting the time step  $\Delta t = t^{n+1} - t^n$ , and given  $f_i^n$  for the previous time step, the solution  $f_i^{n+1}$  for the current time step is determined from

$$\frac{f_i^{n+1} - f_i^n}{\Delta t} + \theta \bar{c} \cdot \nabla f_i^{n+1} + (1 - \theta) \bar{c} \cdot \nabla f_i^n = \theta \Omega_i^{n+1} + (1 - \theta) \Omega_i^n \quad (5-6)$$



In this work,  $\theta=1/2$  is implemented, which corresponds to the Crank-Nicolson scheme, providing for second order accuracy in time. Under this condition, a standard form of LSFE can be obtained by rearranging equation (5-6):

$$\begin{aligned}
c_x \frac{\partial f_i^{n+1}}{\partial x} + c_y \frac{\partial f_i^{n+1}}{\partial y} + A f_i^{n+1} &= p_i \\
A &= \frac{2}{\Delta t} + \frac{1}{\tau} \\
p_i &= \left(\frac{2}{\Delta t} - \frac{1}{\tau}\right) f_i^n + \frac{1}{\tau} (f_i^{eq,n+1} + f_i^{eq,n}) - \left(c_x \frac{\partial f_i^{n+1}}{\partial x} + c_y \frac{\partial f_i^{n+1}}{\partial y}\right)
\end{aligned} \tag{5-7}$$

For brevity, operator  $L$  is used, and equation (5-7) can be written in the following form:

$$L f^{n+1} = p \tag{5-8}$$

For finite element analysis, the problem domain can first be subdivided into a set of finite elements, and then approximated by the solution  $f_h^{e,n+1}$  in a finite element subspace as:

$$f_h^{e,n+1} = \sum_{j=1}^{\alpha} N_j f_j^{n+1} \tag{5-9}$$

where  $N_j$  denotes the element shape function,  $\alpha$  represents the number of nodes in an element, and  $f_j$  is the nodal value at the  $j$ -th node. Introducing equation (5-9) into equation (5-8) for an element, we get

$$E = L f_h^{e,n+1} - p_h^e \tag{5-10}$$

where  $E$  is the residual due to elemental approximation. The LSFE is based on the minimization of the squares of the residual for the subspace

$$\varphi(f^{n+1}) = \int_{\Omega_e} E^2 d\Omega_e = \int_{\Omega_e} (L f_h^{e,n+1} - p_h^e)^2 d\Omega_e \tag{5-11}$$

$$\frac{\partial \varphi(f^{n+1})}{\partial f_\alpha^{n+1}} = \int_{\Omega_e} (LN_\alpha)^T (Lf_h^{e,n+1} - p_h^e) d\Omega_e = 0, \quad \alpha = 1, 2, \dots, n \quad (5-12)$$

where  $\Omega_e$  is the domain of the  $e$ -th element, and the exponent  $T$  denotes the transpose.

For each element, the following set of linear algebraic equations can be derived from equation (5-12):

$$K_e F_e^{n+1} = P_e \quad (5-13)$$

where  $F_e^{n+1}$  is the vector of nodal values at the current time step.  $K_e$  is the elemental matrix given by

$$K_e = \int_{\Omega_e} Q^T Q d\Omega_e \quad (5-14)$$

where  $Q$  is a  $(1 \times \alpha)$  vector defined by:

$$\begin{aligned} Q &= CB + AN \\ &= \begin{bmatrix} c_x & c_y \end{bmatrix} \begin{bmatrix} \frac{\partial N_1}{\partial x} & \dots & \frac{\partial N_\alpha}{\partial x} \\ \frac{\partial N_1}{\partial y} & \dots & \frac{\partial N_\alpha}{\partial y} \end{bmatrix} + A \begin{bmatrix} N_1 & \dots & N_\alpha \end{bmatrix}. \end{aligned} \quad (5-15)$$

The element vector  $P_e$  in equation (5-13) is

$$P_e = \int_{\Omega_e} Q^T p_h^e d\Omega_e \quad (5-16)$$

As presented in equation (5-7),  $p_h^e$  is related to the previous time step  $f_i^n$  and  $f_i^{eq,n}$  values, and the current time step  $f_i^{eq,n+1}$  value. An extrapolation is applied to express  $f_i^{eq,n+1}$  as proposed by Mei and Shyy (Mei and Shyy 1998),

$$f_i^{eq,n+1} = 2f_i^{eq,n} - f_i^{eq,n-1} \quad (5-17)$$

where  $f_i^n$ ,  $f_i^{eq,n}$  and  $f_i^{eq,n-1}$  can be approximated in the subspace similar to  $f_i^{n+1}$ :

$$\mathbf{f}_h^n = \sum_{j=1}^{\alpha} N_j \mathbf{f}_j^n, \quad \mathbf{f}_h^{\text{eq},n} = \sum_{j=1}^{\alpha} N_j \mathbf{f}_j^{\text{eq},n}, \quad \mathbf{f}_h^{\text{eq},n-1} = \sum_{j=1}^{\alpha} N_j \mathbf{f}_j^{\text{eq},n-1} \quad (5-18)$$

### 5.2.2 Boundary Conditions

A typical boundary condition for first order differentiation equations can be expressed as:

$$f_i = g \quad \text{on } \Gamma \quad (5-19)$$

where,  $\Gamma$  denotes a homogeneous boundary condition when  $g$  equals 0, and a heterogeneous boundary condition when  $g$  is not 0.

This essential type of boundary condition is of great convenience to LSFE-LBM. Well-established LBM boundary methods (Chen, Martinez et al. 1996; Maier, Bernard et al. 1996; Zou and He 1997), e.g., bounce back conditions, constant velocity conditions, and pressure gradient conditions, can be readily applied. At each time step, the boundary values of  $f_h^{n+1}$  can be calculated in similar manner to traditional LBMs, which are then applied to the LSFE-LBM scheme as essential boundary conditions. Meanwhile, macroscopic boundary conditions are imposed through the equilibrium function,  $f_h^{\text{eq}}$ . For unstructured mesh, special attention should be noted when implementing periodic boundary conditions, where corresponding nodes for inlet and outlet boundary are required.

### 5.2.3 Implementation Issues

LSFE method leads to a linear system of equations, as described by equation (5-13), which requires solving at each time step. Since  $K_e$  in equation (5-13) is always

symmetric and positive definite, a preconditioned conjugate gradient (CG) method can be well applied as a tool for efficient solution. The CG iterative updating formula can be expressed as:

$$F^{n+1} = F^n - M^{-1}(KF^n - P) \quad , \quad (5-20)$$

where,  $M$  is a non-singular preconditioning matrix serving to accelerate convergence of the iteration. In this study, Jacobi preconditioned CG (JPCG) (Jiang 1998) is applied, where the diagonal matrix of  $K$  is utilized as the preconditioner matrix  $M$ .

As presented in equation (5-20), matrix multiplication,  $K \times F$ , is involved in the JPCG algorithm. Traditionally, a sparse and large global matrix system will require assemblage prior to the multiplication operation, necessitating a large amount of computer memory usage and significant computing time, thus restricting the size of the problem. To overcome this issue, an element-by-element approach (Wathen 1989), which stores information only at the element level, was implemented. Avoiding the assembling of global matrices, this approach requires greatly reduced memory storage compared to the traditional approach. Following is a brief description of this element-by-element approach.

A global matrix may be expressed as:

$$K = \sum_{e=1}^{N_e} K_g^e \quad , \quad (5-21)$$

where,  $N_e$  is the number of elements in the system, and  $K_g^e$  is a matrix with global size.

The components of  $K_g^e$  are all zero except those corresponding to the nodes in element  $e$ .

Meanwhile, the global vector  $P$  can be expressed as:

$$P = KF = \left( \sum_{e=1}^{N_e} K_g^e \right) F = \sum_{e=1}^{N_e} (K_g^e F_g^e) = \sum_{e=1}^{N_e} P_g^e, \quad (5-22)$$

where  $F_g^e$  is a modified global vector, whose components are all zero, except those corresponding to the nodes of element  $e$  whose values remain the same as in global vector  $F$ . Thus, individual matrix-vector products  $P_g^e$  may be obtained by computing an element matrix vector product

$$P^{de} = K^e F^{de}, \quad (5-22)$$

and expanding the vector  $P^{de}$  into appropriate position of  $P_g^e$ . In equation (5-22),  $F^{de}$  is an element level vector which extracts values from corresponding components of  $F_g^e$ . In this way, matrix-vector multiplication can be conducted at the element level, independently and concurrently without storing the global matrix.

It is noteworthy that large benefits of this element-by-element approach have been observed in this study. For a system with 2500 nodes, the memory usage of the element-by-element approach is about 130 times less than a typical assembled global matrix approach, and the computing speed is approximately 4 times faster. These advantages will likely become even more obvious for larger systems, where memory leakage may occur while storing global matrices.

### 5.3 Analysis of LSFE-LBM

#### 5.3.1 Accuracy Analysis

Since the collision term has no effect on numerical accuracy, for simplicity, a one-dimensional pure advection equation is utilized to analyze the accuracy of LSFE-LBM.

$$\frac{\partial f_i}{\partial t} + c_i \cdot \frac{\partial f_i}{\partial x} = 0 \quad (i = 1, 2, \dots, N) \quad (5-23)$$

Applying the  $\theta$ -method to treat time-space approximations, and implementing LSFE scheme as presented above with uniform linear element, equation (5-23) will lead to a discretized format for a typical node  $j$ :

$$\left[ 1 + \left( \frac{1}{6} - \beta^2 \theta^2 \right) \delta^2 \right] (F_j^{n+1} - F_j^n) = -\frac{\beta}{2} (F_{j+1}^n - F_{j-1}^n) + \theta \beta^2 (F_{j+1}^n - 2F_j^n + F_{j-1}^n), \quad (5-24)$$

where,  $\delta^2$  denotes the second order variation operator, and  $\beta = c\Delta t / \Delta x$ .

In order to determine the accuracy of equation (5-24), a Taylor series expansion of  $f$  around time  $t$  and the node  $j$  is considered:

$$\begin{aligned} f(x \pm \Delta x, t + \Delta t) = & f(x, t) \pm \Delta x f_x(x, t) + \Delta t f_t(x, t) + \frac{\Delta x^2}{2} f_{xx}(x, t) \pm \Delta x \Delta t f_{xt}(x, t) + \frac{\Delta t^2}{2} f_{tt}(x, t) \\ & \pm \frac{\Delta x^3}{6} f_{xxx}(x, t) + \frac{\Delta x^2 \Delta t}{2} f_{xxt}(x, t) \pm \frac{\Delta x \Delta t^2}{2} f_{xtt}(x, t) + \frac{\Delta t^3}{6} f_{ttt}(x, t) + \dots \end{aligned} \quad (5-25)$$

Implementing Taylor series expansion on  $F_j^{n+1}$ ,  $F_j^n$ ,  $F_{j+1}^n$ ,  $F_{j-1}^n$ ,  $F_{j+1}^{n+1}$ ,  $F_{j-1}^{n+1}$  in equation (5-24), and utilizing the recursive application relationship of the advection equation (Comini, Manzan et al. 1995), i.e.

$$f_{tt} = c^2 f_{xx}, \quad f_{xxt} = -c f_{xxx}, \quad f_{xtt} = c^2 f_{xxx}, \quad f_{ttt} = -c^3 f_{xxx}, \quad (5-26)$$

the transient truncation error can be derived as:

$$\varepsilon_i = f_i + cf_x = \Delta t \left( \theta c^2 - \frac{c^2}{2} \right) f_{xx} + \Delta t^2 \left( \frac{c^3}{6} - c^3 \theta^2 \right) f_{xxx} + O(\Delta t^3, \Delta x^4) \quad (5-27)$$

When  $\theta=1/2$ , corresponding to the Crank-Nicolson scheme, the transient trunk error is:

$$\varepsilon_i = -\frac{\Delta t^2}{12} f_{xxx} + O(\Delta t^3, \Delta x^4) = O(\Delta t^2, \Delta x^4). \quad (5-28)$$

Thus, for uniform linear elements, LSFE-LBM enjoys similar accuracy as the CGDBE method presented by Lee and Lin (Lee and Lin 2001), i.e., fourth-order accuracy in space and second order accuracy in time. Compared to the second-order accuracy in space for FD-based LBM, it is clear that FE-based LBM greatly increases numerical accuracy. Further, the spatial accuracy is dependent on the order of the shape functions. If higher order shape functions are employed, higher order accuracy will be expected. In this work, linear shape functions are utilized for all test examples. It is important to note that the temporal and spatial accuracy discussed here is for LSFE, not for the incompressible Navier-Stokes equation. When applying LSFE to recover the incompressible Navier-Stokes equation, there exists an additional error in the order of  $O(M_a^2)$ , where  $M_a$  is the Mach number of the flow.

### 5.3.2 Stability Analysis

Stability analysis is applied to the pure advection equation in similar fashion to the accuracy analysis. Application of von Neumann stability analysis to the discretized format of LSFE-LBM, i.e., equation (5-23), reveals unconditional stability with any Courant-Friedrichs-Lewy (CFL) number for the pure advection equation on a uniform mesh if  $\theta$  in equation (5-6) is in the range of  $[1/2, 1]$ . This unconditional stability, derived from the implicit nature of LSFE, provides a significant advantage over CGDBE,

which is only conditionally stable due to its explicit treatment of the advection term. A comparison of accuracy and stability among LSFE-LBM, CGDBE, and FD-LBM is given in Table 5-1.

**Table 5-1. A Comparison of Accuracy and Stability Characteristics of FD-LBM, CGDBE, and LSFE-LBM for the Pure Advection Equation on a Uniform Mesh.**

		<b>FD-LBM</b>	<b>CGDBE</b>	<b>LSFE-LBM</b>
<b>Accuracy</b>	<b>Space</b>	Second order	Fourth order	Fourth order
	<b>Time</b>	Second order	Second order	Second order
<b>Stability<sup>a</sup></b>		Conditional /Unconditional	$\Delta t \leq \frac{\Delta x}{3 e }$	Unconditional

<sup>a</sup>Stability of FD-LBM is based upon the specific time discretization scheme used.

$\Delta x$  = element size

$\Delta t$  = time step

$e$  = discrete velocity in the characteristic direction (Lee and Lin 2001)

Stability analysis based upon the pure advection equation simplifies the analysis procedure by neglecting the nonlinear collision term. Although this simplified analysis may represent some stability property of LSFE-LBM, it is not sufficient to reflect the true stability feature of the method. Thus, the numerical stability of the LSFE-LBM is further studied via the linearization approach proposed by Sterling and Chen (Sterling and Chen 1996), as detailed below.

Rearranging equation (5-13) into a more desirable format for stability analysis:

$$U_e \left( f_i^{n+1} + \frac{1-\theta}{\theta} f_i^n \right) + \frac{W_e}{\theta \Delta t} (f_i^{n+1} - f_i^n) = W_e \left( \Omega_i^{n+1} + \frac{1-\theta}{\theta} \Omega_i^n \right), \quad (5-29)$$

where,  $U_e = \int_{\Omega_e} Q^T C B d\Omega_e$ ,  $W_e = \int_{\Omega_e} Q^T N d\Omega_e$ , and  $C, B, N$  are as defined in equation (5-

15). In order to implement von Neumann stability analysis, it is necessary to transform



equation (5-29) into a discrete form. For the purpose of simplicity, a uniform triangular mesh is utilized here, as illustrated in Figure 5-1.

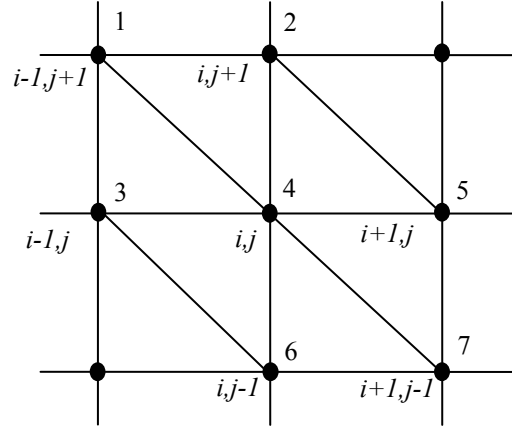


**Figure 5-1. Schematic Plot of Neighboring Point Distribution around the Point  $(i,j)$  in a Uniform Triangular Mesh for LSFE-LBM.**

Assembling global matrixes based on this mesh, a discrete formula for point  $(i,j)$  can be expressed as:

$$\sum_{p=1}^7 U_p \left( f_i^{n+1} + \frac{1-\theta}{\theta} f_i^n \right) + \frac{1}{\theta \Delta t} \sum_{p=1}^7 W_p (f_i^{n+1} - f_i^n) = \sum_{p=1}^7 W_p \left( \Omega_i^{n+1} + \frac{1-\theta}{\theta} \Omega_i^n \right), \quad (5-30)$$

where,  $p$  is the node number as denoted in Figure 5-1. As proposed by Sterling and Chen (Sterling and Chen 1996),  $f_i$  can be expanded as:

$$f_i = \overline{f^{(0)}} + f_i', \quad (5-31)$$

where,  $f_i'$  is the fluctuating quantity, and  $\overline{f^{(0)}}$  is the global equilibrium population, not varying in space or time. It can be shown that the constant property of  $\overline{f^{(0)}}$  results in the relationship:

$$U_p \overline{f^{(0)}} = 0. \quad (5-32)$$

Applying a Taylor series expansion to the collision operator around  $\overline{f^{(0)}}$  gives:

$$\begin{aligned}\Omega_i(f_j) &= \left( \frac{\partial \Omega_i}{\partial f_j} \right)_{\overline{f^{(0)}}} f_j' + \Omega_i(\overline{f^{(0)}}) + O(f_j'^2) \\ &\approx \left( \frac{\partial \Omega_i}{\partial f_j} \right)_{\overline{f^{(0)}}} f_j' = G_{ij} f_j'\end{aligned}\quad (5-33)$$

Substituting this first order approximation of the collision operator after the expansion of  $f_i$  by equation (5-30) in equation (5-31), and utilizing the relationship in equation (5-32), equation (5-30) is reduced to the following form:

$$\begin{aligned}\sum_{p=1}^7 U_p \left( f_i'^{n+1} + \frac{1-\theta}{\theta} f_i'^n \right) + \frac{1}{\theta \Delta t} \sum_{p=1}^7 W_p (f_i'^{n+1} - f_i'^n) \\ = \sum_{p=1}^7 W_p G \left[ f_j'^{n+1} + \frac{1-\theta}{\theta} f_j'^n \right],\end{aligned}\quad (5-34)$$

Performing a Fourier transform of equation (5-34), it follows

$$F_i(\vec{k}, t + \Delta t) = Z_{ij} F_j(\vec{k}, t), \quad (5-35)$$

where,  $F_j(\vec{k}, t) = \int f_j'(\vec{x}, t) \exp(-\vec{k} \cdot \vec{x}) d\vec{x}$  and  $\vec{k} = (k_x, k_y)$  is the wave number. Matrix  $Z$  is given by:

$$Z = \left[ \sum_{p=1}^7 (A_p - W_p G) E_p \right]^{-1} \left[ \sum_{p=1}^7 (B_p + \frac{1-\theta}{\theta} W_p G) E_p \right], \quad (5-36)$$

where,  $A_p = \text{diag} \left\{ \frac{W_p}{\theta \Delta t} + U_p \right\}_{9 \times 9}$ ,  $B_p = \text{diag} \left\{ \frac{W_p}{\theta \Delta t} - \frac{1-\theta}{\theta} U_p \right\}_{9 \times 9}$ , and

$$E_p = \exp(i\vec{k} \cdot \vec{d}\vec{l}_p) I_{9 \times 9}.$$

When the spectral radius of matrix  $Z$ , i.e., the largest value of eigenvalues, is not larger than unity, the system approaches stability. When the wave number is zero,  $E_p$  matrices become identity matrices, resulting in eigenvalues of matrix  $Z$ :

$\left\{1, \frac{(\theta - 1)\Delta t + \tau}{\theta\Delta t + \tau}\right\}$ , with three and six multiplicity respectively, independent of macroscopic velocity. In this special case, the stability of the system is guaranteed when  $\tau > \max\{0, (1/2 - \theta)\Delta t\}$ .

When the wave number is non-zero, the stability of LSFE-LBM is dependent on a number of parameters, including time step, element size, wave number, and relaxation time, similar to that reported in other studies for LBM on irregular mesh (Sterling and Chen 1996; Guo and Zhao 2003). It is therefore not feasible to evaluate the full effects of these parameters on stability; rather, simplifications and restrictions may be imposed. In this study, the influences of collision frequency  $\omega = \Delta t / \tau$ , ratio  $dt/dl$ , and mean velocity  $u$  are evaluated with several simplifications. These include, (i) fix  $\theta = 0.5$ ; (ii) evaluate wave number vector only in the range  $[0, \pi]$ ; (iii) use uniform mesh, i.e.,  $dx = dy = dl$ ; (iv) keep the mean velocity and the wave number vector horizontal corresponding to the likely most unstable condition identified by Sterling and Chen (Sterling and Chen 1996).

A program written in MATLAB (version 6.5.1, The MathWorks, Inc., Natick, Massachusetts) was employed to numerically calculate eigenvalues of the matrix  $Z$ , and thus to determine the stability boundary. An iterative scheme is used in which values of  $\omega$ ,  $dt/dl$ , and  $\tau$  were selected, and the mean flow velocity  $u$  is incrementally increased until the maximum eigenvalue exceeds unity. The resulting mean flow velocity is coined in terms of a maximum stable velocity, which is utilized to construct the stability boundary by varying the value of  $\omega$  for several different  $dt/dl$  and  $\tau$  values. Although it is very difficult to present a complete illustration of the dependence of the LSFE-LBM stability on physical parameters and numerical discretization, Figure 5-2 and Figure 5-3 shed light on the stability feature of LSFE-LBM with selected  $\tau$  and  $dt/dl$  values.

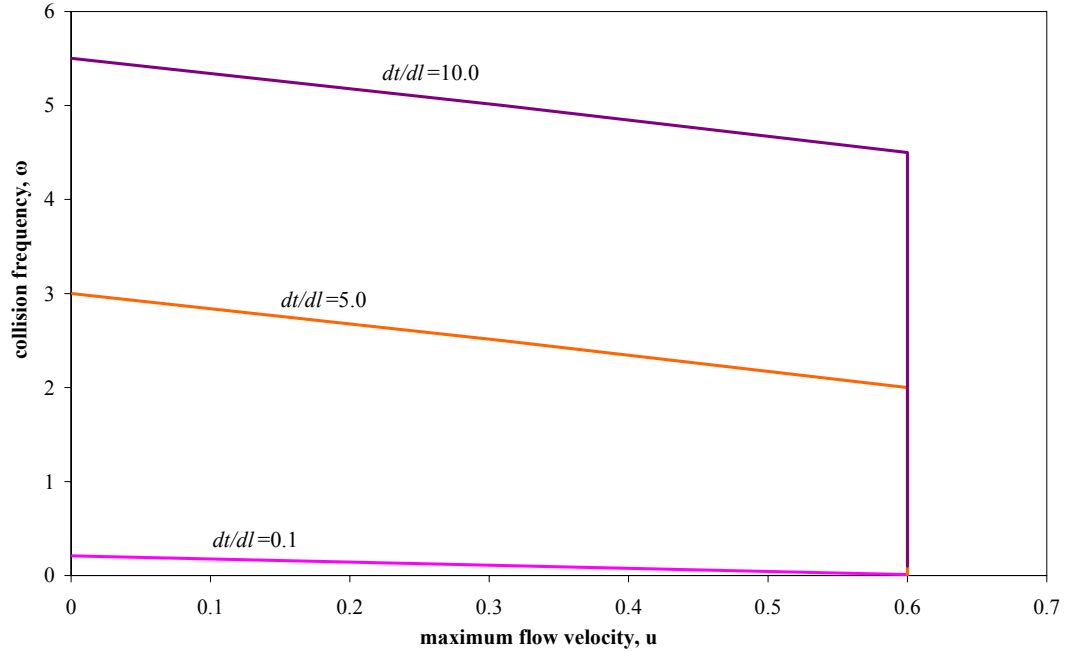


**Figure 5-2. Stability Boundaries as Function of Mean Velocity  $u$  and Collision Frequencies  $\omega$  for Selected  $dt/dl$  when  $\tau = 1.0$ .**

Figure 5-2 presents the correlation between maximum stable velocity  $u$  and collision frequency  $\omega$  for different  $dt/dl$  under a fixed  $\tau$  value. As the value of  $\omega$  decreases, the maximum stable velocity first increases, and then is held constant near 0.58. This existence of a limiting stable velocity was also observed by Sterling and Chen (Sterling and Chen 1996) for traditional LBM, implying the underlying inability of using a finite set of particle velocities to represent high flow velocity. The observed limiting stable velocity for the LSFE-LBM of 0.58, corresponding to a Mach number  $M_a = u/c_s = 1.0$ , however, is higher than 0.42 for a traditional D2Q9 model derived by Sterling and Chen (Sterling and Chen 1996), indicating that the LSFE scheme actually enhanced the

stability of LBM. Meanwhile, Figure 5-2 shows that the stability region is increased with increased of  $dt/dl$  values.

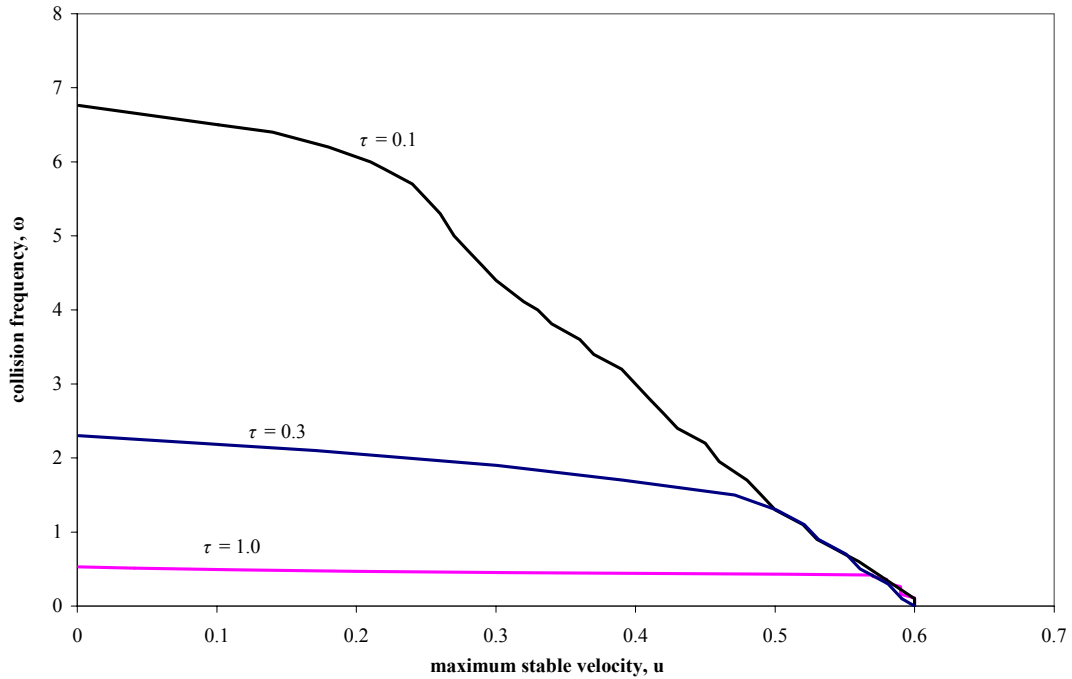


**Figure 5-3. Stability Boundaries as Function of Mean Velocity  $u$  and Collision Frequencies  $\omega$  for Selected  $\tau$  when  $dt/dl = 1.0$ .**

Similar to Figure 5-2, Figure 5-3 presents the relationship between  $\omega$  and maximum stable velocity, but for different  $\tau$  values. Again, with decreased  $\omega$ , the maximum stable velocity increases until the largest possible value of 0.58 is reached. The smaller curve slopes for larger  $\tau$  values agree well with other simulation results that suggest that LBM tends toward stability at higher values of velocity for a larger  $\tau$  value. Moreover, it is observed in Figure 5-3 that smaller  $\tau$  values possess larger stability regions relative to larger  $\tau$  values, which implicates some trends about the dependency of stability

on the numerical discretization. For a certain  $\omega$ , a smaller  $\tau$  value corresponds to a smaller  $dt$  value, and thus a smaller  $dl$  value due to the fixed  $dt/dl$  in Figure 5-3. Therefore, the smaller  $dt$  and  $dl$  values may lead to larger stability regions, although, on the other hand, a higher  $dt/dl$  ratio tends to be more stable, based on Figure 5-2.

## 5.4 Numerical Results

Demonstration of the validity and power of LSFE-LBM is illustrated in the following test problems in this section, including: Poiseuille flow, Couette flow, flow past a circular cylinder, and flow in porous media.

### 5.4.1 Poiseuille Flow

Poiseuille flow, i.e., channel flow driven by a constant pressure gradient, is first simulated to validate LSFE-LBM. An analytical solution to plan Poiseuille flow in a channel is provided by equation (5-37) (Deen 1998):

$$v_x(y) = u_{\max} \left[ 1 - \left( \frac{y}{H} \right)^2 \right], \quad -H \leq y \leq H \quad (5-37)$$

where  $x$  is the spatial longitudinal dimension,  $y$  is the spatial transverse dimension,  $u_{\max}$  is the maximum velocity at the parabolic velocity profile, and  $H$  is the half width of the channel. In our LSFE-LBM implementation, the initial flow velocity is zero, relaxation time,  $\tau$ , is 0.05, particle density,  $\rho$ , is 1.0,  $u_{\max}$  is 0.1, and  $H$  is 5/6. A periodic boundary condition is applied in the  $x$ -direction, and a body force  $G = \frac{2\nu u_{\max}}{H^2}$  is applied in the  $x$ -direction to initiate the flow, where  $\nu$  is the viscosity. This system possesses a Reynolds

number ( $Re = \frac{u_{max} 2H}{\nu}$ ) of 10, and a Mach number ( $Ma = \frac{u_{max}}{c_s}$ ) of 0.173. Results presented in Figure 5-4 illustrate that LSFE-LBM achieves close agreement with the analytical solution.

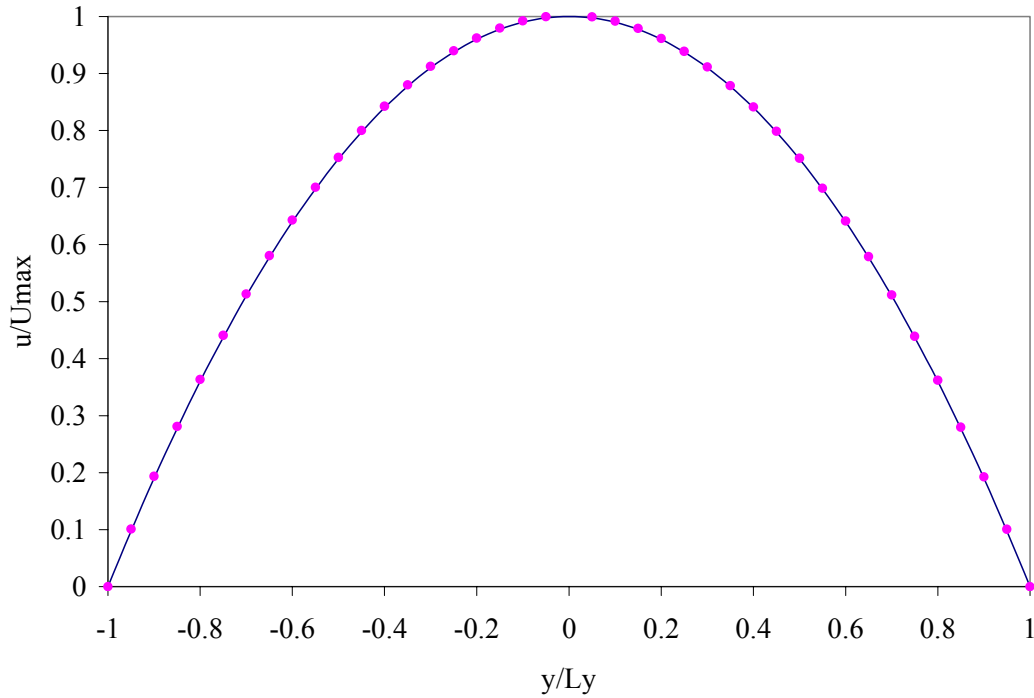


**Figure 5-4. Comparison of LSFE-LBM Solution (points) and Analytical Solution (line) for Normalized Velocity Profile for Poiseuille Flow. In LSFE-LBM, the relaxation time,  $\tau$ , is 0.05, and particle density,  $\rho$ , is 1.0, the maximum velocity,  $u_{max}$ , is 0.1, and the half width of the channel,  $H$ , is 5/6.**

It is observed in modeling Poiseuille flow, and later in Couette flow, that the viscosity of fluid follows the relationship  $\nu = \tau/3$ . In a traditional D2Q9 lattice Boltzmann model, the viscosity is  $\nu = (\tau - dt/2)/3$ , in which the negative component derives from numerical errors. Thus, it is indicated that LSFE-LBM will be less subjected to numerical diffusion. Further, the absence of the negative component implies

the possibility of very small viscosity values, which may lead to higher Reynolds numbers. However, to fully explore the efficiency of LSFE-LBM with high Reynolds number, we suggest that more thorough theoretical and numerical tests are necessary.

#### 5.4.2 Couette Flow

The second application of unsteady Couette flow is used to evaluate the temporal accuracy of LSFE-LBM. Different from Poiseuille flow, here the top plate is moving along the  $x$ -direction at a constant velocity,  $u_{\max}$ , while the bottom plate remains stationary. The analytical solution for Couette flow is (Deen 1998):

$$u(y,t) = u_{\max} \frac{y}{D} + \sum_{i=1}^{\infty} \frac{2u_{\max} (-1)^i}{\lambda_i D} e^{-1/\lambda_i^2 t} \sin \lambda_i y, \quad 0 \leq y \leq D, \quad (5-38)$$

where  $\lambda_i = \frac{i\pi}{D}$ ,  $m = 1, 2, 3, \dots$

A periodic boundary condition is applied in the  $x$ -direction, and the Reynolds number  $R_e = \frac{u_{\max} D}{\nu}$  is again set equal to 10, where  $D$  represents the width of the channel. The time step is 0.03, relaxation time,  $\tau$ , is 0.05, particle density is 1.0,  $u_{\max}$  is 0.1, and  $D$  is 5/3. A comparison of numerical results and the analytical solution is shown in Figure 5-5.



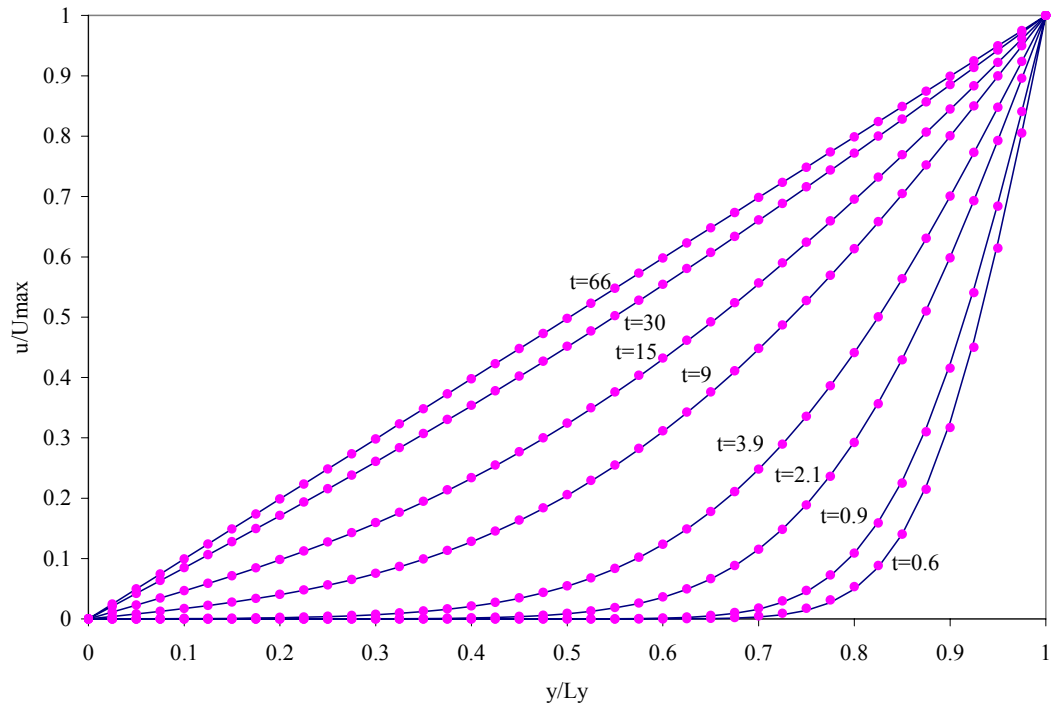


**Figure 5-5. Comparison of LSFE-LBM Solution and Analytical Solution for Couette flow. The points represent the LSFE-LBM solution, while the lines denote the analytical solution. The time step is 0.03, and relaxation time,  $\tau$ , is 0.05, the maximum velocity,  $u_{max}$ , is 0.1, and the width of the channel,  $D$ , is  $5/3$ .**

#### 5.4.3 Flow past a Circular Cylinder

LSFE-LBM was also applied to simulate steady-state flow past a circular cylinder, since this problem has been widely employed (He and Doolen 1997; Lee and Lin 2001; Guo and Zhao 2003) as a benchmark problem to validate different numerical methods. Here, the results are compared with previous numerical and experimental studies. Simulation is carried out in a square domain with width  $W = 100d$ ,  $Ma = 0.1$ , and  $Re = u_{\infty}d/\nu = 20$ , where  $u_{\infty}$  is the free stream velocity and  $d$  is the diameter of the circular cylinder. Unstructured triangular mesh is applied, as shown in Figure 5-6, which includes 2544 nodes and 4992 elements.

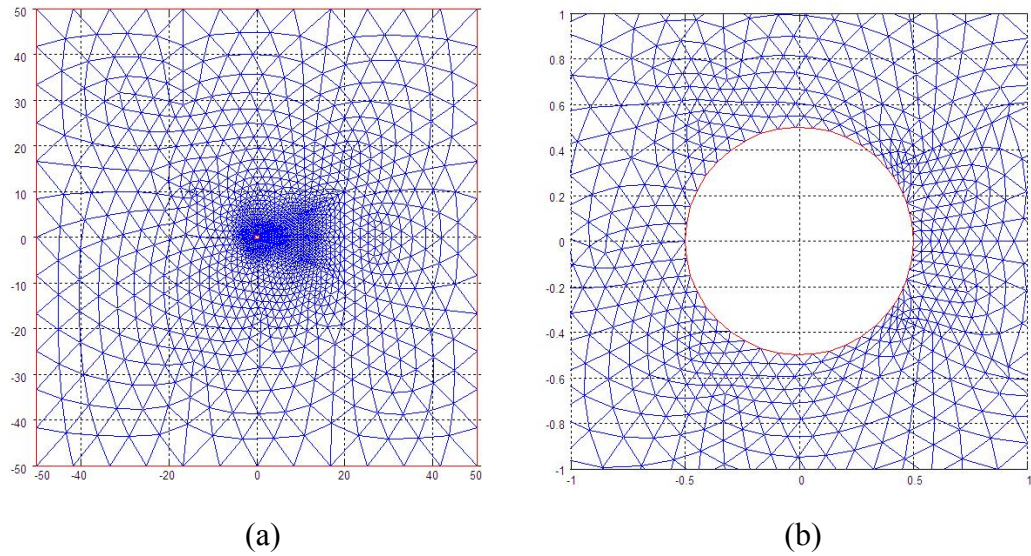


**Figure 5-6. Unstructured Mesh for Flow past a Circular Cylinder in (a) the entire computational domain and (b) the vicinity of the cylinder.**

Simulation starts from an irrotational potential flow. Free stream velocity  $u_\infty$  is enforced on the domain boundaries, while keeping the distribution function in its equilibrium state. Periodic boundary conditions are implemented for the inlet and outlet of the simulation domain, while a bounce back rule is imposed to ensure the non-slip condition at the surface of cylinder.

LSFE-LBM simulation results show a pair of stationary recirculation eddies appearing behind the cylinder, as reported in many previous studies (He and Doolen 1997; Lee and Lin 2001; Guo and Zhao 2003). Geometric parameters of the flow are measured and listed in Table 5-2, including the separation angle  $\Theta_s$  and the ratio of wake length to cylinder radius  $L/r_0$ , where wake length  $L$  is defined as the distance from the rearmost point of the cylinder to the end of the wake. Dynamic parameters, including the

drag coefficient ( $C_D$ ) and the stagnation pressure coefficients at the front,  $C_p(\pi)$ , and at the end,  $C_p(0)$ , of the cylinder, were also measured and listed in Table 5-2.

**Table 5-2 Comparison of Geometric and Dynamic Parameters of Flow past a Circular Cylinder with Previous Studies.**

Authors	$L/r_0$	$\theta_s$	$C_D$	$-C_p(0)$	$C_p(\pi)$
Tritton <sup>a</sup> (Tritton 1959)	1.86	41.6	-	-	-
Coutanceau and Bouard <sup>a</sup> (Coutanceau and Bouard 1977)	1.86	44.8	-	-	-
Nieuwstadt and Keller <sup>b</sup> (Nieuwstadt and Keller 1973)	1.786	43.37	2.053	0.582	1.274
Dennis and Chang <sup>b</sup> (Dennis and Chang 1970)	1.88	43.7	2.045	0.589	1.269
Fornberg <sup>b</sup> (Fornberg 1980)	-	-	2.000	0.54	1.28
He and Doolen <sup>c</sup> (He and Doolen 1997)	1.843	42.96	2.152	0.567	1.233
Guo and Zhao <sup>d</sup> (Guo and Zhao 2003)	1.824	43.59	2.048	0.512	1.289
Lee and Lin <sup>e</sup> (Lee and Lin 2001)	1.85	44.08	1.998	0.530	1.248
Present <sup>f</sup>	1.835	44.64	2.011	0.551	1.262

<sup>a</sup> Experiment.

<sup>b</sup> Numerical simulation of Navier-Stokes equations.

<sup>c</sup> Interpolation-supplemented LBM on structured mesh with  $181 \times 241$  grid points.

<sup>d</sup> Explicit finite-difference LBM on structured mesh with  $129 \times 64$  grid points.

<sup>e</sup> Characteristic Galerkin discrete LBM on unstructured mesh with 2568 grid points

<sup>f</sup> Least squares finite-element LBM on unstructured mesh with 2544 grid points.

The stagnation pressure coefficient  $C_p$  is defined as:

$$C_p = \frac{p - p_\infty}{1/2 \rho u_\infty^2} \quad (5-39)$$

where,  $p$  is the pressure which can be evaluated directly using:

$$p = c_s^2 \rho \quad (5-40)$$

The drag coefficient,  $C_D$ , is defined as

$$C_D = \frac{1}{\rho u_\infty^2 r_0} \int S \cdot ndl \quad (5-41)$$

where,  $n$  is the normal direction of the cylinder wall and  $S$  is the stress tensor given by:

$$S = pI + \rho\nu(\nabla u + [\nabla u]^T) \quad (5-42)$$

As shown in Table 5-2, the results of LSFE-LBM are in good agreement with previous experimental studies (Tritton 1959; Coutanceau and Bouard 1977) and finite-difference based CFD methods by Nieuwstadt and Keller (Nieuwstadt and Keller 1973) and Dennis and Chang (Dennis and Chang 1970). Compared to LBM on structured mesh (He and Doolen 1997; Guo and Zhao 2003), LSFE-LBM achieves good agreement with simulation results while using a much smaller number of grid points. Approximately the same number of grid points as CGDBE (Lee and Lin 2001) on the unstructured mesh is utilized by LSFE-LBM in this study. However, LSFE-LBM is not restricted by the CFL condition due to the implicit feature of the LSFE scheme, which can be implemented with a larger time step.

#### 5.4.4 Flow in Porous Media

Traditional LBM has been successfully applied to study fluid flow in porous media by numerous studies (Rothman 1988; Cancelliere, Chang et al. 1990; Chen, Diemer et al. 1991; Zhang, Zhang et al. 2000; Talon, Martin et al. 2003; Pan, Hilpert et al. 2004; Spaid, Phelan et al. 2004; Sukop and Or 2004; Zhang and Kang 2004; Li, LeBoeuf et al. 2005). To demonstrate its ability to address complex geometries and compare its performance with traditional LBM, we here apply LSFE-LBM to simulate flow in a porous medium and estimate permeability of the simulation domain. At low Reynolds number for single-phase flow, specific permeability  $k$  of porous media, in unit of  $L^2$  or *Darcy*, can be described within the context of Darcy's law

$$q = -\frac{k}{\mu} \cdot \nabla p \quad (5-43)$$

where,  $q$  [L/T] is the specific flow rate,  $\mu$  [M/LT] is the viscosity of the fluid, and  $\nabla p$  [M/L<sup>2</sup>T<sup>2</sup>] represents the pressure gradient.

In this study, porous media are envisioned as a statistical distribution of non-overlapping circular disks representing soil particles distributed in a rectangular two-dimensional uniform continuum representing the pore space through which a fluid flows. Simulation is conducted on a 1mm × 1mm domain with porosity 0.5, and randomly generated particle diameters obeying a lognormal distribution with geometric mean 100 μm and coefficient of variance (COV) 0.3. For comparison, both traditional LBM with uniform mesh and LSFE-LBM with unstructured mesh are considered. Figure 5-7 illustrates an example irregular triangular mesh for LSFE-LBM.

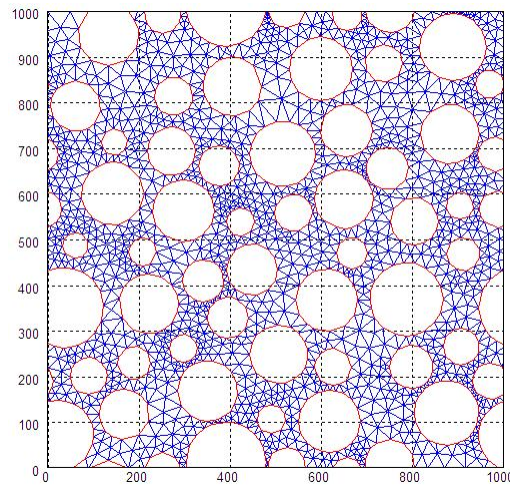


**Figure 5-7. An Example of Unstructured Mesh for Flow in the Porous Media.**

No-flow boundary conditions were applied on upper and lower edges, which are parallel to the main flow direction. Periodic boundary conditions were applied at the inlet and outlet of the domain, which require that the last column of nodes face nodes of the same y-axis values at the first column. For porous media with complex geometry, an unstructured mesh commonly will not provide such a symmetric node structure for domain inlet and outlet. To overcome this problem, an additional buffer area without any soil particles was added at the domain inlet and outlet. A similar handling technique was also utilized by S. Ubertini and coworkers (Ubertini, Bella et al. 2003; Ubertini and Succi 2005) to treat zero-gradient boundary conditions for unstructured mesh, where acceptable results were found. Bounce back boundary conditions are applied to guarantee the non-slip condition at the surface of particles. To mimic the effects of a pressure gradient along the horizontal direction, an external body force was enforced on the fluid in the porous media, which generates fluid flow at low Reynolds number of approximately 0.05. Darcy's law equation (5-43) may thus be applied to calculate the permeability of the porous media.

Traditional LBM was carried out with increasing numerical resolution until the effects of spatial discretization were negligible. As presented in Figure 5-8, at grid point number  $2001 \times 2001$ , the permeability estimated by traditional LBM approaches a stable value of 35.56 *Darcy*, which is utilized as a standard value to compare with LSFE-LBM simulation results. 8866 grid points are utilized in LSFE-LBM simulation, leading to a permeability value of 33.59 *Darcy*. While the relative error between the two methods is only approximately 5.5%, the number of grid points utilized by traditional LBM is about 452 times that used by LSFE-LBM. Although LSFE-LBM inherits the computational

complexity from the LSFE method, the reduced grid point requirement for unstructured mesh potentially offsets the negative influence on computational efficiency. In this specific example, LSFE-LBM with 8866 nodes and traditional LBM with  $2001 \times 2001$  nodes require approximately the same amount of time to achieve equilibrium, while producing permeability values within the same order of accuracy. Further, in this study, the memory usage of LSFE-LBM is only about 4% of traditional LBM, suggesting the potential benefits of applying LSFE-LBM to larger and more complex domains.

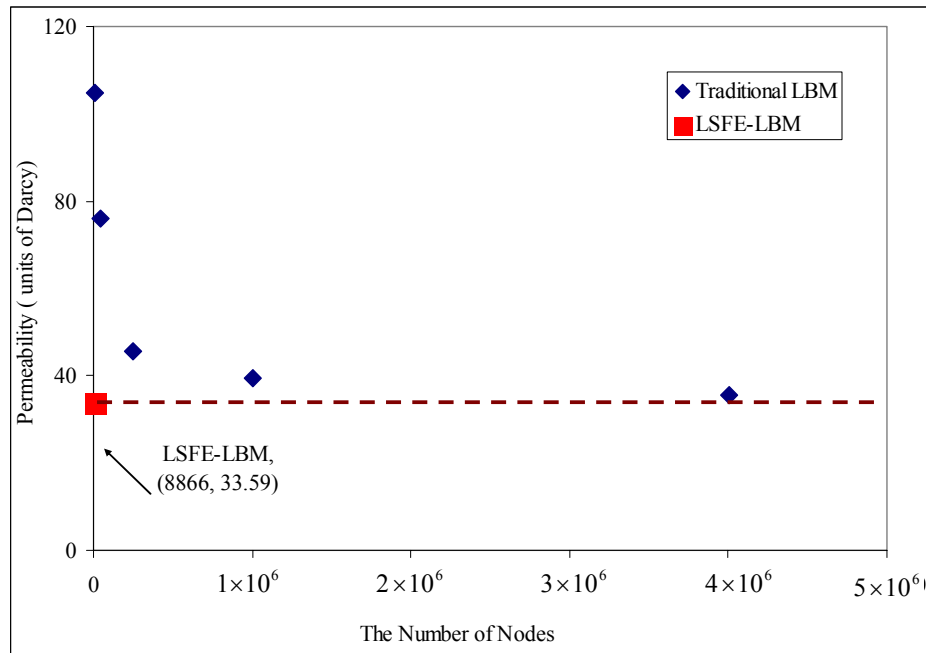


**Figure 5-8. A Comparison of the Performance of Traditional LBM and LSFE-LBM on Simulating Flow in the Porous Media.**

## 5.5 Summary

In this chapter, we present a new numerical model for LBM by implementing a least squares finite element scheme on unstructured mesh. Through theoretical accuracy

and stability analysis, and successful application of LSFE-LBM to a variety of test problems, including Poiseuille flow, Couette flow, flow past a cylinder, and flow in porous media, it is suggested that the LSFE-LBM possesses the following attributes:

- *High accuracy*: Accuracy analysis of the pure advection equation suggests that LSFE-LBM enjoys fourth-order accuracy in space and second-order accuracy in time. LSFE-LBM results agree well with the analytical solutions for Poiseuille and Couette flow, and the previous numerical and experimental study results for flow past a cylinder.
- *High stability*: For the pure advection equation, LSFE-LBM presents unconditional stability in the time domain, which is superior to other finite-difference and finite-element based LBMs. Although the von Neumann linearized stability analysis indicates that the stability of LSFE-LBM is dependent on physical and numerical discretization parameters as other numerical LBMs, its improved stability property is further confirmed by a higher limiting stable velocity.
- *High flexibility*: Application of LSFE-LBM to flow past a circular cylinder suggests good agreement with previous numerical and experimental results, providing initial evidence of its applicability to curved boundaries. Later, LSFE-LBM was successfully applied to model fluid flow in a randomly generated porous media using an unstructured mesh; good agreement with traditional LBM results further demonstrate the geometric flexibility of LSFE-LBM.
- *High efficiency*: Although more complex computations are required in LSFE-LBM relative to traditional LBM, LSFE-LBM requires fewer grid points by utilizing unstructured mesh, while consuming less memory by implementing an innovative element-by-element approach in the LSFE scheme. As demonstrated by the flow in



porous media problem, LSFE-LBM requires  $1/452$  of the number of grids points and  $1/25$  of the memory of traditional LBM to achieve a similar order of accuracy with a similar amount of computational time. It is worthy to note that advantages derived from this increased efficiency may not be obvious for problems with simple geometries; rather, it is expected to be better demonstrated when applied to larger domains with more complex geometries.

Encouraging results from this work suggest that LSFE-LBM will be a promising addition to the family of LBM, especially for geometric complex domains. Further improvements of LSFE-LBM, however, are suggested. First, LSFE-LBM numerical tests were primarily applied to complex geometries with low Reynolds numbers, corresponding to our research focus area. Although it is predicted that LSFE-LBM will provide potential for employment in high Reynolds number conditions, additional efforts are required to validate this point. Second, LBM is well-suited for distributed computing. Since element contributions are computed independently, element-by-element based LSFE-LBM can also be easily implemented in parallel. It is thus worthwhile to provide a more thorough study on the performance of LSFE-LBM following parallelization. Finally, since finite volume based CFDs are more commonly employed relative to finite element based CFDs, it will be meaningful to further assess and compare the performance of LSFE-LBM, FV-LBM, and FV based CFDs.

## CHAPTER VI

### USE OF LSFE-LBM TO STUDY MASS TRANSFER PROCESSES

#### 6.1 Introduction

To provide for effective and efficient groundwater contamination prevention and remediation, it is important to possess a clear understanding of the complex mass transfer processes governing solute transport in the subsurface environment. Solute mass transfer in the subsurface includes several processes acting simultaneously: (i) advective-dispersive transport from bulk solution to the boundary layer of a soil or sediment particle; (ii) film diffusion across adsorbed water to the surface of a particle; (iii) sorption/desorption processes at the surface of the soil particle; and (iv) intrasorbent diffusion. Experimental observations of these processes often reveal non-ideal behaviors, for example, long term sorption/desorption processes may follow a pattern of initial rapid uptake/release, followed by a stage of slow uptake/release. These non-ideal behaviors were attributed to transport-related non-equilibrium factors, e.g. different advection patterns due to complex soil particle geometries (Brusseau, Jessup et al. 1989; Brusseau, Jessup et al. 1991), and sorption-related non-equilibrium factors (Pignatello and Xing 1996), e.g. chemical non-equilibrium reactions, pore diffusion and intrasorbent diffusion processes.

Successful mass transfer models that capture these non-ideal behaviors need to possess the ability to: (i) accurately interpret the rate-limiting mass transfer processes at the particle scale; and (ii) accurately model the complex flow advection behavior within

the porous media. While traditional advective-dispersive equations with a local equilibrium assumption (LEA) often fail to predict non-ideal behaviors, mass transfer models range from one-site models (Lapidus and Amundson 1952) to multi-site models (Brusseau, Jessup et al. 1989; Pedit and Miller 1994; Haggerty and Borelick 1995; Pedit and Miller 1995), multiple diffusion mechanism models (Miller and Weber 1984; Miller and Weber 1988; Ball and Roberts 1991; Pedit and Miller 1994; Cunningham, Werth et al. 1997; Haggerty and Gorelick 1998; Werth and Hansen 2002), and stochastic based models (Cunningham, Werth et al. 1997; Haggerty and Gorelick 1998; Werth and Hansen 2002). Although these models provide enhanced abilities for describing sorption-related nonequilibrium, their ability to account for transport-related nonequilibrium at the microscale is deficient. Extension of these mass transfer models through improved representation of the physics of fluid flow and solute transport in porous media is necessary.

Recently, a lattice Boltzmann method was successfully applied to simulate fluid flow in porous media (Chen and Doolen 1998), providing a powerful alternative to model transport-related nonequilibrium processes. Corresponding to LBM's inability to allow irregularity in the lattice (Sterling and Chen 1996), we developed a least squares finite element lattice Boltzmann method (LSFE-LBM), which uses a LSFE method (Jiang 1998) in space and Crank-Nicolson method in time to solve the lattice Boltzmann equation. As described in Chapter 5, LSFE-LBM was successfully implemented on unstructured mesh to simulate fluid flow in porous media, requiring fewer grid points and consuming significantly less memory than traditional LBM. In this chapter, we extend LSFE-LBM is to simulate solute transport in bulk fluid and couple it with non-linear

sorption/desorption processes at particle surfaces and intraparticle diffusion processes. In this way, we present a novel approach to integrate transport-related nonequilibrium factors with sorption-related nonequilibrium factors.

Following this introduction, a brief description of a LBM model is provided. Validations of LSFE-LBM for solute transport on simple geometric problems are provided in Section 6.3. In Section 6.4, we applied LSFE-LBM to study mass transfer in a simplified system. Sensitivity analysis is performed to elucidate the relative contributions of mass transfer processes. In Section 6.5, LSFE-LBM is applied to study mass transfer processes in porous media.

## 6.2 LSEF-LBM for solute transport

In this study, we assume that the solute concentration is sufficiently low that it will not influence solvent flow. In this case, the solute can be described by a separate particle distribution function (Wolf-Gladrow 2000). To recover the advection-diffusion equation, a simple square lattice with four possible velocities, i.e., D2Q4 model, is sufficient, which can be described as:

$$\frac{\partial g_i}{\partial t} + \bar{c}_i \cdot \bar{\nabla} g_i = -\frac{1}{\tau_s} (g_i - g_i^{\text{eq}}) \quad (i = 1, 2, 3, 4) \quad (6-1)$$

where  $g_i$  represents a particle distribution function for the solute,  $\tau_s$  is the relaxation time,  $\bar{c}_i$  is the microscopic velocity associated with each link, given by:

$$\bar{c}_i = \left( \cos \frac{\pi(i-1)}{2}, \sin \frac{\pi(i-1)}{2} \right), i = 1, 2, 3, 4 \quad (6-2)$$

and  $g_i^{\text{eq}}$  is the corresponding equilibrium distribution function, which is defined by:

$$g_i^{eq} = \frac{C}{4} + \frac{C}{2c^2} (\bar{c}_i \cdot \bar{u}), \quad (6-3)$$

where  $C$  is the solution concentration defined by

$$C = \sum_{i=1}^4 g_i, \quad (6-4)$$

and  $\bar{u}$  is fluid flow velocity provided by solving flow field.

Implementing the same numerical approach as for fluid flow, i.e., Crank-Nicolson method for time and least squares finite element method for space, a LSFE-LBM for solute transport can be derived based on this four velocity model.

### 6.3 Validation of LSFE-LBM

In this section, validations of LSFE-LBM simulating solute transport are performed by several diffusion problems on a very simple geometry for both steady state and unsteady state conditions. LSFE-LBM results are then compared with analytical solutions.

#### 6.3.1 Diffusion between Two Parallel Walls

As illustrated in Figure 6-1, two walls are assumed to be porous and a constant normal flow  $u_a$  is injected through the lower wall and removed from the upper wall. The concentration of solute at the lower and upper walls is maintained with  $C_L$  and  $C_U$ , respectively. In this specific problem,  $C_U$  is assumed higher than  $C_L$ ; it follows that solute diffuses counter to the flow of the fluid.

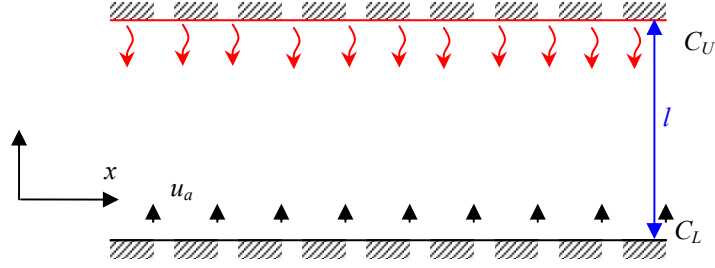


**Figure 6-1. Diffusion between Two Parallel Walls.**

The governing equation for this problem is:

$$\frac{\partial \Phi}{\partial t} = D \frac{\partial^2 \Phi}{\partial y^2} + u_a \frac{\partial \Phi}{\partial y} \quad (6-5)$$

$$\Phi(y,0) = 0, \quad \Phi(0,t) = 0, \quad \Phi(l,t) = 1$$

where,  $\Phi$  is a normalized concentration defined as:  $\Phi = \frac{C - C_L}{C_U - C_L}$ , and  $D$  is the diffusivity of solute. Analytical solutions can be obtained for this problem in two special cases.

Analytical solutions can be obtained for this problem in two special cases.

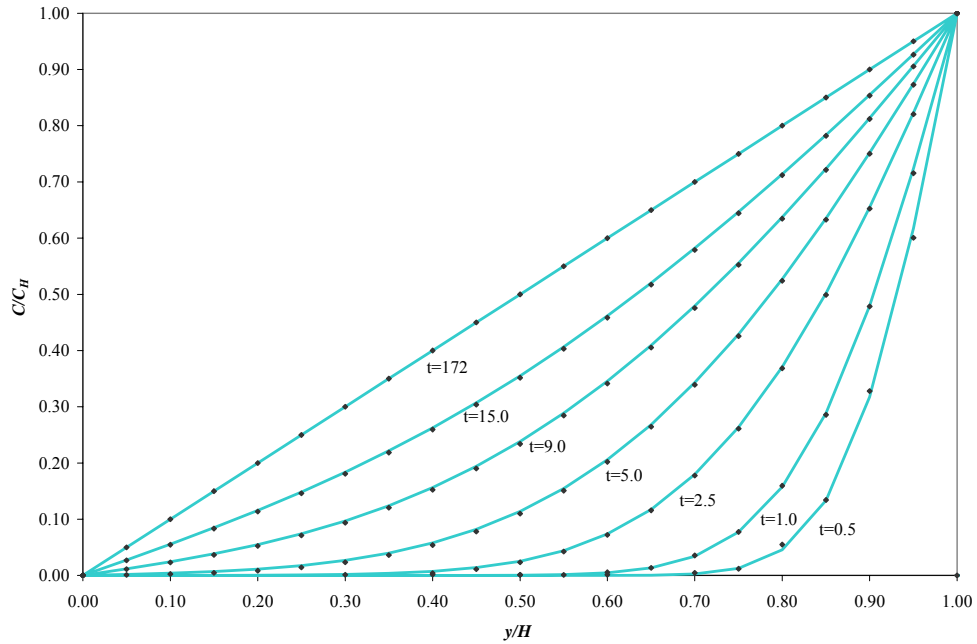
**Case I:** When  $u_a = 0$ , equation (6-5) will reduce to an unsteady state pure diffusion problem. The analytical solution can be expressed as:

$$\Phi(y,t) = \frac{y}{l} + \frac{2}{\pi} \sum_{n=1}^{\infty} \frac{(-1)^n}{n} \sin \frac{n\pi y}{l} e^{-n^2 t / \lambda}, \text{ where } \lambda = \frac{l^2}{\pi^2 D} \quad (6-6)$$

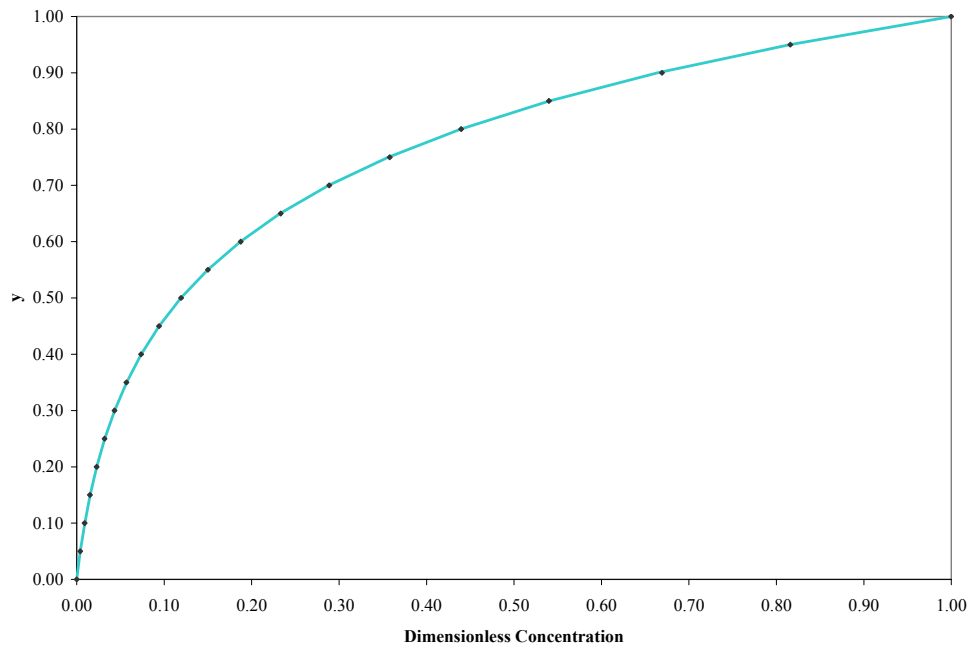
**Case II:** When  $u_a \neq 0$ , analytical solutions are only available for steady-state conditions:

$$\Phi = \frac{e^{(u_a y / D)} - 1}{e^{(u_a l / D)} - 1} \quad (6-7)$$

Results presented in Figure 6-2 illustrate that LSFEE-LBM achieves close agreement with analytical solutions for solute transport in both unsteady state and steady state conditions.



(a)



(b)

**Figure 6-2. Comparison of LSFE-LBM Solution (points) and Analytical Solution (line) for Diffusion between Two Parallel Walls. (a) represents unsteady state solutions when water velocity  $u_a=0$  and (b) represents steady state solution when water velocity  $u_a \neq 0$ .**

### 6.3.2 Diffusion with Reactive Boundary

In this section, applicability of LSFE-LBM to reactive boundary conditions is examined by the classical problem of diffusion between two parallel walls. As illustrated in Figure 6.3, a constant concentration  $C_{A0}$  is maintained at the lower wall, while a first order reaction occurs at the surface of the upper wall. Solute is transported between the two walls due to the concentration gradient.

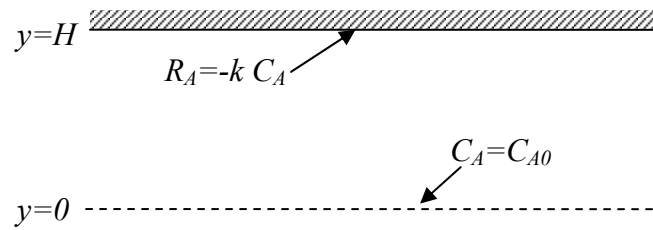


**Figure 6-3. Diffusion between Two Parallel Walls with a Reactive Boundary Condition.**

The governing equation and boundary conditions for this problem are:

$$\frac{d^2 C_A}{dy^2} = 0 \quad (6-8)$$

$$C_A = C_{A0}, \quad @ y=0$$

$$D \frac{dC_A}{dy} = -k C_A, \quad @ y=H$$

where  $C_A$  represents concentration of solute A,  $D$  is the diffusion coefficient of solute A,  $k$  is the first order reaction rate, and  $H$  is the distance between two walls. An analytical solution of this problem is given by:

$$\frac{C_A}{C_{A0}} = 1 - \frac{D_a}{1 + D_a} \frac{y}{H}, \quad D_a = \frac{kH}{D} \quad (6-9)$$



where  $D_a$  is Damkohler number, representing the ratio of reaction rate to the diffusion rate.

To implement the boundary condition at the upper wall, it is important to relate the concentration gradient with the microscale particle distribution function. For a D2Q4 lattice Boltzmann model, a relationship is given by (Noble 1997):

$$\sum_{i=1}^4 g_i c_{i\alpha} \approx C u_\alpha - \frac{\tau_s}{2} \partial_\alpha C \quad (6-10)$$

where  $\alpha$  denotes  $x$  or  $y$  direction. As shown in Figure 6.4,  $g_4$  and concentration  $C$  is unknown.

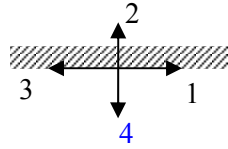


**Figure 6-4. An Illustration of an Upper Wall Boundary Condition at the Micro-Scale.**

Based on the relationship (6-10), and the fact of  $u = 0$  on the wall, we can get:

$$g_2 - g_4 = -\frac{\tau_s}{2} \frac{\partial C}{\partial y}. \quad (6-11)$$

Substituting in the boundary condition on the wall, we have:

$$g_2 - g_4 = -\frac{\tau_s}{2} \frac{\partial C}{\partial y} = \frac{\tau_s}{2} \frac{k}{D} C \quad (6-12)$$

Further, we know:

$$g_1 + g_2 + g_3 + g_4 = C \quad (6-13)$$

Solving equation (6-12) and (6-13), unknown distribution  $g_4$  and concentration  $C$  can be calculated. LSFE-LBM simulation results were compared with analytical solutions under different Damkohler numbers. As presented in Figure 6-5, very good accuracy is achieved, demonstrating the ability of LSFE-LBM to simulate reactive boundary diffusion problems.

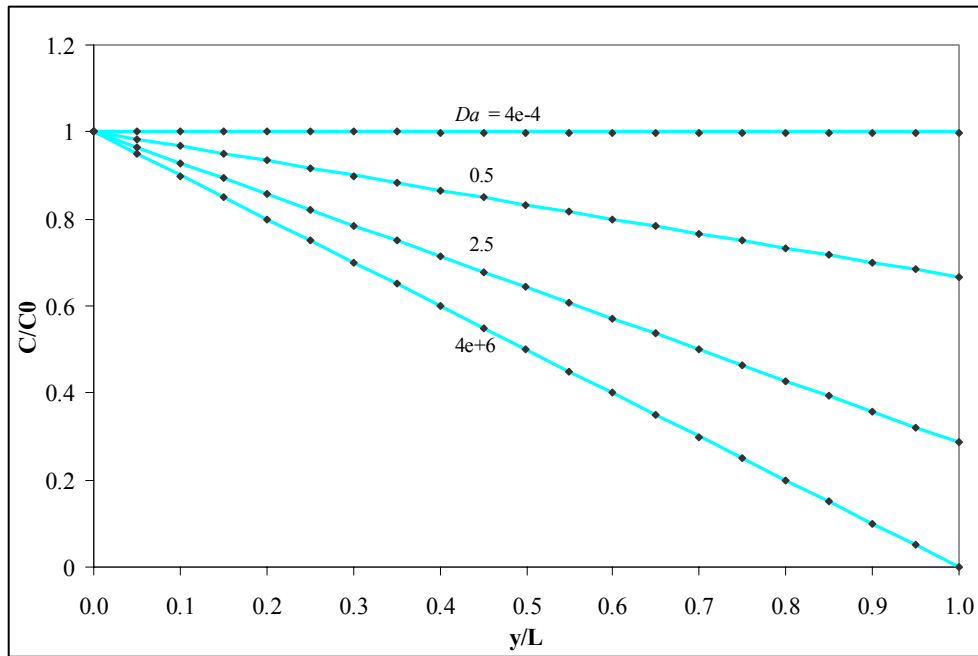


**Figure 6-5. Comparison of LSFE-LBM Solution (points) and Analytical Solution (line) for Diffusion Between Two Parallel Walls with a Reactive Boundary Condition under Different Damkohler Numbers.**

## 6.4 Use of LSFE-LBM to simulate mass transfer in a single particle system

### 6.4.1 Problem Description

To explore influences of transport-related and sorption-related non-equilibrium factors on mass transfer processes, we first apply LSFE-LBM to simulate flow and

transport through and around a single circular particle, set in a two-dimensional domain with a uniform far-field velocity, as illustrated in Figure 6-6.

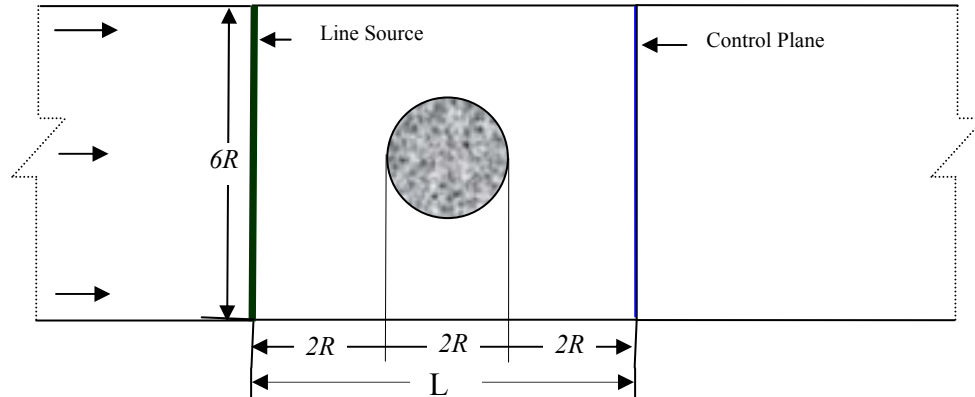


**Figure 6-6. An Illustration of Fluid Flow and Solute Transport Through and Around a Circular Particle.**

As shown in Figure 6-6, a constant body force is imposed to as the driving force to move the fluid from the left to right. In the steady state fluid flow field, a solute source with a constant concentration is applied as a line source. Solute transport in the bulk fluid is driven by advection and diffusion processes. Some solutes will arrive at the surface of the particle, where sorption/desorption processes will occur. The sorption rate at the particle surface can be expressed (Brusseau and Rao 1990) as a function of the concentration difference between the solid and solution phases:

$$\frac{\partial s}{\partial t} = k_a C^m - k_d s \quad (6-14)$$

where:

- $s$  = the solute concentration in the solid phase [M/L<sup>2</sup>];
- $C$  = the solute concentration in solution [M/L<sup>3</sup>];
- $m$  = Freundlich sorption intensity exponent [-];
- $k_a$  = sorption rate coefficient [L/T] [L<sup>3</sup>/M]<sup>m-1</sup>; and

$k_d$  = desorption rate coefficient [1/T].

At equilibrium, i.e.  $\frac{\partial s}{\partial t} = 0$ , adsorption may be described by a Freundlich isotherm as:

$$s = (k_a / k_d) C^m, \quad (6-15)$$

Following adsorption at the surface, the solute may diffuse into the soil particle. A simple Fickian diffusion model is employed to describe this intra-particle process:

$$\frac{\partial q}{\partial t} = D_{in} \left( \frac{\partial^2 q}{\partial r^2} + \frac{1}{r} \frac{\partial q}{\partial r} + \frac{1}{r^2} \frac{\partial^2 q}{\partial \theta^2} \right) \quad (6-16)$$

where:

$q$  = the solid phase concentration [M/L<sup>3</sup>];  
 $D_{in}$  = the intraparticle diffusion coefficient [M<sup>2</sup>/T];  
 $r$  = the radial coordinate; and  
 $\theta$  = the azimuthal coordinate.

#### 6.4.2 Liquid Phase Boundary Condition

Boundary conditions at the solid-liquid interface are derived by mass conservation. Considering a typical control volume at the surface noted in Figure 6-7, mass balance of the liquid phase solute may be expressed as:

$$\frac{\partial}{\partial t} \int C dV = \int \left( -r_c + D \frac{\partial C}{\partial n} \right) dA \quad (6-17)$$

where  $V$  is the volume of control volume,  $A$  is the surface area, and  $r_c$  is the adsorption/desorption rate expressed by:

$$-r_c = k_a C^m - k_d s \quad (6-18)$$

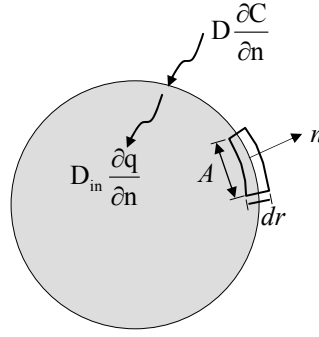


**Figure 6-7. An Illustration of Boundary Conditions at the Solid-Liquid Interface.**

For a small control volume, it is reasonable to assume that solute concentration, solute adsorption/desorption rates, and diffusion rates are all uniform at the surface, then we have:

$$\frac{\partial}{\partial t} \int C A dr = \left( -r_c + D \frac{\partial C}{\partial n} \right) A \quad (6-19)$$

or

$$\frac{\partial}{\partial t} (\bar{C} \cdot dr) = -r_c + D \frac{\partial C}{\partial n} \quad (6-20)$$

where  $\bar{C}$  is an average concentration over the depth of the control volume. When  $dr$  is sufficiently small, the local adsorption/desorption and diffusion rates will be equal to the diffusion rate:

$$r_c = D \frac{\partial C}{\partial n}, \quad (6-21)$$

or

$$D \frac{\partial C}{\partial n} = k_a C^m - k_d s \quad (6-22)$$

This formula reflects a boundary condition at the macroscale. To implement this in LSFE-LBM, it is necessary to use the relationship between the macroscale concentration gradient and microscale particle distribution functions, equation (6-10):

$$\sum_{i=1}^4 g_i c_{i\alpha} \approx C u_\alpha - \frac{\tau_s}{2} \partial_\alpha C \quad (6-10)$$

Applying this relationship to boundary nodes as shown in Figure 6-8,

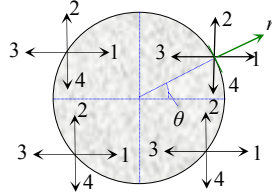


**Figure 6-8. An Illustration of the LBM Boundary Condition at the Solid-Liquid Interface.**

We have the following expressions:

$$g_2 - g_4 = -(k_a C^n - k_d s) \sin \theta \quad (6-23)$$

$$g_1 - g_3 = -(k_a C^n - k_d s) \cos \theta \quad (6-24)$$

Further, we know:

$$g_1 + g_2 + g_3 + g_4 = C \quad (6-25)$$

Unknown distribution functions are different for each portion of the circular surface. For example, at the upper left quadrant of the circle,  $g_2$  and  $g_3$  are unknown; at the upper right quadrant,  $g_1$  and  $g_2$  are unknown; at the lower left quadrant,  $g_3$  and  $g_4$  are unknown; and at the lower right quadrant  $g_1$  and  $g_4$  are unknown. Meanwhile, concentration  $C$  is unknown for all four domains. At each time step, boundary conditions are applied by solving the non-linear equation system (6-23), (6-24), and (6-25) with different unknowns corresponding to each domain.

### 6.4.3 Intraparticle Diffusion

Following adsorption at the particle surface, intraparticle diffusion will occur either by pore diffusion or intra-organic matter diffusion. For simplification, it is assumed in this study that the soil particle possesses uniform diffusivity everywhere. A Fickian diffusion model is employed to describe intraparticle diffusion, as described in equation (6-16):

$$\frac{\partial q}{\partial t} = D_{in} \left( \frac{\partial^2 q}{\partial r^2} + \frac{1}{r} \frac{\partial q}{\partial r} + \frac{1}{r^2} \frac{\partial^2 q}{\partial \theta^2} \right) = D_{in} \nabla^2 q \quad (6-16)$$

In a similar manner to the liquid phase solute, a boundary condition at the surface of particle for the solid phase solute can be derived:

$$D_{in} \left. \frac{\partial q}{\partial n} \right|_{r=R} = -(k_a C^m - k_d s) \quad (6-26)$$

Due to the non-uniform feature of  $C$  and surface concentration  $s$  at the surface of the particle, no analytical solution is available to describe this intraparticle diffusion process. In this work, a numerical technique with finite-difference in space and Crank-Nicolson method in time space was implemented, as illustrated in Figure 6-9.

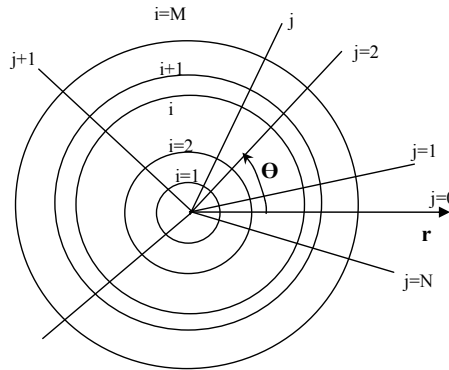


**Figure 6-9. An Illustration of a Finite Difference Discretization of a Circular Particle with a Cylindrical Coordinate System.**

Using a central difference scheme, first and second order differentiation in equation (6-16) can be approximated as:

$$\frac{\partial^2 q}{\partial r^2} = \frac{q_{i+1,j} - 2q_{i,j} + q_{i-1,j}}{(dr)^2} \quad (6-27)$$

$$\frac{1}{r} \frac{\partial q}{\partial r} = \frac{1}{i(dr)} \frac{q_{i+1,j} - q_{i-1,j}}{2dr} \quad (6-28)$$

$$\frac{1}{r^2} \frac{\partial^2 q}{\partial \theta^2} = \frac{1}{(idr)^2} \frac{q_{i,j+1} - 2q_{i,j} + q_{i,j-1}}{(d\theta)^2} \quad (6-29)$$

Thus,

$$\begin{aligned} \nabla^2 q = \\ \frac{1}{dr^2} \left[ \left(1 - \frac{1}{2i}\right) q_{i-1,j} + \left(1 + \frac{1}{2i}\right) q_{i+1,j} - 2 \left(1 + \frac{1}{i^2 d\theta^2}\right) q_{i,j} + \frac{1}{i^2 d\theta^2} q_{i,j-1} + \frac{1}{i^2 d\theta^2} q_{i,j+1} \right] \end{aligned} \quad (6-30)$$

Applying a Crank-Nicolson method to the time discretization:

$$\frac{q_{i,j}^{t+1} - q_{i,j}^t}{dt} = \frac{D_{in}}{2} (\nabla^2 q^{t+1} + \nabla^2 q^t) \quad (6-31)$$

Substituting equation (6-30) and (6-31) into equation (6-16):

$$\begin{aligned} (R1)q_{i-1,j}^{t+1} + (R2)q_{i,j-1}^{t+1} + (R3)q_{i,j}^{t+1} + (R4)q_{i,j+1}^{t+1} + (R5)q_{i+1,j}^{t+1} & \quad i = 2, \dots, M-1 \\ = -(R1)q_{i-1,j}^t - (R2)q_{i,j-1}^t - (R3b)q_{i,j}^t - (R4)q_{i,j}^t - (R5)q_{i+1,j}^t & \quad j = 0, 1, \dots, N \end{aligned} \quad (6-32)$$

$$\text{where, } R1 = -\alpha \left(1 - \frac{1}{2i}\right); \quad R2 = -\frac{\alpha}{i^2 d\theta^2}; \quad R3 = 1 + 2\alpha \left(1 + \frac{1}{i^2 d\theta^2}\right); \quad R4 = -\frac{\alpha}{i^2 d\theta^2};$$

$$R5 = -\alpha \left(1 + \frac{1}{2i}\right); \quad R3b = 1 - 2\alpha \left(1 + \frac{1}{i^2 d\theta^2}\right); \quad \text{and } \alpha = \frac{D_{in} dt}{2dr^2}.$$

At the surface of the particle, i.e.  $i=M$ ,  $q_{M+1,j}$  can only be derived by approximating the boundary condition equation (6-26)



$$D_{in} \left. \frac{\partial q}{\partial n} \right|_{r=R} = -(k_a C^m - k_d s) \quad (6-26)$$

as:

$$\frac{q_{M+1,j} - q_{M-1,j}}{2dr} = -\frac{\gamma}{D_{in}} (k_a C_{M,j}^m - k_d s_{M,j}) = w_M \quad (6-33)$$

Rearranging:

$$q_{M+1,j} = 2drw_M + q_{M-1,j} \quad (6-34)$$

and substituting in equation (6-32) yields:

$$\begin{aligned} -2\alpha q_{i-1,j}^{t+1} + (R2)q_{i,j-1}^{t+1} + (R3)q_{i,j}^{t+1} + (R4)q_{i,j+1}^{t+1} & \quad i = M \\ = 2\alpha q_{i-1,j}^t - (R2)q_{i,j-1}^t + (R3b)q_{i,j}^t - (R4)q_{i,j}^t - 4(dr)w_M \alpha R5 & \quad j = 0,1,\dots,N \end{aligned} \quad (6-35)$$

In the inner most circle  $i=1$ ,  $q_{0,j}$ , the concentration in the center of particle, is not directly available, and is thus approximated as follows. It can be shown (Smith 1978) that  $\nabla^2 q$  can be approximated in a second order accuracy as:

$$\nabla^2 q = \frac{4(q_{\text{mean}} - q_0)}{dr^2} + o(dr)^2 \quad (6-36)$$

where  $q_{\text{mean}}$  is a mean value of concentration around the inner most circle. At  $r = 0$ , the governing equation is then reduced to:

$$\frac{1}{D_{in}} \frac{\partial q}{\partial t} = \frac{4(q_{\text{mean}} - q_0)}{dr^2} \quad (6-37)$$

Applying a Crank-Nicolson method, we have:

$$q_0^{t+1} - q_0^t = \frac{2D_{in} dt}{dr^2} (q_{\text{mean}}^{t+1} - q_0^{t+1} + q_{\text{mean}}^t - q_0^t) \quad (6-38)$$

Combining (6-32), (6-35), (6-38), a linear equation system can be derived:

$$[A]\{q\}^{t+1} = [B]\{q\}^t + \{k\} \quad (6-39)$$

where A and B are two  $M^*(N+1) \times M^*(N+1)$  matrices, and  $\{q\}$  and  $\{q\}^{t+1}$  illustrate that  $\{k\}$  is a  $M^*(N+1)$  vector, with

$$k = \begin{cases} 0 & i \neq M \\ 4(dr)w_M \alpha \left(1 + \frac{1}{2M}\right) & i = M \end{cases} \quad (6-40)$$

With a given initial condition, the solid phase concentration at current time step  $\{q\}^{t+1}$  in equation (6-40) may be calculated.

#### 6.4.4 Analysis of the Single Particle System

As illustrated in Figure 6-10, mass transfer processes in this single particle system include diffusion and advection in the bulk fluid, adsorption/desorption at the surface of the particle, and intraparticle diffusion. Advection and diffusion in the bulk fluid act in parallel, which similarly act in parallel with mass transfer processes in the solid particle. Mass transfer processes in the solid particle act in series, where surface adsorption processes occur first, followed by intraparticle diffusion.

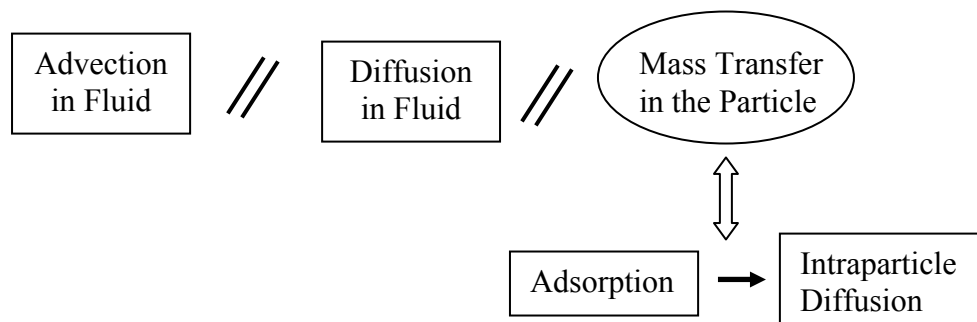


**Figure 6-10. An Illustration of Relationships among Mass Transfer Processes in a Single Particle System.**

For parallel processes, the fastest one will control; while for series processes, the slowest one will control. To quantitatively analyze mass transfer characteristics, we defined several dimensionless numbers.

### 1. Pe

The Peclet number represents the ratio of the time scale of diffusion in the bulk fluid to the time scale of advection in the bulk fluid:

$$P_e = \frac{L^2 / D}{L / u} = \frac{uL}{D}, \quad (6-41)$$

where  $u$  is an average velocity of the domain, and  $L$  is the characteristic length of the domain defined as the distance between the source line and the control panel. A large Pe indicates that advection is important, while a small Pe means diffusion will control.

### 2. Dna

Dna is defined as the ratio of adsorption reaction time to the intraparticle diffusion time. For simplicity, only linear adsorption processes are considered, so that  $k_a$  is possesses units of [L/T], where Dna may be expressed as:

$$Dna = \frac{R / k_a}{R^2 / D_{in}} = \frac{D_{in}}{Rk_a} \quad (6-42)$$

Since adsorption and intraparticle diffusion act in series, the slower process will dominate. A large Dna thus indicates that surface adsorption will control, while a small Dna implies that intraparticle diffusion will control.

### 3. Dad

Dad is defined as the ratio of the time scale of diffusion in bulk fluid to the adsorption reaction time. Again,  $k_a$  possesses units of [L/T] for linear adsorption, which gives:

$$D_{ad} = \frac{L^2/D}{R/k_a} = \frac{L^2 k_a}{RD} \quad (6-43)$$

Since diffusion in the bulk fluid and adsorption are parallel processes, the faster process will control. A large  $D_{ad}$  means adsorption will control, while a small  $D_{ad}$  indicates that diffusion in the bulk fluid will control.

Figure 6-11 graphically represents different mass transfer regions based on these defined dimensionless numbers.

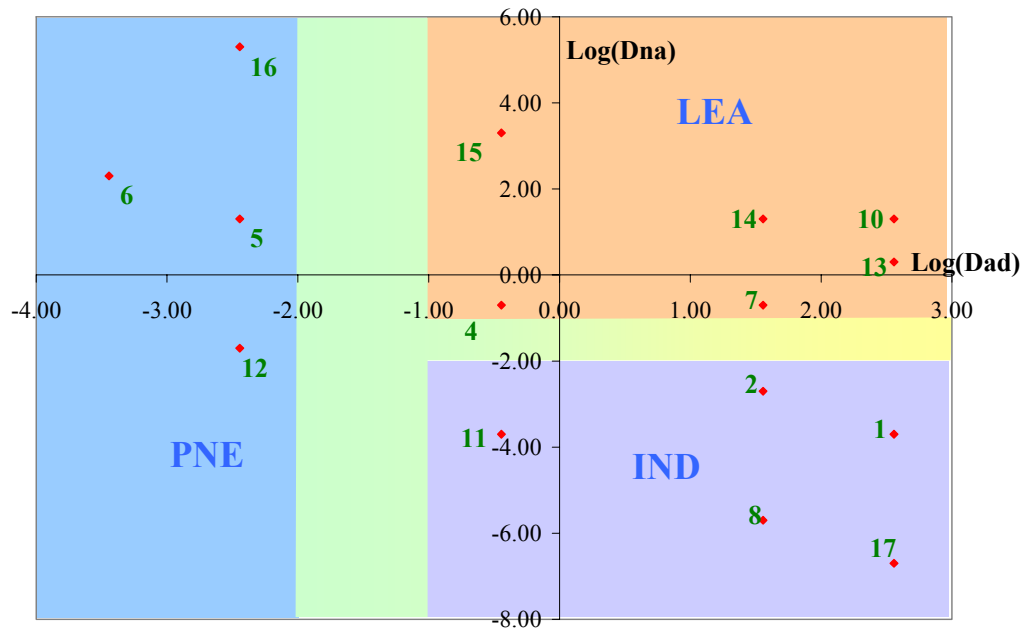


**Figure 6-11. Graphic Representation of Mass Transfer Regimes of a Single Particle System.**

When the adsorption reaction rate is smaller than the diffusion rate in the bulk fluid (i.e.  $D_{ad} \ll 1$ ), the contribution of sorption-related nonequilibrium is relatively insignificant. In this case, physical nonequilibrium will control, which is represented as region PNE in

the figure. When both the adsorption reaction rate and the intraparticle diffusion rate are larger than the diffusion rate in the bulk fluid (i.e.  $D_{ad} \gg 1$ , and  $D_{na} \gg 1$ ), the overall mass transfer rate in the particle will be very fast, indicating a local equilibrium condition, which is denoted as region LEA in the figure. When the adsorption reaction rate is faster than the diffusion rate in the bulk fluid (i.e.  $D_{ad} \gg 1$ ) and the intraparticle diffusion rate is smaller than the adsorption reaction rate (i.e.  $D_{na} \ll 1$ ), intraparticle diffusion will control, represented as region IND.

#### 6.4.5 Numerical Simulations

Mass transfer characteristics of each region were studied by conducting numerical experiments with varied intraparticle diffusion coefficients,  $D_{in}$ , and adsorption reaction rates,  $k_a$ , for a single particle system. General system characteristic parameters are as listed in Table 6-1.

**Table 6-1. Parameters of the Single Particle System.**

<b>L (<math>\mu\text{m}</math>)</b>	<b>R (<math>\mu\text{m}</math>)</b>	<b>D (<math>\text{mm}^2/\text{s}</math>)</b>	<b>Re</b>
300.00	50.00	5.00E-05	0.14

##### 6.4.5.1 Region PNE

Mass transfer characteristics of region PNE was first studied. Parameters of numerical tests are listed in Table 6-2. Corresponding locations of these tests in region PNE are denoted as dots in Figure 6-11.

**Table 6-2. Parameters of Numerical Tests for Region PNE.**

Case	$k_a(\mu\text{m/s})$	$D_{in}(\text{mm}^2/\text{s})$	$\log(D_{ad})$	$\log(D_{na})$
6	1.00E-05	1.00E-07	-3.44	2.30
12	1.00E-04	1.00E-10	-2.44	-1.70
5	1.00E-04	1.00E-07	-2.44	1.30
16	1.00E-04	1.00E-03	-2.44	5.30

As illustrated in Figure 6-12, numerical test Cases 5, 6, 12, and 16 produced identical breakthrough curves (BTCs), although their  $k_a$  spanned one order of magnitude and  $D_{in}$  varied over seven orders of magnitude. The identical BTCs are probably due to small  $D_{ad}$  values, which imply a small adsorption reaction rate relative to the diffusion rate in the bulk fluid. Thus, when  $D_{ad}$  is sufficiently low, the sorption-related nonequilibrium component will have minimum effects on solute transport. In this example, when  $D_{ad}$  is less than -2.44, influences of sorption-related nonequilibrium may be neglected.

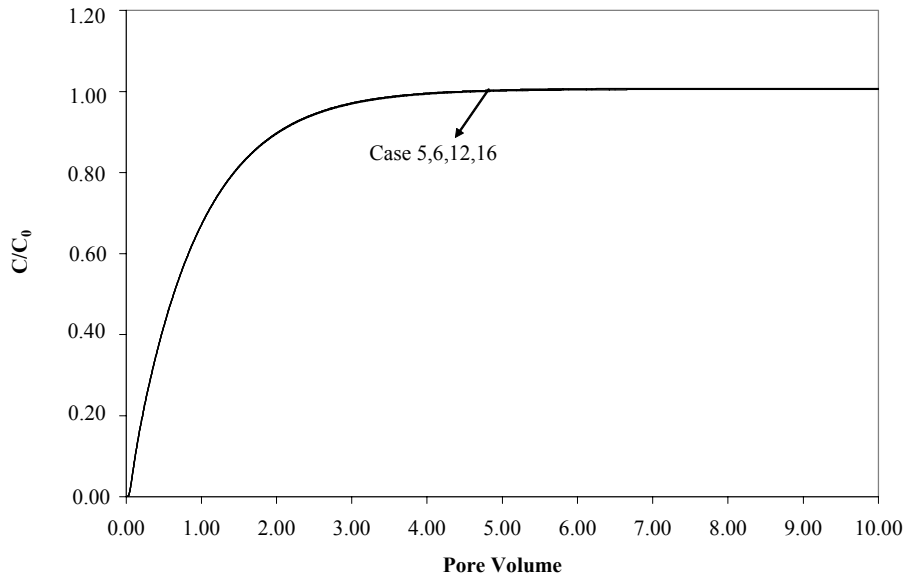


**Figure 6-12. Break Through Curves in Region PNE.**

6.4.5.2. Region LEA

When both  $k_a$  and  $D_{in}$  are large enough, the time scale of mass transfer in the solid phase will be very small compared to the time scale of solute transport in the bulk fluid, in which case the local equilibrium assumption is valid. Numerical experiment Cases 7, 10, 14 and 13 were conducted in region LEA, as presented in Table 6-3 and Figure 6-13.

**Table 6-3. Parameters of Numerical Tests for Region LEA.**

Case	$k_a$ ( $\mu\text{m/s}$ )	$D_{in}$ ( $\text{mm}^2/\text{s}$ )	$\log(D_{ad})$	$\log(D_{na})$
7	1.00E+00	1.00E-05	1.56	-0.70
14	1.00E+00	1.00E-03	1.56	1.30
13	1.00E+01	1.00E-03	2.56	0.30
10	1.00E+01	1.00E-02	2.56	1.30

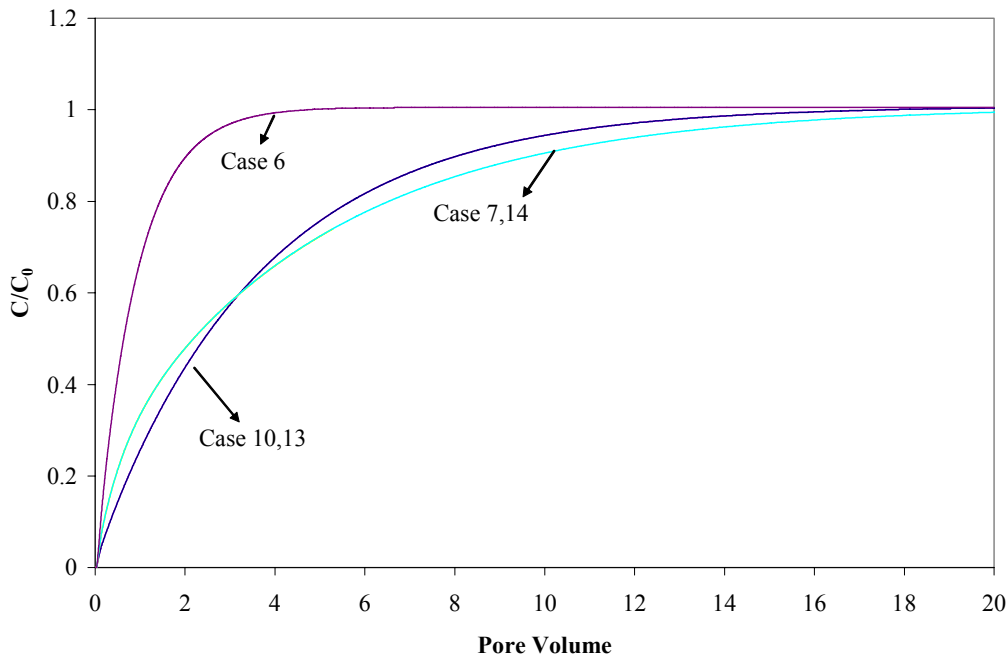


**Figure 6-13. Break Through Curves in Region LEA.**

Compared with BTCs in region PNE, e.g., Case 6, BTCs in region LEA present much later breakthrough. This is due to the presence of much higher  $D_{ad}$  values in region LEA, which allow more solutes enter solid particle, producing lower outlet concentration at the control point.

It is interesting to note that Cases 7 and 14 possess identical BTCs, as do Cases 10 and 13, which can be attributed to large  $D_{na}$  values in region LEA. A large  $D_{na}$  indicates a smaller adsorption rate relative to the intraparticle diffusion rate. Since adsorption and intraparticle diffusion are in series, adsorption will control if it is slower. In this condition, variations in the intraparticle diffusion rate will not influence mass transfer characteristics.

It is also interesting to examine the intersection of BTCs of Cases 7 and 14 and Cases 10 and 13. At early times, since Cases 10 and 13 possess higher adsorption rates than Cases 7 and 14, more solute will attach on the surface of the solid particle, resulting in a lower outlet concentration. With the concentration at the surface of the particle increasing, the concentration gradient at solid-liquid interfaces will decrease, leading to a slower mass uptake within the solid particle. At this point, less solute will enter Cases 10 and 13, resulting in a higher outlet concentration relative to Cases 7 and 14.

#### *6.4.5.3 Region IND*

In region IND, the adsorption rate is faster than the diffusion rate in the bulk fluid, but the intraparticle diffusion rate is slower than the adsorption rate. In this region, intraparticle diffusion will control. Numerical tests for region IND and their results are presented in Table 6-4 and Figure 6-14.



**Table 6-4. Parameters of Numerical Tests for Region IND.**

Case	$k_a(\mu\text{m/s})$	$D_{in}(\text{mm}^2/\text{s})$	$\log(D_{ad})$	$\log(D_{na})$
8	1.00E+00	1.00E-10	1.56	-5.70
2	1.00E+00	1.00E-07	1.56	-2.70

As shown in Figure 6-14, while Cases 7 and 14 share a similar BTC in region LEA, Cases 2 and 8 possess different BTCs. This confirms that when  $D_{ad}$  is large and  $D_{na}$  is small, intraparticle diffusion will be an important factor in the overall mass transfer rate. Since the intraparticle diffusion rate of Case 8 is lower than Case 2, less solute will enter the particle in Case 8 than in Case 2, resulting in higher outlet solute concentration in Case 8.

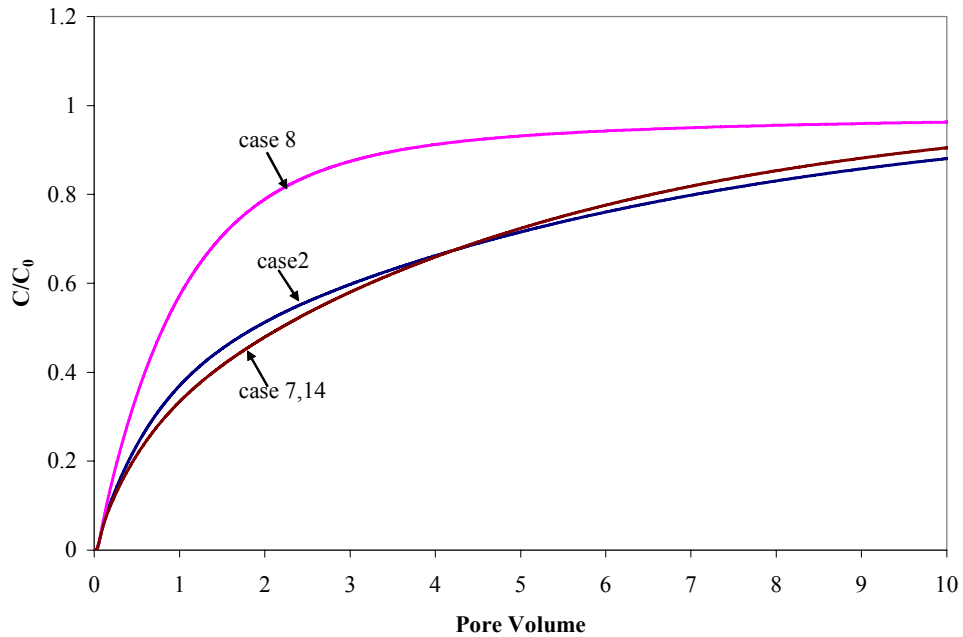


**Figure 6-14. Break Through Curves in Region IND.**

Cases 1, 4, 11, 15, and 17 were conducted to elucidate under what circumstances intraparticle diffusion will begin to govern, as presented in Table 6-5.

**Table 6-5. Parameters of Numerical Tests for Defining the Intraparticle Diffusion Region.**

Case	$k_a(\mu\text{m/s})$	$D_{in}(\text{mm}^2/\text{s})$	$\log(D_{ad})$	$\log(D_{na})$
11	1.00E-02	1.00E-10	-0.44	-3.70
4	1.00E-02	1.00E-07	-0.44	-0.70
15	1.00E-02	1.00E-03	-0.44	3.30
17	1.00E+01	1.00E-10	2.56	-6.70
1	1.00E+01	1.00E-07	2.56	-3.70

As noted in the previous section, BTCs of Cases 5, 6, 12 and 16 in region PNE are identical, representing insignificant effects of sorption-related factors. BTCs of Case 4, 11 and 15 appear different than BTCs of Case 5, 6, 12 and 16, suggesting that larger  $D_{ad}$  values increase the role of sorption-related non-equilibrium. It is reasonable to consider the existence of a transition area that sorption-related factors will begin to function, which is about  $\log(D_{ad}) \in (-2.0, -1.0)$  for this example.

While  $\log(D_{ad}) > -1.0$ , Cases 11, 4, 15, Cases 8, 2, 7, 14, and Cases 17, 1, 13, 10 represent three groups whose members possess similar  $D_{ad}$  values but varied  $D_{na}$ . As shown in Table 6-6, BTCs will be insensitive to intraparticle diffusion when  $\log(D_{na})$  is larger than -0.7. Since a similar trend holds true for  $\log(D_{ad})$ , it is reasonable to consider a transition region instead of a distinct line along which the overall mass transfer rate will be influence by intraparticle diffusion, which is approximately  $\log(D_{na}) \in (-2.0, -1.0)$  for this example.

**Table 6-6. An Analysis of BTCs of Numerical Tests for Defining the Intraparticle Diffusion Region.**

Case	Log(Dad)	log(Dna)	BTC
15	-0.44	3.30	Same as Case 4
4	-0.44	-0.70	Same as Case 15
11	-0.44	-3.77	Different
14	1.56	1.30	Same as Case 7
7	1.56	-0.70	Same as Case 14
2	1.56	-2.77	Different
8	1.56	-5.77	Different
10	2.56	1.30	Same as Case 13
13	2.56	0.30	Same as Case 10
1	2.56	-3.70	Different
17	2.56	-6.70	Different

*6.4.5.4 Summary of a Single Particle System*

Thus, for this single particle system, we have: (i) when  $\log(\text{Dad}) < (-2.0, -1.0)$ , sorption-related non-equilibrium will have a minimal effect on solute transport, and physical nonequilibrium will control. (ii) when  $\log(\text{Dad}) > (-2.0, -1.0)$  and  $\log(\text{Dna}) > (-2.0, -1.0)$ , both the adsorption reaction rate and the intraparticle diffusion rate are fast. In this situation, a local equilibrium assumption will be valid, and mass transfer is insensitive to intraparticle diffusion; (iii) when  $\log(\text{Dad}) > (-2.0, -1.0)$  and  $\log(\text{Dna}) < (-2.0, -1.0)$ , intraparticle diffusion will significantly influence the overall mass transfer rate.

## **6.5 Use of LSFE-LBM to simulate mass transfer in porous media**

### 6.5.1 Introduction

Experimental observations of fate and transport of hydrophobic organic chemicals (HOCs) in subsurface environment often reveal non-ideal behaviors, for example, long term sorption/desorption processes may follow a pattern of initial rapid uptake/release, followed by a stage of slow uptake/release (Brusseau and Rao 1989). Traditional models employing ideal contaminant transport processes represented by local equilibrium assumptions and linear sorption processes often fail to adequately model observed processes, suggesting other, non-ideal factors are influencing observed behaviors. Heterogeneities of soils and sediments, including soil and sediment structural configurations and composition, are known to play important roles for these non-ideal behaviors.

Variable structural configurations can result in complex advection patterns in porous media, leading to transport-related non-ideal behaviors (Brusseau, Jessup et al. 1989; Brusseau, Jessup et al. 1991). Research has shown that complex pore configurations, including root channels, earth worm burrows, and intrapedal voids, contribute significantly to nonideal solute transport behaviors (Beven and Germann 1982; Willoughby and Klavivko 2002). For example, preferential transport of water and solute in macropore channels will lead to early solute breakthrough. Experimental studies and numerical modeling efforts were carried out to investigate the influence of intraparticle porosity (Brusseau 1993), macropore networks (Haws, Das et al. 2004), and soil aggregations (Rao, Rolston et al. 1980; Van Genuchten and Dalton 1986). These

numerical modeling efforts, however, focus at the Darcy-scale. It remains a very difficult challenge to explicitly quantify pore tortuosity, particle geometry, and pore size distribution within models. While it is obvious that the variability of flow rate and solute concentration at the pore scale will affect mass transfer characteristics, proper pore-scale modeling efforts will thus enhance our ability to explore the influence of microscale soil structure configurations on mass transfer.

Meanwhile, the variable soil and sediment composition can contribute to sorption-related non-ideal behaviors (Pignatello and Xing 1996), e.g., chemical non-equilibrium reactions, pore diffusion, and intrasorbent diffusion processes. Studies (Pignatello and Xing 1996) have attributed some non-ideal behaviors of HOC transport, e.g., slow desorption, to a combination of contributions of different reactivity fractions, i.e., mineral fraction and soil organic matter (SOM) in their different physical states, i.e., glassy or condensed states and rubbery or gel-like states. The Distributed Reactivity Model (DRM), proposed by Weber and co-workers (Weber, McGinley et al. 1992; Young and Weber 1995; Weber and Huang 1996; Huang, Young et al. 1997; LeBoeuf and Weber 1997; Huang and Weber 1998), characterizes soil particles as three functional domains that contribute differently to equilibrium and non-equilibrium sorption/desorption processes.

Domain I consists of mineral sites which may play a minor role for HOC sorption/desorption processes (Huang, Schlautman et al. 1996). Domain II contains soft fractions of SOM, such as humic acids and fulvic acids in their rubbery states. Humic acids, soluble in bases but insoluble in acids, are dominant SOM components (Stevenson 1994). Humic acids may transfer from a glassy state to a rubbery state at temperature

range between 36 °C to 62 °C (LeBoeuf and Weber 1997; LeBoeuf and Weber 2000; LeBoeuf and Weber 2000; Schaumann and Antelmann 2000; Young and LeBoeuf 2000; DeLapp and LeBoeuf 2004; DeLapp, LeBoeuf et al. 2004). Although it has been observed that HOCs may present slow sorption/desorption rate in aged humic materials (Shor, Rockne et al. 2003), humic acids in their rubbery states, possessing high macromolecular mobility, often provide sites for relatively fast and linear sorption/desorption processes. Domain III refers to condensed fractions of SOM, such as kerogen, black carbon, and humic acids in their glassy states, and are believed to be primarily responsible for adsorption-type behaviors. Kerogen, the nonextractable fraction of SOM, is an important component of Domain III, where it has been shown to possess much larger sorption capacities for HOCs than humic acids, and always presents highly nonlinear sorption isotherms (Young and Weber 1995; Kleineidam, Rugner et al. 1999).

Identification of kerogen and detection of glass transition phenomenon for humic acids improved the mechanistic understanding of HOC sorption and desorption processes. However, efforts of incorporating these laboratory observations with pore-scale simulation of HOCs fate and transport are insufficient (Huang, Peng et al. 2003). As an initial effort to bridge comprehensive sorption/desorption mechanistic studies with pore-scale modeling, LSFE-LBM was employed to study the influences of the heterogeneity of both soil structure configurations and soil compositions on solute transport in porous media.

### 6.5.2 System Setting

The desorption of phenanthrene, a typical HOC, from soils and sediments under saturated conditions was simulated. Numerical simulations were conducted for the system illustrated in Figure 6-15.

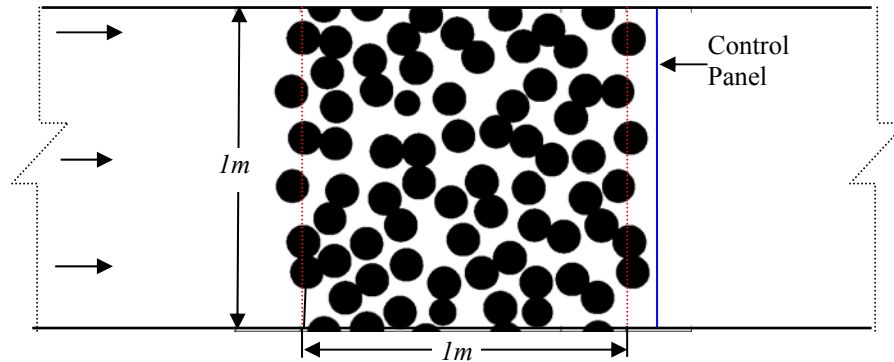


**Figure 6-15. An Illustration of Fluid Flow and Solute Transport through a Porous Medium.**

A 1 mm × 1 mm soil domain consisting of circular particles with geometric mean diameter of 100 μm, depicting particle size representative of coarse sand, was studied. The particle size distribution function of the domain obeys a modified lognormal distribution, employing a 95% confidence interval for particle size to eliminate extreme values. The geometric mean porosity of the domain is 0.5. The phenanthrene concentration was initially set as a uniform concentration  $C_0$  of 1.0 mg/L, close to its aqueous solubility at 25 °C (Schwarzenbach, Gschwend et al. 1993). The bulk fluid flows from left to right, with a Reynolds number close to 0.002, representing laminar flow conditions in porous media. Phenanthrene transport in the bulk fluid is driven by

advection and diffusion processes, with a diffusion coefficient of  $8.0\text{E-}06 \text{ cm}^2/\text{s}$  (Schwarzenbach, Gschwend et al. 1993).

The influence of soil structure configuration was first evaluated by modeling the transport of phenanthrene in randomly generated porous media with varied structural configurations, without the presence of SOM. The effects of SOM were then studied by simulations of porous media with varied SOM contents and compositions.

### 6.5.3 Influence of Pore Structural Configurations

#### *6.5.3.1 Domains of Simulation*

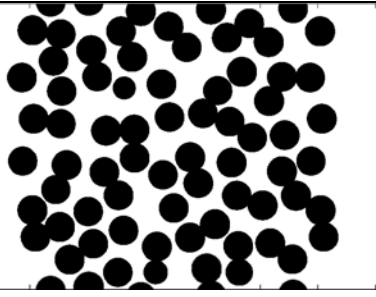
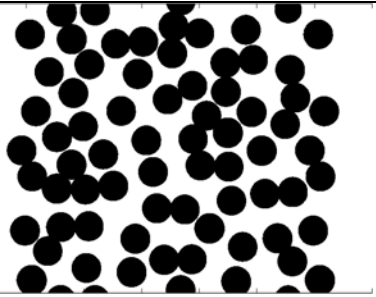
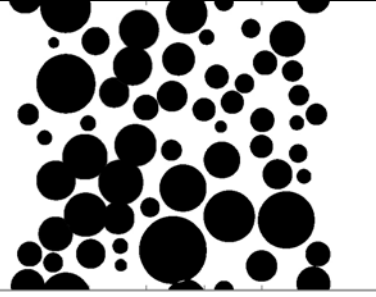
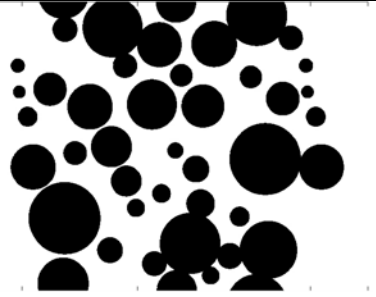
The influence of pore structure configurations was examined by simulating porous media domain with varied particle diameter coefficient of variance (COV), i.e. COV of 0.01 and 0.6, corresponding to very well-sorted and poorly sorted soils and sediments. Since soil configurations may be different, even for soils possessing similar particle diameters and COV, two configurations were simulated for soils possessing similar particle diameters and COV. Illustrations of the simulated domains are presented in Table 6-7.

In this portion of the simulation, porous media are envisioned as soils and sediments with negligible SOM; mineral materials thus comprise the main component of the soil. Research (Weber and Huang 1996) has shown that HOC sorption/desorption processes on mineral materials are described by relatively low sorption capacity, rapid uptake, and rapid release. Huang (Huang, Schlautman et al. 1996) conducted a systematic experimental investigation of the sorption of phenanthrene by mineral materials, which reported Freundlich sorption capacities of four to six orders of magnitude lower than the



SOMs employed by LeBoeuf (LeBoeuf and Weber 2000). Because of this relatively minor role for HOC sorption on mineral solids, sorption/desorption processes of phenanthrene at the surfaces of mineral particles were ignored. Mass transfer processes in such a system thus only include advection and diffusion of phenanthrene in the bulk fluid. This simplification reduces the primary variable of concern to soil structure configuration.

**Table 6-7. Porous Media Domains Used for Studying the Influence of Soil Structure Configurations on Solute Transport.**

	Soil 5	Soil 6
<b>D = 100 <math>\mu\text{m}</math> COV=0.01</b>		
	Permeability K = 38 Darcy	Permeability K = 44 Darcy
	Soil 7	Soil 9
<b>D = 100 <math>\mu\text{m}</math> COV=0.6</b>		
	Permeability K= 61 Darcy	Permeability K= 100 Darcy

### 6.5.3.2 Results and Discussion

Figure 6-16 below illustrates break through curves (BTCs) for four porous media domains. The most obvious observation is that all BTCs are subjected to a long tailing.

Further, tailing concentrations are dependent on soil particle diameter COVs. At 30 pore volumes, the outlet concentration of soil configurations with COV of 0.01 is approximately 5% of the original saturated concentration. Meanwhile, outlet concentrations of soil configurations with COV of 0.6 are approximately 2% of the original concentration.

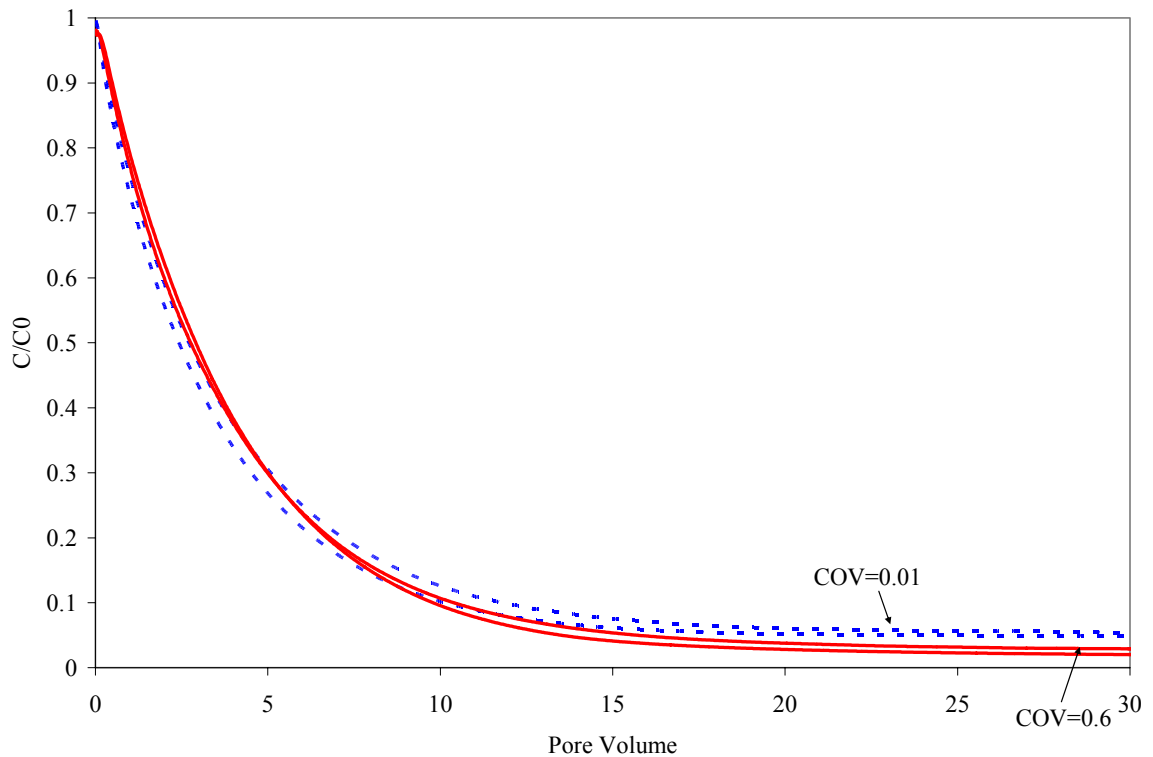
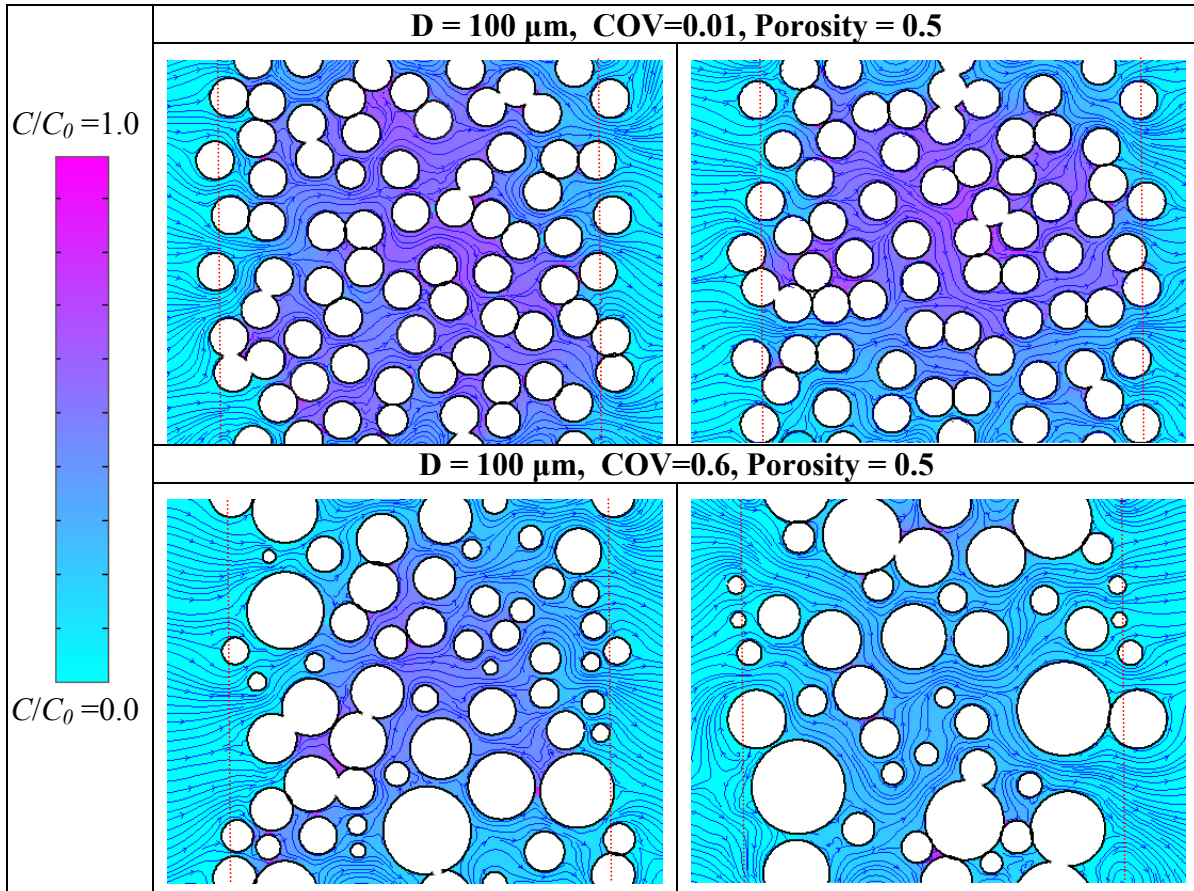


**Figure 6-16. BTCs of Phenanthrene Removal from Contaminated Porous Media with Varied Particle Sorting Levels. The y-axis represents a ratio of observed outlet concentration to the original phenanthrene concentration in porous media.**

It is reasonable to hypothesize that some phenanthrene was trapped inside the porous media, serving as long term sources for the tailing. A closer observation of phenanthrene distributions upon transmission of 30 pore volumes is shown in Table 6-8.

**Table 6-8. Distributions of Remaining Phenanthrene in Simulated Porous Media Domains at a Time of 30 Pore Volumes. The color bar represents a ratio of the residual concentration to the original concentration; blue arrow lines denote fluid flow lines.**



Snap shots of residual phenanthrene distributions vividly show the influence of soil configurations on tailing. In pore throats with higher velocities, advection will control phenanthrene transport. Phenanthrene was easily advected by the bulk fluid flow, resulting in low residual concentrations. Within nearly stagnant zones, diffusion will control phenanthrene transport, resulting in higher concentrations of phenanthrene residual. Soil configurations with a lower COV tend to be denser, which provide increased regions of low velocity, resulting in higher residual concentrations. On the

contrary, soil configurations with a higher COV generally possess higher velocity flow fields, resulting in lower residual concentrations.

Although COVs play an important role on tailing effects, domains consisting of a similar particle mean diameter, COV, and porosity presented different tailing concentrations, due to differing soil structure configurations. COV itself is thus not sufficient to describe the mass transfer rate within a porous media. Considering permeability is a parameter representing averaged microscale characteristics of the fluid and the porous media, the relationship between permeability and the residual mass was investigated, as presented in Figure 6-17. The mass of phenanthrene residual decreases in a nonlinear fashion with increases in permeability. The rate of decrease at lower permeability values is greater than at higher permeability values.

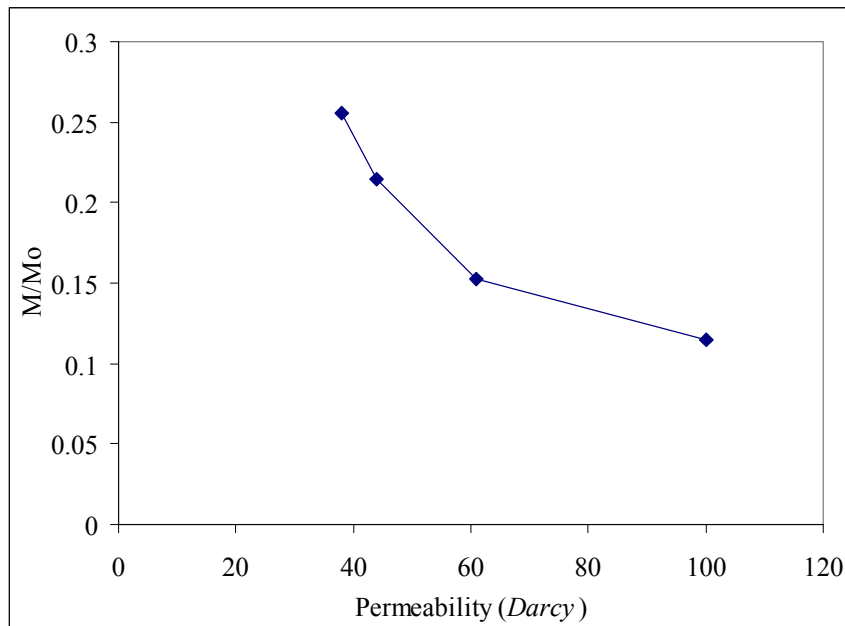


**Figure 6-17. A Relationship between Permeability and the Amount of Mass remaining in a Porous media. The y-axis represents a ratio of phenanthrene mass remaining in a porous media at a time of 30 pore volumes to the original mass at time 0.**

Low permeability porous media often possess significantly large stagnant zones or dead ends, where solutes may become entrapped. Slight incremental increases in permeability in these low permeability media, however, can greatly decrease the proportion of stagnant zones, allowing for significant increases in the release of trapped solute. For high permeability porous media, however, the percentage of stagnant zones or dead ends is low, such that an equivalent incremental increase in permeability will not display a similar reduction in the portion of stagnant zones compared with porous media with lower permeability. Thus, the influence of incremental permeability increases will have a decreased effect on the mass of phenanthrene residual as the overall permeability increases; as exemplified in the non-linear behavior depicted in Figure 6-17.

The aforementioned simulations imply an underlying relationship between the permeability of porous media and the amount of solute residual. However, permeability, as a function of particle size distribution, porosity, and packing, is often subject to uncertainty. Clear identification of the uncertainties and the relationship between permeability and phenanthrene residual actually will require a comprehensive stochastic study. Considering the large computational requirements for traditional Monte-Carlo simulations, employment of an analytical reliability method, e.g., first order reliability method (FORM), may be beneficial. As demonstrated by a similar application (Li, LeBoeuf et al. 2005), a combination of LSFE-LBM and FORM may help elucidate the relationship between permeability and solute residual while capturing particle scale uncertainties.

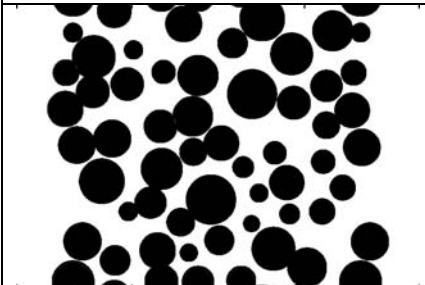
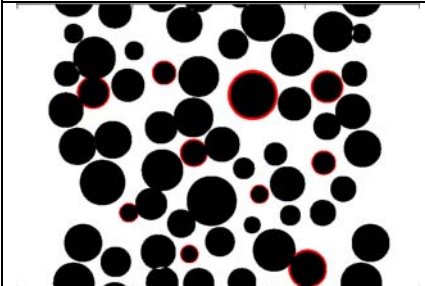
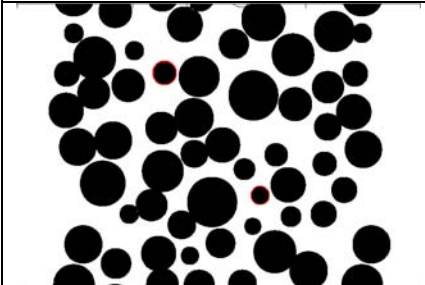
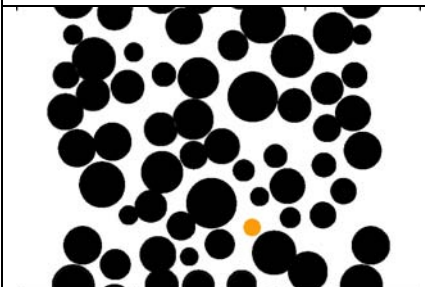
## 6.5.4 Influences of Soil Organic Matter

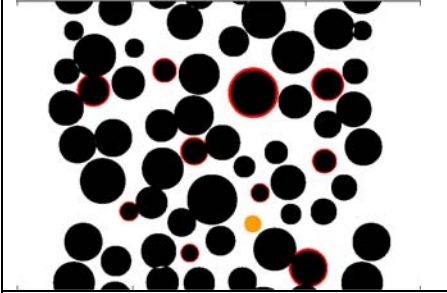
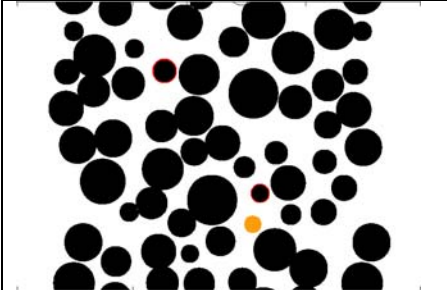
### 6.5.4.1 Numerical Simulations

The influence of SOM was examined by simulating porous media domain with varied SOM contents. Humic acid and kerogen, representing SOM of Domain II and Domain III respectively, are randomly scattered in the porous medium. Humic acid is depicted by a thin layer on randomly-selected particles. This layer represents the outer 10% of the original particle radius. Kerogen is represented by select porous media particles, with a radius of 28  $\mu\text{m}$ . Although the representations of the simulated humic acid and kerogen components represent a simplification of their actual physical shape, simplification enables the maintenance of the original soil configuration, such that the fluid flow simulation results can be readily compared among a variety of SOM contents.

Initially, phenanthrene concentrations in the humic acid and kerogen are in equilibrium with the liquid phase phenanthrene concentration in the bulk fluid, based on their corresponding Freundlich isotherm models. As noted in Table 6-9, porous media with various proportions of humic acid and kerogen, including humic acid contents of 3% and 0.3%, a kerogen content of 0.48%, and their combination, were simulated to investigate behaviors of phenanthrene transport under different SOM contents, which are compared with the same porous medium but without SOM.

**Table 6-9. Porous Media Domains with Varied Humic Acids and Kerogen Contents Used for Studying the Influence of SOMs on Solute Transport. Red circles represent humic acid coatings; orange particles denote kerogen particles.**

<b>NOSOM</b>	
	<b>Humic Acid 0%</b> <b>Kerogen 0%</b>
<b>SOM 2</b>	
	<b>Humic Acid 3%</b> <b>Kerogen 0%</b>
<b>SOM 3</b>	
	<b>Humic Acid 0.3%</b> <b>Kerogen 0%</b>
<b>SOM 4</b>	
	<b>Humic Acid 0%</b> <b>Kerogen 0.48%</b>
<b>SOM 5</b>	

	<p><b>Humic Acid 3%</b> <b>Kerogen 0.48%</b></p>
<b>SOM 6</b>	
	<p><b>Humic Acid 0.3%</b> <b>Kerogen 0.48%</b></p>

Again, due to the minor role of mineral materials (Huang, Schlautman et al. 1996), sorption/desorption processes of phenanthrene at the surfaces of mineral particles were ignored. Mass transfer processes in such a system thus include advection and diffusion of phenanthrene in the bulk fluid, sorption/desorption at the surfaces of the humic acid and kerogen, and intraparticle diffusion in the humic acid and kerogen.

#### 6.5.4.2 Parameter Determinations

When phenanthrene arrives at the surface of SOM, sorption/desorption processes will occur. Nonequilibrium sorption processes were considered as (Brusseau, Jessup et al. 1991):

$$\frac{\partial q}{\partial t} = \gamma(K_f C^m - q) \quad (6-45)$$

where,  $\gamma$  is a reaction rate [1/T], and  $K_f$  is a Freundlich capacity parameter [ $\mu\text{g/g}$ ][ $\text{L}/\mu\text{g}$ ]<sup>m</sup>.

In equilibrium, i.e.,  $\frac{\partial q}{\partial t} = 0$ , adsorption is described by a Freundlich isotherm as:



$$q = K_f C^m, \quad (6-46)$$

Following sorption at the surface, the solute will diffuse into the particle. A simple Fickian diffusion model is employed to describe this intra-particle process, as expressed by equation (6-16):

$$\frac{\partial q}{\partial t} = D_{in} \left( \frac{\partial^2 q}{\partial r^2} + \frac{1}{r} \frac{\partial q}{\partial r} + \frac{1}{r^2} \frac{\partial^2 q}{\partial \theta^2} \right) \quad (6-16)$$

LeBoeuf (LeBoeuf and Weber 2000; LeBoeuf 1998) conducted equilibrium and non-equilibrium experiments for phenanthrene sorption on an Aldrich humic acid and an Ohio Shale II kerogen, the results of which can be readily applied to estimate  $K_f$ ,  $\gamma$  and  $D_{in}$  for humic acids and kerogen. Freundlich isotherm model parameters derived from LeBoeuf's sorption equilibrium experiments at 25 °C are summarized in Table 6-10.

**Table 6-10. Freundlich Isotherm Model Parameters for Phenanthrene Sorption on Humic Acids and Kerogen at 25 °C (LeBoeuf and Weber 2000).**

	<b>log K<sub>f</sub><sup>a</sup></b>	<b>n<sup>b</sup></b>	<b>R<sup>2</sup></b>	<b>N<sup>c</sup></b>
<b>Aldrich Humic Acid</b>	1.138 (0.058)	0.965 (0.030)	1.000	22
<b>Ohio Shale II kerogen</b>	3.164 (0.026)	0.548 (0.049)	1.000	22

<sup>a</sup>  $K_f$  units are  $[\mu\text{g/g}][\text{L}/\mu\text{g}]^n$ , 95% confidence interval for log $K_f$  in parentheses.

<sup>b</sup> Freundlich exponent [-], 95% confidence interval in parentheses.

<sup>c</sup> Number of observations.

Non-equilibrium sorption experiments provided C and q values at different time points. Coupled with a simple least squares linear optimization program, the reaction rate  $\gamma$  of equation (6-45) can be derived, as summarized in Table 6-11.

**Table 6-11. Nonequilibrium Reaction Rates of Phenanthrene Sorption on Humic Acid and Kerogen.**

	$\gamma$ (1/s)	$R^2$
<b>Aldrich Humic Acid</b>	1.21E-05	0.96
<b>Ohio Shale II kerogen</b>	5.69E-06	0.95

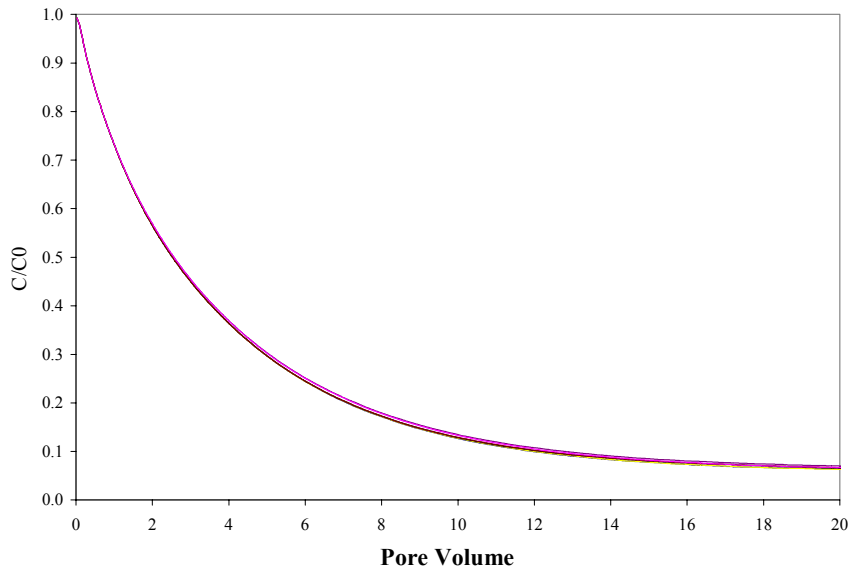
Further, intraparticle diffusion coefficients equation (6-11) were also provided by LeBoeuf's non-equilibrium sorption studies:

**Table 6-12. Intraparticle Diffusion Coefficients for Phenanthrene Diffusion into Humic Acids and Kerogen (LeBoeuf and Weber 2000).**

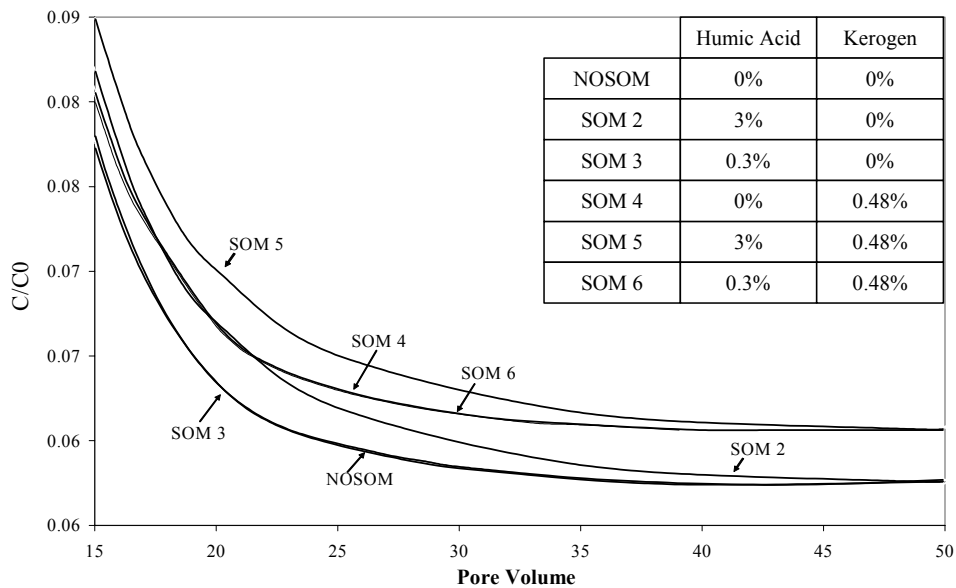
	$D_{in}$ (mm <sup>2</sup> /s)	$R^2$
<b>Aldrich Humic Acid</b>	5.96E-8	0.999
<b>Ohio Shale II kerogen</b>	13.91E-8	0.996

#### 6.5.4.3 Results and Discussions

As illustrated in Figure 6-18, while each possesses long tailing effects, shapes of BTCs for soils with differing humic acid and kerogen contents are almost identical. As explained in Section 6.5.1.3, the complex pore configuration contributes significantly to this tailing effect.



**Figure 6-18. Breakthrough Curves of Phenanthrene Removal from Contaminated Porous Media with Varied SOM Contents. The y-axis represents a ratio of observed outlet concentrations to the original phenanthrene concentration in the porous media.**



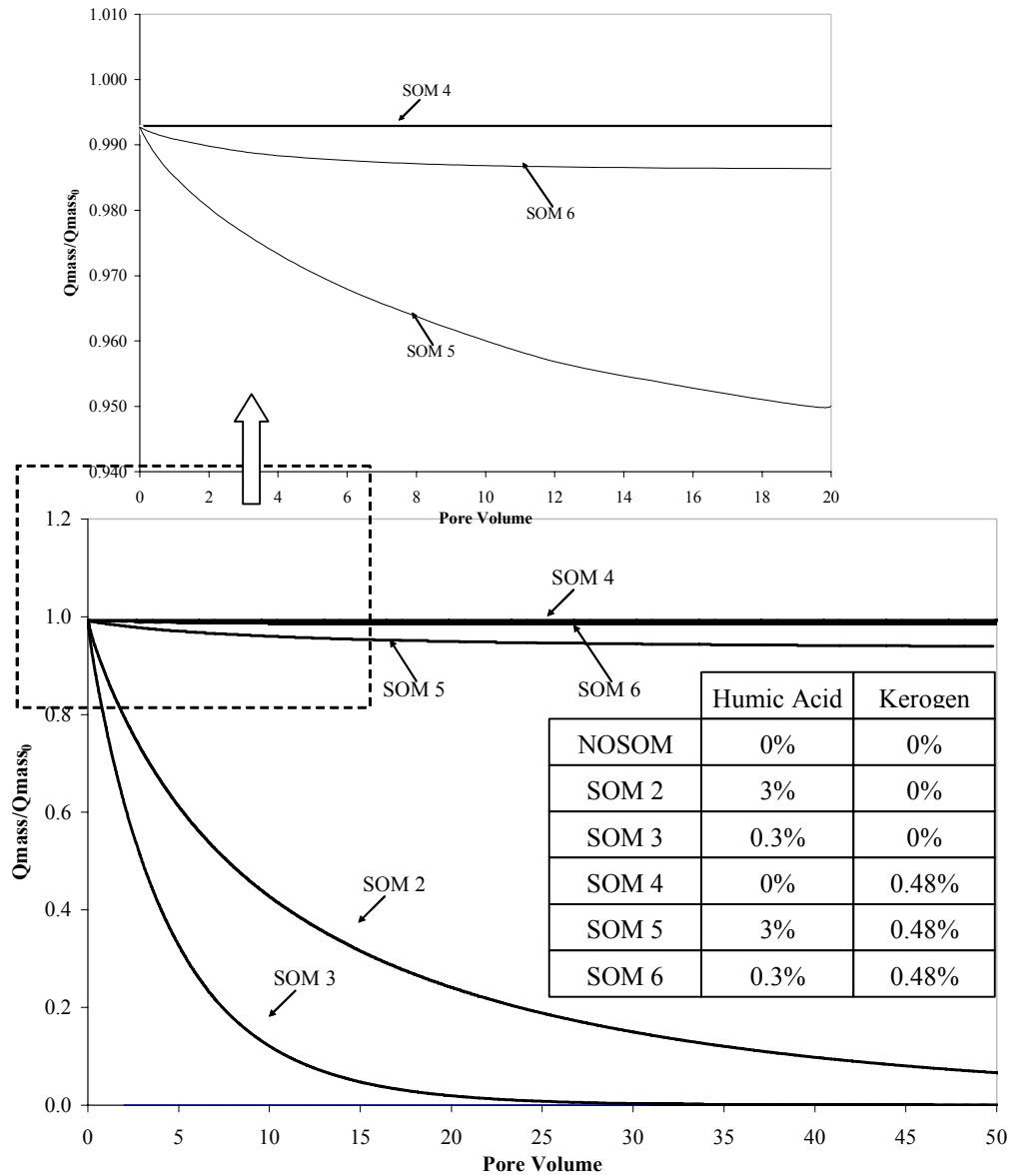
**Figure 6-19. Tailing Concentrations of Phenanthrene Removal from Contaminated Porous Media with Varied Humic Acids and Kerogen contents. The y-axis represents a ratio of observed outlet concentrations to the original phenanthrene concentration in the porous media.**

Figure 6-19 presents two groups of tailing behaviors, i.e., a group without kerogen SOM 2, SOM 3, and NOSOM, and a group with kerogen, i.e., SOM 4, SOM 5, and SOM 6. Several interesting phenomena are observed among these two groups. First, the group with kerogen possesses much higher tailing concentrations than the group without kerogen, indicating that significant amounts of phenanthrene were added into the bulk fluid from the desorption from high sorption capacity kerogen. Second, the two groups possess parallel tails, which suggests that that desorption from kerogen will be a very slow and long lasting process, comparable to the time scale of tailing due to pore structure complexity. Third, SOM 3 (0.3% humic acid) and NOSOM (without SOM) possess almost identical BTCs, suggesting that that very low humic acid contents will have limited effects on the tailing concentration. This point can be further illustrated by the similar BTCs of SOM 4 (0% humic acid, 0.48% kerogen) and SOM 6 (0.3% humic acid, 0.48% kerogen). Fourth, SOM 2 (3% humic acid) presents larger concentration than NOSOM (without SOMs) at the early time. The difference of tailing concentration, however, continues to decrease, and eventually disappears somewhere between 45 to 50 pore volumes. Here, phenanthrene entered the bulk fluid by desorbing from the humic acid at early time, which might be depleted after 45 to 50 pore volumes. A similar phenomenon was also observed for SOM 5 (3% humic acid, 0.48% kerogen) and SOM 4 (0% humic acid, 0.48% kerogen).

Based on these observations, it is reasonable to note that the humic acid will contribute to an early-time influence on solute breakthrough curve tailing effects, while kerogen plays a very important role in late-time tailing effects. To further elucidate this point, the fractions of remaining phenanthrene in different domains are investigated, as

shown in Figure 6-20. Here, phenanthrene desorption rates from SOM 2 (3% humic acid, 0% kerogen) and SOM 3 (0.3% humic acid, 0% kerogen) are very fast. Upon passing of approximately 50 pore volumes, only 7% of the original phenanthrene mass residing in SOM 2 remains, while less than 0.1% of the original phenanthrene remains in SOM 3; further illustrating the early-time influence of humic acid on tailing effects, due to the limited sorption capacity and rapid desorption rates.

A closer investigation, as shown at the upper portion of Figure 6-20, indicates the group with kerogen generally presents much slower desorption rates. First, the amount of phenanthrene in SOM 4 (0% humic acid, 0.48% kerogen) has barely decreased. Further, the amount of phenanthrene in SOM 5 (3% humic acid, 0.48% kerogen) and SOM 6 (0.3% humic acid, 0.48% kerogen) after about 50 pore volumes are 94.0% and 98.6%, respectively. Most of the observed decrease of phenanthrene represents desorption of from the humic acid portion of SOM. The overall higher percentages of remaining phenanthrene for SOM 4, SOM 5 and SOM 6 relative to domains without kerogen, i.e., SOM 2 and SOM 3, can again be explained by the very large sorption capacity and slow desorption rate of kerogen relative to humic acid, illustrating the late-time influence of kerogen on tailing processes.



**Figure 6-20. Changes of Phenanthrene Concentrations in SOMs with Different Humic Acids and Kerogen Contents when Removal of Phenanthrene from Contaminated Porous Media. The y-axis represents a ratio of phenanthrene concentrations in SOMs to the original phenanthrene concentration in SOMs.**

## 6.6 Summary

In this Chapter, a LSFE-LBM, based on a four-velocity lattice Boltzmann model, was developed to simulate solute transport processes at the pore scale. Numerical validations of LSFE-LBM for solute transport were conducted through comparison with analytical solutions of diffusion between two walls. Very good agreements with analytical solutions were achieved for both steady and unsteady states, and for a reactive boundary condition situation.

LSFE-LBM was then applied to study mass transfer processes in a single particle system. The purpose of simulating such a simplified system is to better elucidate roles of different mass transfer processes, while eliminating the influence of complex flow patterns. Advection, diffusion in bulk fluid, adsorption/desorption at the surface of the particle, and intraparticle diffusion were under consideration. Specially, intraparticle diffusion was solved by a two-dimensional finite difference method, which was incorporated with LSFE-LBM through a nonequilibrium adsorption/desorption boundary condition. In such a system, if the sorption rate is very low, or  $\log(Dad) < (-2.0, -1.0)$ , sorption-related nonequilibrium will have minimal effects on solute transport, and physical nonequilibrium will control. If both the sorption reaction rate and intraparticle diffusion rate are fast, or  $\log(Dad) > (-2.0, -1.0)$  and  $\log(Dna) > (-2.0, -1.0)$ , the local equilibrium assumption will be valid, and mass transfer will be insensitive to intraparticle diffusion. If the sorption reaction rate is fast but the intraparticle diffusion rate is slow, or  $\log(Dad) > (-2.0, -1.0)$   $\log(Dna) < (-2.0, -1.0)$ , then intraparticle diffusion will significantly influence the overall mass transfer rate.

LSFE-LBM was then applied to study mass transfer processes in randomly generated porous media. Phenanthrene removal from contaminated porous media with varied pore configurations was simulated. Results show that complex pore configurations contributed significantly to a long tailing phenomenon. While the particle sorting level does affect solute tailing behavior, it appears more reasonable to relate soil/sediment permeability with the amount of solute mass remaining within a porous media as a function of time.

The influence SOM on phenanthrene transport in porous media was examined based on parameters derived from LeBoeuf's phenanthrene equilibrium and non-equilibrium sorption batch experiments. As expected, humic acids, possessing small sorption capacity and large desorption rates, will contribute to early time tailing effects. The effect of the presence of a kerogen, possessing large sorption capacity and low desorption rates, however, is manifested in long lasting tailing effects. Although the results are not surprising; this effort represents a proof-of-concept demonstration of bridging comprehensive representations of fluid-flow with more mechanistic sorption/desorption processes. Further efforts will expand this analysis to include additional diffusion mechanisms known to operate in SOM; namely non-Fickian diffusion and Case II diffusion processes.



## CHAPTER VII

### CONCLUSIONS AND FUTURE RESEARCH NEEDS

#### 7.1 Overview

This dissertation provides comprehensive Web-based modeling tools and advanced numerical methods for students and researchers to better investigate mass transfer processes in natural and model systems under water-saturated conditions. Development of a mass transfer virtual laboratory provides a convenient and efficient tool for engineering students to gain an improved understanding of state-of-the-art mass transfer mechanisms at the particle scale. Development of a novel least squares finite element lattice Boltzmann method (LSFE-LBM) improved the kinetic theory-based lattice Boltzmann method (LBM) by extending LBM to unstructured meshes. LSFE-LBM provided the foundation for the numerical modeling efforts to elucidate the relative contributions of transport-related and sorption/desorption-related nonequilibrium factors on mass transfer processes in a whole class of porous media exemplified by randomly generated particle size and pore size distributions. Important findings from this work are summarized in the following paragraph and detailed in the following sections. Although each of the stated conclusions provides an answer to a challenge in modeling of these systems, every discovery unravels new questions; thus, recommendations for future work are provided in the final section of this chapter.

## 7.2 Summary

This study began with development of a Web-based mass transfer process virtual laboratory (MTVLab) for students and researchers to study mass transfer mechanisms at the particle scale. Chapter III provides a detailed depiction of MTVLab and its system architecture. Later, this research went beyond well-mixed systems considered in MTVLab and focused on utilizing and improving LBM to simulate fluid flow and mass transfer processes in porous media. As an initial effort of LBM modeling, Chapter IV presents an innovative stochastic method to construct probability density functions for permeability of porous media by coupling a first order reliability method (FORM) with LBM. To further improve LBM, a novel LSFE-LBM was developed. LSFE-LBM breaks the uniform grid restriction of traditional LBM and is able to more efficiently simulate fluid flow and solute transport in domains that contain complex or irregular geometric boundaries. Chapter V details the numerical derivations, validations, stability and accuracy analysis, and successful applications of LSFE-LBM to simulate flow fields in randomly generated porous media. Chapter VI extends LSFE-LBM to study solute transport in porous media, improved elucidation of the relative contributions of mass transfer processes, including advection and diffusion in bulk fluid, sorption/desorption at the surface of particles, and intraparticle diffusion. Applications of LSFE-LBM to simulate phenanthrene transport in porous media present an initial effort to bridge comprehensive sorption/desorption mechanistic studies with pore-scale modeling, the results of which assist in advancing our understanding of the effects of soil organic matter and soil structure configurations on fate and transport of organic chemicals in subsurface systems.

### 7.2.1 Development of a Web-Based Mass Transfer Process Laboratory (MTVLab) (<http://www.vanderbilt.edu/mtvlab>)

The state-of-the-art understanding of mass transfer processes at the particle scale brought in complex concepts and necessitated highly nonlinear numerical models, which thus provide a great educational challenge. In Chapter III, a user-friendly, graphical user interface, Web-based mass transfer processes laboratory was developed to serve as an educational tool to assist in the instruction of mass transfer processes. Twelve types of diffusion models, representing state-of-the-art understanding of solute transport in soil organic matter, were solved by a finite element method and were incorporated into MTVLab as numerical modules.

MTVLab is comprised of interactive user-friendly input interfaces, customizable output interfaces, illustrative help and tutorial sections, a relational database, and a numerical engine. The system was designed based on a Model-View-Controller (MVC) model. Relative to the currently available Web-based model systems, the MTVLab system architecture is novel in its multi- and mixed- language supporting ability, its ability to physically separate the numerical engine and Web server using CORBA technology, its flexibility for database management system, and its downloadable, easily edited EXCEL Web-component output. MTVLab system architecture will provide a proof-of-principle framework from which to develop more sophisticated Web-based models that can employ computationally efficient, high-level computer programs. This part of work leads to one published paper and one manuscript in review:

- *Li, Y., E. J. LeBoeuf, et al. Development of a Web-Based Mass Transfer Processes Laboratory: System Development and Implementation. Computer Applications in Engineering Education. 11: 25-39, 2003.*

- Li, Y., E. J. LeBoeuf, et al. A Web-based interactive virtual laboratory system for environmental mass transfer processes. *International Journal of Engineering Education* (in review).

### 7.2.2 Stochastic Modeling of the Permeability of Randomly Generated Porous Media

While only well-mixed systems were considered in MTVLab, efforts were put forward to simulate fluid flow in porous media in Chapter IV. In this study, porous media were envisioned as a statistical distribution of non-overlapping circular disks representing soil particles distributed in a rectangular two-dimensional uniform continuum representing the pore space through which a fluid flows. The particle size distribution function obeys a modified lognormal distribution, with a 95% confidence interval for particle size to eliminate extreme values. A two-step collective rearrangement technique based algorithm was developed to generate random porous media.

Although permeability has previously been assumed as a random variable in groundwater modeling, the restriction on computational resources and the difficulty in relating microscale and macroscale uncertainties have resulted in reduced efforts to construct probability density functions for permeability. In Chapter IV, we proposed a new approach, LBM FORM, based on more easily derived porosity statistics and particle size distribution, to construct permeability CDFs through the combination of LBM and FORM. LBM FORM was implemented to construct permeability CDFs of five randomly generated porous media; each possessing different particle size distributions. Results show that the domains with larger mean particle diameter or higher particle diameter COV tend to possess a higher probability of achieving larger permeability. Permeability values are subjected to higher uncertainty than the porosity and particle diameters because of the uncertainty of the micropore structure configurations. Lognormal

distributions modeled well the permeability CDF constructed for a variety of domains examined in this study. Accuracy of the proposed method was confirmed by comparison with Monte Carlo simulations for one example simulation domain. The largest relative error is approximately 3.4% when the probability exceeds 0.4, and is 8.5% when the probability is less than 0.4, both of which are within the relative error associated with the Monte Carlo method. Further, this work demonstrated that the Monte Carlo method is severely limited by computational requirements, making it extremely difficult to accurately construct an entire permeability CDF curve by Monte Carlo; LBM FORM, however, was found to be approximately 13 to 120 times more efficient than traditional Monte Carlo simulations. This part of work leads to one published paper:

- *Li, Y., LeBoeuf, E. J., Basu, P. K., and Mahadaven, S. Stochastic Modeling of the Permeability of Randomly-Generated Heterogeneous Porous Media. Advances in Water Resources, 28 (8): 835-844, 2005.*

### 7.2.3 Development of a Least Squares Finite Element Lattice Boltzmann Method (LSFE-LBM)

Lattice Boltzmann methods (LBM) have been demonstrated as promising tools for simulating fluid flow. In practical applications, the potential of LBM is restricted because it can only be applied to uniform lattice structures. To overcome this problem, Chapter V presented a new LBM, i.e. LSFE-LBM, which uses a least-squares finite element method in space and a Crank-Nicolson method in time. The new method is able to solve fluid flow in domains that contain complex or irregular geometric boundaries by using the finite-element method's unstructured mesh while employing accurate least-squares optimization. Through theoretical accuracy and stability analysis, and successful applications of LSFE-LBM to a variety of test problems, including Poiseuille flow,

Couette flow, flow past a cylinder, and flow in porous media, it is suggested that LSFE-LBM is highly accurate, stable, flexible and efficient:

*High accuracy:* Accuracy analysis of the pure advection equation suggests that LSFE-LBM enjoys fourth-order accuracy in space and second-order accuracy in time. LSFE-LBM results agree well with the analytical solutions for Poiseuille and Couette flow, and the previous numerical and experimental study results for flow past a cylinder.

*High stability:* For the pure advection equation, LSFE-LBM presents unconditional stability in the time domain, which is superior to other finite-difference and finite-element based LBMs. Although the von Neumann linearized stability analysis indicates that the stability of LSFE-LBM is dependent on physical and numerical discretization parameters as other numerical LBMs, its improved stability property is further confirmed by a higher limiting stable velocity.

*High flexibility:* Application of LSFE-LBM to flow past a circular cylinder suggests good agreement with previous numerical and experimental results, providing initial evidence of its applicability to curved boundaries. Later, LSFE-LBM was successfully applied to model fluid flow in a randomly generated porous media using an unstructured mesh; good agreement with traditional LBM results further demonstrate the geometric flexibility of LSFE-LBM.

*High efficiency:* Although more complex computations are required in LSFE-LBM relative to traditional LBM, LSFE-LBM requires fewer grid points by utilizing unstructured mesh, while consuming less memory by implementing an innovative element-by-element approach in the LSFE scheme. As demonstrated by the flow in porous media problem, LSFE-LBM requires 1/452 of the number of grids points and 1/25

of the memory of traditional LBM to achieve a similar order of accuracy with a similar amount of computational time. It is worthy to note that advantages derived from this increased efficiency may not be obvious for problems with simple geometries; rather, it is expected to be better demonstrated when applied to larger domains with more complex geometries. This part of work leads to one rapid communication published and one manuscript in review:

- *Li, Y., E.J. LeBoeuf, and P.K. Basu, Least squares finite element lattice Boltzmann method. Physical Review E, 69 (6), Art. No., 06570(R). 2004.*
- *Li, Y., E.J. LeBoeuf, and P.K. Basu, A Least Squares Finite Element Scheme for Lattice Boltzmann Method on Unstructured Meshes. Physical Review E (in review).*

#### 7.2.4 Use of a Least Squares Finite Element Lattice Boltzmann Method to Study Fluid Flow and Mass Transfer Processes

In Chapter VI, LSFE-LBM based on a four-velocity lattice Boltzmann model was developed to simulate solute transport processes at the pore scale. Numerical validations of LSFE-LBM for solute transport were conducted by comparison with analytical solutions of problems regarding diffusion between two walls. Very good agreements with analytical solutions were achieved for both steady and unsteady states, and for a reactive boundary condition situation.

LSFE-LBM was then applied to study mass transfer processes in a single particle system. The purpose of simulating such a simplified system is to better elucidate roles of different mass transfer processes, while eliminating the influence of complex flow patterns. Advection, diffusion in bulk fluid, adsorption/desorption at the surface of the particle, and intraparticle diffusion were under consideration. Specially, intraparticle diffusion was solved by a two-dimensional finite difference method, which was

incorporated with LSFE-LBM through a nonequilibrium adsorption/desorption boundary condition. Sensitivity analysis shows that if the adsorption rate is 10 to 100 times slower than the bulk fluid diffusion rate, sorption-related non-equilibrium will have minimum effects on solute transport. If the adsorption reaction rate is fast and intraparticle diffusion rate is 10 to 100 faster than the adsorption reaction rate, the local equilibrium assumption will be valid, and mass transfer will be insensitive to intraparticle diffusion. If the adsorption reaction rate is fast but the intraparticle diffusion rate is 10 to 100 times slower than the adsorption rate, then intraparticle diffusion will govern the solute transport process.

LSFE-LBM was then applied to simulate phenanthrene removal from contaminated porous media with varied pore configurations. Results show that complex pore configurations contributed significantly to a long tailing phenomenon. While the particle sorting level does affect the tailing effect, it appears more reasonable to relate permeability with the amount of mass trapped within porous media. The influence of SOM on phenanthrene transport in porous media was examined based on parameters derived from LeBoeuf's phenanthrene equilibrium and non-equilibrium sorption batch experiments (LeBoeuf 1998). The presence of soil and sediment organic matter (SOM) further contributes to the tailing effect. Sufficiently high contents of humic acids, representing soft SOM, will contribute to an early-time influence on solute breakthrough curve tailing effects. Kerogen, representing hard SOM, however, plays a very important role in late-time tailing effects. Although the results are not surprising; they do, however, present an initial effort to bridge comprehensive mechanistic studies with pore-scale



simulating of HOCs fate and transport. This portion of work leads to one conference paper published and a manuscript under preparation:

- *Li, Y., LeBoeuf, E.J. and Basu, P.K. Use of a Least Squares Finite Element Lattice Boltzmann Method to Study Fluid Flow and Mass Transfer Processes. Proceedings of the 2005 International Conference on Computational Science, May, 2005.*
- *Li, Y., LeBoeuf, E. J. and Basu, P. K. Pore-scale modeling of the effects of transport - related and sorption/desorption processes on solute transport in heterogeneous porous media. Water Resources Research (in preparation).*

### **7.3 Recommendations for Future Research**

This research presented a Web-based modeling system and advanced numerical methods, e.g., LBM FORM and LSFE-LBM, for students and researchers to further explore fate and transport of solute in subsurface systems. While each of these contributions provide answers to several challenges in numerical modeling of mass transfer processes, they also reveal further research needs, especially in expanding MTVLab for broader applicability, further advancing numerical methods LBM FORM and LSFE-LBM, and more extensively investigating mass transfer processes using LSFE-LBM.

#### **7.3.1 Future directions on expanding MTVLab**

The mass transfer processes system illustrated in MTVLab focused on understanding fundamental sorption and diffusion processes for spherical particles in various reactor configurations. Although comprehensive in its coverage of different diffusion and sorption models that may be applicable in most environmental systems, additional phases of work are suggested to expand the model capabilities for wider applicability. Future work includes:

- Improvement of the numerical engine, to include other standard particle shapes (slabs and cylinders) and user-defined shapes (e.g., polygons), parameter optimization, stochastic simulation, and expansion to multiscale modeling.
- Enhancement of the graphical user interface, to include addition of 3-D animation for result visualization.
- Development of improved feedback mechanisms to provide prompt, two-way communication between the users and the program developers.
- Increase multi-client capacity through use of parallel programming, and use of high-performance distributed computing systems.

### 7.3.2 Future directions on advancing LBM FORM

Although LBM FORM provides higher accuracy and efficiency than Monte-Carlo simulations to construct permeability CDFs, it is worthy to note several directions for enhancements of the method:

- First, the LBM method implemented in this study is in the BGK form (Bhatnagar, Gross et al. 1954) with a linear collision operator. The accuracy of permeability based on BGK LBM is dependent on the fluid viscosity and thus on the relaxation time. We chose an optimized value of the relaxation time  $\tau$  ( $\tau = 0.8$ ) to eliminate this dependency. In the future, we suggest the use of more sophisticated LBM schemes to simulate fluid flow in porous media. For example, a two relaxation time (TRT) LBM (d'Humieres, Ginzburg et al. 2002; Lallemand, d'Humieres et al. 2003) will be able to annihilate the permeability dependence on the viscosity with a specific choice of the

free eigen values. Further, the convergence rate will be accelerated when using higher viscosity values for a TRT LBM.

- A second potential enhancement of the method is associated with the reliability method employed. While FORM performed well in example domains in this study, more advanced methods, such as SORM or other modified forms of FORM, might be required for situations that are more complicated.
- Finally, the simulation results in this work are based on randomly generated, two-dimensional simplified porous media. Future modeling efforts will benefit from use of more sophisticated porous media packing modules to more closely reflect actual field situations, and extension to three-dimensions.

### 7.3.3 Future directions on advancing LSFE-LBM

Encouraging results from this work suggest that LSFE-LBM will be a promising addition to the family of LBM, especially for geometrically complex domains. For further improvements of LSFE-LBM, the following future directions are suggested:

- First, LSFE-LBM numerical tests were primarily applied to complex geometries with low Reynolds numbers, corresponding to authors' research foci. Although it is likely that LSFE-LBM will have similarly high potential for application to flows with high Reynolds numbers, we suggest more efforts to validate this point.
- Second, the superior performance of LBM following parallelization is one of the most important features of LBM. Since element contributions are computed independently, element-by-element based LSFE-LBM can also be easily implemented in parallel. It is

thus worthwhile to provide a more thorough study on the performance of LSFE-LBM after parallelization.

- Finally, since finite volume-based CFDs are much in vogue relative to finite element-based CFDs, it will be meaningful to further assess and compare the performances of LSFE-LBM-, FV-LBM- and FV-based CFDs.

#### 7.3.4 Future directions on investigating mass transfer processes using LSFE-LBM

LSFE-LBM has been demonstrated as a powerful method to study fluid flow and mass transfer processes in porous media. The example applications of LSFE-LBM employed in this study are purposefully simple, as the main objective of this effort was to demonstrate new methods to incorporate experimental mechanistic studies with pore scale modeling. To more fully utilize LSFE-LBM, the following future research efforts are suggested:

- HOC diffusion in SOM is concentration-dependent and sorbent property-dependent. For the purpose of simplicity, a Fickian diffusion model was used to describe intraparticle diffusion in this study. It will be very interesting to link LSFE-LBM with more sophisticated intraparticle diffusion models, e.g. non-Fickian diffusion and SOM relaxation models. The link can be achieved by coupling LSFE-LBM with traditional numerical methods through sorption/desorption boundary interfaces, as demonstrated in this study. Moreover, the link can also be achieved by further developing LSFE-LBM to directly model multi-phase transport among water, sorbates, and sorbents.
- Humic acids and kerogen were randomly scattered on solid circular particles, in very simplified shapes. To further explore the influence of SOMs to the transport of organic

chemicals, it will be beneficial to consider more realistic distributions of SOMs, for example, considering kerogen as smaller scattered junks and humic acids as coatings at both surfaces of particles and intraparticle pore surfaces.

- Techniques, such as X-ray microtomography (XMT) characterization of porous media, can provide accurate visualizations of real soil configurations. Further advancements of LSFE-LBM to three dimensions and parallelization, will allow LSFE-LBM to be more easily applied to simulate transport in real soil configurations. These advanced applications of LSFE-LBM will certainly progress the understanding of mass transfer processes at the pore scale, likely leading to improvements to existing mass transfer theories.
- Finally, the findings developed in this work necessitate application to current remediation problems. Upscaling of LSFE-LBM will be a first step towards practical applications. Properly coupling of LSFE-LBM with available upscaling techniques will be a good direction to explore.

## REFERENCES

- Abbas, A. and N. Al-Bastaki (2002). "The use of software tools for the education: Students' evaluations." Chemical Engineering Education **36**(3): 236-241.
- Abu-Khalaf, A. M. (1998). "Getting the most out of a laboratory course." Chemical Engineering Education **32**(3): 184-189.
- Adamson, A. W. (1990). Physical Chemistry of Surfaces. New York, John Wiley & Sons, Inc.
- Adler, P. M., J.-F. Thovert, et al. (2002). "Real porous media: Local geometry and transports." Journal of Engineering Mechanics **128**(8): 829-839.
- Alvarez-Ramirez, J., S. Nieves-Mendoza, et al. (1996). "Calculation of the effective diffusivity of heterogeneous media using the lattice-Boltzmann method." Physical Review E **53**(3): 2298-2303.
- Amati, G., S. Succi, et al. (1997). "Turbulent channel flow simulations using a coarse-grained extension of the lattice Boltzmann method." Fluid Dynamics Research **19**: 289-302.
- Anderson, M. R. (1991). Characterization of the graduate career change woman in engineering: Recruitment and retention. Proceedings of ASEE/IEEE Frontiers in Education Conference, IEEE.
- Aviles, B. E. and M. D. LeVan (1991). "Network models for nonuniform flow and adsorption in fixed beds." Chemical Engineering Science **46**(8): 1935-1944.
- Bakke, S. and P.-E. Oren (1997). "3-D pore-scale modeling of sandstones and flow simulations in the pore networks." SPE Journal **2**: 136-149.
- Ball, W. P. (1989). Equilibrium sorption and diffusion rate studies with halogenated organic chemicals and sandy aquifer material. Stanford, Stanford University.
- Ball, W. P. and P. V. Roberts (1991). "Long-term sorption of halogenated organic chemical by aquifer material. 2. Intraparticle diffusion." Environmental Science and Technology **25**(7): 1237-1249.
- Ball, W. P. and P. V. Roberts (1991). "Long-term sorption of halogenated organic chemicals by aquifer material. 1. Equilibrium." Environmental Science and Technology **25**(7): 1223-1237.

- Basu, P. K., G. Hsiao, et al. (1993). "Pointwise performance of finite element method in the case of boundary layer problems." Simulation **61**(2).
- Bear, J. (1972). Dynamics of Fluids in Porous Media. New York, Dover Publications, Inc.
- Benefield, L. D., J. F. Judkins, et al. (1982). Process Chemistry for Water and Wastewater Treatment. Englewood Cliffs, NJ, Prentice-Hall, Inc.
- Bennett, C. H. (1972). "Serially deposited amorphous aggregates of hard spheres." Journal of Applied Physics **43**(6): 2727-& 1972.
- Benzi, R., S. Succi, et al. (1992). "The lattice Boltzmann-equation - Theory and applications." Physics Reports - Review Section of Physics Letters **222**(3): 145-197.
- Berens, A. R. (1978). "Analysis of Transport Behavior in Polymer Powders." Journal of Membrane Science **3**: 247-264.
- Berens, A. R. and H. B. Hopfenberg (1978). "Diffusion and relaxation in glassy polymer powders: 2. Separation of diffusion and relaxation parameters." Polymer **19**(May): 489-497.
- Bergsten, H. (2001). JavaServer Pages, O'Reilly & Associates, Inc.
- Bernsdorf, J., F. Durst, et al. (1999). "Comparison of cellular automata and finite volume techniques for simulation of incompressible flows in complex geometries." International Journal for Numerical Methods in Fluids **29**: 251-264.
- Beven, K. and P. Germann (1982). "Macropores and water flow in soils." Water Resources Research **18**(5): 1311-1325.
- Bhatnagar, P., E. P. Gross, et al. (1954). "A model for collision processes in gases. I. Small amplitude processes in charged and neutral one-component systems." Physical Review **94**: 511-525.
- Bloomberg, J., J. Kawski, et al. (1997). "Web page scripting techniques." Social Science Computer Review **15**(3): 336-337.
- Blunt, M. J. (2001). "Flow in porous media - pore-network models and multiphase flow." Current Opinion in Colloid & Interface Science **6**(3): 197-207.
- Boek, E. S., J. Chin, et al. (2003). "Lattice Boltzmann simulation of the flow of non-Newtonian fluids in porous media." International Journal of Modern Physics B **17**(1-2): 99-102.

- Book, W. J., K. Koeppen, et al. (2002). "Virtual access hydraulic experiment for system dynamics and controls education." Mechatronics **12**(2): 261-270.
- Bott, E. and W. Leonhard (1999). Using Microsoft Office 2000, Indianapolis, Ind.
- Brusilovsky, P., J. Eklund, et al. (1998). "Web-based education for all: a tool for development adaptive courseware." Computer Networks and ISDN Systems **30**(2): 291-300.
- Brusseau, M. L. (1993). "The influence of solute size, pore water velocity, and intraparticle porosity on solute dispersion and transport in soil." Water Resources Research **29**(4): 1071-1080.
- Brusseau, M. L. (1994). "Transport of Reactive Contaminants in Heterogeneous Porous Media." Reviews of Geophysics **32**(3): 285-313.
- Brusseau, M. L. (1998). "Non-ideal transport of reactive solutes in heterogeneous porous media: 3. Model testing and data analysis using calibration versus prediction." Journal of Hydrology **209**(1-4): 147-165.
- Brusseau, M. L., R. E. Jessup, et al. (1989). "Modeling the Transport of Solutes Influenced by Multiprocesses Nonequilibrium." Water Resources Research **25**(9): 1971-1988.
- Brusseau, M. L., R. E. Jessup, et al. (1991). "Nonequilibrium Sorption of Organic Chemicals: Elucidation of Rate-Limiting Processes." Environmental Science and Technology **25**(1): 134-142.
- Brusseau, M. L. and P. S. C. Rao (1989). "Sorption nonideality during organic contaminant transport in porous media." Critical Reviews in Environmental Control **19**(1): 33-95.
- Brusseau, M. L. and P. S. C. Rao (1990). "Modeling solute transport in structured soils: A review." Geoderma **46**: 169-192.
- Cameron, D. R. and A. Klute (1977). "Convective-dispersive solute transport with a combined equilibrium and kinetic adsorption model." Water Resources Research **13**: 183.
- Cancelliere, A., C. Chang, et al. (1990). "The permeability of a random medium: Comparison of simulation with theory." Physics of fluids. A, Fluid dynamics **12**(2): 2085-2088.
- Cao, N., S. Chen, et al. (1997). "Physical symmetry and lattice symmetry in the lattice Boltzmann method." Physical Review E **55**(1): R21-R23.



- Carbonell, R. G. and S. Whitaker (1983). "Dispersion in pulsed systems. 2. Theoretical developments for passive dispersion in porous-media." Chemical Engineering Science **38**(11): 1795-1802.
- Carroll, K. M., M. R. Harkness, et al. (1994). "Application of a permeant/polymer diffusional model to the desorption of polychlorinated biphenyls from hudson river sediments." Environmental Science and Technology **28**(1): 253-258.
- Castilla, H. J., C. J. Werth, et al. (2000). "Structure evaluation of slow desorbing sites in model and natural solids using temperature stepped desorption profiles: 2. Column result." Environmental Science and Technology **34**: 2966-2972.
- Chatong, A. and F. E. Massoth (1993). "Restrictive diffusion in Aluminas." American Institute of Chemical Engineers Journal **29**: 725-731.
- Chen, H. (1998). "Volumetric formulation of the lattice Boltzmann method for fluid dynamics: Basic concept." Physical Review E **58**(3): 3955-3963.
- Chen, H., S. Chen, et al. (1992). "Recovery of the Navier-Stokes equations using a lattice-gas Boltzmann method." Physical Review E **45**(8): R5339-R5342.
- Chen, S., H. Chen, et al. (1991). "Lattice Boltzmann model for simulation of magnetohydrodynamics." Physical Review Letters **67**: 3776-3779.
- Chen, S., S. P. Dawson, et al. (1995). "Lattice methods and their applications to reacting systems." Computers & Chemical Engineering **19**(6/7): 617-646.
- Chen, S., K. Diemer, et al. (1991). "Lattice gas automata for flow through porous media." Physica D **47**: 72-84.
- Chen, S. and G. D. Doolen (1998). "Lattice Boltzmann method for fluid flow." Annual Review of Fluid Mechanics **30**: 329-364.
- Chen, S., D. Martinez, et al. (1996). "On boundary conditions in lattice Boltzmann methods." Physics of Fluids **8**(9): 2527-2536.
- Chen, W. and R. J. Wagenet (1995). "Solute transport in porous media with sorption-site heterogeneity." Environmental Science and Technology **29**(11): 2725-2734.
- Choy, T. C. (1999). Effective medium theory - Principles and applications, Oxford Science Publications.
- Chu, K. C. (1999). "The development of a web-based teaching system for engineering education." Engineering Science and Education Journal **8**(3): 115-118.

- Coats, K. H. and B. D. Smith (1964). "Dead-end pore volume and dispersion in porous media." Journal of Society of Petroleum Engineering **4**: 73-84.
- Comini, G., M. Manzan, et al. (1995). "Analysis of finite element schemes for convection-type problems." International Journal of Numerical Methods in Fluids **20**: 443-458.
- Connaughton, D. F., J. R. Stedinger, et al. (1993). "Description of Time-Varying Desorption Kinetics: Release of Naphthalene from Contaminated Soils." Environmental Science and Technology **27**(12): 2397-2403.
- Cooke, R. A., S. Mostaghimi, et al. (1995). "Effect of hydraulic conductivity probability distribution function on simulated solute leaching." Water Environment Research **67**(2): 159-168.
- Coutanceau, M. and R. Bouard (1977). "Experimental determination of the main features of the viscous flow in the wake of a circular cylinder in uniform translation. Part 1. Steady flow." Journal of Fluid Mechanics **79**(2): 231-256.
- Crank, J. (1975). The mathematics of diffusion, Oxford Science Publications.
- Crittenden, J. C., N. J. Hutzler, et al. (1986). "Transport of organic compounds with saturated groundwater flow: Model development and parameter sensitivity." Water Resources Research **22**: 271-284.
- Crown, S. W. (1999). "Web-based learning: enhancing the teaching of engineering graphics." Interactive Multimedia Electronic Journal of Computer-Enhanced Learning **1**(2): on-line.
- Crown, S. W. (2001). "Improving visualization skills of engineering graphics students using simple JavaScript web based games." Journal of Engineering Education **90**(3): 347-355.
- Culver, T. B., S. P. Hallisey, et al. (1997). "Modeling the desorption of organic contaminants from long-term contaminated soil using distributed mass transfer rates." Environmental Science and Technology **31**(6): 1581-1588.
- Cunningham, J. A., C. J. Werth, et al. (1997). "Effects of grain-scale mass transfer on the transport of volatile organics through sediments 1. Model development." Water Resources Research **33**(12): 2713-2726.
- Dawson, S. P., S. Chen, et al. (1993). "Lattice Boltzmann computations for reaction-diffusion equations." The Journal of Chemical Physics **98**(2): 1514-1523.
- Deen, W. M. (1998). Analysis of Transport Phenomena. New York, Oxford University Press.

- DeLapp, R. C. and E. J. LeBoeuf (2004). "Thermal analysis of whole soil and sediment." Journal of Environmental Quality **33**(1): 330-337.
- DeLapp, R. C., E. J. LeBoeuf, et al. (2004). "Thermodynamic Properties of Several Soil- and Sediment-Derived Natural Organic Materials." Chemosphere **54**(4): 527-539.
- Dennis, S. C. R. and G. Z. Chang (1970). "Numerical solutions for steady flow past a circular cylinder at Reynolds number up to 100." Journal of Fluid Mechanics **42**: 471.
- d'Humieres, D., I. Ginzburg, et al. (2002). "Multiple-relaxation-time lattice Boltzmann models in three dimensions." Philosophical Transactions of the Royal Society of London Series A - Mathematical Physical and Engineering Sciences **360**(1792): 437-451.
- Di Toro, D. M. and L. M. Horzempa (1982). "Reversible and resistant components of PCB adsorption-desorption: Isotherms." Environmental Science and Technology **16**(9): 594-602.
- Ding, X. (1999). Large eddy simulation of turbulent transport processes by a least-squares finite element method. Lexington, Kentucky, University of Kentucky.
- Dong, Y. and M. Zhu (2002). "Web-based VR-form virtual laboratory." Chemical Engineering Education **36**(2): 102-107.
- Drake, J. M. and J. Klafter (1990). "Dynamics of confined molecular systems." Physics Today **43**: 46-55.
- Dupuis, A. and B. Chopard (2003). "Theory and applications of an alternative lattice Boltzmann grid refinement algorithm." Physical Review E **67**: Art No. 066707.
- Durlofsky, L. J. (1991). "Numerical calculation of equivalent grid block permeability tensors for heterogeneous porous media." Water Resources Research **27**(5): 699-708.
- Eckel, B. (2000). Thinking in Java, Prentice Hall PTR.
- Efendiev, Y. and L. J. Durlofsky (2002). "Numerical modeling of subgrid heterogeneity in two phase flow simulations." Water Resources Research **38**(8): 3-1 to 3-11.
- Egan, K. (1997). The Educated Mind. Chicago, IL, University of Chicago Press.
- Eggleston, J. and S. Rojstaczer (2001). "The value of grain-size hydraulic conductivity estimation: Comparison with high resolution in-situ field hydraulic conductivity." Geophysical Research Letters **28**(22): 4255-4258.

- Eidsath, A., R. G. Carbonell, et al. (1983). "Dispersion in pulsed systems. 3. Comparison between theory and experiments for packed-beds." Chemical Engineering Science **38**(11): 1803-1816.
- England, R. and R. Field (1989). "Using the laboratory to develop engineering awareness." Chemical Engineering Education **23**(3): 144-148.
- Farrell, J. and M. Reinhard (1994). "Desorption of halogenated organics from model solids, sediments, and soil under unsaturated conditions. 1. Isotherms." Environmental Science and Technology **28**(1): 53-62.
- Farrell, J. and M. Reinhard (1994). "Desorption of halogenated organics from model solids, sediments, and soil under unsaturated conditions. 2. Kinetics." Environmental Science and Technology **28**(1): 63-72.
- Fatt, I. (1956). "The network model of porous media: I. Capillary pressure characteristics." Transactions of the AIME **207**: 144-159.
- Fatt, I. (1956). "The network model of porous media: II. Dynamic properties of a single size tube network." Transactions of the AIME **207**: 160-163.
- Fatt, I. (1956). "The network model of porous media: III. Dynamic properties of networks with tube radius distribution." Transactions of the AIME **207**: 164-181.
- Filippova, O. and D. Hanel (1998). "Grid refinement for lattice-BGK models." Journal of Computational Physics **147**: 219-228.
- Flekkøy, E. G. (1993). "Lattice Bhatnagar-Gross-Krook models for miscible fluids." Physical Review E **47**: 4247.
- Flory, P. J. (1941). Journal of American Chemical Society **63**: 3083.
- Freeman, D. H. and L. S. Cheung (1981). "A gel partition model for organic desorption from a pond sediment." Science **214**: 790-792.
- Freeze, R. A. and J. A. Cherry (1979). Groundwater. Englewood Cliffs, NJ, Prentice-Hall Inc.
- Frisch, U., B. Hasslacher, et al. (1986). "Lattice-gas automata for the Navier-Stokes equation." Physical Review Letters **56**(14): 1505-1508.
- Gallivan, M. A., D. R. Noble, et al. (1997). "An evaluation of the bounce-back boundary condition for lattice Boltzmann simulations." International Journal for Numerical Methods in Fluids **25**: 249-263.

- Gillett, J. E. (2001). "Chemical engineering education in the next century." Chemical Engineering Technology **24**(6): 561-570.
- Goeller, K. E. (1998). "Web-based collaborative learning: a perspective on the future." Computer Networks and ISDN Systems **30**(6): 634-635.
- Good, T. L. and J. E. Brophy (1990). Educational psychology: A realistic approach, New York : Longman.
- Gu, B., J. Schmitt, et al. (1994). "Adsorption and desorption of natural organic matter on iron oxide: Mechanisms and models." Environmental Science and Technology **28**(1): 38-46.
- Guo, Z. and T. S. Zhao (2003). "Explicit finite-difference lattice Boltzmann method for curvilinear coordinates." Physical Review E **67**: 066709-1~066709-12.
- Haggerty, R. and S. M. Borelick (1995). "Multiple-rate mass transfer for modeling diffusion and surface reactions in media with pore-scale heterogeneity." Water Resources Research **31**(10): 2383-2400.
- Haggerty, R. and S. M. Gorelick (1998). "Modeling Mass Transfer Processes in Soil Columns with Pore-Scale Heterogeneity." Soil Science Society of America Journal **62**(January-February): 62-74.
- Haldar, A. and S. Mahadevan (2000). Probability, Reliability, and Statistical Methods in Engineering Design, John Wiley & Sons, Inc.
- Hamed, M. M., P. B. Bedient, et al. (1996). "Numerical stochastic analysis of groundwater contaminant transport and plume containment." Journal of Contaminant Hydrology **24**: 1-24.
- Hamed, M. M., P. B. Bedient, et al. (1996). "Probabilistic modeling of aquifer heterogeneity using reliability methods." Advances in Water Resources **19**(5): 277-295.
- Harmon, J. P., S. Lee, et al. (1987). "Methanol Transport in PMMA: The Effect of Mechanical Deformation." Journal of Polymer Science : Part A : Polymer Chemistry **25**: 3215-3229.
- Harmon, T. C. (1992). Determining and modeling diffusion-limited desorption rates in heterogeneous aquifer solids. Stanford, CA, Stanford University.
- Harr, M. E. (1977). Mechanics of particulate media: A probability approach, McGraw-Hill International Book Company.

- Haws, N. W., B. S. Das, et al. (2004). "Dual-domain solute transfer and transport processes: evaluation in batch and transport experiments." Journal of Contaminant Hydrology **75**: 257-280.
- He, X. and G. D. Doolen (1997). "Lattice Boltzmann method on curvilinear coordinates system: Flow around a circular cylinder." Journal of Computational Physics **134**: 306-315.
- He, X., L.-S. Luo, et al. (1996). "Some progress in lattice Boltzmann method. Part I. Nonuniform mesh grids." Journal of Computational Physics **129**: 357-363.
- He, X., N. Li, et al. (2000). "Lattice Boltzmann simulation of diffusion-convection systems with surface chemical reaction." Molecular Simulation **25**: 145-156.
- Heijs, A. W. J. and C. P. Lowe (1995). "Numerical evaluation of the permeability and Kozeny constant for two types of porous media." Physical Review E **51**(5): 4346-4352.
- Held, R. J. and M. A. Celia (2001). "Modeling support of functional relationships between capillary pressure, saturation, interfacial areas and common lines." Advances in Water Resources **24**: 325-343.
- Higuchi, H. (2001). "Multi-level, interactive web-based simulations to teach fluid mechanics and aerodynamics from middle school to college levels." International Journal of Engineering Education: on-line issue.
- Higuera, F., S. Succi, et al. (1989). "Lattice gas-dynamics with enhanced collisions." Europhysics Letters **9**(4): 345-349.
- Higuera, F. J. and J. Jimenez (1989). "Boltzmann approach to lattice gas simulations." Europhysics Letters **9**: 663-668.
- Holme, R. and D. H. Rothman (1992). "Lattice-gas and lattice-Boltzmann models of miscible fluids." Journal of Statistical Physics **68**: 409-430.
- Hopfenberg, H. B. and H. L. Frisch (1969). "Transport of organic micromolecules in amorphous polymers." Polymer Letters **7**: 405-409.
- Huang, W., P. a. Peng, et al. (2003). "Effects of organic matter heterogeneity on sorption and desorption of organic contaminants by soils and sediments." Applied Geochemistry **18**(955-972).
- Huang, W., M. A. Schlautman, et al. (1996). "A distributed reactivity model for sorption by soils and sediments: 5. The influence of near-surface characteristics in minear domains." Environmental Science and Technology **30**(1): 105-113.

- Huang, W. and W. J. Weber (1998). "A distributed reactivity model for sorption by soils and sediments. 11. Slow concentration-dependent sorption rates." Environmental Science and Technology **32**(22): 3549-3555.
- Huang, W., T. M. Young, et al. (1997). "A distributed reactivity model for sorption by soils and sediments. 9. General isotherm nonlinearity and applicability of the dual reactive domain model." Environmental Science and Technology **31**(6): 1703-1710.
- Hyde, R. A. and B. W. Karney (2001). "Environmental education research: Implications for engineering education." Journal of Engineering Education **90**(2): 267-275.
- Inamura, T., K. Suzuki, et al. (2005). "Acceleration of steady-state lattice Boltzmann simulations on non-uniform mesh using local time step method." Journal of Computational Physics **202**: 645-663.
- Inamuro, T., M. Yoshino, et al. (2002). "A lattice Boltzmann method for a Binary miscible fluid mixture and its application to a heat-transfer problem." Journal of Computational Physics **179**: 201-215.
- Inamuro, T., M. Yoshino, et al. (1995). "A non-slip boundary condition for lattice Boltzmann simulations." Physics of Fluids **7**(12): 2928-2930.
- Iskander, M. F. (2002). "Technology-based electromagnetic education." IEEE transactions on microwave theory and techniques **50**(3): 1015-1020.
- Jansons, S. and G. J. Cook (2002). "Web-enabled database connectivity: A comparison of programming, scripting, and application-based access." INFORMATION SYSTEMS MANAGEMENT **19**(1): 14-22.
- Jiang, B.-n. (1998). The least-squares finite element method : theory and applications in computational fluid dynamics and electromagnetics. New York, Springer.
- Johnston, P. R. (1998). "Revisiting the most probable pore-size distribution in filter media:: The gamma distribution." Filtration & Separation **35**(3): 287-292.
- Jullien, R. and P. Meakin (1987). "Simple 3-dimensional models for ballistic deposition with restructuring." Europhysics Letters **4**(12): 1385-1390.
- Kaiser, K. and G. Guggenberger (2000). "The role of DOM sorption to mineral surfaces in the preservation of organic matter in soils." Organic Geochemistry **31**(8): 711-725.
- Kang, Q., D. Zhang, et al. (2002). "Unified lattice Boltzmann method for flow in multiscale porous media." Physical Review E **66**(056307): 1-11.

- Kang, Q., D. Zhang, et al. (2002). "Lattice Boltzmann simulation of chemical dissolution in porous media." Physical Review E **65**: 036318-1~8.
- Kang, Q., D. Zhang, et al. (2003). "Simulation of dissolution and precipitation in porous media." Journal of Geophysical Research **108**(B10): Art. No. 2505.
- Karickhoff, S. W. and D. S. Brown (1978). "Paraquat sorption as a function of particle size in natural sediments." Journal of Environmental Quality **7**(2): 246-252.
- Katz, L. E., L. J. Weathers, et al. (1998). A multimedia based laboratory course for environmental engineering. ASEE Annual Conference.
- Katz, L. E., L. J. Weathers, et al. (1997). A multimedia based laboratory course for environmental engineering fundamentals and process design. 1997 ASEE/IEEE Frontiers in Education Conference.
- Keehm, Y., T. Mukerji, et al. (2004). "Permeability prediction from thin sections: 3D reconstruction and lattice-Boltzmann flow simulation." Geophysical Research Letters **31**(4): Art. No. L04606.
- Kennedy, P. and A. Woodbury (2002). "Geostatistics and Bayesian updating for transmissivity estimation in a multiaquifer system in Manitoba, Canada." Ground Water **40**(3): 273-283.
- Kerrey, B. and J. Isakson (2000). The Power of the Internet for Learning: Moving from Promise to Practice, Web-based education commission: 185.
- Kim, I. and W. B. Lindquist (2003). "Fracture flow simulation using a finite-difference lattice Boltzmann method." Physical Review E **67,046708**: 1-9.
- King, P. R. (1989). "The use of renormalization for calculating effective permeability." Transport in Porous Media **4**: 37-58.
- Kingdon, R. and P. Schofield (1992). "A reaction-flow lattice Boltzmann model." Journal of Physics A - Mathematical and General **25**: 145-156.
- Kirkpatrick, A., A. Lee, et al. (1997). The engine in engineering - development of thermal/fluids web based applications. 1997 Frontiers in Education Conference.
- Kirkpatrick, S. (1973). "Percolation and conduction." Reviews of Modern Physics **45**(4): 574-588.
- Kirschner, P. A. and F. Paas (2001). "Web-enhanced higher education: a tower of Babel." Computers in Human Behavior **17**(4): 347-353.



- Kleineidam, S., H. Rugner, et al. (1999). "Organic matter facies and equilibrium sorption of phenanthrene." Environmental Science and Technology **33**(10): 1637-1644.
- Knapek, S. (1998). "Matrix-Dependent multigrid homogenization for diffusion problems." SIAM Journal on Scientific Computing **20**(2): 515-533.
- Knutson, C. E., C. J. Werth, et al. (2001). "Pore-scale modeling of dissolution from variably distributed nonaqueous phase liquid blobs." Water Resources Research **37**(12): 2951-2963.
- Ko, C. C., B. M. Chen, et al. (2000). "A large-scale web-based virtual oscilloscope laboratory experiment." Engineering Science and Education Journal **9**(2): 69-76.
- Koehn, E. E. (2001). "ABET program criteria: Review and assessment for a civil engineering program." Journal of Engineering Education **90**(3): 445-455.
- Kolari, S. and C. Savander-Ranne (2000). "Will the application of constructivism bring a solution to today's problems of engineering education?" Global Journal of Engineering Education **4**(3): 275-280.
- Kolb, D. A. (1984). Experiential learning: experience as the source of learning and development, Englewood Cliffs, N.J. : Prentice-Hall.
- Koplik, J. and T. J. Lasseter (1984). "One- and two-phase flow in network models of porous media." Chemical Engineering Communications **26**: 285-295.
- Koponen, A., M. Kataja, et al. (1997). "Permeability and effective porosity of porous media." Physical Review E **56**(3): 3319-3325.
- Lallemand, P., D. d'Humieres, et al. (2003). "Theory of the lattice Boltzmann method: Three-dimensional model for linear viscoelastic fluids." Physical Review E **67**(2): Art. No. 021203 Part 1.
- Langrish, T. A. and W. Davies (1995). "Putting commercial relevance into the unit operations laboratory." Chemical Engineering Education **28**(1): 40-46.
- Lapidus, L. and N. R. Amundson (1952). "Mathematics of adsorption in beds. VI. The effects of longitudinal diffusion in ion exchange and chromatographic columns." Journal of Physical Chemistry **56**: 984.
- LeBoeuf, E. J. (1998). Ph.D. Dissertation. Macromolecular Characteristics of Natural Organic Matter and Their Influence on Sorption and Desorption Behavior of Organic Chemicals. Department of Civil and Environmental Engineering, University of Michigan.

- LeBoeuf, E. J. and W. Weber, Jr. (1997). "A distributed reactivity model for sorption by soils and sediments. 8.Sorbent organic domains: Discovery of a humic acid glass transition and an argument for a polymer-based Model." Environmental Science and Technology **31**(Addi): 1697-1702.
- LeBoeuf, E. J. and W. Weber, Jr. (2000). "Macromolecular Characteristics of Natural Organic Matter. 1. Insights from Glass Transition and Enthalpic Relaxation Behavior." Environmental Science and Technology **34**(17): 3623-3631.
- LeBoeuf, E. J. and W. Weber, Jr. (2000). "Macromolecular Characteristics of Natural Organic Matter. 2. Sorption and Desorption Behavior." Environmental Science and Technology **34**(17): 3632-3640.
- Lee, T. and C.-L. Lin (2001). "A characteristic Galerkin method for discrete Boltzmann equation." Journal of Computational Physics **171**: 336-356.
- Lee, T. and C.-L. Lin (2003). "An Eulerian description of the streaming process in the lattice Boltzmann equation." Journal of Computational Physics **185**(2): 445-471.
- Lerman, A. (1979). Geochemical processes: water and sediment environments. New York, Wiley.
- Li, Y., E. J. LeBoeuf, et al. (Accepted, 2005). Use of a Least Squares Finite Element Lattice Boltzmann Method to Study Fluid Flow and Mass Transfer Processes. 2005 International Conference on Computational Science.
- Li, Y., E. J. LeBoeuf, et al. (2005). "Stochastic modeling of the permeability of randomly-generated heterogeneous porous media." Advances in Water Resources **28** (8): 835-844.
- Li, Y., E. J. LeBoeuf, et al. (2004). "Least-squares finite-element lattice Boltzmann method." Physical Review E **69**(6): Art. No. 065701.
- Li, Y., E. J. LeBoeuf, et al. (2003). "Development of a Web-Based Mass Transfer Processes Laboratory: System Development and Implementation." Computer Applications in Engineering Education **11**(1): 25-39.
- Liang, Z. R., P. C. Philippi, et al. (1999). "Prediction of permeability from the skeleton of three-dimensional pore structure." SPE Reservoir Engineering **2**(2): 161-168.
- Lin, C.-L. and Y. G. Lai (2000). "Lattice Boltzmann method on composite grids." Physical Review E **62**(2): 2219-2225.
- Ling, R. R., D. C. Yen, et al. (2000). "From database to web browser: The solutions to data access." Journal of Computer Information Systems **41**(2): 58-63.

- Lowry, M. I. and C. T. Miller (1995). "Pore-scale modeling of nonwetting-phase residual in porous media." Water Resources Research **31**(3): 455-473.
- Lu, Z. and D. Zhang (2003). "On importance sampling Monte Carlo approach to uncertainty analysis for flow and transport in porous media." Advances in Water Resources **26**: 1177-1188.
- Luo, L.-S. and S. S. Girimaji (2003). "Theory of the lattice Boltzmann method: Two-fluid model for binary mixtures." Physical Review E **67**: Art No. 036302.
- Luthy, R. G., G. R. Aiken, et al. (1997). "Sequestration of Hydrophobic Organic Contaminants by Geosorbents." Environmental Science and Technology **31**(12).
- Maier, H. R., B. J. Lence, et al. (2001). "First-order reliability method for estimating reliability, vulnerability, and resilience." Water Resources Research **37**(3): 779-790.
- Maier, R. S., R. S. Bernard, et al. (1996). "Boundary conditions for the lattice Boltzmann method." Physics of Fluids **8**(7): 1788-1801.
- Maier, R. S., D. M. Kroll, et al. (1998). "Simulation of flow through bead packs using the lattice Boltzmann method." Physics of Fluids **10**(1): 60-74.
- Manwart, C., U. Aaltosalmi, et al. (2002). "Lattice-Boltzmann and finite-difference simulations for the permeability for three-dimensional porous media." Physical Review E **66**(061702): 1-11.
- Marin, A. (2000). "A simulation engine for custom project management education." International Journal of Project Management **18**(3): 201-213.
- McNamara, G. R. and G. Zanetti (1988). "Use of the Boltzmann equation to simulate lattice-gas automata." Physical Review Letters **61**: 2232-2235.
- Mei, R., L.-S. Luo, et al. (1999). "An accurate curved boundary treatment in the lattice Boltzmann method." Journal of Computational Physics **155**: 307-330.
- Mei, R. and W. Shyy (1998). "On the finite difference-based lattice Boltzmann method in curvilinear coordinates." Journal of Computational Physics **143**: 426-448.
- Merks, R. M. H., A. G. Hoekstra, et al. (2002). "The moment propagation method for advection-diffusion in the lattice Boltzmann method: Validation and Peclet number limits." Journal of Computational Physics **183**: 563-576.
- Miller, C. T. and W. J. Weber (1984). "Modeling organic contaminant partitioning in groundwater systems." Ground Water **22**(5): 584-592.

- Miller, C. T. and W. J. Weber (1986). "Sorption of Hydrophobic Organic Pollutants in Saturated Soil System." Journal of Contaminant Hydrology **1**: 243-261.
- Miller, C. T. and W. J. Weber (1988). "Modeling the Sorption of Hydrophobic Contaminants by Aquifer Materials .2. Column Reactor Systems." Water Research **22**(4): 465-474.
- Mohtar, R. H., T. Zhai, et al. (2000). "A world wide web-based grazing simulation model (GRASIM)." Computers and Electronics in Agriculture **29**(3): 243-250.
- Mosterman, P. J., M. A. M. Dorlandt, et al. (1994). "Virtual engineering laboratories: design and experiments." Journal of Engineering Education **85**(3): 279-286.
- Moulton, J. D., J. E. Dendy, et al. (1998). "The black box multigrid numerical homogenization algorithm." Journal of Computational Physics **142**(2): 80-108.
- Myers, K. J. (1994). "Troubleshooting in the unit operations laboratory." Chemical Engineering Education **28**(2): 120-132.
- Nakavachara, C. (2001). Facilitating learning and teaching in engineering education: a problem-based approach. Electrical Engineering and Computer Science Department. Nashville, TN, Vanderbilt University.
- Nannelli, F. and S. Succi (1992). "The lattice Boltzmann-equation on irregular lattices." Journal of Statistical Physics **68**(3-4): 401-407.
- Nieuwstadt, F. and H. B. Keller (1973). "Viscous flow past circular cylinders." Computers and Fluids **1**: 59-71.
- Noble, D. R. (1997). Lattice Boltzmann study of the interstitial hydrodynamics and dispersion in steady inertial flows in large randomly packed beds. Department of Mechanical and Industrial Engineering, University of Illinois at Urbana-Champaign.
- Noble, D. R., S. Chen, et al. (1995). "A consistent hydrodynamic boundary condition for the lattice Boltzmann method." Physics of Fluids **7**(1): 203-209.
- Pan, C., M. Hilpert, et al. (2001). "Pore-scale modeling of saturated permeabilities in random sphere packings." Physical Review E **64**: 0066702-1~9.
- Pan, C., M. Hilpert, et al. (2004). "Lattice-Boltzmann simulation of two-phase flow in porous media." Water Resources Research **40**(1): Art. No. W01501.
- Pedit, J. A. and C. T. Miller (1994). "Heterogeneous Sorption Processes in Subsurface Systems. 1. Model Formulations and Applications." Environmental Science and Technology **28**(12): 2094-2104.

- Pedit, J. A. and C. T. Miller (1995). "Heterogeneous Sorption Processes in Subsurface Systems. 2. Diffusion Modeling Approaches." Environmental Science and Technology **29**(7): 1766-1772.
- Peng, G., H. Xi, et al. (1998). "Lattice Boltzmann on irregular meshes." Physical Review E **58**(4): R4124-R4127.
- Peng, G., H. Xi, et al. (1999). "Finite volume scheme for the lattice Boltzmann method on unstructured meshes." Physical Review E **59**(4): 4675-4682.
- Pignatello, J. J. and B. Xing (1996). "Mechanisms of slow sorption of organic chemicals to natural particles." Environmental Science and Technology **30**(1): 1-11.
- Portielje, R., T. Hvitved-Jacobsen, et al. (2000). "Risk analysis using stochastic reliability methods applied to two cases of deterministic water quality models." Water Research **34**(1): 153-170.
- Qian, Y. and S. Orszag (1995). "Scalings in diffusion-driven reaction  $A+B \rightarrow C$ -- Numerical simulations by lattice BGK models." Journal of Statistical Physics **81**(1-2): 237-253.
- Quintard, M. and S. Whitaker (1994). "Convection, dispersion, and interfacial transport of contaminants: Homogeneous porous media." Advances in Water Resources **17**: 221-239.
- Quintard, M. and S. Whitaker (2000). Theoretical analysis of transport in porous media. Handbook of Porous Media. K. Vafai. New York, Marcel Dekker.
- Rackwitz, R. and B. Fiessler (1978). "Structural reliability under combined random loading sequences." Computers and Structures **9**(5): 484-494.
- Rao, P. S. C. and R. E. Jessup (1982). "Experimental and Theoretical Aspects of Solute Diffusion in Spherical and Nonspherical Aggregates." Soil Science **133**(6): 342-349.
- Rao, P. S. C., D. E. Rolston, et al. (1980). "Solute transport in aggregated porous media: theoretical and experimental evaluation." Soil Science Society of America Journal **44**: 1139-1146.
- Rasmuson, A. (1985). "The effect of particles of variable size, shape and properties on the dynamics of fixed-beds." Chemical Engineering Science **40**(4): 621-629.
- Rasmuson, A. (1985). "The influence of particle-shape on the dynamics of fixed-beds." Chemical Engineering Science **40**(7): 1115-1122.

- Reardon, F. H. (2001). Internet use in a beginning thermodynamics course. Proceedings of the 2001 American Society for Engineering Annual Conference & Exposition.
- Reed, J. A. and A. A. Afjeh (1998). "Developing interactive educational engineering software for the world wide web with Java." Computers & Education **30**(3/4): 183-194.
- Renard, P. and G. d. Marsily (1997). "Calculating equivalent permeability: a review." Advances in Water Resources **20**: 253-278.
- Reyes, S. C. and K. F. Jensen (1985). "Estimation of effective transport coefficients in porous solids based on percolation concepts." Chemical Engineering Science **40**(9): 1723-1734.
- Roschelle, J., J. Kaput, et al. (1998). "Scaleable integration of educational software: exploring the promise of component architectures." Journal of Interactive Media in Education **6**: 1-31.
- Rothman, D. H. (1988). "Cellular-automaton fluids: A model for flow in porous media." Geophysics **53**(4): 509-518.
- Rothman, D. H. (1997). Lattice-gas cellular automata: simple models of complex hydrodynamics. New York, Cambridge University Press.
- Russell, B. P. and M. D. LeVan (1997). "Nonlinear adsorption and hydrodynamic dispersion in self-similar networks." Chemical Engineering Science **52**(9): 1501-1510.
- Sahimi, M. (1994). Applications of percolation theory. Bristol, PA, Taylor & Francis.
- Sahimi, M. (1995). Flow and Transport in Porous Media and Fractured Rock: from classical methods to modern approaches. Weinheim (Federal Republic of Germany), VCH Verlagsgesellschaft mbH.
- Sangani, A. S. and A. Acrivos (1983). "The effective conductivity of a periodic array of spheres." Proceedings of the Royal Society of London Series A - Mathematical Physical and Engineering Sciences.
- Schaumann, G. E. and O. Antelmann (2000). "Thermal characteristics of soil organic matter measured by DSC: a hint on a glass transition." Journal of Plant Nutrition Soil Science **163**(179-181).
- Schaumann, G. E. and E. J. LeBoeuf (2004). "Glass transitions in peat: their relevance and the impact of water." Environmental Science and Technology((in review)).

- Scheidegger, A. E. (1974). The Physics of Flow Through Porous Media. Buffalo [N.Y.], University of Toronto Press.
- Schwarzenbach, R. P., P. M. Gschwend, et al. (1993). Environmental Organic Chemistry, John Wiley & Sons, Inc.
- Selim, H. M., J. M. Davidson, et al. (1976). Evaluation of a two site adsorption-desorption model for describing solute transport in soil. Proceedings of the Computer Simulation Conference, Washington, D. C., Am. Inst. of Chem. Eng.
- Sere, M. G., J. Leach, et al. (1998). Improving science education: issues and research on innovative empirical and computer-based approaches to labwork in Europe, European Project: Labwork in Science Education (Contract No. ERB-SOE2-CT-95-2001): 121.
- Shan, X. and G. D. Doolen (1996). "Diffusion in a multicomponent lattice Boltzmann equation model." Physical Review E **54**(4): 3614-3620.
- Shin, D. and E. S. Yoon (2000). " Web-based, interactive virtual laboratory system for unit operations and process systems engineering education." Computers and Chemical Engineering **24**(5): 1381-1385.
- Shin, D., E. S. Yoon, et al. (2002). "A web-based, interactive virtual laboratory system for unit operations and process systems engineering education: issues, design and implementation." Computers and Chemical Engineering **26**(2): 319-330.
- Shin, Y. (2002). "Virtual reality simulations in Web-based science education." Computer Applications in Engineering Education **10**(1): 18-25.
- Shor, L. M., K. J. Rockne, et al. (2003). "Desorption kinetics for field-aged polycyclic aromatic hydrocarbons from sediments." Environmental Science and Technology **37**(8): 1535-1544.
- Shu, C., X. D. Niu, et al. (2002). "Taylor-series expansion and least-squares-based lattice Boltzmann method: Two-dimensional formulation and its applications." Physical Review E **65**: 036708-1~036708-13.
- Sitar, N., J. D. Cawfield, et al. (1987). "First-order reliability approach to stochastic analysis of subsurface flow and contaminant transport." Water Resources Research **23**(5): 794-804.
- Skaggs, T. H. and D. A. Barry (1996). "Assessing uncertainty in subsurface solute transport: efficient first-order reliability methods." Environmental Software **11**(1-3): 179-184.

- Skaggs, T. H. and D. A. Barry (1997). "The first-order reliability method of predicting cumulative mass flux in heterogeneous porous formations." Water Resources Research **33**(6): 1485-1494.
- Skorodos, P. A. (1993). "Initial and boundary conditions for the lattice Boltzmann method." Physical Review E **43**(6): 4823-4828.
- Smith, G. D. (1978). Numerical Solution of Partial Differential Equations. Oxford, Clarendon Press.
- Sofonea, V. and R. F. Sekerka (2003). "Viscosity of finite difference lattice Boltzmann models." Journal of Computational Physics **184**: 422-434.
- Spaid, M. A. A., F. R. Phelan, et al. (2004). "Lattice Boltzmann methods for modeling microscale flow in fibrous porous media." Physics of Fluids **9**(9): 2468-2474.
- Sterling, J. D. and S. Chen (1996). "Stability analysis of lattice Boltzmann methods." Journal of Computational Physics **123**: 196-206.
- Stern, M. K. and B. P. Woolf (2000). Adaptive content in an online lecture system. Proceedings of the International Conference on Adaptive Hypermedia and Adaptive Web-based Systems.
- Stevenson, F. J. (1994). Humus Chemistry: Genesis, Composition, Reaction. New York, John Wiley & Sons.
- Stice, J. E. (1987). "Using Kolb's learning cycle to improve student learning." Engineering Education **77**(5): 291-296.
- Strang, G. and G. J. Fix (1973). An Analysis of the Finite Element Method. Englewood Cliffs, Prentice-Hall.
- Su, Y. and I. T. Huang (1999). "The relationship between laboratory climate and students' attitudes toward science." Chinese Journal of Science Education **7**(4): 393-410.
- Succi, S. (2001). The Lattice Boltzmann equation for fluid dynamics and beyond, New York : Oxford University Press.
- Succi, S., G. Amati, et al. (1995). "Challenges in lattice Boltzmann computing." Journal of Statistical Physics **81**(1/2): 5-16.
- Succi, S., E. Foti, et al. (1989). "Three-dimensional flows in complex geometries with the lattice Boltzmann method." Europhysics Letters **10**: 433-438.



- Sukop, M. C. and D. Or (2004). "Lattice Boltzmann method for modeling liquid-vapor interface configurations in porous media." Water Resources Research **40**(1): Article No. W01509.
- Talon, L., J. Martin, et al. (2003). "Lattice BGK simulations of macrodispersion in heterogeneous porous media." Water Resources Research **39**(5): Art. No. 1135.
- Thomas, N. L. and A. H. Windle (1980). "A deformation model for CaseII diffusion." Polymer **21**: 613-619.
- Thomas, N. L. and A. H. Windle (1982). "A theory of CaseII diffusion." Polymer **23**: 529-541.
- Torquato, S. (2002). "Statistical description of microstructures." Annual Review of Materials Research **37**: 77-111.
- Travis, C. C. and E. L. Etnier (1981). "A survey of sorption relationships for reactive solutes in soil." Journal of Environmental Quality **10**(1): 8-17.
- Tritton, J. D. (1959). "Experiments on the flow past a circular cylinder at low Reynolds numbers." Journal of Fluid Mechanics **6**: 231-256.
- Tsakiroglou, C. D. and A. C. Payatakes (2000). "Characterization of the pore structure of reservoir rocks with the aid of serial sectioning analysis, mercury porosimetry and network simulation." Advances in Water Resources **23**: 773-789.
- Turcke, M. and B. Kueper (1996). "Geostatistical analysis of the Borden aquifer hydraulic conductivity." Journal of Hydrology **178**(1-4): 223-240.
- Ubertini, S., G. Bella, et al. (2003). "Lattice Boltzmann method on unstructured grids: Further developments." Physical Review E **68**: Art. No. 016701.
- Ubertini, S. and S. Succi (2005). "Recent advances of lattice Boltzmann techniques on unstructured grids." Progress in Computational Fluid Dynamics **5**(1/2): 85-96.
- Van Genuchten, M. T. (1985). "A General Approach for Modeling Solute Transport in Structured Soils." Hydrogeology of rocks of low permeability: 513-526.
- Van Genuchten, M. T. and F. N. Dalton (1986). "Model for simulating salt movement in aggregated field soil." Geoderma **38**: 165-183.
- Van Genuchten, M. T. and P. J. Wierenga (1976). "Mass transfer studies in sorbing porous media I. Analytical Solutions." Soil Science Society of America Journal **40**(4): 430-480.

- Vermeulen, T., M. D. LeVan, et al. (1987). Adsorption and Ion Exchange. Perry's Chemical Engineer's Handbook, Section 16. R. H. Perry and D. W. Green. New York, McGraw-Hill.
- Vieth, W. R. and J. M. Howell (1976). "Review paper: Dual Sorption Theory." Journal of Membrane Science **1**: 177-220.
- Vogel, H. J. and K. Roth (1998). "A new approach for determining effective soil hydraulic functions." European Journal of Soil Sciences **49**(4): 547-556.
- Vogel, H. J. and K. Roth (2001). "Quantitative morphology and network representation of soil pore structure." Advances in Water Resources **24**(3-4): 233-242.
- Wang, M., J. Laffey, et al. (2001). "The construction of shared knowledge in an Internet-based shared environment for expeditions (iExpeditions)." International Journal of Educational Technology **2**(2): on-line.
- Wankat, P. C. and F. S. Oreovicz (1993). Teaching Engineering, McGraw-Hill, Inc.
- Wathen, A. J. (1989). "An analysis of some element-by-element techniques." Computer Methods in Applied Mechanics and Engineering **74**(3): 271-287.
- Weber, W. J. and F. A. DiGiano (1996). Process dynamics in environmental systems. New York, John Wiley & Sons Inc.
- Weber, W. J. and W. Huang (1996). "A Distributed Reactivity Model for Sorption by Soils and Sediments. 4. Intraparticle Heterogeneity and Phase-Distribution Relationships under Nonequilibrium Conditions." Environmental Science and Technology **30**(3): 881-888.
- Weber, W. J., E. J. LeBoeuf, et al. (2001). "Contaminant interactions with geosorbent organic matter: Insights drawn from polymer science." Water Research **35**(4): 853-868.
- Weber, W. J., P. M. McGinley, et al. (1991). "Sorption phenomena in subsurface systems: concepts, models and effects on contaminant fate and transport." Water Research **25**(5): 499-528.
- Weber, W. J., P. M. McGinley, et al. (1992). "A distributed reactivity model for sorption by soils and sediments. 1. Conceptual Basis and Equilibrium Assessments." Environmental Science and Technology **26**(10): 1955-1962.
- Weber, W. J. and C. T. Miller (1988). "Modeling the Sorption of Hydrophobic Contaminants by Aquifer Materials .1. Rates and Equilibria." Water Research **22**(4): 457-464.

- Weimar, J. R. and J. P. Boon (1996). "Nonlinear reactions advected by a flow." Physica A **224**: 207-215.
- Wells, J. T., D. R. Janecky, et al. (1991). "A lattice gas automata model for heterogeneous chemical reactions at mineral surfaces and in pore networks." Physica D **47**: 115-123.
- Wen, X. and J. J. Gomez-Hernandez (1996). "Upscaling hydraulic conductivities in heterogeneous media: An overview." Journal of Hydrology **183**: ix-xxxii.
- Werth, C. J. and K. M. Hansen (2002). "Modeling the effects of concentration history on the slow desorption of trichloroethene from a soil at 100% relative humidity." Journal of Contaminant Hydrology **54**(4): 307-327.
- Werth, C. J. and M. Reinhard (1997). "Effects of temperature on trichloroethylene desorption from silica gel and natural sediments. 1. Isotherms." Environmental Science and Technology **31**(3): 689-696.
- Werth, C. J. and M. Reinhard (1997). "Effects of temperature on trichloroethylene desorption from silica gel and natural sediments. 2. Kinetics." Environmental Science and Technology **31**(3): 697-703.
- Werth, C. J. and M. Reinhard (1999). "Counter-diffusion of isotopically labeled trichloroethylene in silica gel and geosorbent micropores: column results." Environmental Science and Technology **33**(5): 730-736.
- Whelan, P. F. (1997). "Remote access to continuing engineering education (RACeE)." Engineering Science and Education Journal **6**(5): 205-211.
- Whitaker, S. (1999). The Method of Volume Averaging. Dordrecht, The Netherlands, Kluwer Academic Publishers.
- Willoughby, G. L. and E. J. Klavivko (2002). "Water infiltration rates following reintroduction of lubricous territories into no-till fields." Journal of Soil and Water Conservation **57**(2): 82-88.
- Wolf-Gladrow, D. A. (2000). Lattice-gas cellular automata and lattice Boltzmann models : an introduction. New York, Springer.
- Woodbury, A. D. and E. A. Sudicky (1991). "The geostatistical characteristics of the Borden Aquifer." Water Resources Research **27**(4): 533-546.
- Xi, H., G. Peng, et al. (1999). "Finite-volume lattice Boltzmann method." Physical Review E **59**(5): 6202-6205.

- Xia, G. and W. P. Ball (1999). "Adsorption-Partitioning Uptake of Nine Low-Polarity Organic Chemicals on a Natural Sorbent." Environmental Science and Technology **33**(2): 262-269.
- Xia, G. and W. P. Ball (2000). "Polanyi-Based Models for the Competitive Sorption of Low-Polarity Organic Contaminants on a Natural Sorbent." Environmental Science and Technology **34**(7): 2000.
- Xia, G. and J. J. Pignatello (2001). "Detailed Sorption Isotherms of Polar and Apolar Compounds in a High-Organic Soil." Environmental Science and Technology **35**(1): 84-94.
- Xing, B. and J. J. Pignatello (1997). "Dual-mode sorption of low-polarity compounds in glassy poly(vinyl chloride) and soil organic matter." Environmental Science and Technology **31**(3): 792-799.
- Yang, A., C. T. Miller, et al. (1996). "Simulation of correlated and uncorrelated packing of random size spheres." Physical Review E **53**(2): 1516-1524.
- Yoshino, M. and T. Inamuro (2003). "Lattice Boltzmann simulations for flow and heat/mass transfer problems in a three-dimensional porous structure." International Journal for Numerical Methods in Fluids **43**: 183-198.
- Young, K. D. and E. J. LeBoeuf (2000). "Glass Transition Behavior in a Peat Humic Acid and an Aquatic Fulvic Acid." Environmental Science and Technology **34**(21): 4549-4553.
- Young, T. M. and W. J. Weber (1995). "A Distributed reactivity model for sorption by soil and sediments. 3. Effects of diagenetic processes on sorption energetic." Environmental Science and Technology **27**(8): 92-97.
- Zhang, D. and Q. Kang (2004). "Pore scale simulation of solute transport in fractured porous media." Geophysical Research Letters **31**: Art. No. L12504.
- Zhang, D., R. Zhang, et al. (2000). "Pore scale study of flow in porous media: Scale dependency, REV, and statistical REV." Geophysical Research Letters **27**(8): 1195-1198.
- Zhang, X., A. G. Bengough, et al. (2002). "A lattice BGK model for advection and anisotropic dispersion equation." Advances in Water Resources **25**: 1-8.
- Zhang, X., A. G. Bengough, et al. (2003). "A novel three-dimensional lattice Boltzmann model of solute transport in variably saturated porous media." Water Resources Research **38**(9): Art No. 1167.

Zhang, X. and L. Ren (2003). "Lattice Boltzmann model for agrochemical transport in soils." Journal of Contaminant Hydrology **67**: 27-42.

Ziegler, D. (1993). "Boundary conditions for lattice Boltzmann simulation." Journal of Statistical Physics **71**(5/6): 1171-1177.

Zou, Q. and X. He (1997). "On pressure and velocity boundary conditions for the lattice Boltzmann BGK model." Physics of Fluids **9**(6): 1591-1598.

(<http://java.sun.com/products/jsp/tomcat/>). Apache Tomcat.

(<http://www.netlib.org/>). Netlib Repository at UTK and ORNL.